

Copyright  
by  
Yunshen Chen  
2014

**The Dissertation Committee for Yunshen Chen Certifies that this is the approved  
version of the following dissertation:**

**Surfactant Stabilization of CO<sub>2</sub>-in-Water Foams at High Temperatures**

**Committee:**

---

Keith P. Johnston, Supervisor

---

George J. Hirasaki

---

Quoc P. Nguyen

---

Isaac C. Sanchez

---

Christopher J. Ellison

---

Steven L. Bryant

**Surfactant Stabilization of CO<sub>2</sub>-in-Water Foams at High Temperatures**

**by**

**Yunshen Chen, B.E.; M.E.; M.E.**

**Dissertation**

Presented to the Faculty of the Graduate School of

The University of Texas at Austin

in Partial Fulfillment

of the Requirements

for the Degree of

**Doctor of Philosophy**

**The University of Texas at Austin**

**August 2014**

## **Dedication**

To Yao, our parents and Justin for their love, support and encouragement

## **Acknowledgements**

First I would like to thank Dr. Keith Johnston for providing me the research opportunities and training me in all kinds of research skills. Also, I would like to thank Dr. George Hirasaki (at Rice University) and Dr. Quoc Nguyen for all the discussions, suggestions, and comments on my research work as well as Dr. Isaac Sanchez, Dr. Christopher Ellison and Dr. Steven Bryant for their time in evaluating my dissertation.

I own deep thanks to Amro Elhag and Andrew Worthen. Their hard work and scientific contributions have been invaluable to this dissertation. I would like to thank visiting scholar, Hao Chen from China University of Petroleum, Beijing for CO<sub>2</sub>-water interfacial tension measurements at high temperature and pressure, and our collaborators at Rice University, Dr. Leyu Cui, Dr. Kun Ma, Dr. Sibani Biswal and Maura Puerto for their experimental and scientific helps in high temperature cloud point tests, surfactant adsorption measurement on mineral surface and core flood experiments. I thank Dr. Xi Chen and Dr. Stephanie Adkins who taught me all the high pressure experiments included in this dissertation even after they left our group. Thanks to all undergraduate students I worked with, Benjamin Poon, Sonia Liao, Prathima Reddy, Anne Maria Ou, Jose Noguera and Amr Omar for their hard work and contributions on experimental data.

I also share my thanks to all previous and current Johnston's group members: Dr. Li Ma, Dr. Ki Youl Yoon, Dr. Daniel Slanac, Dr. Andrea Miller, Dr. Avinash Murthy, Dr. Jiannan Dong, Dr. Guangzhe Yu, Dr. Hitesh Bagaria, Dr. Csaba Kotsmar, Dr. Lynn Foster, Dr. Edward Foster, Zheng Xue, Ameya Borwankear, Aileen Dinin, Bobby Stover, William Hardin, Edward Lin, Jessica Hung, Bart Dear and Joshua Laber.

Lastly, I thank my wife, Yao for her understanding and support through all of the late nights of writing and long days of experiments. This dissertation and degree is as much hers as it is mine.

# Surfactant Stabilization of CO<sub>2</sub>-in-Water Foams at High Temperatures

Yunshen Chen, PhD

The University of Texas at Austin, 2014

Supervisor: Keith P. Johnston

The interfacial properties of a surfactant in a CO<sub>2</sub>-aqueous system at a temperature above 100 °C, and how they influence foams are essentially unknown. A cationic surfactant, C<sub>12-14</sub>N(EO)<sub>2</sub> in the protonated state below pH 5.5, was demonstrated to be soluble in an aqueous phase with up to 22% total dissolved salt (TDS) at 120 °C. Moreover, the strong solvation in brine (high cloud point) and simultaneous affinity for CO<sub>2</sub> led to significant adsorption of the surfactant at the CO<sub>2</sub>-water interface. Given that the surfactant favored the brine phase over the CO<sub>2</sub> phase, the preferred curvature was a CO<sub>2</sub>-in-water (C/W) macroemulsion (foam). The surfactant stabilized foam in the presence of crushed calcium carbonate at ~ pH 4 upon suppressing the dissolution of calcium carbonate upon addition of Ca<sup>2+</sup> and Mg<sup>2+</sup> according to the common ion effect.

Cationic alkyltrimethylammonium surfactants with an alkyl tail of average carbon number less than 15 were soluble in 22% TDS brine up to 120 °C. The head group was properly balanced with a C<sub>12-14</sub> hydrocarbon tail for a sufficiently dense surfactant layer at the CO<sub>2</sub>-water interface to reduce the interfacial tension. For C<sub>12-14</sub>N(CH<sub>3</sub>)<sub>3</sub>Cl the solubility in brine and the surfactant adsorption were sufficient to stabilize C/W foam at 120 °C in both a crushed calcium carbonate packed bed (76 Darcy) and a capillary tube at the downstream of the bed. The stability of the foam at high temperature may be attributed to the high surfactant adsorption at the interface.

The use of nonionic surfactants as a foam stabilizer is usually limited by their poor aqueous solubility at elevated temperatures, particularly at high salinity. A nonionic surfactant  $C_{12-14}(EO)_{22}$  with high degree of ethoxylation gave higher salt tolerance at elevated temperature. The surfactant stabilize C/W foam at 80 °C in the presence of 90 g/L NaCl brine in a 30 Darcy sand pack, which has not yet been reported by a nonionic surfactant. Both the formation of strong foam in the porous media and the low of oil-brine partition coefficient suggest  $C_{12-14}(EO)_{22}$  is a potential candidate for a CO<sub>2</sub> EOR field trial.



## Table of Contents

List of Tables .....	xiv
List of Figures .....	xvii
Chapter 1: Introduction .....	1
1.1 Motivation .....	1
1.2 Objectives .....	6
1.3 Dissertation outline .....	7
Chapter 2: Switchable Nonionic to Cationic Ethoxylated Amine Surfactants for CO <sub>2</sub> Enhanced Oil Recovery in High Temperature, High Salinity Carbonate Reservoirs .....	10
2.1 Introduction .....	11
2.2 Experimental .....	14
2.2.1 Materials .....	14
2.2.2 Cloud–point temperature .....	14
2.2.3 Solubility of surfactant in CO <sub>2</sub> .....	15
2.2.4 Interfacial tension measurement between CO <sub>2</sub> and aqueous surfactant solutions .....	15
2.2.5 Partition coefficient of surfactant between brine and CO <sub>2</sub> .....	16
2.2.6 C/W foam formation and apparent viscosity .....	16
2.2.7 Partition coefficient of surfactant between water or brine and dodecane at 90 °C .....	18
2.2.8 Static dodecane/water emulsion stability .....	19
2.2.9 Adsorption test under 2 atm CO <sub>2</sub> .....	19
2.3 Results and discussion .....	20
2.3.1 Cloud–point temperature .....	20
2.3.2 Solubility of surfactant in CO <sub>2</sub> .....	22
2.3.3 Interfacial tension between CO <sub>2</sub> and aqueous surfactant solutions .....	23
2.3.4 Partition coefficients of surfactant between water and CO <sub>2</sub> with gentle stirring .....	24
2.3.5 C/W foam formation and apparent viscosity .....	24

2.3.5.1	Effect of temperature at a given salinity .....	25
2.3.5.2	Effect of salinity at a given temperature .....	25
2.3.5.3	Effect of initial pH of surfactant solution .....	26
2.3.5.4	Surfactant injection in the CO <sub>2</sub> phase .....	26
2.3.5.5	Effect of foam quality .....	27
2.3.5.6	Comparison of the apparent viscosity in sand Pack and capillary.....	28
2.3.6	Partition coefficients of surfactant between water or brine and dodecane at 90 °C .....	29
2.3.7	Static dodecane/water emulsion stability.....	30
2.3.8	Adsorption of surfactant on carbonate surface .....	30
2.4	Conclusions.....	31
Chapter 3: CO <sub>2</sub> -in-water Foams Stabilized at High Temperature with a Cationic Ethoxylated Amine Surfactant.....		
3.2	Experimental.....	51
3.2.1	Materials .....	51
3.2.2	Cloud–point temperature and potentiometric titration.....	52
3.2.3	Interfacial tension measurement between CO <sub>2</sub> and aqueous surfactant solutions .....	52
3.2.3	Partition coefficient of surfactant between brine and CO <sub>2</sub> .....	53
3.2.4	C/W foam formation and apparent viscosity .....	53
3.2.5	PHREEQC simulation .....	54
3.3	Results and Discussion .....	54
3.3.1	Cloud point temperatures and the degree of protonation.....	54
3.3.1.1	Effect of temperature on protonation state and solvation in aqueous phase. ....	55
3.3.1.2	Effect of salinity on protonation state and solvation in aqueous phase .....	56
3.3.1.3	Effect of pH on cloud point of C <sub>12-14</sub> N(EO) <sub>2</sub> .....	56
3.3.2	Solubility in CO <sub>2</sub> and CO <sub>2</sub> -brine partition coefficients of C <sub>12-14</sub> N(EO) <sub>2</sub> .....	57
3.3.2.1	Solubility in CO <sub>2</sub> .....	57

3.3.2.2	CO <sub>2</sub> -brine partition coefficients .....	58
3.3.3	Interfacial properties at CO <sub>2</sub> -22% TDS brine interface up to 120 °C .....	59
3.3.3.1	Interfacial tension at C-W interface .....	59
3.3.3.2	Critical micelle concentration .....	60
3.3.3.3	Adsorption at the C-W interface and efficiency in lowering the interfacial tension (pC20).....	60
3.3.4	Bulk foam apparent viscosity in capillary .....	62
3.3.5	C/W foam formation and apparent viscosity in glass bead pack .....	64
3.3.6	C/W foam formation and apparent viscosity in calcium carbonate packed bed .....	65
3.3.6.1	Effect of divalent ions on pH and foam apparent viscosity.....	65
3.3.6.2	Effect of foam quality on apparent viscosity .....	67
3.3.6.3	Effect of temperature .....	68
3.4	Conclusions.....	69
Chapter 4: CO <sub>2</sub> -in-Water Foam Stabilized with Cationic Ammonium Salt Surfactants at High Temperature .....		
4.1	Introduction.....	80
4.2	Experimental .....	85
4.2.1	Materials .....	85
4.2.2	Surfactant aqueous solubility measurements .....	85
4.2.3	Interfacial tension measurements at CO <sub>2</sub> -brine and air-brine interfaces .....	85
4.2.4	C/W foam formation and apparent viscosity measurements .....	86
4.2.5	Partition coefficient of surfactant between 22% TDS brine and dodecane .....	87
4.3	Results and Discussion .....	88
4.3.1	Solvation in water and brine .....	88
4.3.2	Interfacial properties at C-W and A-W interfaces .....	88
4.3.2.1	C-W IFT.....	88
4.3.2.2	Adsorption at the C-W interface and pC20.....	90
4.3.2.3	Interfacial properties at A-W interface .....	91

4.3.3 C/W foam formation and apparent viscosity .....	92
4.3.3.1 Effect of tail length .....	92
4.3.3.2 Effect of temperature .....	93
4.3.3.3 Effect of foam quality .....	95
4.3.3.4 Effect of surfactant concentration .....	97
4.3.4 Partitioning of surfactants between brine and dodecane.....	97
4.4 Conclusions.....	98
Chapter 5: CO <sub>2</sub> -in-Water Foam at Elevated Temperature and Salinity Stabilized with a Nonionic Surfactant with a High Degree of Ethoxylation .....	110
5.1 Introduction.....	111
5.2 Experimental .....	114
5.2.1 Materials .....	114
5.2.2 Cloud point temperature .....	114
5.2.3 CO <sub>2</sub> -brine partition coefficient determination .....	115
5.2.4 Interfacial tension measurement between CO <sub>2</sub> and aqueous surfactant solutions .....	115
5.2.5 Foam formation and apparent viscosity in sand/glass bead packs	116
5.2.6 Core flood .....	117
5.2.7 Oil-brine partition coefficient determination .....	118
5.3 Results and Discussion .....	118
5.3.1 Cloud point temperature .....	118
5.3.2 CO <sub>2</sub> -brine partition coefficient .....	119
5.3.3 Interfacial tension at CO <sub>2</sub> -brine interface .....	120
5.3.4 Foam formation and apparent viscosity in sand/glass bead pack	121
5.3.4.1 Effect of temperature and salinity on apparent viscosity at high superficial velocity.....	121
5.3.4.2 Minimum pressure gradient for foam generation .....	124
5.3.4.3 Effect of total superficial velocity and shear thinning on apparent viscosity.....	124
5.3.4.4 Effect of surfactant concentration on apparent viscosity	126
5.3.4.5 Effect of foam quality on apparent viscosity .....	127

5.3.5 Apparent viscosity of C/W foam in core floods .....	129
5.3.6 Partition coefficient between dodecane and 0.8%TDS brine ...	130
5.4 Conclusions.....	130
Chapter 6: Conclusions and Recommendations .....	145
6.1 Conclusions.....	145
6.2 Recommendations.....	145
Appendix A.....	147
A.1 Theory of bulk foam formation, apparent viscosity, and stability .....	147
A.2 Foam in porous media.....	149
A.2.1 Single-phase fluid flow in porous media .....	149
A.2.2 Foam generation.....	151
A.2.2.1 Lamellae creation.....	152
A.2.2.2 Lamellae mobilization.....	154
A.3 Smooth capillaries model and shear thinning in porous media .....	156
A.4 Limiting capillary pressure and disjoining pressure .....	157
Appendix B.....	160
B.1 Potentiometric titration for determination of the degree of protonation	160
B.2 Apparatus for apparent viscosity measurement .....	161
B.3 PHREEQC simulation (continued) .....	161
B.4 Minimum pressure gradient for foam generation.....	164
Appendix C .....	167
Appendix D.....	169
Bibliography .....	173

## List of Tables

Table 2.1:	Composition of surfactants .....	33
Table 2.2:	Cloud point temperature of 1 % w/w ethoxylated cocoamine aqueous solution with different NaCl concentrations and pH (adjusted by HCl) at atmospheric pressure.....	34
Table 2.3:	Apparent viscosities of CO <sub>2</sub> foams. Surfactants were injected from aqueous phase. pH of aqueous phase was adjusted to 4 by HOAc or HCl initially .....	35
Table 2.4:	Apparent viscosities of CO <sub>2</sub> and aqueous phase mixture with no surfactant.....	36
Table 2.5:	Apparent viscosities of CO <sub>2</sub> foams. Surfactants were injected from aqueous phase. pH of aqueous phase was adjusted to 6 by HOAc or HCl initially .....	36
Table 2.6:	Apparent viscosities of CO <sub>2</sub> foams. Surfactant was injected from CO <sub>2</sub> phase .....	37
Table 2.7:	Partition coefficient (weight fraction in oil/weight fraction in brine) of C <sub>12-14</sub> N(EO) <sub>2</sub> between NaCl brine solution and dodecane at 90 °C, 1 atm .....	37
Table 3.1:	Cloud point temperatures of 1% w/w C <sub>12-14</sub> N(EO) <sub>2</sub> aqueous solution with different salinity and pH (adjusted with HCl) .....	71
Table 3.2:	Partition coefficients of C <sub>12-14</sub> N(EO) <sub>2</sub> (weight fraction in CO <sub>2</sub> /weight fraction in brine) between CO <sub>2</sub> and brine with gentle stirring at 25-90 °C, 1000 or 3400 psia. (CO <sub>2</sub> and brine were equal in mass. 0.25 % w/w surfactant in total mass of CO <sub>2</sub> and brine .....	71

Table 3.3:	The interfacial properties of $C_{12-14}N(EO)_2$ at the $CO_2$ -22% TDS brine interface at 3400 psia .....	72
Table 4.1:	Composition and HLB of alkyltrimethylammonium surfactants....	100
Table 4.2:	Aqueous solubility of 1% w/w alkyltrimethylammonium surfactants from 25 to 120 °C in 22% total dissolved solids (see text for salt composition) .....	101
Table 4.3:	Properties of $C_{12-14}N(CH_3)_3Cl$ at the $CO_2$ -22% TDS brine and air-22% TDS brine interfaces .....	101
Table 4.4:	Apparent viscosities of $CO_2$ -in-brine foams with 1% w/w alkyl trimethyl ammonium salts in 22% TDS brine solution at 90% foam quality with total superficial velocity 938 ft/day in a 76 Darcy crushed calcium carbonate packed bed at 120 °C and 3400 psia .....	101
Table 4.5:	Partition coefficient (weight fraction in oil/weight fraction in 22% TDS brine) of quaternary ammonium salts between aqueous solution and dodecane at 90 °C and 1 atm.....	102
Table 5.1:	Structures of surfactants.....	141
Table 5.2:	Effect of salinity on cloud points of nonionic surfactants .....	142
Table 5.3:	Partition coefficients of $C_{12-14}(EO)_{22}$ , $C_{12-15}(EO)_{12}$ and $C_{12-15}(EO)_9$ between $CO_2$ and 0.8% TDS brine at 1700 psia, 24 and 40 °C .....	142
Table 5.4:	Interfacial tension between $CO_2$ and 1 % w/w $C_{12-14}(EO)_{22}$ 0.8% TDS brine at 24-60 °C, 940 or 1700 psia .....	143

Table 5.5:	Apparent viscosity of C/W foams stabilized with 1% w/w C <sub>12-14</sub> (EO) <sub>22</sub> brine solution in a 30 Darcy sand pack at 90% foam quality, total superficial velocity 622 ft/day at a CO <sub>2</sub> density of 0.413 g/mL. (Temperature and pressure was adjusted to give the constant CO <sub>2</sub> density).....	143
Table 5.6:	Partition coefficients of nonionic surfactants between dodecane and 0.8% TDS brine at 40 °C, 1 atm.....	144
Table B1:	Apparent viscosity of C/W foam stabilized with 1% w/w C <sub>12-14</sub> N(EO) <sub>2</sub> 22%TDS brine or 182 g/L NaCl brine solution (pH of aqueous phase was adjusted to 6 by HCl initially.) at 120 °C, 3400 psia, total superficial velocity 938 ft/day in a 76 Darcy calcium carbonate packed bed with foam quality from 70% to 95%.....	166



## List of Figures

Figure 2.1:	Schematic of the high-pressure apparatus for phase behavior.....	38
Figure 2.2:	Schematic of equipment used for CO <sub>2</sub> -water foam viscosity measurements. BPR means back pressure regulator. The sand pack is used as the foam generator.....	39
Figure 2.3:	Cloud point pressure of 0.2 % w/w ethoxylated cocoamines .....	40
Figure 2.4:	Interfacial tension (IFT) between CO <sub>2</sub> and 1 % w/w C <sub>12-14</sub> N(EO) <sub>2</sub> at pH6 30 g/L NaCl aqs. vs CO <sub>2</sub> density ( $\rho$ ) at 24 and 60 °C.....	41
Figure 2.5:	Partition coefficient of C <sub>12-14</sub> N(EO) <sub>2</sub> between CO <sub>2</sub> and 182 g/L NaCl with gentle stirring at 24, 60 and 90 °C, 3400 psia.....	42
Figure 2.6:	Foam apparent viscosity in sand pack of C/W foam stabilized with 1 % w/w C <sub>12-14</sub> N(EO) <sub>2</sub> versus foam quality .....	43
Figure 2.7:	Apparent viscosity in sand pack vs apparent viscosity in capillary at the same condition .....	44
Figure 2.8:	Partition coefficients of ethoxylated cocoamines with 2- 15 EO between pH4 182 g/L NaCl solution and dodecane at 90 °C, 1 atm.....	44
Figure 2.9:	Initial (A) and 72 hours (B) images of emulsion of different volumetric ratios of dodecane and 1 % w/w pH4 (adjusted by HCl) C <sub>12-14</sub> N(EO) <sub>2</sub> 120g/L NaCl solution at 90 °C, prepared by hand mixing .....	45
Figure 2.10:	The adsorption of C <sub>12-14</sub> N(EO) <sub>2</sub> on calcite in DI water and 22% TDS brine .....	45
Figure 3.1:	(A) Effect of formulation variables on the phase behavior and interfacial tension of CO <sub>2</sub> -water-ionic surfactant system; (B) Formation of a hole in a water lamella for a C/W foam.....	73

- Figure 3.2: Apparatus for CO<sub>2</sub>-water foam viscosity measurements in porous media and in a capillary tube. BPR: back pressure regulator. PT: pressure transducer. A glass bead pack or crushed calcium carbonate packed bed is used as the foam generator.....74
- Figure 3.3: Degree of protonation of C<sub>12-14</sub>N(EO)<sub>2</sub> (1% w/w) vs pH at 1 atm.: (A) 22% TDS brine at 24 (◇), 50 (△) and 90 (○)°C. (B) DI water (no salt) (◇), 120g/L NaCl brine (△) or 22% TDS brine (○) at 90 °C. (Phase boundaries where the solution became clear upon lowering pH are marked with red circles.).....75
- Figure 3.4: Interfacial tension (IFT) for C<sub>12-14</sub>N(EO)<sub>2</sub> at the CO<sub>2</sub>-22%TDS brine interface at 24 (◇), 90 (△) and 120 (□) °C versus the logarithm of surfactant concentration. The intersection of the curves denotes the critical micelle concentration (CMC). The pH of the aqueous phase is ~3. ....76
- Figure 3.5: Apparent viscosity of bulk foam in the capillary tube stabilized with 1% w/w C<sub>12-14</sub>N(EO)<sub>2</sub> 22% TDS brine at pH 6 (adjusted by adding HCl) solution with a total velocity 82897 ft/day at 3400 psia. (Foam was generated in a 76 Darcy calcium carbonate pack): (A) Effect of temperature at foam quality of 90%; (B) Effect of foam quality at 120 °C.....77

Figure 3.6: Apparent viscosity of C/W foam stabilized with  $C_{12-14}N(EO)_2$  at 3400 psia. (A) Co-injecting 1% w/w  $C_{12-14}N(EO)_2$  in 182 g/l NaCl brine pH 4 solution with pure  $CO_2$  in a 1.2 Darcy glass bead pack at 40% ( $\diamond$ ) and 80%( $\square$ ) foam quality or a 30 Darcy sand pack at 80%(+) and 90% ( $\triangle$ ) foam quality at 120 °C (See reference 42). (B) Co-injecting 1% w/w  $C_{12-14}N(EO)_2$  in 22%TDS brine pH6 solution with  $CO_2$ ( $\diamond$ ), 0.2% w/w  $C_{12-14}N(EO)_2$   $CO_2$  solution with 22%TDS brine ( $\square$ ) or 1% w/w  $C_{12-14}N(EO)_2CH_3Cl$  22%TDS brine solution with  $CO_2$  ( $\triangle$ )at 120 °C, total superficial velocity 938 ft/day in 76 Darcy calcium carbonate packed bed with foam quality from 70% to 95%. (C) Co-injecting 1% w/w  $C_{12-14}N(EO)_2$  22%TDS brine pH 6 solution with  $CO_2$  at 24-120 °C, with a total superficial velocity 938 ft/day in 76 Darcy calcium carbonate pack.....79

Figure 3.7: Effect of concentration of  $Ca^{2+}$  in injected brine on concentration of various species:  $CO_3^{2-}$ (+),  $H^+$ ( $\diamond$ ),  $HCO_3^-$ ( $\circ$ ) and  $Ca^{2+}$ ( $\square$ ) at equilibrium in the presence of excess calcium carbonate and  $CO_2$  at 120 °C and 3400 psia. The results are simulated suing PHREEQC.....79

Figure 4.1: (A) Effect of formulation variables on the phase behavior and interfacial tension of  $CO_2$ -water-ionic surfactant system; (B) Formation of a hole in a water lamella for a C/W foam.....103

Figure 4.2: Apparatus for  $CO_2$ -water foam viscosity measurements. BPR: back pressure regulator. The crushed calcium carbonate packed bed is used as the foam generator. ....104

Figure 4.3:	Interfacial tension (IFT) for $C_{12-14}N(CH_3)_3Cl$ at the $CO_2$ -22%TDS brine interface at 24, 90 and 120 °C. The arrows indicate the critical micelle concentrations. ....	105
Figure 4.4:	Surface tension for $C_{12-14}N(CH_3)_3Cl$ at the air-22%TDS brine interface at 24 °C. The arrow indicates the critical micelle concentration ....	106
Figure 4.5:	Effect of temperature on apparent viscosities of $CO_2$ -in-brine foams with 1% w/w $C_{12-14}N(CH_3)_3Cl$ in 22% TDS brine solution at total superficial velocity of 938 ft/day, 90% foam quality in a 76 Darcy calcium carbonate packed bed at 3400 psia.....	107
Figure 4.6:	Effect of foam quality on apparent viscosities of $CO_2$ -in-brine foams stabilized with 1% w/w $C_{12-14}N(CH_3)_3Cl$ in 22% TDS brine solutions at total superficial velocity of 938 ft/day in a 76 Darcy calcium carbonate packed bed at 120 °C and 3400 psia .....	108
Figure 4.7:	View cell photographs of $CO_2$ -in-brine foams stabilized with 1% w/w $C_{12-14}N(CH_3)_3Cl$ 22% TDS brine solutions at total superficial velocity 938 ft/day, 70-98% foam quality in 76 Darcy calcium carbonate packed bed, 120 °C and 3400 psia .....	109
Figure 4.8:	Effect of surfactant concentration in brine on apparent viscosities of $CO_2$ -in-brine foams stabilized with $C_{12-14}N(CH_3)_3Cl$ 22% TDS brine solutions at total superficial velocity 938 ft/day, 90% foam quality in a 76 Darcy calcium carbonate packed bed, 120 °C and 3400 psia ....	109
Figure 5.1:	Effect of formulation variables on the phase behavior and interfacial tension of $CO_2$ -water-nonionic surfactant system .....	132
Figure 5.2:	Schematic of equipment used for $CO_2$ -water foam viscosity measurements. BPR: back pressure regulator.....	133

Figure 5.3: C/W foam core flood apparatus .....	133
Figure 5.4: Temperature and salinity effects on the apparent viscosity of C/W foams stabilized with 1% w/w $C_{12-14}(EO)_{22}$ brine solution in a 30 Darcy sand pack at 25-60 °C, in the presence of 0.8% TDS brine, 30 g/L NaCl brine or 90 g/L NaCl brine at 90% foam quality, total superficial velocity 622 ft/day and 1700 psia .....	134
Figure 5.5: Effect of total superficial velocity on the pressure gradient in a 30 Darcy sand pack for co-injection of 1% w/w $C_{12-14}(EO)_{22}$ 0.8% TDS brine with $CO_2$ at 90% foam quality, 40 °C and 1700 psia. The minimum pressure gradient (MPG) for foam generation is marked with a dash line. ...	135
Figure 5.6: Effect of total superficial velocity on apparent viscosity of C/W foams stabilized with 1% w/w $C_{12-14}(EO)_{22}$ or $C_{12-15}(EO)_9$ 0.8% TDS brine solution in 30 Darcy sand pack or 1.2 Darcy glass bead pack at 40 °C, and 1700 psia .....	136
Figure 5.7: Effect of $C_{12-14}(EO)_{22}$ concentration in brine on foam apparent viscosity in 1.2 Darcy glass bead pack at superficial velocity 10 ft/day, foam quality 60%, 40 °C, 1700 psia with 0.8% TDS brine .....	137
Figure 5.8: Effect of foam quality on the apparent viscosity of C/W foams stabilized with 1% and 0.1% w/w $C_{12-14}(EO)_{22}$ 0.8% TDS brine solution in 30 Darcy sand pack at total superficial velocity of 156 ft/day, 40 °C, and 1700 psia in a 30 Darcy sand pack.....	138
Figure 5.9: Effect of foam quality on apparent viscosity of C/W foam stabilized with 1% w/w $C_{12-14}(EO)_{22}$ 0.8% TDS brine solution, 40 °C, and 1700 psia in a 1.2 Darcy bead pack at total superficial velocity 6 ft/day.....	139

Figure 5.10: The apparent viscosity history for co-injection of 1% w/w C <sub>12-14</sub> (EO) <sub>22</sub> water solution or DI water and CO <sub>2</sub> in a 49 mDarcy dolomite core at total superficial velocity 4 ft/day, 80% foam quality, 25 °C and 3400 psia .....	140
Figure 5.11: The apparent viscosity history for SAG process of injecting 1% w/w C <sub>12-14</sub> (EO) <sub>22</sub> water solution or DI water and CO <sub>2</sub> in a 49 mDarcy dolomite core at total superficial velocity 4 ft/day, with an injection pattern of 0.1 PV aqueous solution /0.4 PV CO <sub>2</sub> , 25 °C and 3400 psia .....	140
Figure A1: Schematic of an “isolated” droplet deforming in an external phase composed of either a concentrated surfactant solution or a concentrated emulsion.....	147
Figure A2: Scheme of emulsion droplets are distorted and shifted as shear is applied .....	148
Figure A3: Scheme of liquid accumulating in a pore throat .....	152
Figure A4: Scheme of snap-off in a pore throat.....	153
Figure A5: Scheme of leave-behind a pore throat.....	154
Figure A6: Scheme of lamellae division a pore throat.....	154
Figure A7: Effect of water saturation on the curvature of CO <sub>2</sub> -water interface in water-wet porous media: R <sub>low Sw</sub> and R <sub>high Sw</sub> are the radii of the curvatures at relative low and high water saturation .....	158
Figure A8: Stability of lamellae: disjoining pressure versus capillary pressure	159
Figure B1: Effect of CO <sub>2</sub> pressure on simulated pH of effluent at 120 °C in the presence of 22% TDS brine and excess calcium carbonate.....	162

Figure B2:	Effect of foam quality on apparent viscosity of CO <sub>2</sub> /brine mixture without surfactant in a 76 Darcy crushed calcium carbonate packed bed (◇) and a downstream capillary tube (660 μm ID) (□) at total superficial velocity 938 ft/day in the calcium carbonate packed bed, 120 °C and 3400 psia .....	163
Figure B3:	Effect of total superficial velocity on the pressure gradient in 1.2 Darcy glass bead pack by injecting 1% w/w C <sub>12-14</sub> N(EO) <sub>2</sub> 182 g/L NaCl brine pH 4 (adjusted by HCl initially) solution with CO <sub>2</sub> at 40% (◇) or 80% (□) foam quality at 120 °C and 3400 psia. ....	164
Figure B4:	Effect of initial concentration of Ca <sup>2+</sup> (◇) or Mg <sup>2+</sup> (□) on simulated pH at equilibrium at 120 °C, 3400 psia in the presence of excess calcium carbonate and CO <sub>2</sub> .....	165
Figure C1:	Scheme (A) and apparatus photos (B) for IFT measurement at high pressures.....	167
Figure C2:	Effect of foam quality on apparent viscosity of CO <sub>2</sub> -brine mixture without surfactant in a 76 Darcy crushed calcium carbonate packed bed at total superficial velocity 938 ft/day, 120 °C and 3400 psia .....	168
Figure D1:	Effect of surfactant concentration on the surface tension for C <sub>12-14</sub> (EO) <sub>22</sub> at the air-0.8 TDS brine interface at 24 °C and 1 atm (an example of a calibration curve used for measuring surfactant concentration in a sample for CO <sub>2</sub> -brine or oil-brine partition coefficient determination).....	169
Figure D2:	Photos for screen holder used in 1.2 Darcy glass bead pack .....	170

Figure D3: Effect of foam quality on apparent viscosity of C/W foams stabilized with 1% w/w  $C_{12-14}(EO)_{22}$  0.8% TDS brine solution at 15500 ft/day, 40 °C and 1700 psia in a capillary at the downstream of a 30 Darcy sand pack (total superficial velocity 156 ft/day in the porous media) ....171

Figure D4: Effect of foam quality on apparent viscosity of C/W foams stabilized with 1% w/w  $C_{12-14}(EO)_{22}$  0.8% TDS brine solution at 3100 ft/day, 40 °C and 1700 psia in a capillary at the downstream of a 1.2 Darcy bead pack (total superficial velocity 6 ft/day in the porous media) .....172



## Chapter 1: Introduction

### 1.1 MOTIVATION

The interest in CO<sub>2</sub> Enhanced Oil Recovery (EOR) has grown significantly over the past 40 years throughout the world,<sup>1-3</sup> and expanded despite fluctuations in oil price. In the United States, the number of CO<sub>2</sub> EOR projects increased from 20 in 1980 to 86 in 2008. Over 600 million tons of CO<sub>2</sub> (11 trillion standard cubic feet) transported through 3,500 miles of high pressure CO<sub>2</sub> pipelines were injected over 13,000 CO<sub>2</sub> EOR wells. The oil production rate from CO<sub>2</sub> projects in 2008 was 245,000 barrels of oil per day. Due to the low density and viscosity of CO<sub>2</sub>, as well as the heterogeneities in the reservoirs, problems such as CO<sub>2</sub> gravity override, viscous fingering and channeling off through high permeability regions limit the sweep efficiency.<sup>4,5</sup> The sweep efficiency for may be improved by forming CO<sub>2</sub>-in-water (C/W) foams to minimize these complication in the CO<sub>2</sub> flow through the reservoir. These foams may be considered as C/W emulsions where water is the continuous phase and supercritical fluid CO<sub>2</sub> is the dispersed phase.<sup>6-9</sup> The foam viscosity is orders of magnitude greater than that of pure CO<sub>2</sub>. Thus the foam can stabilize the displacement front in CO<sub>2</sub> flooding zones.<sup>10-12</sup> In addition, “smart” foams may be designed that would break in the presence of residual oil. Here the CO<sub>2</sub> viscosity will be low in regions where it contacts the oil, such that it may aid mobilization and production in oil rich regions.<sup>13,14</sup>

Mobility control by CO<sub>2</sub> foam has been tested in the field many times during the past 20 years. However, CO<sub>2</sub> foam has not been widely adopted, even though field trials have shown increased oil recovery. Although many surfactants were initially screened, the surfactants chosen for many of the trials were: CD-128, an alcohol ethoxylate sulfate, and CD-1045, a proprietary surfactant. These surfactants were generally selected on the

basis of the greatest reduction of CO<sub>2</sub> mobility. However, issues such as overall cost, high demands on operator time to run the process, injectivity decrease upon foam formation at the well head, limited improvement in sweep efficiency and other issues thwarted adoption.

Reservoir mineralogy, temperature and salinity play important roles in surfactant selection for CO<sub>2</sub> EOR. For sandstone formations, sulfate or nonionic surfactants can be used at low to moderate temperatures. Sulfates are chemically unstable at elevated temperatures due to hydrolytic reactions. Consequently, sulfonates are often used at high temperature rather than sulfates, or alternatively, nonionic surfactants, if their cloud points are high enough. Sulfonates with alkoxy chains have been studied at high temperature for chemical EOR to form microemulsions to mobilize oil.<sup>15,16</sup> In the case of divalent cations, ethoxylated or propoxylated alcohols, sulfates or sulfonates are needed given carboxylates and other surfactants precipitate.

Increasing numbers of carbonate reservoirs in the Middle East are becoming candidates for CO<sub>2</sub> EOR.<sup>17</sup> However, the high temperatures and high salinities widely encountered require surfactants candidate with high cloud points in the presence of concentrated brine. Above the cloud point temperature, precipitation of the surfactant from water limits the ability of the surfactant to stabilize water lamellae in C/W foam.<sup>18</sup> The cloud points of ethoxylated nonionic surfactants are often below 50 to 80 °C and nearly always below 120 °C, as hydrogen bonding between ethylene oxide groups and water weakens with temperature.<sup>18</sup> Anionic sulfate and sulfonate surfactants are used at high salinities in both lab scale tests and EOR processes,<sup>19-22</sup> but will often adsorb strongly on positively charged limestone surfaces in the presence of dissolved acidic CO<sub>2</sub> at high pressure. Cationic surfactants can be used to increase the cloud points of nonionic-cationic mixed surfactant system.<sup>23</sup> To our knowledge, there are no published

examples of CO<sub>2</sub> field trials using cationic surfactants, though lab-scale CO<sub>2</sub> foam/emulsion stabilized by cationic surfactants has been investigated.<sup>24,25</sup> More effort is needed to find promising surfactant candidates for CO<sub>2</sub> foams that are stable at high temperatures and salinities, particularly for carbonate reservoirs.

CO<sub>2</sub> foam may be achieved by injecting surfactant through the CO<sub>2</sub> phase although very few surfactants are soluble. The injection of surfactant in CO<sub>2</sub> would make the surfactant available wherever the CO<sub>2</sub> is flowing. Otherwise, if the surfactant does not flow with CO<sub>2</sub>, then the formation of foam will be limited.<sup>26</sup> Although ionic surfactants tend to have high aqueous cloud points, they also have limited CO<sub>2</sub> solubility with very few exceptions.<sup>25,27</sup> Nonionic surfactants may be soluble in the CO<sub>2</sub> phase if the tail-tail interactions are sufficiently weak, for example in the case of branched tails.<sup>18,28</sup> However, their cloud points are mostly too low for a high temperature (>100 °C), high salinity reservoirs. New surfactant concepts are needed to satisfy simultaneously the requirements of a high cloud point in the aqueous phase and high CO<sub>2</sub> solubility.

The partition coefficient of surfactant between brine, CO<sub>2</sub>, and oil phases is an important parameter for the transport of surfactant through a porous reservoir. Surfactant candidates need to favor the water phase over the oil phase to minimize losses to the oil phase. Also, the ability to form foam in presence of heavy residual oil, without forming foam upon contacting light oil at the CO<sub>2</sub> displacement front, has the potential to lead to improved sweep efficiency.<sup>29-31</sup> The hydrocarbon composition profile during a CO<sub>2</sub> flood can be conceptualized with a ternary diagram where the crude oil is represented as a mixture of a light pseudo-component and a heavy pseudo-component. The swept region will be nearly pure CO<sub>2</sub> and a residual, heavy oil pseudo-component. The CO<sub>2</sub> foam should be designed to be stable in the presence of this heavy, residual oil, so that the CO<sub>2</sub>

does not bypass the light oil. Near the displacement front both phases become enriched in the light oil pseudo-component. Since this light oil is being displaced by CO<sub>2</sub>, the foam/emulsion films should be designed to be unstable so that CO<sub>2</sub> can contact oil and the mobilized oil is not retarded as a viscous emulsion. A potential solution is to design CO<sub>2</sub> foams that are stable in the presence of a heavy residual oil but yet destabilized by the light oil at the displacement front.

Typically, the design of C/W emulsions for EOR has been based on interfacial properties for air-in-water (A/W) foams, where the air is essentially an ideal gas.<sup>5</sup> This approach may not lead to optimal surfactant selection, since C/W emulsions have very different interfacial properties and phase behavior than ideal gas/water foams. The interfacial tension (IFT) between water and compressed CO<sub>2</sub> is about 20-30 mN/m, lower than that of water and air, 72 mN/m. Consequently, the area per surfactant molecule at the planar CO<sub>2</sub>-water (C-W) interface is often larger than at oil-water (O-W) and water-air interfaces as shown by experiment<sup>32,33</sup> and molecular dynamics simulation.<sup>34</sup> For emulsions of water and CO<sub>2</sub>, measurements of interfacial tension and surfactant adsorption, with complimentary measurements of phase behavior, rheology, and emulsion stability are scarce.<sup>35</sup> Recently, the interfacial properties at A/W and C/W interfaces of approximately a dozen of nonionic surfactants were compared by our group,<sup>36</sup> which provides important information for surfactant selection for CO<sub>2</sub> EOR at low salinity and low temperature. A better understanding of the interfacial properties of C/W emulsions with other kinds of surfactant candidates, such as cationic or zwitterionic surfactants, and how these properties influence the emulsion morphology and stability would be highly beneficial for advancing EOR and other applications at even higher temperatures and salinities.

A limiting factor in the economics of EOR is the loss of surfactant to adsorption on the mineral surfaces of the formation. The industry has sought a single surfactant that fits all conditions rather than recognizing that different reservoirs require different surfactants. Anionic surfactants generally have less adsorption than nonionic surfactants on sandstones, which are anionic, but nonionic surfactants generally have less adsorption on carbonate formations. Cationic surfactants may exhibit significantly less adsorption on positively charged carbonate minerals at pH values on the order of 4-5 produced by dissolved CO<sub>2</sub> in the aqueous phase<sup>37</sup> than exhibited by anionic surfactants as a result of electrostatic repulsion<sup>38</sup>. However, charged surfactants are rarely soluble in CO<sub>2</sub> as mentioned above. Given all these limitations, it remains a major challenge to design CO<sub>2</sub> soluble surfactants that form C/W foams at high temperature with small levels of adsorption on limestone surfaces.

## 1.2 OBJECTIVES

The objective is to understand the formation, texture, rheology and stability of C/W foams as a function of the surfactant structure and formulation variables including temperature, pressure, foam quality (volumetric ratio of CO<sub>2</sub> in total injected fluid), surfactant concentration, salinity and concentration of oil. Surfactant structure and concentration will be optimized for desired foam stability and rheology in a 30 Darcy sand pack, a 1.2 Darcy glass bead pack, a 76 Darcy crushed calcium carbonate pack and a capillary tube up to 120 °C in the presence of low and high salinity brine at conditions relevant to carbonate as well as sandstone reservoirs.

The hydrophilic-CO<sub>2</sub>philic balance (HCB) of the surfactant will be characterized in terms of complimentary measurements of the surfactant distribution coefficient and the surfactant adsorption and interfacial tension at the C-W interface. The structure of the CO<sub>2</sub>philic and hydrophilic groups of the surfactant will be varied systematically to adjust the surfactant HCB to achieve the following objectives: solubility of the surfactant in CO<sub>2</sub> (with cloud point density measurements), strong adsorption of the surfactant at the C-W interface, and stable high internal phase C/W foams stabilized with minimal amounts of surfactant.

The overall goal is to control the foam propagation in porous media with favorable economics, to minimize surfactant adsorption on the rock and loss toward oil. Surfactants will be screened at high and low temperature with the small scale equipment to identify candidates with the proper phase behavior, rheology, and adsorption on carbonate and sandstone formations for scale up in the experiments with the rock cores.

### 1.3 DISSERTATION OUTLINE

Chapter 2 introduces ethoxylated amines which are switchable<sup>9,39</sup> from the nonionic state in dry CO<sub>2</sub> to cationic in the presence of an acidic aqueous phase. With a proper balance in the number of carbons in the alkyl chains and number of EO groups attached to nitrogen atom in the head group, ethoxylated alkyl amines are shown to satisfy several key criteria for efficient CO<sub>2</sub> EOR. The nitrogen atom is unprotonated in the CO<sub>2</sub> phase, and thus the surfactant is highly soluble in CO<sub>2</sub>. However, in a low pH aqueous phase, the positively charged protonated amine makes the surfactant more hydrophilic, raising the cloud point up to 120 °C. Thus, ethoxylated amine surfactants may be used to generate foams by injection of the surfactant from either the CO<sub>2</sub> or brine phase. Moreover, the cationic head group is shown to significantly reduce the adsorption of ethoxylated alkyl amines on calcite, which is also positively charged in the presence of CO<sub>2</sub> dissolved in brine.

In Chapter 3, a much detailed analysis of the mechanisms for the switchable surfactant in Chapter 2 is presented. A thermally stable cationic surfactant, protonated C<sub>12-14</sub>N(EO)<sub>2</sub>, is determined to be soluble in brine below pH 5.5 at high temperatures up to 120 °C and stabilizes C/W foams. The switchability of the surfactant between nonionic and cationic states is determined by measuring the degree of protonation versus pH as a function of temperature and salinity. The high cloud point and thermal stability of this surfactant provided an opportunity to study the C-W IFT, CMC, and the surfactant adsorption at the C-W interface at very high temperatures up to 120 °C for the first time. The phase equilibria and interfacial properties are explained in terms of the interaction of the head and tail groups with the relevant phases. In addition, the behavior of bulk C/W foam in a 660 μm ID capillary tube is described in terms of temperature and foam quality, and explained with stabilization mechanisms for the lamellae in the foams

including prevention of film drainage and hole formation. In porous media, the apparent viscosities of C/W foam stabilized with  $C_{12-14}N(EO)_2$  in a 1.2 Darcy glass bead pack at a low superficial velocity are shown to be an order of magnitude larger than in higher permeability media at much higher superficial velocities as a consequence of shear thinning effect<sup>40</sup>. To form foam in a crushed calcium carbonate packed bed, excess divalent ions were required to lower the concentration of  $CO_3^{2-}$  and  $HCO_3^-$  and consequently the pH to  $\sim 4$  according to the common ion effect to ensure the surfactant was protonated.<sup>41</sup>

In Chapter 4, several permanent cationic alkyltrimethylammonium surfactants are investigated, in contrast with the switchable surfactants in the above chapters. These surfactants are demonstrated to be soluble in water and concentrated brine up to 120 °C, lower the interfacial tension, and consequently stabilize viscous C/W foams. For the chosen trimethylammonium head group, the highest carbon number in the surfactant tail is identified whereby the surfactant solubility is not less than 1% w/w surfactant in 22% TDS brine up to 120 °C. This level of solubility is sufficient for studies of the IFT, critical micelle concentration (CMC), and surfactant adsorption at the C-W interface.. The results are compared with those for the switchable surfactant  $C_{12-14}N(EO)_2$  in the protonated state from Chapter 3 and found to be similar. The apparent viscosities of the foams are characterized in a crushed calcium carbonate packed bed and a downstream capillary tube in terms of the alkyl tail length, temperature, foam quality, and surfactant concentration, and explained in terms of lamellae stabilization mechanisms and theories for bulk foam and foam in porous media<sup>42-46</sup>. The oil-water (O-W) partition coefficients of the surfactants are investigated in terms of alkyl tail length.

In Chapter 5, interfacial properties and foams were studied for a nonionic surfactant at somewhat lower temperatures. nonionic alkyl ethoxylate surfactant with a



relatively high degree of ethoxylation ( $C_{12-14}(EO)_{22}$ ) and thus high cloud point temperature is identified for stabilization of a viscous  $CO_2$  foam at temperatures up to  $90\text{ }^\circ\text{C}$  and a salinity up to  $30\text{ g/L NaCl}$ . To choose this surfactant, the cloud point and O-W partition coefficients of eight nonionic surfactants were studied as a function of surfactant structure and/or aqueous phase salinity. The C-W partition coefficients of the nonionic surfactants were investigated in terms of surfactant structure, temperature, and pressure to give insight on the curvature of the emulsion (C/W foam in this case) and ultimately, surfactant transport in the  $CO_2$  EOR process.<sup>47-49</sup> In addition, the effects of temperature, salinity, total superficial velocity, foam quality and surfactant concentration on the apparent viscosity of C/W foams stabilized with the surfactant in a 30 Darcy sand pack or a 1.2 Darcy glass bead pack are presented and explained in terms of the phase behavior, interfacial properties and existing foam models.<sup>42,43</sup>

Supplementary material is included in Appendices A, B, C and D. Appendix A presents a summary of theories and equations on bulk foam and foam in porous media related to this dissertation. Appendices B, C and D are supporting information for Chapters 3, 4 and 5 respectively.

## **Chapter 2: Switchable Nonionic to Cationic Ethoxylated Amine Surfactants for CO<sub>2</sub> Enhanced Oil Recovery in High Temperature, High Salinity Carbonate Reservoirs**

In order to improve sweep efficiency for CO<sub>2</sub> enhanced oil recovery up to 120 °C in the presence of high salinity brine (182 g/L NaCl), novel C/W foams have been formed with surfactants composed of ethoxylated amine head groups with cocoalkyl tails. These surfactants are switchable from the nonionic (unprotonated amine) state in dry CO<sub>2</sub> to cationic (protonated amine) in the presence of an aqueous phase with a pH below 6. The high hydrophilicity in the protonated cationic state was evident in the high cloud point temperature up to 120 °C. The high cloud point facilitated stabilization of lamella between bubbles in CO<sub>2</sub>/water foams. In the nonionic form the surfactant was soluble in CO<sub>2</sub> at 120 °C, and 3300 psia at a concentration of 0.2 % w/w. C/W foams were produced by injecting the surfactant either in the CO<sub>2</sub> phase or the brine phase, which indicated good contact between phases for transport of surfactant to the interface. Solubility of the surfactant in CO<sub>2</sub> and a favorable CO<sub>2</sub>/water partition coefficient, are beneficial for transport of surfactant with CO<sub>2</sub> flow pathways in the reservoir, to minimize viscous fingering and gravity override. The ethoxylated cocoamine with two ethylene oxide (EO) groups was shown to stabilize C/W foams in a 30 Darcy sand pack with NaCl concentrations up to 182 g/L at 120 °C, 3400 psia and foam qualities from 50 to 95%. The foam produces an apparent viscosity of 6.2 cP in the sand pack and 6.3 cP in a 762 μm inner diameter capillary tube (downstream of the sand pack) in contrast with values well below 1 cP without surfactant present. Moreover, the cationic head group reduces the adsorption of ethoxylated alkyl amines on calcite, which is also positively charged in the presence of CO<sub>2</sub> dissolved in brine. The surfactant partition coefficients (0 to 0.04) favored the water phase over the oil phase, which is beneficial for minimizing losses of

surfactant to the oil phase for efficient surfactant utilization. Furthermore, the surfactant was used to form C/W foams, without forming stable/viscous O/W emulsions. This selectivity is desirable for mobility control whereby CO<sub>2</sub> will have low mobility in regions where oil is not present and high contact with oil at the displacement front. In summary, the switchable ethoxylated alkyl amine surfactants provide both high cloud points in brine and high interfacial activities of ionic surfactants in water for foam generation, as well as significant solubilities in CO<sub>2</sub> in the nonionic dry state for surfactant injection.

## 2.1 INTRODUCTION

The interest in CO<sub>2</sub> EOR has grown significantly over the past 40 years throughout the world<sup>1,2,50,51</sup>. Due to the low density and viscosity of CO<sub>2</sub>, as well as heterogeneity in reservoirs, the sweep efficiency can be limited by CO<sub>2</sub> gravity override, viscous fingering and channeling through high permeability regions.<sup>3-5</sup> The sweep efficiency can be improved by forming C/W foams which also may be considered C/W emulsions given the moderate CO<sub>2</sub> density and substantial solvent strength of CO<sub>2</sub><sup>6-9</sup>. The foam can stabilize the displacement front in CO<sub>2</sub> flooded zones.<sup>10-12</sup> In addition, a smart foam may be designed to be unstable in the presence of residual oil at the CO<sub>2</sub> displacement front whereby CO<sub>2</sub> can contact light oil, but stable in the CO<sub>2</sub> swept regions containing heavy residual oil.<sup>13,14</sup>

Increasing numbers of oil reservoirs in the Middle East are becoming candidates for CO<sub>2</sub> EOR.<sup>17</sup> However, widely encountered high temperatures and high salinities require surfactant candidates with high cloud points in the presence of concentrated brine. Above the cloud point temperature, precipitation of the surfactant from brine limits the

ability of a surfactant to stabilize water lamellae in C/W foams<sup>18</sup>. For example, the cloud points of ethoxylated nonionic surfactants are often below 50 to 80 °C and nearly always below 120 °C, as hydrogen bonding between EO groups and water become weaker with temperature.<sup>18</sup> Anionic sulfate and sulfonate surfactants are used at high salinities in both lab scale tests and EOR processes,<sup>19-22</sup> but they often adsorb strongly on positively charged limestone surfaces in the presence of dissolved acidic CO<sub>2</sub> at high pressure. Sulfonates with alkoxy chains have been studied at high temperature for surfactant EOR.<sup>15,16</sup>

CO<sub>2</sub> foam may be achieved by injecting surfactant through the CO<sub>2</sub> phase although very few surfactants are CO<sub>2</sub> soluble. The injection of surfactant in CO<sub>2</sub> would make the surfactant more available to follow CO<sub>2</sub> flow paths than in the case of alternating injection of aqueous surfactant solutions and CO<sub>2</sub> gas.<sup>26</sup> Although ionic surfactants tend to have high cloud points, they also have limited CO<sub>2</sub> solubility with very few exceptions.<sup>25,27</sup> Nonionic surfactants may be soluble in the CO<sub>2</sub> phase if the tail-tail interactions are sufficiently weak, for example in the case of branched tails<sup>18,28</sup>. However, their cloud points have been too low for a high temperature, high salinity reservoir. New surfactant concepts are needed to satisfy simultaneously the requirements of a high cloud point in the aqueous phase and high CO<sub>2</sub> solubility.

The partition coefficient of surfactant between brine, CO<sub>2</sub>, and oil phases is an important parameter for the transport of surfactant through a porous reservoir. Surfactant candidates should favor the water phase over the oil phase to minimize losses to the oil phase.<sup>52</sup> Also, the ability to form foam in presence of heavy residual oil, without forming foam upon contacting light oil or water in oil emulsion at the CO<sub>2</sub> displacement front, has the potential to lead to improved sweep efficiency.<sup>29-31</sup>

Another major challenge is to limit adsorption of surfactant on positively charged limestone surfaces at pH values on the order of 4-5 produced by dissolved CO<sub>2</sub> in the aqueous phase<sup>37</sup>. Cationic surfactants may exhibit significantly less adsorption on positively charged carbonate minerals in the presence of CO<sub>2</sub> than exhibited by anionic surfactants as a result of electrostatic repulsion<sup>38</sup>. However, charged surfactants are rarely soluble in CO<sub>2</sub> as mentioned above. Given all these limitations, it remains a major challenge to design CO<sub>2</sub> soluble surfactants that form C/W foams at high temperature with small levels of adsorption on limestone surfaces.

Our objective is to design surfactants that are soluble in CO<sub>2</sub> and stabilize C/W foams at 120 °C in the presence of concentrated brine. The stability and strength of the foams are characterized by the apparent viscosities in a porous sand pack and in a capillary tube downstream of the sand pack. Additionally, the surfactant structure was optimized to minimize adsorption on limestone. Alkyl amidine surfactants were reported to be reversibly transformed into a cationic state by exposure to CO<sub>2</sub> saturated water at atmospheric pressure to stabilize water/alkane emulsions.<sup>39</sup> To achieve our goals, we introduce ethoxylated amines which are also switchable<sup>9,39</sup> from the nonionic state in dry CO<sub>2</sub> to cationic in the presence of an acidic aqueous phase. Ethoxylated amines may readily be formed by reacting alkyl amines with an appropriate alkoxyating agent.<sup>53</sup> Relative to the starting alkyl amines, the cationic head group becomes more hydrophilic with small degrees of ethoxylation. With a proper balance in the number of carbons in the alkyl chains and number of EO groups attached to nitrogen atom in the head group, ethoxylated alkyl amines are shown to satisfy several key criteria for efficient CO<sub>2</sub> EOR. The nitrogen atom is unprotonated in the CO<sub>2</sub> phase, and thus the surfactant is highly soluble in CO<sub>2</sub>. However, in a low pH aqueous phase, the positively charged protonated amine makes the surfactant more hydrophilic, raising the cloud point up to 120 °C.

Moreover, the cationic head group is shown to significantly reduce the adsorption of ethoxylated alkyl amines on calcite, which is also positively charged in the present of CO<sub>2</sub> dissolved in brine.

## **2.2 EXPERIMENTAL**

### **2.2.1 Materials**

Bis(2-hydroxyethyl) cocoalkylamine (C<sub>12-14</sub>N(EO)<sub>2</sub>), polyoxyethylene (5) cocoalkylamine (C<sub>12-14</sub>N(EO)<sub>5</sub>) and polyoxyethylene (15) cocoalkylamine (C<sub>12-14</sub>N(EO)<sub>15</sub>) were gifts from Akzo Nobel and used without further purification.(Table 2.1). Research-grade carbon dioxide was used as received.

Sodium chloride (NaCl, certified ACS, Fisher), calcium chloride dehydrate (CaCl<sub>2</sub>·2H<sub>2</sub>O, 99+% Acros), magnesium chloride hexahydrate (MgCl<sub>2</sub>·6H<sub>2</sub>O, Fisher), glacial acetic acid (HOAc, certified ACS plus, Fisher), hydrochloric acid (HCl, technical, Fisher) and isopropanol (certified ACS plus, Fisher) were used as received.

Brine was composed of deionized (DI) water (Nanopure II, Barnstead, Dubuque, IA), and NaCl in which the concentration of NaCl was varied from 30 g/L to 182 g/L. Furthermore, 22% TDS brine (182 g/L NaCl, 77 g/L CaCl<sub>2</sub>·2H<sub>2</sub>O, 26 g/L MgCl<sub>2</sub>·6H<sub>2</sub>O) was used in the cloud point and adsorption tests. The surfactant concentration in the water/brine solution was 1.0 % w/w. In some cases, the initial pH of surfactant water/brine solutions was adjusted to 4 or 6 by adding either HOAc or HCl initially before mixing with CO<sub>2</sub>.

### **2.2.2 Cloud–point temperature**

Cloud-point temperature measurement up to 120 °C was carried out with a sealed glass pipette method developed by Puerto et al<sup>16,54</sup> following careful safety

precautions. The sealed pipettes containing surfactant aqueous solution were placed inside a 10 mL test tube filled with the same bath oil as in a temperature controlled oil bath. The surfactant concentration was 1.0 % w/w. The uncertainty in the cloud point temperature is  $\pm 0.2$  °C.

### **2.2.3 Solubility of surfactant in CO<sub>2</sub>**

The cloud point density of a CO<sub>2</sub>–surfactant solution was measured with a stirred high-pressure variable-volume view cell<sup>55</sup> containing a piston as shown in Figure 2.1. A magnetic stir-bar coated with polytetrafluoroethylene (Fisher, 3 mm in diameter, 10 mm in length, Octagonal) was used for mixing. The pressure on the backside of the piston in the cell was controlled by a computer-controlled syringe pump (Isco, model 260D), with CO<sub>2</sub> as the pressurizing fluid. The temperature of the system was controlled to within  $\pm 0.1$  °C with heating tape (Omegalux, model STH051-020) and a temperature controller (Omega, model CN76000). The pressure of the system was increased to 5000 psia where the contents in the cell became clear without excess undissolved surfactant. Upon reducing the pressure slowly with a computer-controlled syringe pump at a rate of 1 psi/second, the pressure, at which the solution became so hazy that the piston was no longer visible, was recorded. This procedure was repeated at least 3 times for every temperature and the pressure was averaged with a typical uncertainty was 10–15 psi.

### **2.2.4 Interfacial tension measurement between CO<sub>2</sub> and aqueous surfactant solutions**

The interfacial tension between CO<sub>2</sub> and aqueous surfactant solutions is determined from axisymmetric drop shape analysis of a captive bubble.<sup>56</sup> The detailed procedure is the same as in our recent work.<sup>57</sup>

### **2.2.5 Partition coefficient of surfactant between brine and CO<sub>2</sub>**

To determine the equilibrium partition coefficient, 5 g CO<sub>2</sub> and 5 g brine plus 0.25% w/w surfactant, relative to the total weight, were loaded in the front part of the variable volume view cell shown in Figure 2.1 following our earlier procedure<sup>57</sup>. The above stir bar was used for gentle mixing to avoid emulsification. The temperature of the system was controlled to within  $\pm 0.1$  °C by submerging the cell into a water bath equipped with a temperature controller (MP-BASIS, Julabo). After equilibration, samples of the upper CO<sub>2</sub> phase were extracted via a 6-port valve (Valco Instrument Co., Inc.) and a 50  $\mu$ L stainless steel loop (Valco Instrument Co., Inc.). The first sample was discarded and three samples were obtained by discharging the loop into a vial with DI water of known volume, typically 7ml. The loop was flushed 3 times with a total of 3ml of DI water to recover all of the surfactant.

The concentration of surfactant in the solution was then determined by Epton's method<sup>58</sup> of two-phase titration with methylene blue solution (0.03 g/L methylene blue, 50 g/L sodium sulfate (Na<sub>2</sub>SO<sub>4</sub>), 10 mL/L sulfuric acid (98%)) as an indicator, and sodium dodecyl ether sulfate with 3EO from Stepan (trade name: STEOL CS330, MW=422 g/mol) as titrant.(colorless end point).

### **2.2.6 C/W foam formation and apparent viscosity**

The apparatus for measurement of the foam viscosity up to 120 °C and 3400 psia is depicted in Figure 2.2. Before each flow experiment, the sand pack was rinsed with 200 ml of isopropanol/water 1:1 v/v mixture, several liters of pH 2 HCl solution and several liters of DI water until the effluent was surfactant-free. A forced convection air oven was used to control system temperature., An ISCO syringe pump (model 260D) with a series D pump controller and an HPLC dual head pump (LDC/Milton Roy consta Metric III) were used to inject the CO<sub>2</sub> and aqueous solution, respectively, at set flow



rates. The mixture of CO<sub>2</sub> and surfactant solution entered a sand pack with hydrophilic pores for foam generation.

For surfactants fed from the aqueous phase, surfactant pre-adsorption was accomplished by running a sufficient volume of surfactant solution (60 mL) through the sand pack (pore volume: 1.73 mL). For injecting surfactant from the CO<sub>2</sub> phase, surfactant and CO<sub>2</sub> were loaded into the front part of an accumulator and pressurized to ~1500 psia for several days to equilibrate. (High Pressure Equipment Company, HIP316SS, Length 121.92 cm, O.D. 2.54 cm, I. D. 1.71 cm, volume 280.00 cm<sup>3</sup>) In each case, the sand pack was a 14.7 cm long, 0.76 cm inner diameter tube packed with pre-washed 20-40 Mesh non-spherical sand (420-840 μm in diameter) with an average 50 μm pore throat<sup>18</sup>.

A differential pressure meter (Validyne, model DP22) with 100 psi diaphragm was inserted across the sand pack. An average ΔP was obtained over at least 2 min while the foam was flowing at approximately steady state, with ΔP varying by less than 15% of the mean value. To determine apparent viscosity of CO<sub>2</sub> foam in sand pack μ, the permeability k (29.8 Darcy) was first calculated from Darcy's law for 1-D horizontal flow with water as the reference fluid

$$k = \frac{q\mu L}{A\Delta P} \quad [2.1]$$

where q is the flow rate, L is the length of sand pack, and A is the cross-sectional area.

$$\mu = \frac{kA\Delta P}{qL} \quad [2.2]$$

The viscosity of the bulk foam in the effluent from the sand pack was also measured with a capillary (762 μm inner diameter, 195 cm long) tube. Either a high-range (200 psi diaphragm) differential pressure meter (Validyne, model DP22) or a low-range (50 psi diaphragm) differential pressure meter (Validyne, model DP303) was used

to measure the differential pressure ( $\Delta P_{cap}$ ) across the capillary. An average  $\Delta P_{cap}$  was obtained by averaging the values recorded over at least 2 min while the foam was flowing at approximately steady state, with  $\Delta P_{cap}$  varying by less than 15% of the mean value. The apparent viscosity of a bulk foam ( $\eta_{foam}$ ) in the capillary is calculated by the Hagen-Poiseuille equation from the known shear rate ( $\dot{\gamma}$ ) and measured  $\Delta P_{cap}$  across the capillary with a length ( $L_c$ ) of 195 cm

$$\mu = \frac{\tau}{\dot{\gamma}} = \frac{\left( \frac{\Delta P \cdot R_{cap}}{2L} \right)}{\left( \frac{4U}{R_{cap}} \right)} = \frac{R_{cap}^2 \Delta P_c}{8L_c U} \quad [2.3]$$

The average velocity,  $U$ , was determined from the total volumetric flow rate of the foam (the sum of the flow rates for the two phases,  $Q_{total}$ , divided by the cross sectional area of the capillary tube, where  $R_{cap}$  is the capillary tube radius (381  $\mu\text{m}$ ).

The effluent of the capillary flowed through a stainless steel cylindrical visual cell with two sapphire windows (0.97 cm thickness and 2.54 cm diameter) for macroscopic visual observations of the bulk flowing foam. Finally, the foam flowed through a heated ( $> 60^\circ\text{C}$ , with a water bath) backpressure regulator (BPR) (Swagelok model SS-4R3A adjustable relief valve with a 177-R3A-K1-F spring for 3000-4000 psia), where  $\text{CO}_2$  expanded to atmospheric conditions. The system pressure reported was the pressure at the BPR.

### **2.2.7 Partition coefficient of surfactant between water or brine and dodecane at $90^\circ\text{C}$**

1 % w/w ethoxylated cocoamine surfactant solutions in water or brine at pH 4 or 6 were mixed with dodecane at equal volume by gentle hand-shaking. The mixtures were put into an oven at  $90^\circ\text{C}$  for 24 h and shaken again and put back in the oven. After

another 24 h, the partition coefficient of ethoxylated cocoamine between water or brine and dodecane at 90 °C was investigated by measuring the surfactant concentration in a sample obtained from the aqueous phase using the same two-phase titration method mentioned above.

### **2.2.8 Static dodecane/water emulsion stability**

1 % w/w pH4 C<sub>12-14</sub>N(EO)<sub>2</sub> 120 g/L NaCl brine solutions were prepared and mixed in different ratios. The samples were gently hand mixed to generate the emulsions and then placed in an oven at 90 °C. Periodic images were taken to monitor the behavior of the emulsion over 72 hours.

### **2.2.9 Adsorption test under 2 atm CO<sub>2</sub>**

Because of the low cloud points of ethoxylated amine surfactants at their original pH (9-10), the surfactant solution was purged with CO<sub>2</sub> and static adsorption was tested at 2 atm in a pressure vessel. At this pressure, the surfactant solution was clear. CO<sub>2</sub> was purged into cloudy surfactant solution just above the liquid surface to lower the pH to around 6. The surfactant solution was stirred overnight to produce a clear solution for adsorption tests. Surfactant at a known concentration was added into a pressure cell and mixed with calcite sands. The equilibrium surfactant concentration was controlled above the critical micelle concentration to ensure that the adsorption plateau is obtained. CO<sub>2</sub> was purged through the pressure cell in order to remove air. CO<sub>2</sub> was then injected into the cell to 5 atm absolute pressure and then released to 1 atm. The above purging process was repeated 5 times. Thus, the volume fraction of air in the cell equalled 1/3125 which was negligible. CO<sub>2</sub> was injected to 2 atm pressure in the cell. The pressure cell was sealed and a decrease in pressure in the cell was observed, because of the dissolution of CO<sub>2</sub> in water and reaction of carbonate and CO<sub>2</sub>. Injection of CO<sub>2</sub> was repeated until the

pressure was stable at 2 atm and equilibrium was reached. The pressure cell was shaken using a reciprocal shaker (Model E6010, Eberbach Corporation) at 180 osc/min for 24 hours. The pressure cell was left to stand for two days, to allow the adsorbent to settle. The liquid was poured out of the cell and the pH of the liquid was measured. The liquid was centrifuged by 8000 rpm for 30 minutes and the pH of the supernatant was measured again. The surfactant concentration in the supernatant was determined by two-phase titration<sup>58</sup> with methylene blue solution as an indicator (colorless endpoint). The BET (Brunauer-Emmett-Teller) surface area of the calcite sands (1.65 m<sup>2</sup>/g) was measured with a Quantachrome Autosorb-3b BET Surface Analyzer. The adsorption was calculated by the following equation. (This test was conducted by Leyu Cui at Rice University)

$$[\text{Mass adsorbed}] = [\text{solution volume}] \times ([\text{initial solution concentration}] - [\text{residual concentration}]) \quad [2.4]$$

$$[\text{Adsorption}] = \frac{[\text{mass adsorbed}] \times [\text{Molecular Weight of surfact}]}{[\text{BET surface area}] \times [\text{adsorbent mass}]} \quad [2.5]$$

## 2.3 RESULTS AND DISCUSSION

### 2.3.1 Cloud–point temperature

To better understand foam generation, it is instructive to first investigate surfactant phase behavior in brine and in CO<sub>2</sub>. For alkyl ethoxylate non-ionic surfactants, the cloud point usually increases with increasing EO number as the surfactant becomes more hydrophilic due to an increase in hydrogen bonding of the head group with water. However, for these surfactants the cloud point does not reach 120 °C<sup>18,59-61</sup>, because hydrogen bonding becomes weak at high temperature. For non-ethoxylated alkyl amines, for example with a coco alkyl chain, the amine head group cannot provide enough

hydrophilicity to compensate for the hydrophobic interactions between tails to dissolve the surfactant molecule even at pH 2 at ambient temperature. This pH is even lower than the pH of water saturated with CO<sub>2</sub> at high pressure. Thus, we chose to examine ethoxylated amine head groups to attempt to raise the water solubility and the cloud point temperature.

The ethoxylation of the amine functionality modifies the hydrophilic-lipophilic balance (HLB) relative to alkyl amines. The pK<sub>a</sub> for tetraoxyethylene dodecylamine (C<sub>12</sub>NH(EO)<sub>4</sub>) is 9.3, while that of dodecylamine is 10.6.<sup>53</sup> Soluble ethoxylated alkyl amines are highly protonated at pH 3 to 6 in the presence of high pressure CO<sub>2</sub>. Ethoxylated alkyl amines are highly cationic in nature with EO numbers less than about 5. For higher EO numbers the surfactant behaves more like a nonionic surfactant,<sup>53</sup> as the effect of the protonated nitrogen group is screened by the surrounding EO groups.

The cloud points of ethoxylated cocoamines at pH 4 to 10 in DI water, with 30 g/L, 120 g/L, 182 g/L NaCl or 22% TDS brine are listed in Table 2.2. At pH4, all the cloud points for the two ethoxylated cocoamines with 2 or 5 EO groups in water and up to 182 g/L NaCl brine are higher than 120 °C. For the case with 15 EO groups, the cloud point dropped slightly for 120 g/L NaCl at pH 6. It further decreased to 108 °C for 182 g/L NaCl. These cloud points are significantly higher than those of most ethoxylated non-ionic surfactants.<sup>18,59-61</sup> At higher salinity, the cloud points of ethoxylated non-ionic surfactants may be expected to be even lower.<sup>62</sup> The cloud point of ethoxylated cocoamine surfactant decreased with increasing of EO number from 5 to 15 EO groups. At first, this may seem counterintuitive given the increase in hydrophilicity with EO number. However a second important factor must be considered at low pH. The EO hydrophilic group may screen the protonated nitrogen and thus lower the contribution

from hydration of the cation. At pH 10 where the amine is not protonated, the cloud point is much lower at high salinity, and decreases with decreasing of EO number.

Thus, the ethoxylated cocoamine surfactant exhibits both non-ionic and ionic character that may be tuned by varying the EO length to achieve high cloud point of > 120 °C in the presence of 22% TDS brine with optimal EO number of 2 at pH4. The high cloud points of ethoxylated cocoamines are an important milestone for designing a successful surfactant candidate for CO<sub>2</sub> foam generation in high temperature and high salinity conditions.

### **2.3.2 Solubility of surfactant in CO<sub>2</sub>**

Injection of surfactant from the CO<sub>2</sub> phase, instead of by the conventional approach from the aqueous phase, is beneficial for directing surfactant with the CO<sub>2</sub> phase to raise sweep efficiency, for example by reducing gravity override. Surfactants that are more soluble in CO<sub>2</sub> are more likely to be transported with the CO<sub>2</sub> phase. Thus, the CO<sub>2</sub> solubilities of ethoxylated amine surfactants were measured at elevated temperatures. The cloud point pressures of 0.2 % w/w ethoxylated cocoamine in CO<sub>2</sub> at 25 to 120 °C are listed in Figure 2.3. No carbamates were formed since tested ethoxylated amines were tertiary amines. It was found that C<sub>12-14</sub>N(EO)<sub>2</sub> and C<sub>12-14</sub>N(EO)<sub>5</sub> were CO<sub>2</sub> soluble up to 120 °C at a pressure below 3400 psia. To our knowledge, very few surfactants have shown to be soluble at such high temperature<sup>27</sup>. Thus, ethoxylated cocoamines with short EO chains are potential candidates for injection in the CO<sub>2</sub> phase. The cloud point density decreased with an increase in temperature. This lower critical solution temperature phase behavior is well known for CO<sub>2</sub>-based systems<sup>9,63</sup>. The increase in the solubility of surfactant with increasing temperature is due primarily to weakened solute–solute interactions. The thermal energy overcomes the various attractive

forces between surfactant molecules for both the head groups and tails. The EO group has moderate CO<sub>2</sub>-philicity<sup>18,36,63</sup>. However, thermal energy is important for weakening hydrogen bonding between the terminal hydroxyl groups on the EO groups and the oxygen and nitrogen atoms<sup>63</sup>. It is possible that the Lewis acidity of CO<sub>2</sub> provides some degree of interaction with the basic nitrogen groups. The cloud point pressure increases with increasing EO number from 2 to 5 given the increase in the van der Waals forces and surfactant hydrogen bonding with itself, as exemplified by a known decrease in solubility with MW for pure PEO<sup>63</sup>.

### **2.3.3 Interfacial tension between CO<sub>2</sub> and aqueous surfactant solutions**

In order to form water lamellae in CO<sub>2</sub> foams, the surfactant must lower the water-CO<sub>2</sub> interfacial tension. The interfacial tension of 1% w/w C<sub>12-14</sub>N(EO)<sub>2</sub> (in the water phase) at the C/W interface as a function of CO<sub>2</sub> density is presented in [Figure 2.4](#) at 24 and 60 °C. The interfacial tension between CO<sub>2</sub> and pure water or low salinity brine is 25-35 mN/m at 24 to 60 °C, 1500-3400 psia.<sup>64,65</sup> The interfacial tension decreased as the density of CO<sub>2</sub> increased, which is also the case for binary CO<sub>2</sub>-water systems without surfactant. As the density of CO<sub>2</sub> increases, the tail-CO<sub>2</sub> interactions become more attractive, which drives surfactant molecules from water to the C/W interface. At CO<sub>2</sub> density ~0.9 g/mL, the interfacial tension of 1% w/w C<sub>12-14</sub>N(EO)<sub>2</sub> is ~3 mN/m, which is very close to the interfacial tension of 1Hex-PO5-EO15 at the same concentration, as reported previously.<sup>36</sup> This comparison indicates that C<sub>12-14</sub>N(EO)<sub>2</sub> can lower interfacial tension between CO<sub>2</sub> and water as well as nonionic surfactants with a much longer EO head group.

### **2.3.4 Partition coefficients of surfactant between water and CO<sub>2</sub> with gentle stirring**

The partition coefficient of surfactant between water and CO<sub>2</sub> is an important parameter for predicting surfactant adsorption at water-CO<sub>2</sub> interfaces to stabilize foams. It also has a large effect on how the surfactant is transported with the flowing CO<sub>2</sub> phase in the presence of an aqueous phase in the reservoir. The partition coefficient of 0.25 % w/w C<sub>12-14</sub>N(EO)<sub>2</sub> between CO<sub>2</sub> and 182 g/L NaCl at 24-90 °C, 3400 psia is presented in Figure 2.5. C<sub>12-14</sub>N(EO)<sub>2</sub> prefers the aqueous phase much more than CO<sub>2</sub> phase as quantified by partition coefficients of ~0.05. This surfactant partitions only weakly into CO<sub>2</sub> at high pressure, indicating the strength of the solvation of the protonated ethoxylated amine by water. In contrast, the nonionic surfactant 2-ethyl-hexanol-poly(propylene oxide)<sub>4,5</sub>-b-poly(ethylene oxide)<sub>8</sub> (2EH-PO<sub>4,5</sub>-EO<sub>8</sub>) favors water at low pressures, but partitions to CO<sub>2</sub> at high pressure.<sup>57</sup> The C<sub>12-14</sub>N(EO)<sub>2</sub> system forms C/W foams following Bancroft's rule, whereby the continuous phase, water, is the phase favored by the surfactant. Based on recent research work from Ren<sup>48</sup>, surfactants with low, CO<sub>2</sub>/water partition coefficients (~0.1) can give good vertical sweep efficiency.

### **2.3.5 C/W foam formation and apparent viscosity**

The ethoxylation of amines influences the hydrophilicity of the surfactant as seen in the cloud points in water<sup>66</sup> and in Table 2.2. Thus, it may be expected that the number of EO groups will influence the partitioning behavior of the surfactant at the water-CO<sub>2</sub> interface, and thus the stability of the foam. Furthermore, the high cloud point is important for foams at 120 °C, as foams are often unstable if the surfactant is not soluble in water. The apparent viscosity of ethoxylated cocoamines with 2-15 EO groups was investigated at variable temperature, salinity and initial pH in aqueous phase. The surfactant was injected either from the aqueous phase or the CO<sub>2</sub> phase.



### ***2.3.5.1 Effect of temperature at a given salinity***

The viscosity results for ethoxylated cocoamine with total flow rate of 6 mL/min at 3400 psia and a loading in water or brine of 1 % w/w (pH was adjusted by HOAc to pH4 initially), are shown for various temperatures in Table 2.3. For all surfactants at low salinity (30 g/L NaCl), foam was formed at all three temperatures, except for C<sub>12-14</sub>N(EO)<sub>15</sub> which failed at 90 and 120 °C. In all cases, foam viscosity decreased dramatically with an increase in temperature. For the case of 2EO, foams were formed at all salinities and temperatures. However, for 15 EO and 5 EO, no foam was generated at 182g/l NaCl and 120 °C.

Two key reasons may be used to explain the decrease in viscosity for ethoxylated cocoamine surfactant stabilized foams with increasing temperature. First, the viscosity of CO<sub>2</sub>-water/brine mixture without added surfactant decreases with increasing temperature, as shown in Table 2.4 where the aqueous phase was DI water or brine. This decrease in the baseline viscosity will be reflected in viscosities after adding surfactant to form foam. The second factor is the effect of cloud point temperature. As the temperature approaches the cloud point the foam is expected to weaken or break. For example, the cloud point of C<sub>12-14</sub>N(EO)<sub>15</sub> decreased to 118 °C, when salinity increased from 0 to 182 g/L NaCl at pH 4 and the foam was unstable in Table 2.3. This trend is even clearer at pH6 and pH10 where the cloud point was even lower. When temperature approaches the cloud point temperature, surfactants become less effectively solvated by water and may precipitate in the foam lamellae. At this point, various mechanisms may lead to rupture of the lamellae including film drainage and opening of holes in the films.<sup>18</sup>

### ***2.3.5.2 Effect of salinity at a given temperature***

The effect of salinity and number of EO groups on viscosity was different at low temperature from high temperature. At low temperature (50 °C), as salinity increases,

foam viscosity for either 15 or 5 EO in the head groups in the surfactant did not change, while the foam viscosity for 2 EO in the head groups decreased by 2/3. At 90 °C, as salinity increases, the foam viscosity for ethoxylated cocoamine with 15 or 5 EO decreases, while the viscosity of ethoxylated (2EO) cocoamine follows the same trend as at lower temperature. At 120 °C, ethoxylated cocoamine with 15 or 5 EO did not stabilize foams at high salinity, as the cloud point temperature was approached. For ethoxylated (2EO) cocoamine, the viscosity increased and then decreased as seen at the lower two temperatures. With fewer EO groups, the hydrophilic head group of ethoxylated cocoamine behaves more like a cationic surfactant than a nonionic surfactant. The greater aqueous solvation of the cation appeared to improve the stability of the lamellae for a favorable foam formation.

#### ***2.3.5.3 Effect of initial pH of surfactant solution***

The foam viscosity was examined as a function of the initial pH of the aqueous brine containing surfactant. Based on the viscosity results for ethoxylated cocoamine loaded in water or brine at 1 % w/w (pH was adjusted by HOAc to pH6 initially) in Table 2.5, the initial pH of the surfactant solution did not influence foam viscosity as long as the surfactants were fully soluble in the aqueous phase. This behaviour may be explained by the fact that CO<sub>2</sub> lowers the pH of aqueous phase during the mixing process inside sand pack.

#### ***2.3.5.4 Surfactant injection in the CO<sub>2</sub> phase***

The surfactant C<sub>12-14</sub>N(EO)<sub>2</sub> was dissolved in CO<sub>2</sub> and the solution was injected into the sand pack where it mixed with brine to form foam. Upon mixing the phases, the pH is lowered by formation of carbonic acid at high temperature, which may protonate the amine. As shown in Table 2.6, this approach generated foam (apparent

viscosity 16.0 cP) with an aqueous phase consisting of 120 g/L NaCl brine over a wide range in temperature up to 120 °C. The success in generating foam by loading surfactant from the CO<sub>2</sub> phase is consistent with the CO<sub>2</sub> solubility of the surfactant. We are not aware of previous attempts to inject surfactants from the CO<sub>2</sub> phase with a switchable non-ionic surfactant into a high salinity brine phase to generate foam at high temperature. The viscosities of foam generated by loading the surfactant from either the CO<sub>2</sub> phase or the aqueous phase were similar as shown in Table 2.3 and Table 2.6. This equivalence demonstrates efficient mixing of the phase prior to entering and within the sand pack, resulting in good contact between phases and transport of surfactant to the interface from both phases. In heterogeneous reservoirs, options of injecting surfactant in the CO<sub>2</sub> phase may simplify the flow path and increase sweep efficiency in certain scenarios, where the surfactant is more likely to be transported by the flowing CO<sub>2</sub>.

#### ***2.3.5.5 Effect of foam quality***

The effect of foam quality on apparent foam viscosity in the sand pack is shown in Figure 2.6. In each case, as the quality increased from 60% v/v, apparent foam viscosity increased gradually and then markedly above 80%, until it reached the transition foam quality. This transition takes place between the high foam quality regime (where the foam obeys the limiting capillary pressure model) and low foam quality regime (where foam behavior is described by the bubble trapping model) as described in Rossen's unified model for steady-state foam behavior. Often, the apparent viscosity of foams is highest at the transition foam quality.)<sup>67,68</sup> The maximum viscosity was reached at qualities near 95% for a total flow rate of 6 mL/min and 90% for total flow rates of 3 ml/min and 1.5 mL/min.

The ability to increase or decrease foam viscosity via quality changes may provide control of the EOR process. Friedmann et al. found that higher quality foams (90%) were more stable than wet foams (40%) in porous media,<sup>69</sup> A formulation with a high transition foam quality will require injection of less surfactant solution and will have less shielding of oil by water.

#### ***2.3.5.6 Comparison of the apparent viscosity in sand Pack and capillary***

The apparent viscosities may be compared in order to determine if the foam generated in the sandpack remains stable as a bulk foam in the downstream capillary tube. The apparent viscosity in the sand pack and capillary at the same condition are similar as shown in Figure 2.7. The pore diameter in the sand pack is  $\sim 50 \mu\text{m}$ <sup>18</sup> whereas the diameter of the capillary tube is 762  $\mu\text{m}$ . The C/W foam was initially generated in the sand pack, and was accumulated as bulk foam with similar viscosity inside the capillary tube with a much larger pore diameter. In our case, the bubble size may be expected to be less than 10  $\mu\text{m}$  and thus much smaller than the capillary diameter, based on numerous microscopy studies of in situ foam texture at similar velocities and conditions.<sup>18</sup> In the case where the bubble size is similar to or larger than the capillary radius, the apparent viscosity may be expected to be higher in a sand pack than in a capillary due to pore constrictions. When the lamellae span the constrictions, reversible work equal to the product of interfacial tension and the change in area is needed to move the lamellae at steady state.<sup>70</sup> For the lamellae in this work, which are much smaller than the pore throats, this interfacial energy is less important, and thus viscosities were similar in the sand pack and capillary. The ability of forming bulk foam in large channels shed insight into the behavior for CO<sub>2</sub> flooding in fractures with larger pore sizes than in low permeability regions.

### **2.3.6 Partition coefficients of surfactant between water or brine and dodecane at 90 °C**

A low oil/water partition coefficient was desired to avoid loss of surfactant to oil phases.<sup>52</sup> The partition coefficients of ethoxylated cocoamines between pH4 182 g/L NaCl solution and dodecane at 90 °C, 1 atm are presented in Figure 2.8. With 5 or less EO groups, the partition coefficients of ethoxylated cocoamine surfactants were less than 0.2, highly favoring the aqueous phase. Ionic surfactants often partition into aqueous phase even more at higher temperatures<sup>71</sup>. Thus it is likely that the partition coefficients of these protonated ethoxylated alkyl amines will also favor brine at 120 °C. As the EO number increased from 2 to 5, the partition coefficient increased modestly, but still highly favored the aqueous phase. For 15 EO groups, the partition coefficient increased markedly and the surfactant favored the oil phase. At first, this may seem counterintuitive given the increase in hydrophilicity with EO number for classical nonionic surfactants. However, a second important factor must be considered at low pH. For the cationic protonated amine, the soft EO hydrophilic group may partially delocalize the charge protonated cation and thus lower the contribution from the hydration of the cation. Furthermore, steric effects from the EO groups may lower the hydration of the protonated amine.

To further investigate the oil/water partition coefficients, experimental were performed at various salinities and pH. The salinity as well as pH effect on partition coefficient of C<sub>12-14</sub>N(EO)<sub>2</sub> between NaCl brine solution and dodecane at 90 °C, 1 atm was investigated as shown in Table 2.7. At pH 4-6, this surfactant highly favored aqueous phase over oil phase at all tested salinities. At pH8, the partition coefficient increased with increasing of salinity. At pH 8, the surfactant was poorly protonated and it behaved more like a nonionic surfactant, partitioned to oil and further salted out of the aqueous

phase by NaCl. All oil-water partitioning results contained an error below  $\pm 0.02$  in partition coefficients.

### **2.3.7 Static dodecane/water emulsion stability**

Viscous O/W emulsions may block the access of CO<sub>2</sub> to residual oil and thus lower oil production CO<sub>2</sub> EOR process. Initial images of the emulsions made using gentle hand mixing for 1 % w/w pH4 C<sub>12-14</sub>N(EO)<sub>2</sub> in 120 g/L NaCl brine solution mixed with dodecane are shown in Figure 2.9. It is noticeable that it took tens of minutes for the emulsions made for an oil/water ratio near unity to totally separate into two clear layers. In contrast, emulsions made by mixing low aqueous surfactant solution with dodecane (1:9 and 2:8 v:v).underwent phase separation immediately. After 30 minutes, all emulsions broke down to clear water and oil phases. Photos of phase separated unstable emulsions after 72 hours are shown in Figure 2.9. Thus, at low shear, the emulsions generated for 120 g/l NaCl solutions were all highly unstable. These results suggest C<sub>12-14</sub>N(EO)<sub>2</sub> is a successful candidate at low shear conditions for avoiding stable oil/water emulsions, which can be present for other cationic surfactants. The ability to form C/W foams, without forming stable O/W foams would be highly beneficial in EOR to lower CO<sub>2</sub> mobility selectively in regions where oil is not present.

### **2.3.8 Adsorption of surfactant on carbonate surface**

The final criterion for CO<sub>2</sub>/water EOR is to minimize loss of surfactant to adsorption on mineral phases. At pH values greater than 9, the cloud point of non-ionic C<sub>12-14</sub>N(EO)<sub>2</sub> is lower than room temperature in both DI water and 22% TDS brine, as shown in Table 2.2. The pH of the solution can be reduced to around 6 under 2 atm CO<sub>2</sub>, which is in agreement with the prediction using the Phreeqc.<sup>72</sup> At this condition, the surfactant solution remains a clear single phase and the adsorption of C<sub>12-14</sub>N(EO)<sub>2</sub> was

tested on calcite (from Alfa Aesar Co., BET surface area: 1.65 m<sup>2</sup>/g) in both DI water and 22 % TDS brine, as shown in Figure 2.10.

Calcite at pH=6 has a positive charge on the surface, while C<sub>12-14</sub>N(EO)<sub>2</sub> is protonated at low pH. Thus, the adsorption of C<sub>12-14</sub>N(EO)<sub>2</sub> is expected to be low on a carbonate surface due to electrostatic repulsion. Our experimental observation follows this theory with adsorption plateaus less than 0.6 mg/m<sup>2</sup> in both DI water and 22% TDS brine (Figure 2.10). However, the calcite powder is synthetic pure calcium carbonate without any silica or clay. Natural carbonates may contain certain amount of silica and clay which may exhibit stronger electrostatic attraction with cationic surfactants. Silica carries a negative charge at pH=6 (the isoelectric point (IEP) of silica is 1.7-3.5<sup>73</sup>), which results in strong attraction to positive charged surfactant and high adsorption. Clay materials, such as kaolinite, can have high adsorption for both cationic and anionic surfactants<sup>74</sup> due to the fact that kaolinite possesses both positive and negative binding sites<sup>75</sup>. The adsorption of C<sub>12-14</sub>N(EO)<sub>2</sub> on outcrop and reservoir carbonate material will be discussed in a following publication.

## 2.4 CONCLUSIONS

Stable CO<sub>2</sub>/water foams at high temperatures up to 120 °C and high salinities up to 182 g/L NaCl have been formed with ethoxylated cocoamine surfactants. These switchable surfactants may be considered hybrids which combine the high cloud points of ionic surfactants (cationic in acidic carbonic acid) with high solubilities in dry CO<sub>2</sub> of certain non-ionic surfactants. They do not form carbamates, generate C/W foam from pH 4 to 6 and exhibit low adsorption on positively charged calcite surface. Furthermore, the variation of the degree of ethoxylation offers great flexibility for meeting several

important criteria for CO<sub>2</sub> EOR at high temperatures. With 2 and 5 EOs in the surfactant head groups at pH 4-6, the significant ionic character produces high cloud points in brine above 120 °C, and partitioning towards water over oil at high temperature, high salinity conditions.

The ethoxylated cocoamine with 2 EO groups was shown to stabilize C/W foams with high salinity brine for NaCl concentrations up to 182 g/L at 120 °C and 3400 psia with a transition foam quality at 90-95% for high viscosity. Upon injection from the CO<sub>2</sub> phase, this surfactant stabilized CO<sub>2</sub>/brine foam without adding acid other than CO<sub>2</sub>. This ability to generate foam upon introduction of the surfactant in either the CO<sub>2</sub> or brine phase indicates good contact between phases and transport of surfactant to the interface from both phases. The interfacial tension between the brine and CO<sub>2</sub> in the presence of 1% w/w surfactant in the aqueous phase was reduced to 3-6 mN/m at CO<sub>2</sub> density 0.6-0.9 g/mL. Dodecane/brine (120 g/L NaCl) emulsions were found to be unstable at 90 °C, 1 atm, indicating the desired selectivity for CO<sub>2</sub>/water foams. C<sub>12</sub>-<sub>14</sub>N(EO)<sub>2</sub> exhibited low adsorption on calcite with adsorption plateaus less than 0.6 mg/m<sup>2</sup> in both DI water and 22% TDS brine.



Table 2.1: Composition of surfactants

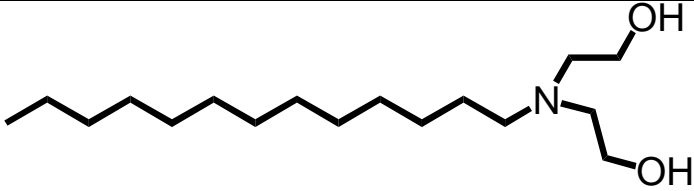
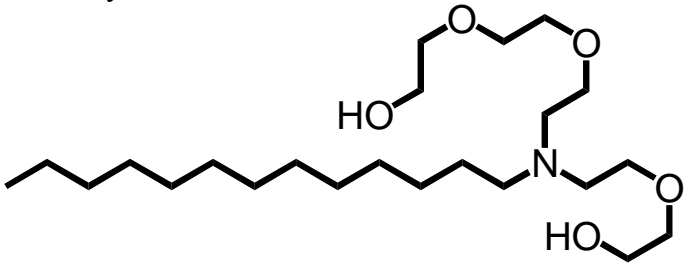
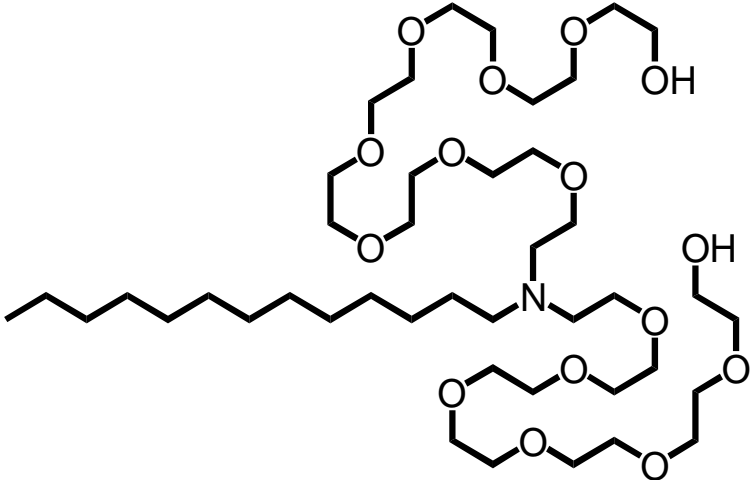
Surfactant	Composition and comments
$C_{12-14}N(EO)_2$	 <p>Hydroxyl groups added hydrophilicity</p> <p>Raised solubility in water</p>
$C_{12-14}N(EO)_5$	 <p>Significant character of nonionic and ionic surfactants</p>
$C_{12-14}N(EO)_{15}$	 <p>Strong character of nonionic surfactant from EO groups and steric hindrance</p> <p>H bonding to EO becomes weak at high T and thus lowered cloud points.</p>

Table 2.2: Cloud point temperature of 1 % w/w ethoxylated cocoamine aqueous solution with different NaCl concentrations and pH (adjusted by HCl) at atmospheric pressure

Surfactant	pH	Salinity				
		0	30 g/L NaCl	120 g/L NaCl	182 g/L NaCl	22% TDS
C <sub>12-14</sub> N(EO) <sub>2</sub>	4	>120	>120	>120	>120	>120
	6	90	-	-	-	110
	10	<25	-	-	-	<25
C <sub>12-14</sub> N(EO) <sub>5</sub>	4	>120	>120	>120	>120	>120
C <sub>12-14</sub> N(EO) <sub>15</sub>	4	>120	>120	>120	118	110
	6	-	>120	116	108	-
	10	>120	116	89	77	-

Table 2.3: Apparent viscosities of CO<sub>2</sub> foams. Surfactants were injected from aqueous phase. pH of aqueous phase was adjusted to 4 by HOAc or HCl initially

Total flow rate of 6 mL/min, 3400 psia, CO<sub>2</sub>: 1 % w/w, ethoxylated cocoamine brine solutions (9:1 v/v ratio)

Surfactant	Salinity (g/L NaCl)	Apparent viscosity in sand pack (cP)			Apparent viscosity in capillary (cP)		
		50 °C	90 °C	120 °C	50 °C	90 °C	120 °C
C <sub>12-14</sub> N(EO) <sub>2</sub>	30	58.1	22.8	9.3	59.3	22.5	9.0
	120	46.4*	22.8	12.9	41.9*	22.0	8.8
	182	20.2	11.6	6.2	24.6	14.2	6.3
C <sub>12-14</sub> N(EO) <sub>5</sub>	30	24.2	4.6	3.1	23.8	7.6	4.5
	182	22.2	1.1	No foam	21.9	1.0	No foam
C <sub>12-14</sub> N(EO) <sub>15</sub>	30	12.0	No foam	No foam	12.8	No foam	No foam
	182	12.2	No foam	No foam	14.6	No foam	No foam

\* This experiment is carried out at 3 mL/min as total flow rate.

Table 2.4: Apparent viscosities of CO<sub>2</sub> and aqueous phase mixture with no surfactant

Total flow rate of 6 mL/min, 3400 psia, CO<sub>2</sub>/aqueous (9:1 v/v ratio)

Aqueous phase	Apparent viscosity in capillary (cP)		
	50 °C	90 °C	120 °C
DI water	0.2	0.1	0.1
182 g/L NaCl	0.3	0.1	0.1

Table 2.5: Apparent viscosities of CO<sub>2</sub> foams. Surfactants were injected from aqueous phase. pH of aqueous phase was adjusted to 6 by HOAc or HCl initially

Total flow rate of 6 mL/min, 3400 psia, CO<sub>2</sub>: 1 % w/w, ethoxylated cocoamine brine solutions (9:1 v/v ratio)

Surfactant	Salinity (g/L NaCl)	Apparent viscosity in sand pack (cP)			Apparent viscosity in capillary (cP)		
		50 °C	90 °C	120 °C	50 °C	90 °C	120 °C
C <sub>12-14</sub> N(EO) <sub>2</sub>	30	57.9	17.3	4.8	54.9	17.9	7.2
	120	60.2	24.4	5.9	60.2	23.1	12.5
C <sub>12-14</sub> N(EO) <sub>5</sub>	30	22.8	5.8	4.6	21.1	7.0	6.5
	120	30.5	2.9	No foam	26.8	3.4	No foam

Table 2.6: Apparent viscosities of CO<sub>2</sub> foams. Surfactant was injected from CO<sub>2</sub> phase

Total flow rate of 6 mL/min, 3400 psia, 0.2 % w/w C12-14N(EO)<sub>2</sub> CO<sub>2</sub> solution: 120 g/L NaCl solution (9:1 v/v ratio).

Surfactant dissolution time without agitation	Apparent viscosity in sand pack (cP)			Apparent viscosity in capillary (cP)		
	50 °C	90 °C	120 °C	50 °C	90 °C	120 °C
2 days	62.3	24.9	14.9	60.4	25.6	16.0

Table 2.7: Partition coefficient (weight fraction in oil/weight fraction in brine) of C<sub>12</sub>-<sub>14</sub>N(EO)<sub>2</sub> between NaCl brine solution and dodecane at 90 °C, 1 atm

	30 g/L NaCl	120 g/L NaCl	182 g/L NaCl
pH4	0.02	0.02	0
pH6	0	0.04	0.02
pH8	7.13	11.23	15.96

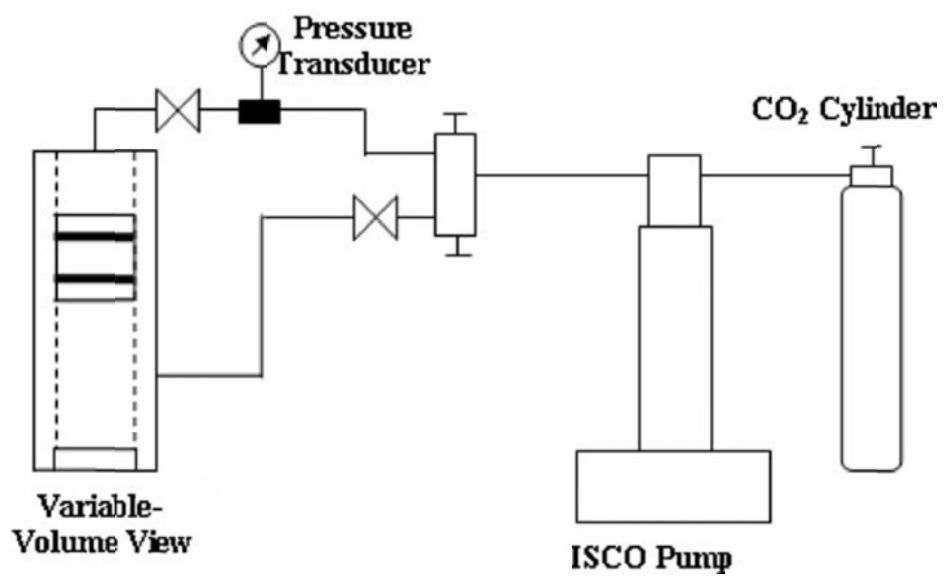


Figure 2.1: Schematic of the high-pressure apparatus for phase behavior

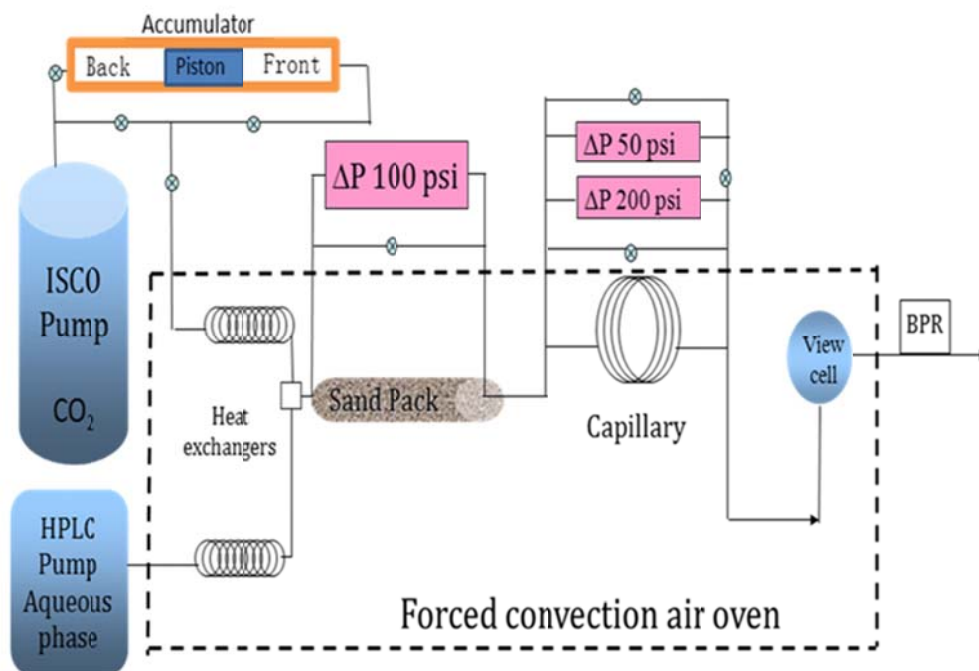


Figure 2.2: Schematic of equipment used for CO<sub>2</sub>-water foam viscosity measurements. BPR means back pressure regulator. The sand pack is used as the foam generator

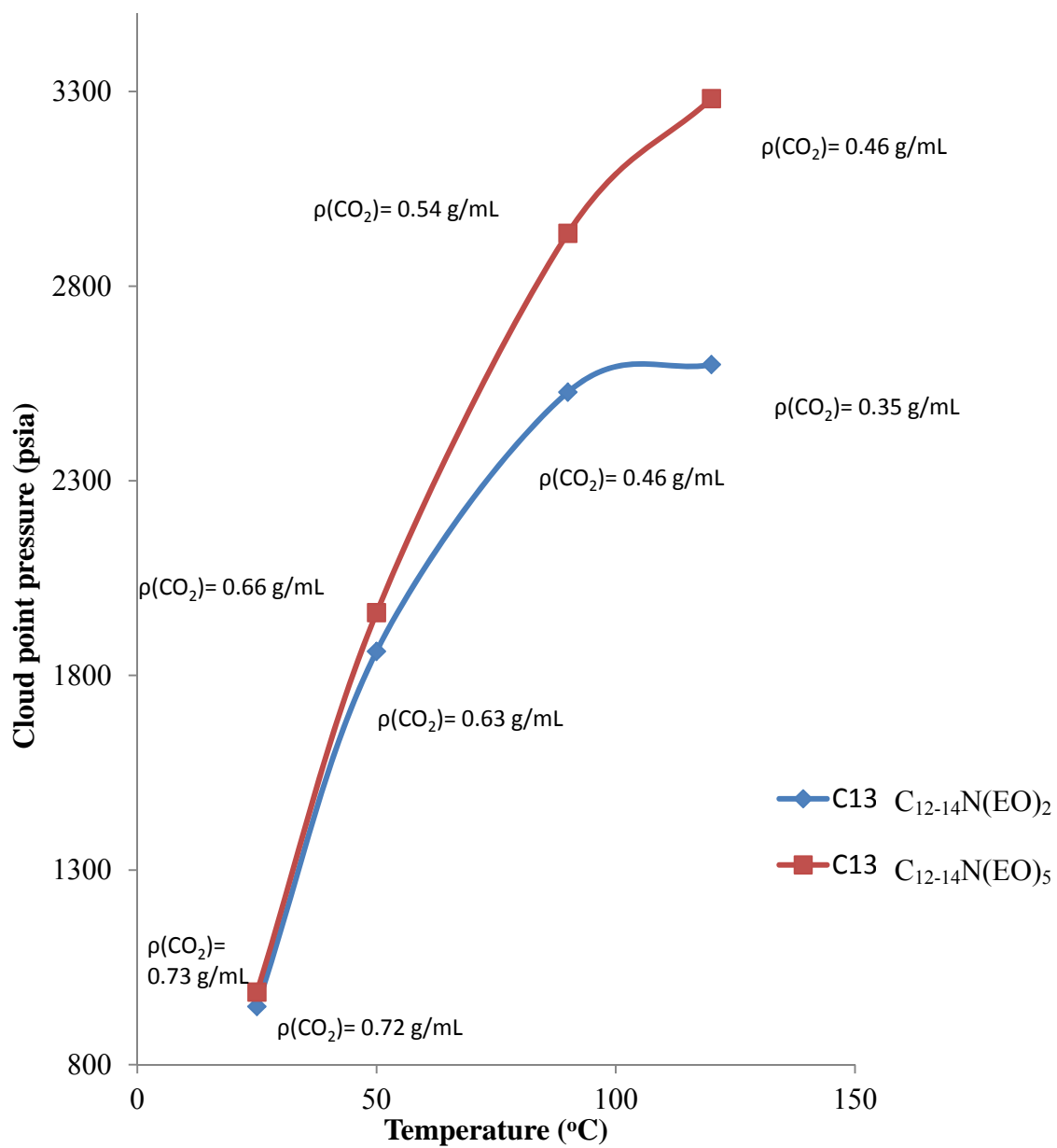


Figure 2.3: Cloud point pressure of 0.2 % w/w ethoxylated cocoamines



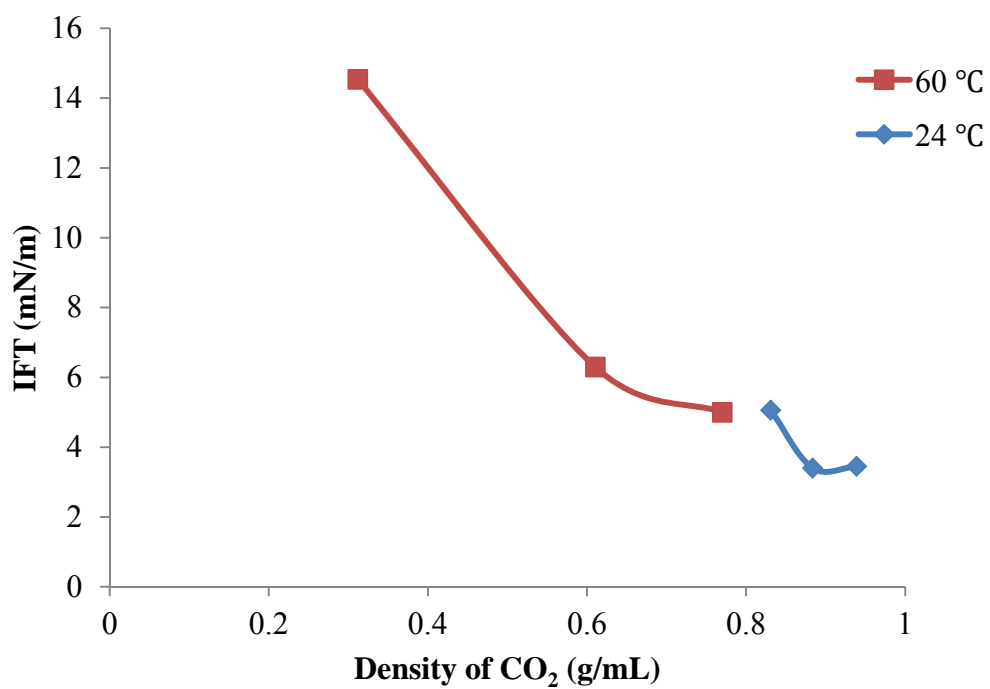


Figure 2.4: Interfacial tension (IFT) between CO<sub>2</sub> and 1 % w/w C<sub>12-14</sub>N(EO)<sub>2</sub> at pH6 30 g/L NaCl aqs. vs CO<sub>2</sub> density ( $\rho$ ) at 24 and 60 °C

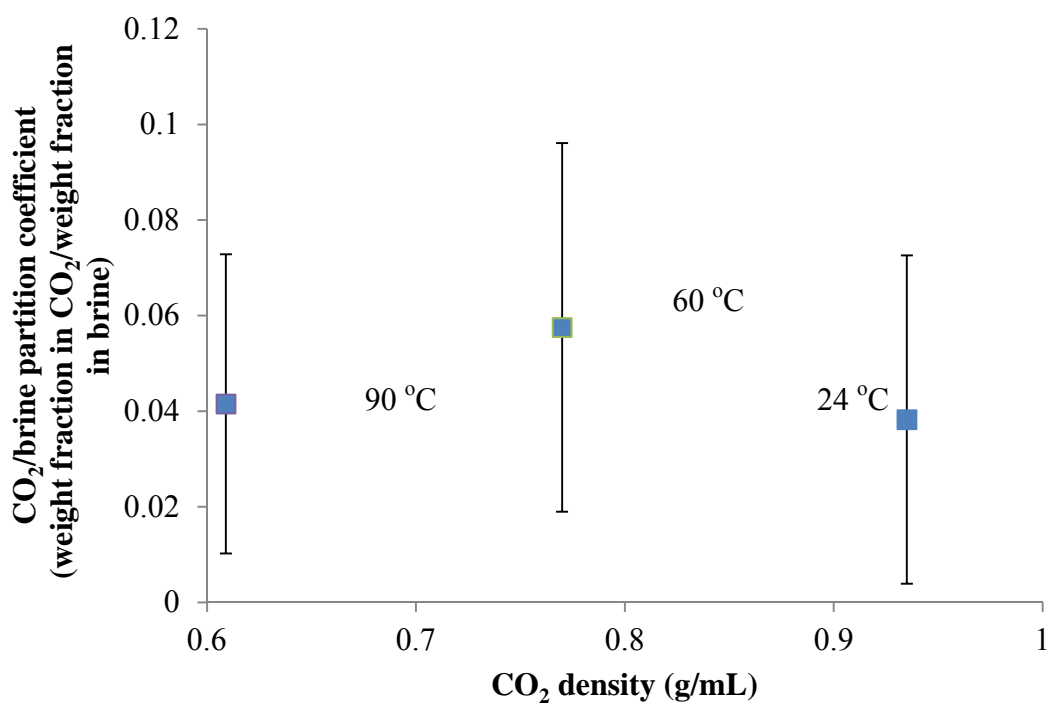


Figure 2.5: Partition coefficient of C<sub>12-14</sub>N(EO)<sub>2</sub> between CO<sub>2</sub> and 182 g/L NaCl with gentle stirring at 24, 60 and 90 °C, 3400 psia

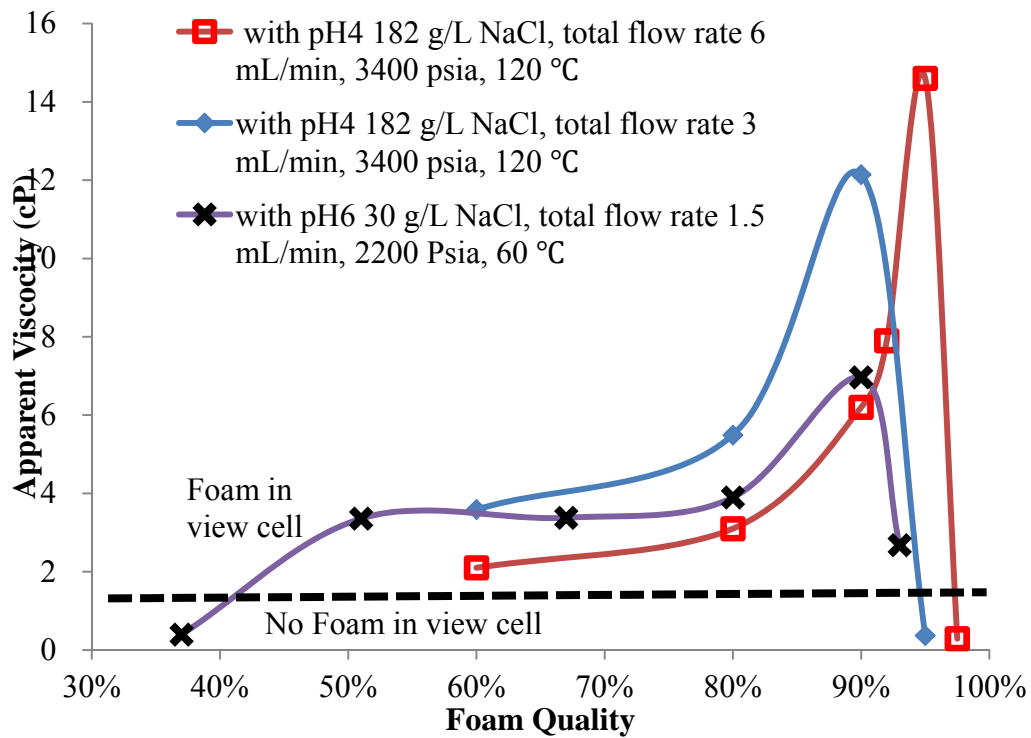


Figure 2.6: Foam apparent viscosity in sand pack of C/W foam stabilized with 1 % w/w  $C_{12-14}N(EO)_2$  versus foam quality

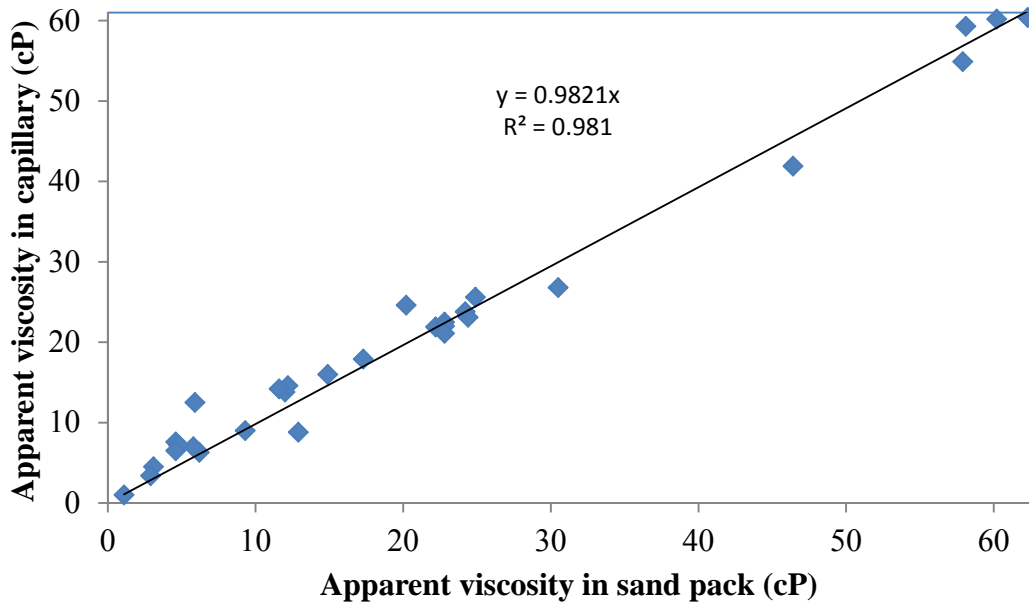


Figure 2.7: Apparent viscosity in sand pack vs apparent viscosity in capillary at the same condition

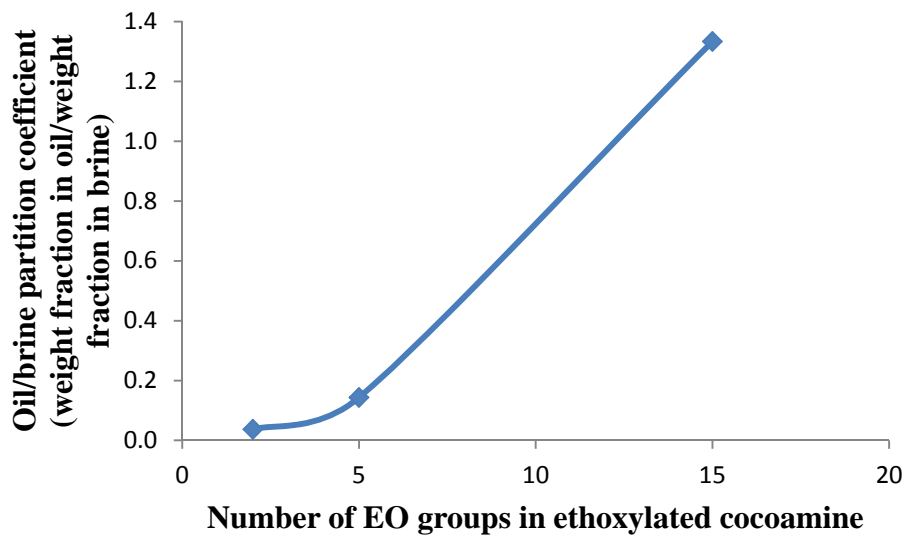


Figure 2.8: Partition coefficients of ethoxylated cocoamines with 2- 15 EO between pH4 182 g/L NaCl solution and dodecane at 90 °C, 1 atm

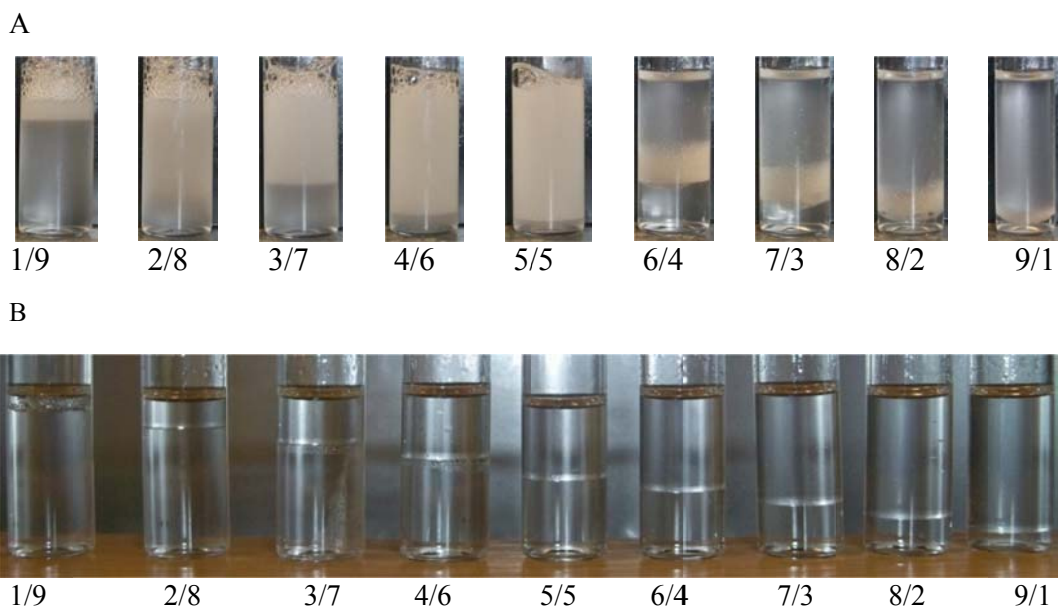


Figure 2.9: Initial (A) and 72 hours (B) images of emulsion of different volumetric ratios of dodecane and 1 % w/w pH4 (adjusted by HCl)  $C_{12-14}N(EO)_2$  120g/L NaCl solution at 90 °C, prepared by hand mixing

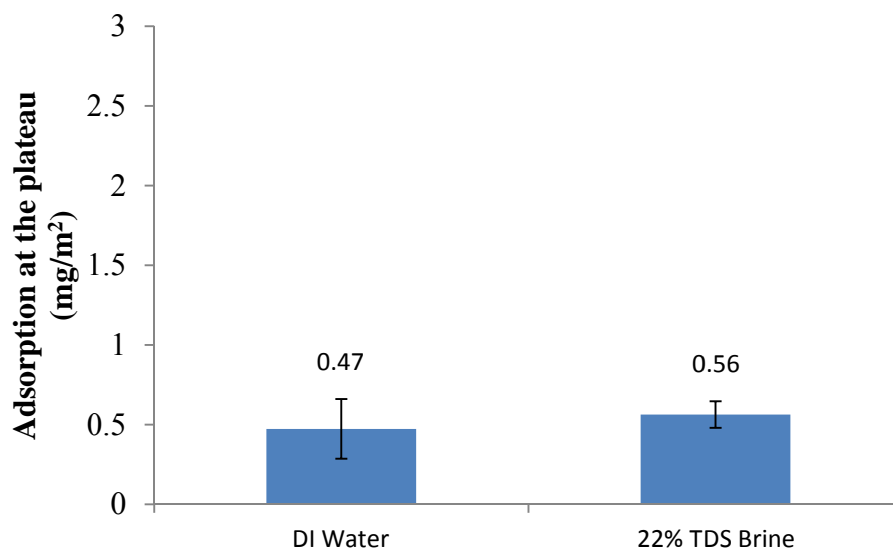


Figure 2.10: The adsorption of  $C_{12-14}N(EO)_2$  on calcite in DI water and 22% TDS brine

## **Chapter 3: CO<sub>2</sub>-in-water Foams Stabilized at High Temperature with a Cationic Ethoxylated Amine Surfactant**

The interfacial properties of a surfactant in a CO<sub>2</sub>-aqueous system at elevated pressures and a temperature above 100 °C, and how they influence foams are essentially unknown. A thermally stable cationic surfactant, C<sub>12-14</sub>N(EO)<sub>2</sub> in the protonated state below pH 5.5, was demonstrated to be soluble in water and brine with up to 22% total dissolved salt (TDS) at 120 °C. Moreover, the strong solvation in brine (high cloud point) and simultaneous affinity for CO<sub>2</sub> led to significant adsorption of the surfactant at the CO<sub>2</sub>-water interface, with an area of 207 Å<sup>2</sup>/molecule. The CO<sub>2</sub>-brine interfacial tension was lowered from ~40 mN/m to ~5 mN/m at surfactant concentrations above the critical micelle concentration (CMC), which was only 0.038 mmol/L. Given that the surfactant favored the brine phase over the CO<sub>2</sub> phase, the preferred curvature was a CO<sub>2</sub>-in-water macroemulsion (foam) according to the Bancroft rule. As the temperature was increased, the apparent viscosity of bulk foam in a 660 μm inner diameter (ID) capillary tube decreased from 23.6 cP at 24 °C to 5.7 cP at 120 °C. In a 1.2 Darcy glass bead pack at 120 °C, the apparent viscosity was very high (146 cP) at low interstitial velocities and exhibited shear thinning behavior over a wide range of foam qualities. The surfactant stabilized foam in the presence of crushed calcium carbonate at ~ pH 4 upon suppressing the dissolution of calcium carbonate upon addition of Ca<sup>2+</sup> and Mg<sup>2+</sup> according to the common ion effect.

### **3.1 Introduction**

Macroemulsions composed of water and CO<sub>2</sub> are of interest in numerous fields including green chemistry, materials science, microelectronics, pharmaceuticals and for

subsurface applications including CO<sub>2</sub> sequestration and EOR.<sup>5,8,18,76-79</sup> The formation of water-in-CO<sub>2</sub> (W/C) emulsions is challenging given the strong interactions between water droplets caused by relatively weak solvation of surfactants with hydrocarbon tails by CO<sub>2</sub>.<sup>8</sup> In contrast, C/W emulsions, (commonly referred to as foams), are formed readily with numerous hydrocarbon surfactants.<sup>18</sup> In this case, the dispersed CO<sub>2</sub> droplets may be stabilized by the favorable disjoining pressure provided by the head groups of the surfactant in the aqueous lamellae between the droplets.<sup>80</sup> Here, the weakly solvated tails are oriented into the CO<sub>2</sub> droplets and thus have a minimal effect on the interdroplet interactions that are problematic for the opposite curvature of W/C emulsions. Relatively few studies have examined C/W foams at temperatures above ~80°C given limitations in surfactant solubility in water or brine and chemical instability of many surfactants.<sup>18</sup> For example, nonionic surfactants with ethylene-oxide (EO) head groups are rarely soluble in brine at high temperatures (>100 °C) as hydrogen bonds between EO and water are weakened at such high temperatures.<sup>81</sup> Whereas anionic and cationic head groups may remain solvated at elevated temperatures, various anionic surfactants include sulfates may undergo hydrolysis.<sup>82</sup> Furthermore, quaternary ammonium salts often undergo dealkylation by Hoffmann elimination or nucleophilic substitution to form tertiary amines.<sup>83</sup> The lack of soluble and chemically stable surfactants in water and concentrated brine above 100 °C has been a major obstacle to the design of high temperature emulsions and foams, particularly for cationic surfactants.

The solubility of hydrocarbon surfactants is often limited in CO<sub>2</sub> given its low polarizability/volume and lack of a dipole moment.<sup>8</sup> Ionic hydrocarbon surfactants are nearly always insoluble in CO<sub>2</sub> as the weak solvation is not sufficient to overcome the ionic head group interactions.<sup>84</sup> For nonionic hydrocarbon surfactants, the solubility in CO<sub>2</sub> often becomes substantial upon branching the surfactant tails to weaken the tail-tail

van der Waals interactions,<sup>36,63</sup> particularly in the case of short EO head groups.<sup>8,40,85</sup> However, Chen et al. found two ethoxylated amine surfactants with linear C<sub>12-14</sub> tails and 2 or 5 EO groups (C<sub>12-14</sub>N(EO)<sub>2</sub> and C<sub>12-14</sub>N(EO)<sub>5</sub>) which were soluble at 0.2 % w/w in dry CO<sub>2</sub> in the unprotonated state at 120 °C and 3400 psia.<sup>40,86</sup>

A key property for understanding the interfacial properties of surfactants, in particular, the curvature of emulsions<sup>8,76,87-92</sup> is the C-W partition coefficient. The partition coefficient is strongly related to the reciprocal of the HCB of the surfactant and depends on the interactions between molecules of surfactant, CO<sub>2</sub> and water (analogous to the Winsor R ratio)

$$\frac{1}{HCB} = \frac{A_{TC} - A_{TT} - A_{CC}}{A_{HW} - A_{HH} - A_{WW}} \quad [3.1]$$

where A<sub>ij</sub> is the interaction potential between CO<sub>2</sub> (C), the hydrocarbon tail (T), water (W) and the surfactant head group (H).<sup>8</sup> The HCB can be manipulated by altering surfactant structure, temperature, pressure or salinity as depicted in Figure 3.1A. When 1/HCB < 1, the solvation of the surfactant head group in water is stronger than that of the tail in CO<sub>2</sub>, and the surfactant partitions into water over CO<sub>2</sub> with the interface curved around CO<sub>2</sub> to form a C/W macroemulsion (or foam).<sup>76,87</sup> When 1/HCB > 1, the surfactant partitions more towards CO<sub>2</sub> and the interface curves about water to form a W/C macroemulsion.<sup>89-92</sup> For an HCB very close to unity (balanced state), the IFT can become low enough for the formation of a W/C<sup>93,94</sup> or C/W<sup>29,57</sup> microemulsion. Here, macroemulsions tend to be unstable as it is easy to bend the interface and generate a hole for coalescence of the dispersed phase (Figure 3.1B). If the HCB is removed from unity in either direction by a modest amount, the adsorption of surfactant will be sufficient to provide stability against coalescence, as seen in this study even for the partition coefficients on the order of 10<sup>-2</sup>. The IFT must be sufficiently small such that the shear



energy input overcomes the capillary pressure to form new interface<sup>81</sup> In the case of porous media, the minimum pressure gradient to allow a foam to flow decreases with a decrease in IFT.<sup>34,35</sup>

To date, the effect of surfactants on the C-W IFT has been studied with nonionic, cationic and anionic/nonionic mixtures at low to moderate temperatures up to 60 °C.<sup>36,40,57</sup> However, above 100 °C, IFTs have been reported for C-W systems without surfactant<sup>95</sup> but not for systems containing equilibrated surfactant at the interface. At high temperature, foams are more susceptible to destabilization by various mechanisms, even if the surfactant is chemically stable. As the temperature increases, the foam lamellae often break if the surfactant aggregates too strongly or precipitates in the brine continuous phase.<sup>18</sup> Holes in the lamellae may be formed by thermal fluctuations leading to coalescence of the dispersed phase as depicted in Figure 3.1B.<sup>18,44,96</sup> Furthermore, the lamellae films will drain more rapidly as the viscosity of the brine decreases at higher temperatures, unless the surfactant maintains a sufficiently high interfacial viscosity.<sup>45</sup> Recently, a thermally stable<sup>97</sup> ethoxylated amine surfactant (C<sub>12-14</sub>N(EO)<sub>2</sub>) was shown to stabilize C/W foams with viscosities up to 6 cP at 120 °C in the presence of 182 g/L NaCl brine.<sup>40</sup> The surfactant was soluble in brine up to 22% TDS and in CO<sub>2</sub> up to 120 °C.<sup>40</sup> While this study introduced the concept of amine surfactants to stabilize C/W foams at high temperature, the significant emphasis on CO<sub>2</sub> enhanced oil recovery precluded a rigorous examination of important physicochemical and interfacial properties. For example, the degree of protonation of the ethoxylated amine surfactant was not investigated. At low temperature, the change in amidine surfactants from the nonionic to the cationic form upon lowering the solution pH has a large effect on the thermodynamic and interfacial properties.<sup>39</sup> Thus, understanding the effect of amine surfactant protonation on the IFT and the surfactant adsorption at the C/W interface remains an

important objective for understanding the formation and stability of high temperature C/W foams.

The objective for this paper is to demonstrate a thermally stable cationic surfactant, protonated  $C_{12-14}N(EO)_2$ , is soluble in brine below pH 5.5 at high temperatures up to 120 °C and stabilizes C/W foams. Furthermore, we demonstrate switchability of the surfactant between nonionic and cationic states, by measuring the degree of protonation versus pH as a function of temperature and salinity. In the protonated state, the C-W partition coefficient was determined quantitatively up to 90 °C and 3400 psia to provide a thermodynamic basis for the emulsion (foam) curvature. The high cloud point and thermal stability of this surfactant provided an opportunity to study the C-W IFT, CMC, and the surfactant adsorption at the C-W interface at very high temperatures up to 120 °C. To our knowledge, these types of measurements have not been reported previously for a surfactant at the C-W interface above 100 °C. The phase equilibria and interfacial properties are explained in terms of the interaction of the  $C_{12-14}N(EO)_2$  head and tail groups with the relevant phases.

The behavior of bulk C/W foam in a 660  $\mu\text{m}$  ID capillary tube is described in terms of temperature and foam quality (volume ratio of  $\text{CO}_2$  in total injected  $\text{CO}_2$  and water fluid). Important stabilization mechanisms for the brine lamellae in the foams are described including prevention of film drainage and hole formation. The foam properties are also investigated in porous media, which were used to generate the bulk foams. Remarkably, the surfactant in the nonionic state is soluble in  $\text{CO}_2$ , and consequently, the foams may be generated by injection the surfactant from either the  $\text{CO}_2$  or brine phase. The apparent viscosities in a 1.2 Darcy glass bead pack at a low superficial velocity are shown to be an order of magnitude larger than in higher permeability media both in this study and our earlier work at much higher superficial velocities as a consequence of shear

thinning effect<sup>40</sup>. In both the porous media and the downstream capillary, the foam formation, apparent viscosity, and stability mechanisms are described in terms of the surfactant protonation state, phase behavior, and the interfacial properties over a wide temperature range. Finally, C/W foams were also formed in the presence of crushed CaCO<sub>3</sub>. In the case of crushed CaCO<sub>3</sub>, excess divalent ions were required to lower the concentration of CO<sub>3</sub><sup>2-</sup> and HCO<sub>3</sub><sup>-</sup> and consequently the pH to ~4 according to the common ion effect, in order to protonate the surfactant.<sup>41</sup> The ability to measure interfacial properties for stable high temperature surfactants and to understand how they stabilize emulsions and foams is of broad interest in colloid science.

## **3.2 EXPERIMENTAL**

### **3.2.1 Materials**

Bis(2-hydroxyethyl) cocoalkylamine (C<sub>12-14</sub>N(EO)<sub>2</sub>) (Ethomeen C/12, 97% actives in water) and coco bis(2-hydroxyethyl)methyl ammonium chloride (C<sub>12-14</sub>N(EO)<sub>2</sub>CH<sub>3</sub>Cl) ammonium salt (Ethoquad C/12, 74-77% actives in 2-propanol) were gifts from Akzo Nobel and used without further purification. Carbon dioxide (Matheson, Coleman grade, 99.99%) was used as received. Sodium chloride (NaCl, certified ACS, Fisher), calcium chloride dehydrate (CaCl<sub>2</sub>·2H<sub>2</sub>O, 99+% Acros), magnesium chloride hexahydrate (MgCl<sub>2</sub>·6H<sub>2</sub>O, Fisher), hydrochloric acid (HCl, technical, Fisher) and isopropanol (certified ACS plus, Fisher) were used as received. Sodium chloride brine was composed of deionized (DI) water (Nanopure II, Barnstead, Dubuque, IA), and NaCl in which the concentration of NaCl from 30 g/L to 182 g/L. In addition, 22% TDS brine (182 g/L NaCl, 77 g/L CaCl<sub>2</sub>·2H<sub>2</sub>O, 26 g/L MgCl<sub>2</sub>·6H<sub>2</sub>O) was used as model reservoir

brine. In some experiments, the initial pH of surfactant water/brine solution/mixture was adjusted to 4 to 7 by adding HCl.

### 3.2.2 Cloud–point temperature and potentiometric titration

Cloud-point temperature measurement up to 120 °C was carried out with a sealed glass pipette method described in our previous publication.<sup>40</sup> The pH titration was carried out with a Mettler Toledo FG2 FiveGo pH meter with pH/ATC electrode as explained in Appendix B to determine the degree of protonation.

### 3.2.3 Interfacial tension measurement between CO<sub>2</sub> and aqueous surfactant solutions

The interfacial tension between CO<sub>2</sub> and aqueous surfactant solutions was determined from axisymmetric drop shape analysis of a captive bubble,<sup>56</sup> as described in detail previously.<sup>57</sup> In earlier studies, the maximum temperature was 60 °C, above which all of the surfactants precipitated. The temperature was raised slowly to avoid overshooting the temperature, particularly above 100 °C. For safety, the entire apparatus was surrounded by 3/8” polycarbonate. The molar surface density of the surfactant monolayer was obtained from the Gibbs adsorption equation below the CMC:

$$\Gamma = -\frac{1}{RT} \left( \frac{\partial \gamma}{\partial \ln C_{surf}} \right)_{T,P} \quad [3.2]$$

where  $C_{surf}$  is the surfactant concentration. The slope was treated as a straight line given the challenges of high temperature. The area occupied by each surfactant in the monolayer is given by  $A_m = 1/(N_A \Gamma)$  where  $N_A$  is Avogadro’s number. The efficiency of adsorption was defined as the negative logarithm of the concentration of surfactant in the bulk phase required to produce a 20 mN/m reduction in the interfacial tension:  $-\log C_{(-\Delta\gamma=20)} \equiv pC_{20}$ .<sup>60</sup>

### **3.2.3 Partition coefficient of surfactant between brine and CO<sub>2</sub>**

To determine the equilibrium partition coefficient, equal masses (~4 g for each) of CO<sub>2</sub> and brine plus 0.25% w/w surfactant solution, relative to the total weight, were loaded in the front part of a variable volume view cell following our earlier procedure.<sup>40,57,86</sup> The temperature of the system was controlled to within  $\pm 0.1$  °C by submerging the cell into a water bath equipped with a temperature controller (MP-BASIS, Julabo). After equilibration for two hours, samples of the upper CO<sub>2</sub> phase were extracted via a 6-port valve (Valco Instrument Co., Inc.) and a 50  $\mu$ L stainless steel loop (Valco Instrument Co., Inc.). The first 50  $\mu$ L were discarded and a sample was obtained by discharging three loads of the loop (150  $\mu$ L in total) into a vial with 0.5 mL pH3 HCl solution. The loop was flushed with a total of 1ml of pH 3 HCl solution followed with 5 mL of air (1 atm) to recover all of the surfactant and HCl solution. The sampling procedure was repeated three times to collect three separate samples. The concentration of surfactant in each sample was then determined by Epton's method<sup>58</sup> of two-phase titration with methylene blue solution (colorless endpoint) as described in recent publications.<sup>40,98</sup> The calculated 3-sample average and standard deviation of partition coefficient was reported.

### **3.2.4 C/W foam formation and apparent viscosity**

The apparatus for measurement of the foam apparent viscosity up to 120 °C and 3400 psia is depicted in Figure 3.2. The experimental procedure for calculating the apparent viscosity of C/W foam from the pressure drop, for both the porous media foam generator and downstream capillary tube were the same as described in our previous publication.<sup>40</sup> In this work, the first porous medium was a crushed calcium carbonate packed bed (22.9 cm long, 0.62 cm inner diameter tube) with a permeability to water of 76 Darcy (calculated from Darcy's law for 1-D horizontal flow) and 38% porosity (2.6

mL pore volume) determined by the mass of loaded material. The crushed calcium carbonate (Franklin Industrial Minerals) was 420-840  $\mu\text{m}$  in diameter (20-40 mesh) after washing with copious amounts of water and ethanol. The non-spherical calcium carbonate particles were held in place by a 100 mesh wire screen at each end of the pack. The second porous medium was a 1 Darcy (determined by the same method described above) glass bead pack (a 17.9 cm long, 1.73 cm inner diameter tube holding pre-washed 30-50  $\mu\text{m}$  in diameter spherical particles from Polysciences, Inc.). The bed was held in place by 100 mesh and 500 mesh wire screens in series at each end of the tube. The porosity was 36%, and the pore volume is 15.2 mL. The capillary tube for measuring bulk foam apparent viscosity was 660  $\mu\text{m}$  ID, 1.5 m in length, and made of hastelloy tubing. Additional details are given in the Appendix B.

### **3.2.5 PHREEQC simulation**

The composition of brines and pH at equilibria were calculated with an excess high pressure  $\text{CO}_2$  phase in the presence/absence of calcium carbonate in terms of the phase behavior and chemical equilibria with PHREEQC (Version 2.18). The calculation included the dissociation of  $\text{CaCO}_3$ ,  $\text{MgCO}_3$  and  $\text{CaMg}(\text{CO}_3)_2$ , acid-base reactions of divalent ions, and carbonic acid-bicarbonate-carbonate equilibria) along with phase equilibria of  $\text{CO}_2$  between the gas and liquid phases. Additional details are given in the Appendix B.

## **3.3 RESULTS AND DISCUSSION**

### **3.3.1 Cloud point temperatures and the degree of protonation**

The cloud point temperatures of 1% w/w  $\text{C}_{12-14}\text{N}(\text{EO})_2$  aqueous solution with pH values between 4 to 7 and salinities between 0 to 22% TDS are listed in Table 3.1. Cloud

point temperatures increase with a decrease of pH for all salinities tested. At lower pH the surfactant will be shown to be cationic and solvated more effectively by the brine. At a pH less than or equal to 5.5, the cloud points of the surfactant are higher than 120 °C, while at pH 7, the surfactant was not completely soluble, irrespective of salinity

### ***3.3.1.1 Effect of temperature on protonation state and solvation in aqueous phase.***

$C_{12-14}N(EO)_2$  becomes protonated in acidic aqueous solutions upon switching from the nonionic to cationic form as shown in the reaction below.



The degree of protonation of ethoxylated amine surfactants versus pH was calculated from pH titration curves as a function of temperature and salinity (Figure 3.3). For each curve, the surfactant is fully soluble at low pH in the protonated state. As the pH is increased, the surfactant solution becomes turbid indicating phase separation of the surfactant at a value shown by the red circle. The degree of protonation versus pH for 1% w/w  $C_{12-14}N(EO)_2$  in 22% TDS brine at 24, 50 and 90 °C is shown in Figure 3.3A. At a pH below 5.4, the surfactant was fully protonated at each temperature. At higher pH values, the degree of protonation decreased with an increase in temperature at a given pH, as indicated by a downward shift of the curves. For example, at pH 6.2, 98% of the surfactant was protonated at 24 °C, compared to only 65% at 90 °C. Exothermic protonation has been reported for alkyl and hydroxyalkyl substituted amines at lower temperatures.<sup>99-101</sup> The heat released may be attributed to the binding of the solvated surfactant amine head group with the hydronium ion, and formation of hydrogen bonds of structured water at the surface of the tails.<sup>101,102</sup>

### ***3.3.1.2 Effect of salinity on protonation state and solvation in aqueous phase***

The degree of protonation versus pH for 1% w/w  $C_{12-14}N(EO)_2$  at 90 °C in water, 120 g/L NaCl brine and 22% TDs brine is shown in Figure 3.3B. At a given pH, the degree of protonation increases with salinity as shown by the upward shift of the curves. For example, at pH 5.3, the degree of protonation of the surfactant was 71% in water and 100% in 22% TDS brine. At the surfactant concentration of 1% w/w, the majority of  $C_{12-14}N(EO)_2$  surfactant will be shown below in the interfacial tension section to be in the micellar state. The protonation of the amine head groups will be inhibited by the electrostatic repulsion between the resulting cations at the palisade micelle surface and the free hydronium ions in the bulk solution. This charging becomes more favorable with an increase in the  $Cl^-$  concentration as the double layer screens this electrostatic repulsion between the surfactant cations and hydronium ions. Thus, protonation of the surfactant is favored with an increase in salinity as observed. A similar mechanism has been provided to describe the effect of salinity on micelles composed of anionic surfactants.<sup>103</sup>

### ***3.3.1.3 Effect of pH on cloud point of $C_{12-14}N(EO)_2$ .***

The effect of pH on the cloud point temperature of  $C_{12-14}N(EO)_2$  depends upon the solvation of the partially or fully protonated nitrogen atom, the hydroxyethyl groups and the hydrocarbon tail. At a pH equal to or below 5.5, the surfactant is highly protonated (above 97% for 24 to 90 °C as shown in Figure 3.3A). The solvation of the cation increases with an increase of temperature, because the solubility of salts depends on dissociation of their cations and anions in water. The dissociation follows Boltzmann distribution which is more favorable at higher temperature and thus leads a higher solubility of ions.<sup>104</sup> Furthermore, the solvation of the hydroxyethyl groups decreases with an increase of temperature, due to weakening of hydrogen bonding.<sup>18,81</sup> For the hydrocarbon tail, the solvation in water increases with temperature, as the structure of



water about the hydrophobic tails is more disordered at higher temperatures.<sup>102,52,55</sup> For the sum of the head and tail groups, the increase in solvation for both protonated nitrogen atom and hydrocarbon tail with temperature is stronger than the reduction in solvation of EO groups, and thus protonated  $C_{12-14}N(EO)_2$  remains soluble at high temperatures, which gives a cloud point over 120 °C at low pH. At a pH above 7, only about 27% of the surfactant is protonated at 90 °C in 22% TDS brine. Here, the small amount of protonated  $C_{12-14}N(EO)_2$  is not enough to solubilize the unprotonated  $C_{12-14}N(EO)_2$  at any temperature (Table 3.1).

### **3.3.2 Solubility in CO<sub>2</sub> and CO<sub>2</sub>-brine partition coefficients of $C_{12-14}N(EO)_2$**

#### ***3.3.2.1 Solubility in CO<sub>2</sub>***

It is instructive to examine the solubility of  $C_{12-14}N(EO)_2$  in CO<sub>2</sub> before describing CO<sub>2</sub>-brine partition coefficients. The surfactant,  $C_{12-14}N(EO)_2$  was reported recently to be soluble in CO<sub>2</sub> at 0.2% w/w up to 120 °C with a cloud point pressure (lowest pressure required to solvate a surfactant in CO<sub>2</sub> at a temperature) below 3400 psia.<sup>40</sup> With an increase in temperature, the cloud point pressure for dissolution of the surfactant increased in order to maintain a sufficient CO<sub>2</sub> density. In dry CO<sub>2</sub>,  $C_{12-14}N(EO)_2$  is unprotonated and thus nonionic, which favors CO<sub>2</sub> solvation. For ionic hydrocarbon surfactants, the weak solvation by CO<sub>2</sub>, as a consequence of its low polarizability/volume is usually insufficient to overcome the lattice energy of ionic surfactant salts.<sup>105</sup> Also, the presence of only two hydroxyethyl groups results in less surfactant intramolecular hydrogen-bonding<sup>63</sup> which favors solvation, as seen for CO<sub>2</sub>-soluble alkyl EO/PO surfactants.<sup>63</sup> Furthermore, the decrease of cloud point density with increasing temperature indicates that thermal energy overcomes surfactant tail-tail interaction and

weakens intramolecular hydrogen-bonding, and thus improves the solvation of  $C_{12-14}N(EO)_2$ .<sup>40,63</sup>

### 3.3.2.2 $CO_2$ -brine partition coefficients

The partition coefficients of 0.25 % w/w  $C_{12-14}N(EO)_2$  between  $CO_2$  and 182 g/L NaCl or 22% TDS brine at 24-90 °C and 1000 or 3400 psia are listed in Table 3.2. At 3400 psia, a low C-W partition coefficient ( $\sim 0.03$ ) was found at all temperatures and salinities with  $CO_2$  densities between 0.61 to 0.94 g/mL. In the presence of high pressure  $CO_2$ , the pH of  $CO_2$  saturated aqueous phase is  $\sim 3$ .<sup>106</sup> Here,  $C_{12-14}N(EO)_2$  is highly protonated as demonstrated by the protonation state curves shown in Figure 3.3. The cationic head in water is solvated by ion-dipole interactions (high  $A_{HW}$ ).<sup>107</sup> The solvation of the straight chain hydrocarbon tail in  $CO_2$  is relatively weak due to the weak van der Waals attraction between  $CO_2$  and the surfactant tail (low  $A_{TC}$ ). The much smaller numerator in Equation 1 relative to the denominator (high HCB) leads to a low C-W partition coefficient. This HCB value will be shown to favor curving of the C-W interface about  $CO_2$  for formation of a C/W macroemulsion.<sup>76,87</sup> In addition, there is an interesting compensation of the solvation of the various parts of the surfactant molecule at 3400 psia. As temperature increases, the solvation of the protonated nitrogen increases, while that of the hydroxyethyl groups decreases. The increase in thermal energy increases tail solvation by overcoming tail-tail interactions, but the lower density of  $CO_2$  also leads to a reduction in the solvent strength of  $CO_2$ .<sup>8</sup> The data indicate that these factors appear to compensate for each other such that the partition coefficient is approximately constant.

The C-W partition coefficient decreased with decrease of pressure at constant temperature as expected. At 90 °C, it decreased from 0.028 at 3400 psia to below 0.004

(detection limit) at 1000 psia. The pressure change from 3400 psia to 1000 psia should not significantly affect solvation of either the protonated nitrogen atom or hydroxyethyl groups. However, a decrease of pressure from 3400 psia to 1000 psia at 90 °C, leads to a decrease of CO<sub>2</sub> density from 0.61 to 0.12 g/mL. The reduction in the solvent strength of CO<sub>2</sub> causes a significant decrease of C-W partition coefficient for C<sub>12-14</sub>N(EO)<sub>2</sub>. Furthermore, has been demonstrated that 0.2% w/w C<sub>12-14</sub>N(EO)<sub>2</sub> is not completely soluble in dry CO<sub>2</sub> at 1000 psia and 90 °C.<sup>40</sup>

### **3.3.3 Interfacial properties at CO<sub>2</sub>-22% TDS brine interface up to 120 °C**

#### ***3.3.3.1 Interfacial tension at C-W interface***

The interfacial tension between CO<sub>2</sub> and 22% TDS brine was measured at 3400 psia and 24-120 °C in the presence of C<sub>12-14</sub>N(EO)<sub>2</sub> with concentrations from 10<sup>-7.4</sup> to 10<sup>-1.4</sup> M (10<sup>-5</sup> to 1 % w/w) as shown in Figure 3.4. To our knowledge, due to the lack of soluble and stable surfactants in water in previous studies,<sup>36,57</sup> this is the first time that the interfacial properties of a surfactant in C-W system has been reported at temperatures above 100 °C. Without surfactant, the IFT ranges from 33 to 44 mN/m from 2500-3900 psia between 25 and 125 °C.<sup>95</sup> Upon adding C<sub>12-14</sub>N(EO)<sub>2</sub> with a surfactant concentration above the CMC, the IFT was reduced to 3-5 mN/m at 3400 psia. In the presence of high pressure CO<sub>2</sub>, the low pH (~3) condition in the brine phase ensured the surfactant was in its cationic form, and thus was sufficiently well solvated even at 120 °C to remain soluble for IFT measurement. Remarkably, the IFT at surfactant concentrations above the CMC remained quite low at less than 6 mN/m even up to 120 °C, indicating significant solvation of the tails by CO<sub>2</sub> is still present despite the low CO<sub>2</sub> density of only 0.48 g/mL. When temperature was increased at constant P, the increased IFT may be attributed to an increase in the HCB; the surfactant cationic head group is solvated more effectively

in water,<sup>104</sup> and the tail is less solvated by CO<sub>2</sub> due to a decrease of CO<sub>2</sub> density. Both of these factors drive the surfactant away from a more balanced state at the interface towards water, which increases the IFT as depicted in Figure 3.1A.

### ***3.3.3.2 Critical micelle concentration***

A discontinuity in the slope of IFT versus log surfactant concentration is evident in Figure 3.4 indicating the CMC. The CMC increases about an order of magnitude with an increase in temperature, indicating the surfactant monomer is favored. When temperature increases, the solvation of protonated nitrogen atom and hydrocarbon tail is improved in brine, which disfavors micellization<sup>108</sup> as observed. However, the dissociation of the micelles is moderated somewhat by the reduction in the solvation of two hydroxyethyl groups.<sup>108</sup> For similar reasons, the CMC of ionic C<sub>10</sub> and C<sub>14</sub> alkyl sulfates increases with increasing temperature from 25-70 °C.<sup>109</sup>

### ***3.3.3.3 Adsorption at the C-W interface and efficiency in lowering the interfacial tension (pC20)***

The adsorption of C<sub>12-14</sub>N(EO)<sub>2</sub> was determined from the slope of the plot of the IFT versus the log of surfactant concentration. At low or moderate temperatures, the adsorption at the CO<sub>2</sub>-22% TDS brine interface, which corresponded to an area per molecule of ~160 Å<sup>2</sup>, was higher than the value of 200-350 Å<sup>2</sup> for alkyl EO/PO nonionic surfactants at the C-W interface.<sup>36</sup> Generally, ionic surfactants tend to have a lower specific adsorption (higher area per molecule) than nonionic surfactants due to electrostatic repulsion between surfactant head groups.<sup>60</sup> However, the high ionic strength in the aqueous phase screened the repulsion which would contribute to the high surfactant adsorption at the interface. Furthermore, the head group for C<sub>12-14</sub>N(EO)<sub>2</sub> contains a single nitrogen atom and two hydroxyethyl groups, which is much smaller than the head

groups of previously studied nonionic alkyl EO/PO surfactants (for example, with 9 or more EO units<sup>36,57</sup>) and thus occupies a smaller area.

When temperature was increased, the specific adsorption of  $C_{12-14}N(EO)_2$  at the  $CO_2$ -brine interface decreased slightly from  $1.05 \times 10^{-6}$  mol/m<sup>2</sup> at 24 °C to  $0.80 \times 10^{-6}$  mol/m<sup>2</sup> at 120 °C, as shown in Table 3.3. The  $\gamma_0$  for the binary C-W system increases with an increase in temperature at constant pressure, as the  $CO_2$  density decreases. A higher IFT alone would provide a greater driving force for surfactant adsorption at the interface.<sup>33</sup> However, this contribution was overshadowed by the reduction of  $CO_2$  density and consequently, the weaker tail solvation in  $CO_2$  compared to the strong head solvation which drove the surfactant towards water. Therefore, the specific adsorption at the interface decreased. In addition, the increased thermal motion also increases the area per surfactant molecule.<sup>60</sup>

The pC20 for  $C_{12-14}N(EO)_2$ , defined as the negative logarithm of the concentration of surfactant in the bulk phase required to produce a 20 mM/m reduction in interfacial tension, decreased a small amount from 24 to 120 °C as shown in Table 3.3. When the temperature increases, the contribution from the larger driving force resulting from the larger  $\gamma_0$  increases<sup>95</sup> would drive the surfactant to move towards the C-W interface to raise pC20<sup>110</sup>. However, this enhancement in driving force for adsorption is overcome by the higher tendency of the surfactant to move towards water as explained above. At 24 °C, the pC20 for  $C_{12-14}N(EO)_2$  for  $CO_2$ -22% TDS brine system is ~8 which is higher than the calculated value of ~5 reported previously for the nonionic surfactant LA-EO<sub>12</sub> ( $C_{12}(EO)_{12}$ ),<sup>36</sup> which has a similar tail length ( $C_{12}$ ). The lower pC20 for LA-EO<sub>12</sub> may indicate an HCB value further from unity, given the relatively large EO number of 12 in LA-EO<sub>12</sub>. The pC20 is expected to increase with increase of alkyl length due to negative free energy of adsorption of a methylene group at the interface.<sup>60</sup> However, if the tails

become too long, they are not solvated sufficiently well by CO<sub>2</sub> and pC20 is expected to decrease.<sup>8</sup> A high pC20 in the presence of concentrated brine indicates C<sub>12-14</sub>N(EO)<sub>2</sub> had the proper tail length to efficiently lower the IFT of C-W system and thus has the potential to be effective for stabilizing C/W emulsions and foams, even at high salinity.

### 3.3.4 Bulk foam apparent viscosity in capillary

To understand the properties of bulk foam, it is first instructive to examine the effect of pH on the protonation state of C<sub>12-14</sub>N(EO)<sub>2</sub>. The pH of 22% TDS brine solution saturated with CaCO<sub>3</sub> and CO<sub>2</sub> at 3400 psia and 120 °C was calculated from the relevant chemical reaction equilibria equations with the software PHREEQC and found to be 3.8 (Figure B1). Here C<sub>12-14</sub>N(EO)<sub>2</sub> is cationic and thus has high a cloud point temperature in brine. The high solubility in brine is important for the surfactant to remain water-soluble in the lamellae films of foams, and to produce a low C-W partition coefficient for the preferred C/W emulsion curvature according to the Bancroft rule. The Bancroft rule states that the phase favored by the surfactant will be the continuous phase, to maximize Marangoni stabilization of the draining lamellae<sup>80</sup> between the CO<sub>2</sub> dispersed bubbles. Also the surfactant lowers the C-W interfacial tension to ~5 mN/m (Figure 3.4), which reduces the capillary pressure and then lowers the tendency for bubble coalescence upon film drainage. Therefore, protonated C<sub>12-14</sub>N(EO)<sub>2</sub> offers the desired phase behavior and interfacial properties for stabilizing lamellae in a C/W foam at high temperature and salinity. To our knowledge previous cationic surfactants have not met all of these requirements at such high temperatures.

To generate a bulk C/W foam stabilized with C<sub>12-14</sub>N(EO)<sub>2</sub>, 1% w/w C<sub>12-14</sub>N(EO)<sub>2</sub> in 22% TDS brine solution at pH 6 (adjusted by adding HCl initially) was injected simultaneously with pure CO<sub>2</sub> into a 76 Darcy calcium carbonate packed bed. The bulk

foam apparent viscosity was measured in a 660  $\mu\text{m}$  ID capillary tube downstream of the calcium carbonate foam generator. The effects of temperature and foam quality on bulk foam apparent viscosity ( $\mu_{\text{foam}}$ ) are shown in Figure 3.5. With an increase of temperature,  $\mu_{\text{foam}}$  decreased from 23.6 cP at 24 °C to 5.7 cP at 120 °C at 90% foam quality, 3400 psia, and a total velocity 29 cm/s in the capillary (Figure 3.5A). At 120 °C, as the foam quality increased from 70 to 90%,  $\mu_{\text{foam}}$  increased from 2.4 cP to 5.7 cP. When the foam quality further increased,  $\mu_{\text{foam}}$  decreased to 1.6 cP at 92% foam quality, and eventually no foam was produced at 95% foam quality (Figure 3.5B). The highest foam apparent viscosity in the capillary achieved at 90% foam quality was more than 50 times of the apparent viscosity of the CO<sub>2</sub>-22% TDS brine mixture without the surfactant at the same condition (Figure B2).

The temperature affects the apparent foam viscosity in various ways. A decrease of  $\mu_e$  with temperature directly contributes to the decrease of bulk foam apparent viscosity as shown in Equation 2. This viscosity reduction in the continuous phase will also lead to more rapid film drainage as shown in Equation 3. In addition,  $\gamma$  increased with temperature (Figure 3.4), which raises  $P_c$  and thus raises  $\Delta P_{\text{film}}$  to accelerate film drainage for a given bubble size. As the aqueous lamellae become thinner, the reduction in work required to create a hole increases the probability of hole formation and thus coalescence (Equation 4).<sup>44</sup> Furthermore, the probability of hole formation is also increased by greater thermal energy fluctuations at higher temperature.<sup>44,96</sup> Thus, the decrease in  $\mu_e$  and the increase in bubble radius  $R$  due to coalescence both contribute to lower  $\mu_{\text{foam}}$  as observed in Figure 3.5A.

With an increase of foam quality from 70% to 90%, the bulk foam apparent viscosity increases as depicted in Equation 2. Above a quality of 74%, the CO<sub>2</sub> bubbles are distorted in the form of polyhedra separated by thin lamellae films.<sup>111</sup> As the lamellae

become too thin (e.g. above 90 % foam quality shown in Figure 3.5B), the low activation energy for hole formation (Equation 4) may lead to the rupture of lamellae.<sup>44</sup> The resulting increase in average bubble size (increased R) causes  $\mu_{\text{foam}}$  to decrease (Equation 2).

### 3.3.5 C/W foam formation and apparent viscosity in glass bead pack

The nature of the foam flow in porous media is more complex than for the bulk foam in the capillary tube, given the complex geometry and interactions with the pore surfaces.<sup>5</sup> For bulk foam at a high shear rate in a single capillary, the bubble radius has been found to be smaller than the capillary radius.<sup>18</sup> However, in porous media where the radius is often similar to the pore size, it is found that single aqueous lamellae separate CO<sub>2</sub> bubbles.<sup>5,42</sup>

To study the foam behavior in porous media, 1% w/w C<sub>12-14</sub>N(EO)<sub>2</sub> in a 182 g/l NaCl solution at pH 4 (adjusted by HCl) was co-injected with CO<sub>2</sub> at a total superficial velocity from 6 to 181 ft/day. The permeability of the glass bead pack (30 to 50  $\mu\text{m}$  diameter beads) was 1.2 Darcy as measured with water. As shown in Figure 3.6A, at 40% foam quality, the apparent viscosity at a low superficial velocity of 6 ft/day was low, below 3.5 cP. As the velocity increased to 10 ft/day, there was a marked increase in apparent viscosity to ~150 cP, which indicates generation of a strong C/W foam. Here, the pressure gradient exceeded the minimum pressure gradient (MPG) need to mobilize the lamellae<sup>112</sup> to generate foam by snap-off and lamellae division.<sup>5</sup> For simultaneous injection of CO<sub>2</sub> and the aqueous phase, upon slowly increasing the total superficial velocity, the MPG for foam generation was found to be 2.7 psi/ft (Figure B3) for 40% foam quality. This results are consistent with an earlier study<sup>112</sup> as discussed in Appendix



B. For 80% foam quality, the behavior was similar but the apparent viscosity curve was shifted to higher velocities.

For both 40% and 80% foam qualities, viscous C/W foams with apparent viscosities above 130 cP were achieved at superficial velocities of 10-20 ft/day. These apparent viscosities in the 1.2 Darcy glass bead pack are an order of magnitude higher than for the same surfactant previously reported<sup>40</sup> in a 30 Darcy sand pack at the same conditions except at a much higher total superficial velocity of 300-600 ft/day (Figure 3.6A). The much lower viscosities at higher superficial velocities indicate a large degree of shear thinning. The shear thinning behavior may be attributed to the contributions to the apparent viscosity from bubble deformation and the interfacial tension gradient as the bubbles flow through the channel of the porous media as explained from a model developed by Hirasaki and Lawson for smooth capillaries.<sup>42</sup> Here, both viscosity contributions are proportional to  $-1/3$  power of the gas phase velocity and thus give a shear-thinning relationship between the apparent viscosity and the superficial velocity. More details on the capillaries model and shear thinning behavior are in Appendix A.

### **3.3.6 C/W foam formation and apparent viscosity in calcium carbonate packed bed**

#### ***3.3.6.1 Effect of divalent ions on pH and foam apparent viscosity***

When an aqueous solution encounters  $\text{CaCO}_3$ , the pH of the solution will increase from the dissociation of  $\text{CaCO}_3$  according to the solubility product and acid-base reactions as shown in Reactions (B2), and (B5-B7).<sup>41</sup> If the solution contains  $\text{C}_{12-14}\text{N}(\text{EO})_2$  and  $\text{CaCO}_3$  increases the pH above  $\sim 6$ , the deprotonation of  $\text{C}_{12-14}\text{N}(\text{EO})_2$  will decrease the hydrophilicity which lowers the solubility of the surfactant in brine, as demonstrated in Figure 3. Furthermore, an increase in pH may increase the C-W IFT as shown in tertiary amine surfactant reported by Smith et al.<sup>25</sup> For this tertiary amine

surfactant, nitrilotripropane-1,2-diyltripivalate, as the pH increased from 3.3 to 6.7, the interfacial tension at C-W interface increased from 2.6 mN/m to ~6 mN/m at 25°C, 5000 psia, as the HCB of the amine became too low to be optimal for strong adsorption at the interface in the unprotonated state.<sup>25</sup> However, by adding divalent ions such as  $\text{Ca}^{2+}$  or  $\text{Mg}^{2+}$ , the dissolution of  $\text{CaCO}_3$  is suppressed by the common ion effect,<sup>41</sup> which is beneficial for lowering pH to maintain amines such as  $\text{C}_{12-14}\text{N}(\text{EO})_2$  in the cationic form to favor adsorption at the interface.

The effect of concentration of  $\text{Ca}^{2+}$  in the feed brine on the simulated concentration of various species in brine in the presence of excess solid  $\text{CaCO}_3$  and high pressure  $\text{CO}_2$  at equilibrium at 120 °C and 3400 psia is shown in Figure 3.7. With an increase of initial concentration of  $\text{Ca}^{2+}$  from 0 to 1 mol/L, the concentration of both  $\text{CO}_3^{2-}$  and  $\text{HCO}_3^-$  decreased by about one order of magnitude, and the equilibrium pH decreased by 0.8. The common ion  $\text{Ca}^{2+}$  depressed the dissolution of excess solid  $\text{CaCO}_3$ , and therefore decreased the pH.<sup>41</sup> A similar reduction of pH was observed by increasing the concentration of  $\text{Mg}^{2+}$  in the feed brine solution (Figure B4). For the model brine (22% TDS) in this paper which contained 0.52 mol/L  $\text{CaCl}_2$  and 0.13 mol/L  $\text{MgCl}_2$ , the simulated pH was 3.8 when saturated with excess  $\text{CaCO}_3$  and  $\text{CO}_2$  at 120 °C, 3400 psia (Figure B1). This low pH condition is beneficial for maintaining  $\text{C}_{12-14}\text{N}(\text{EO})_2$  in the protonated state for stabilizing C/W foams.

To examine effect of divalent ions on the apparent viscosity of foam stabilized with  $\text{C}_{12-14}\text{N}(\text{EO})_2$  at 120 °C and 3400 psia in a crushed calcium carbonate packed bed, the foam apparent viscosity is compared for two brines, 22% TDS (182 g/L NaCl with 77 g/L  $\text{CaCl}_2 \cdot 2\text{H}_2\text{O}$ , 26 g/L  $\text{MgCl}_2 \cdot 6\text{H}_2\text{O}$ , where foam apparent viscosity results are shown in Figure 3.6B ) versus 182 g/L NaCl (where the foam apparent viscosity result shown in Table B1). In each case, the pH of the brine was adjusted to 6 by HCl initially. At 90%

foam quality, the apparent viscosity of the foam was 14.5 cP with an effluent pH of 4.5-5.2, when the divalent ions presented, while it was only 7.9 cP with an effluent pH of 5.7 for the 182 g/L NaCl. Previously, the apparent viscosity of ethoxylated amine in a sand pack almost always decreased as the NaCl concentration increased.<sup>40</sup> This decrease was attributed to the “salting out” effect,<sup>71</sup> which lowered the solubility of surfactant in the foam lamellae. However, when  $\text{Ca}^{2+}$  and  $\text{Mg}^{2+}$  were added into the aqueous phase, they reduced the aqueous phase pH as expected from the common ion effect according to the simulations. By lowering pH with adding divalent ions,  $\text{C}_{12-14}\text{N}(\text{EO})_2$  was maintained in the cationic state in the lamellae without precipitating, which enhanced the stability of the C/W foam in the presence of excess solid  $\text{CaCO}_3$ .

#### ***3.3.6.2 Effect of foam quality on apparent viscosity***

The effect of foam quality on apparent viscosity of C/W foam stabilized with  $\text{C}_{12-14}\text{N}(\text{EO})_2$  or the analogous quaternary ammonium salt  $\text{C}_{12-14}\text{N}(\text{EO})_2\text{CH}_3\text{Cl}$  in a 76 Darcy calcium carbonate packed bed with a total superficial velocity of 938 ft/day is shown in Figure 3.6B. For  $\text{C}_{12-14}\text{N}(\text{EO})_2$ , foam was generated either by co-injection of 1% w/w surfactant at pH6 (adjusted by HCl) in a 22% TDS brine solution and  $\text{CO}_2$ , or by co-injection of a 0.2 % w/w surfactant -  $\text{CO}_2$  solution with a 22% TDS brine solution without pH adjustment. When  $\text{C}_{12-14}\text{N}(\text{EO})_2$  was injected from the brine phase, as the quality increased from 70% v/v, the apparent foam viscosity increased gradually until it reached a maximum of 14 cP at 90% and then decreased. At 95% foam quality, no foam formed. As quality increases, the size of the pores invaded by the gas phase continually decreases (and so does the water saturation) in the calcium carbonate packed bed, increasing the capillary pressure. Eventually, the van der Waals attraction between

CO<sub>2</sub> bubbles exceeds the electrostatic repulsion from the surfactant head groups and the lamellae become unstable.<sup>43,113</sup>

When C<sub>12-14</sub>N(EO)<sub>2</sub> was injected from the CO<sub>2</sub> phase, the behavior was very similar up to a quality of 90%. At this quality, the experiments were designed such that the concentration of C<sub>12-14</sub>N(EO)<sub>2</sub> in the foam (aqueous phase + CO<sub>2</sub> phase) was the same, ~ 0.16% w/w. The equivalence of foam apparent viscosity indicates that the surfactant underwent effective transport to the interface from either the brine or CO<sub>2</sub> phase, indicating good contact between phases. At 95% foam quality, the concentration of C<sub>12-14</sub>N(EO)<sub>2</sub> in the total injected fluid was 0.18% when C<sub>12-14</sub>N(EO)<sub>2</sub> was injected from the CO<sub>2</sub> phase. Here the foam apparent viscosity was the highest. In contrast, for the case of surfactant injected from the brine phase, the concentration of C<sub>12-14</sub>N(EO)<sub>2</sub> in the total injected fluid was only 0.10%. This low concentration was found to provide insufficient disjoining pressure against the higher capillary pressure at a higher foam quality of 95% resulting in destabilization of the C/W foam<sup>113</sup>.

For the two foam qualities studied, the apparent viscosity was similar for the quaternary ammonium C<sub>12-14</sub>N(EO)<sub>2</sub>CH<sub>3</sub>Cl surfactant with the same tail length, where all other conditions were held constant as depicted in Figure 3.6B. Thus, C<sub>12-14</sub>N(EO)<sub>2</sub> appeared to behave as a cationic surfactant, consistent with the expected protonation at these conditions. The disadvantage of the quaternary amine is that it undergoes Hoffman dealkylation at the high temperatures over time. At short times however, it serves as a useful model for the protonated C<sub>12-14</sub>N(EO)<sub>2</sub>.

### ***3.3.6.3 Effect of temperature***

The effect of temperature on the apparent viscosity of C/W foam stabilized with 1% w/w C<sub>12-14</sub>N(EO)<sub>2</sub> in 22% TDS brine solution at pH 6 (adjusted by HCl) in the 76 Darcy

calcium carbonate packed bed at foam quality 90% and total superficial velocity 938 ft/day from 24 to 120 °C is shown in Figure 3.6C. With an increase of temperature, the apparent viscosity decreased from 36 cP at 24 °C to 14 cP at 120 °C. The decrease in apparent viscosity can be explained in a similar manor as the decrease in bulk foam apparent viscosity observed as temperature was increased (Figure 3.5A). With increasing temperature, the viscosity of aqueous phase decreased, which is expected to decrease foam apparent viscosity in porous media (Equation A26).<sup>40</sup> Also, high temperature leads to faster film drainage,<sup>18,45</sup> and a greater tendency to go over the activation energy barrier for hole formation in the lamellae,<sup>44,96</sup> which reduces the number of lamellae per unit length and thus reduces the apparent viscosity of the C/W foam.<sup>42</sup>

### 3.4 CONCLUSIONS

A thermally stable cationic surfactant  $C_{12-14}N(EO)_2$  in the protonated state was demonstrated to be soluble in water at pH values  $< 5.5$  with up to 22% TDS brine at 120 °C. An enhancement in solvation with temperature in brine for both the protonated amine head group and hydrocarbon tail is stronger than the loss in solvation of the hydroxyethyl groups. The  $CO_2$ -brine partition coefficient was  $\sim 0.03$  from 24 to 90 °C at 3400 psia indicated a relatively high HCB. However, the small but measurable amount of surfactant in the  $CO_2$  phase was consistent with the solubility of the surfactant in  $CO_2$  (without brine present) in the nonionic form.<sup>40</sup> Moreover, the strong solvation in brine (high cloud point) and simultaneous affinity for  $CO_2$  (solubility in pure  $CO_2$ ) provided an appropriate HCB for significant adsorption of the surfactant at the C-W interface, with an area of 207 Å<sup>2</sup>/molecule even at 120 °C. The  $CO_2$ -brine interfacial tension decreased from  $\sim 40$  to  $\sim 5$  mN/m at surfactant concentrations above the CMC, which was only 0.038 mmol/L

(0.00094 % w/w). Given the high HCB, the preferred curvature corresponded to a C/W macroemulsion (foam) according to the Bancroft rule. The decrease in apparent viscosities when temperature increased may be attributed to faster film drainage and larger thermal fluctuations that enhance hole formation in the lamellae. Despite these changes, the apparent viscosity of 5.7 cP at 120 °C was more than 50 times of the apparent viscosity of CO<sub>2</sub>-brine mixture without surfactant at the same conditions.

In addition to bulk foams, the surfactant also stabilized foams in porous glass bead packs and crushed calcium carbonate media. With only 1 % w/w C<sub>12-14</sub>N(EO)<sub>2</sub> in brine, C/W foams with qualities of 40% and 80% were formed at a superficial velocity between 10 to 20 ft/day with an apparent viscosity up to 146 cP at low superficial velocities, an order of magnitude larger than than in our previous study<sup>40</sup> at higher superficial velocities. Above the minimum pressure gradient required for foam formation, shear-thinning was observed in the low permeability glass bead pack. For calcium carbonate media, it was necessary to suppress the dissolution of CaCO<sub>3</sub> by adding Ca<sup>2+</sup> and Mg<sup>2+</sup> in the aqueous phase (via the common ion effect) in order to maintain a low enough pH to protonate the surfactant and stabilize a foam. The fundamental phase behavior, interfacial properties, and foam behavior in this study at high temperatures and salinities offer many interesting opportunities for potential applications including CO<sub>2</sub> enhanced oil recovery and sequestration.

Table 3.1: Cloud point temperatures of 1% w/w C<sub>12-14</sub>N(EO)<sub>2</sub> aqueous solution with different salinity and pH (adjusted with HCl)

pH	Salinity			
	0	120 g/L NaCl	182 g/L NaCl	22% TDS
4	>120	>120	>120	>120
5.5	-	>120	-	>120
6	90	110	-	110
6.5	-	100	-	80
7.0	Insoluble	Insoluble	Insoluble	Insoluble

Table 3.2: Partition coefficients of C<sub>12-14</sub>N(EO)<sub>2</sub> (weight fraction in CO<sub>2</sub>/weight fraction in brine) between CO<sub>2</sub> and brine with gentle stirring at 25-90 °C, 1000 or 3400 psia. (CO<sub>2</sub> and brine were equal in mass. 0.25 % w/w surfactant in total mass of CO<sub>2</sub> and brine)

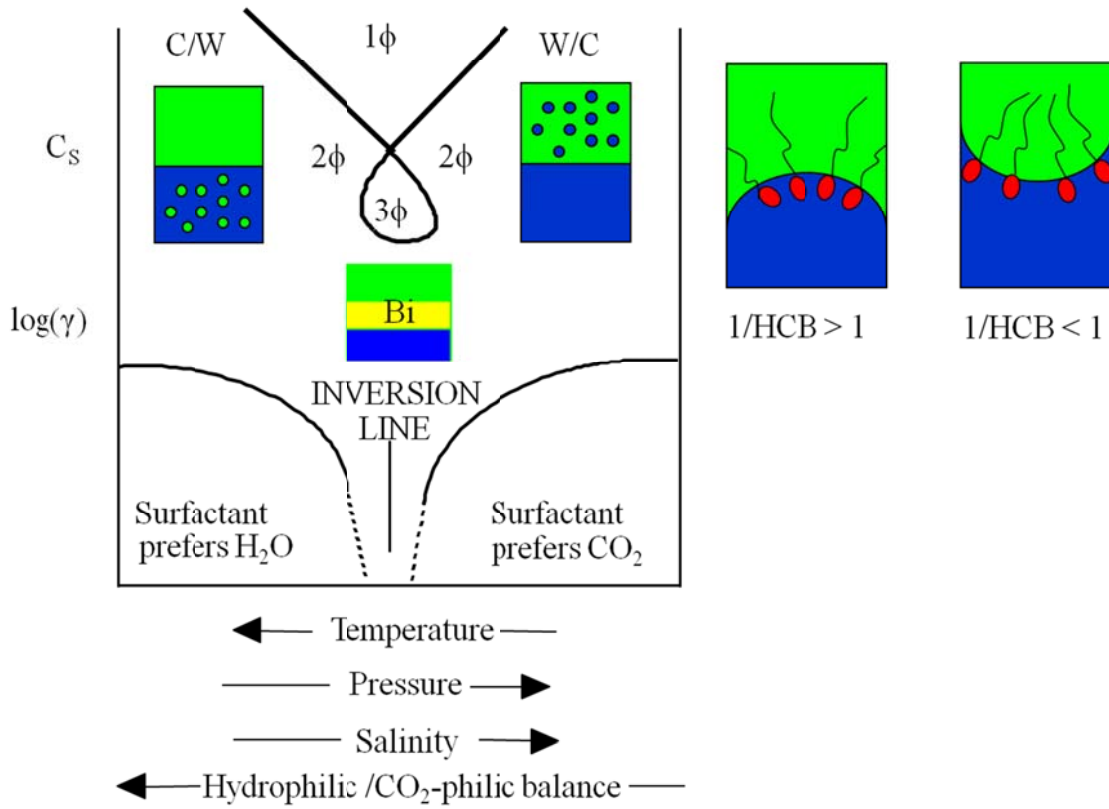
Salinity	Temperature(°C)	Pressure(Psia)	Density of CO <sub>2</sub> (g/mL)	Average partition coefficient
182 g/L NaCl	24	3400	0.94	0.030 ± 0
	60	3400	0.77	0.030 ± 0.001
	90	3400	0.61	0.032 ± 0.001
22% TDS	24	3400	0.94	0.026 ± 0.004
	90	3400	0.61	0.028 ± 0.002
	90	1000	0.12	<0.004

Table 3.3: The interfacial properties of  $C_{12-14}N(EO)_2$  at the  $CO_2$ -22% TDS brine interface at 3400 psia

T (°C)	$\rho(CO_2)$ (g/mL)	CMC (% w/w)	CMC (mmol/L)	$IFT_{cmc}$ (mN/m)	$\pi_{cmc}$ (mN/m)	$\Gamma \cdot 10^6$ (mol/m <sup>2</sup> )	$A_m$ (Å <sup>2</sup> /molecule)	pC20
24	0.94	0.00016	0.007	2.9	34-37	1.05	158	7.6-8.1
90	0.61	0.00053	0.022	3.7	-	0.90	184	-
120	0.48	0.00094	0.038	5.1	35-39	0.80	207	6.9-7.6



A



B

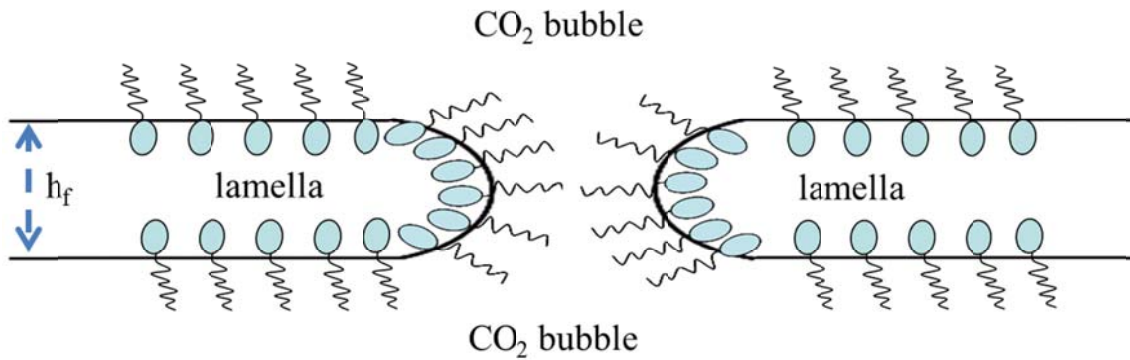


Figure 3.1: (A) Effect of formulation variables on the phase behavior and interfacial tension of CO<sub>2</sub>-water-ionic surfactant system; (B) Formation of a hole in a water lamella for a C/W foam

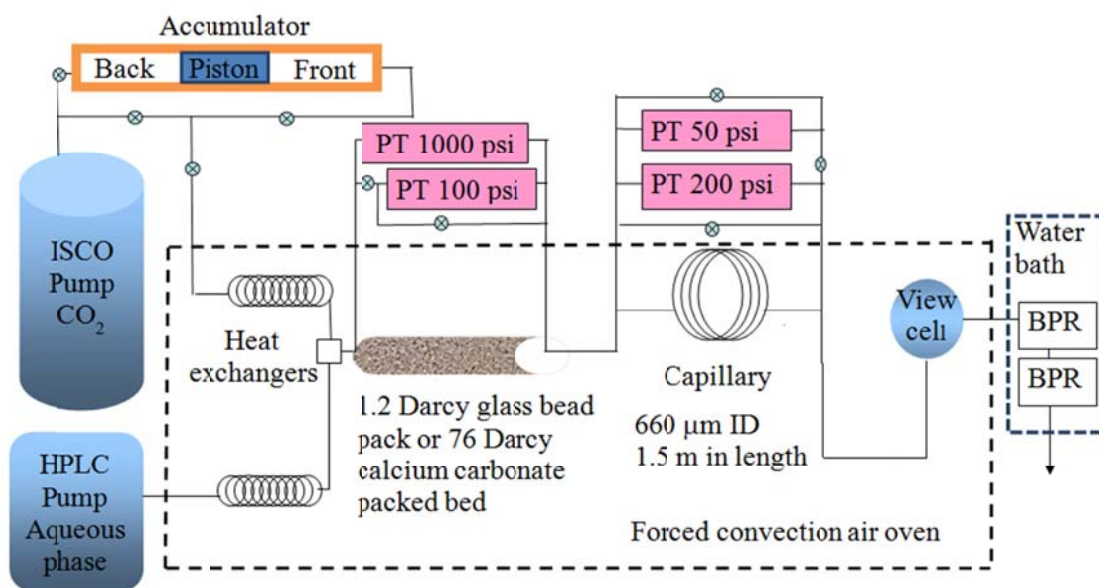


Figure 3.2: Apparatus for CO<sub>2</sub>-water foam viscosity measurements in porous media and in a capillary tube. BPR: back pressure regulator. PT: pressure transducer. A glass bead pack or crushed calcium carbonate packed bed is used as the foam generator.

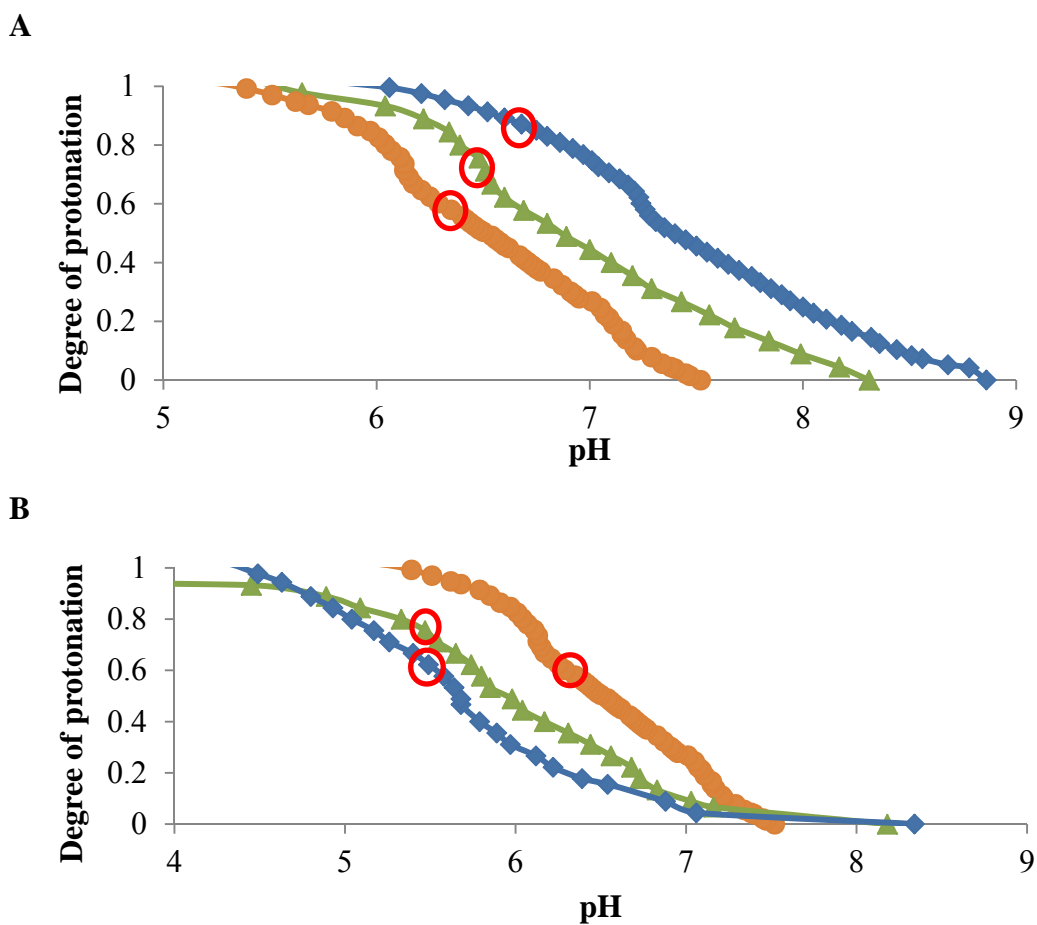


Figure 3.3: Degree of protonation of  $C_{12-14}N(EO)_2$  (1% w/w) vs pH at 1 atm.: (A) 22% TDS brine at 24 ( $\diamond$ ), 50 ( $\triangle$ ) and 90 ( $\circ$ )°C. (B) DI water (no salt) ( $\diamond$ ), 120g/L NaCl brine ( $\triangle$ ) or 22% TDS brine ( $\circ$ ) at 90 °C. (Phase boundaries where the solution became clear upon lowering pH are marked with red circles.)

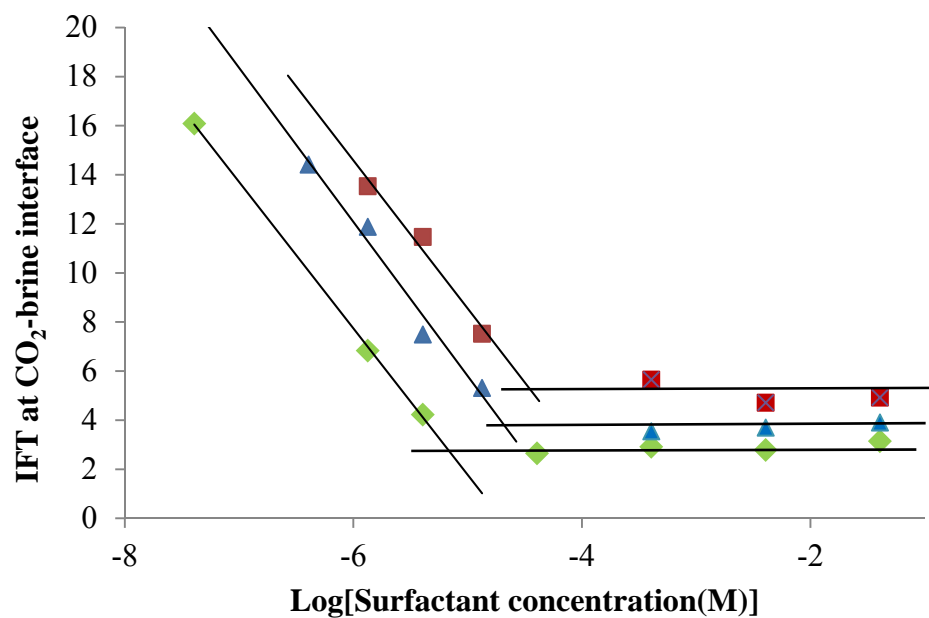


Figure 3.4: Interfacial tension (IFT) for  $C_{12-14}N(EO)_2$  at the CO<sub>2</sub>-22%TDS brine interface at 24 ( $\diamond$ ), 90 ( $\triangle$ ) and 120 ( $\square$ ) °C versus the logarithm of surfactant concentration. The intersection of the curves denotes the critical micelle concentration (CMC). The pH of the aqueous phase is ~3.

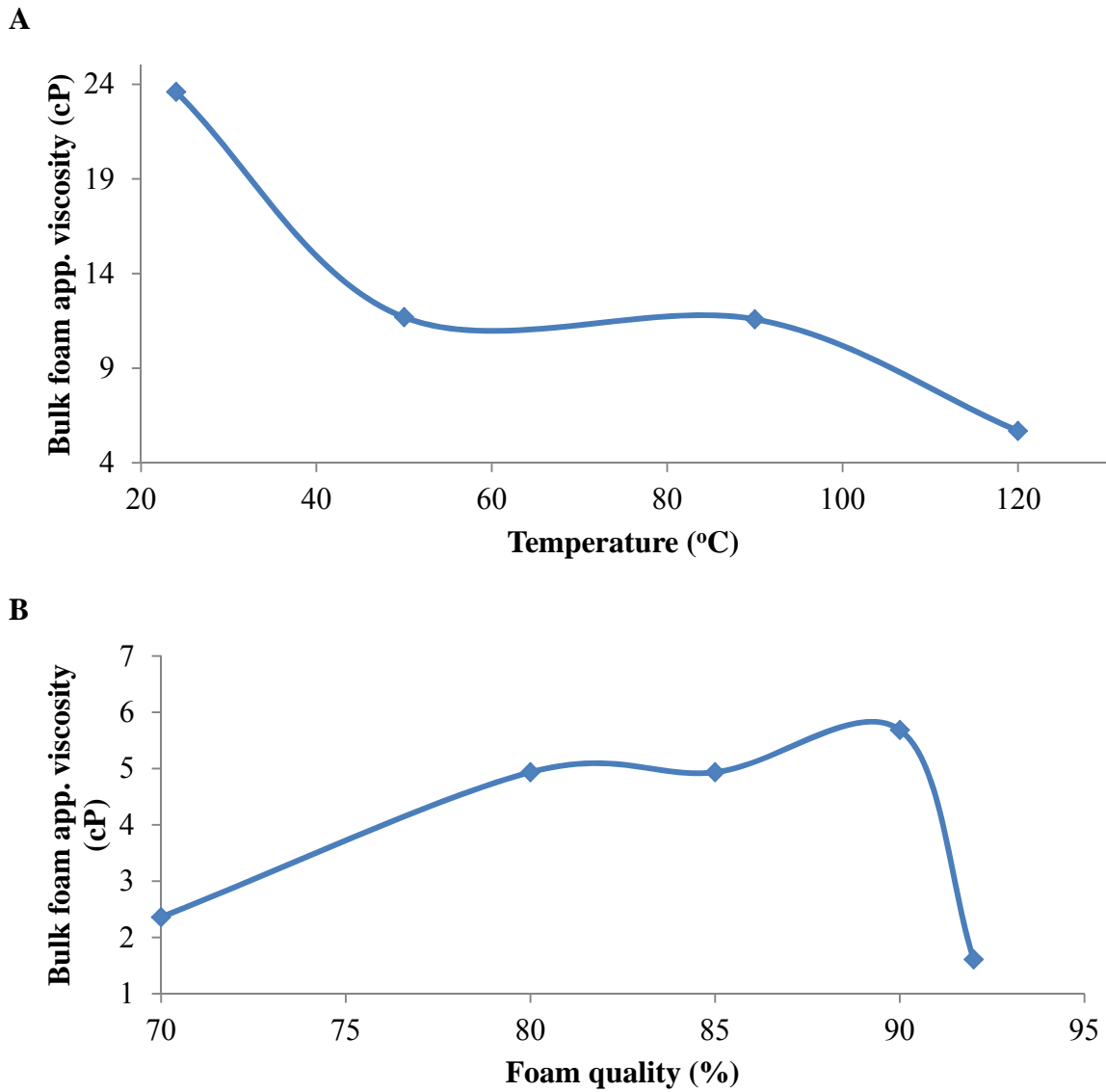
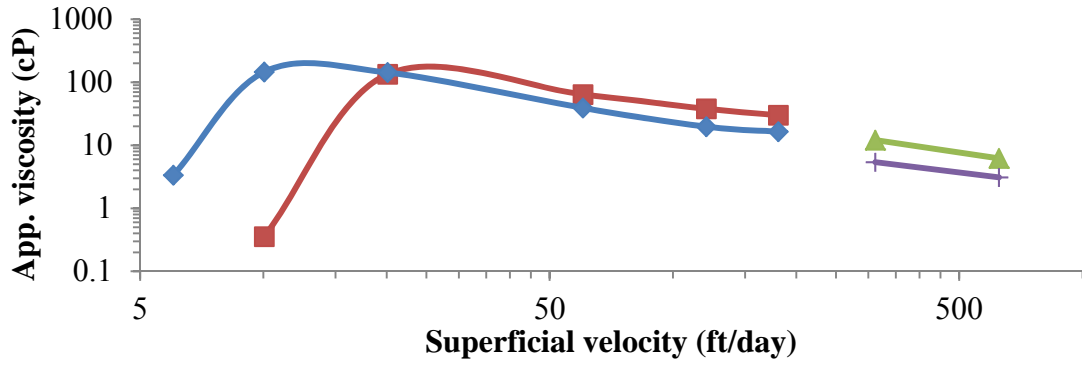
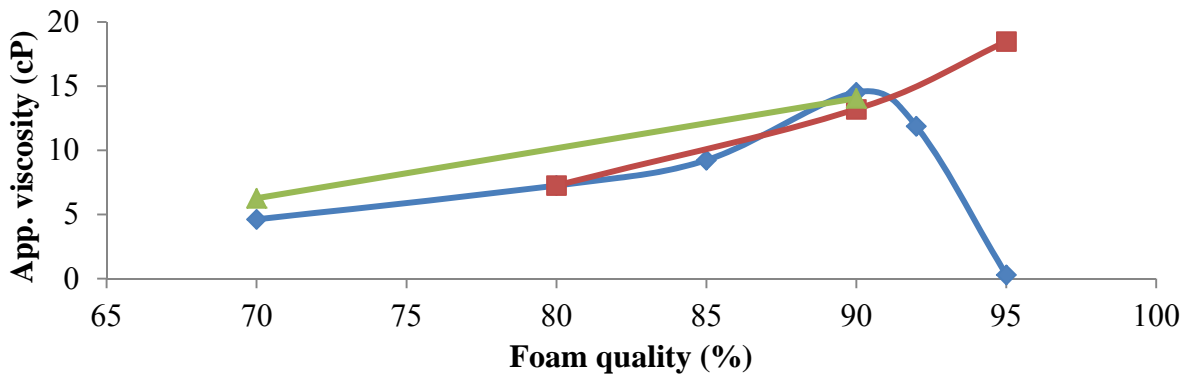


Figure 3.5: Apparent viscosity of bulk foam in the capillary tube stabilized with 1% w/w  $C_{12-14}N(EO)_2$  22% TDS brine at pH 6 (adjusted by adding HCl) solution with a total velocity 82897 ft/day at 3400 psia. (Foam was generated in a 76 Darcy calcium carbonate pack): (A) Effect of temperature at foam quality of 90%; (B) Effect of foam quality at 120 °C.

A



B



C

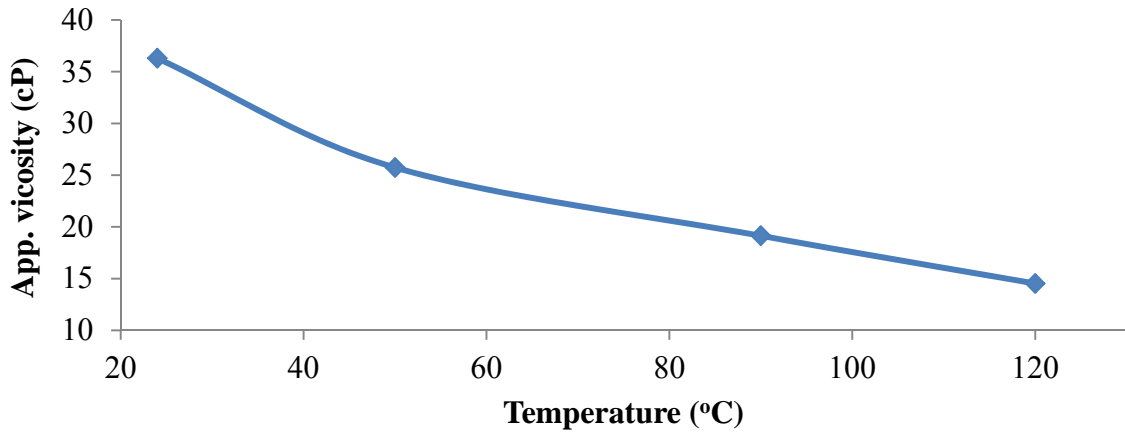


Figure 3.6: Apparent viscosity of C/W foam stabilized with  $C_{12-14}N(EO)_2$  at 3400 psia. (A) Co-injecting 1% w/w  $C_{12-14}N(EO)_2$  in 182 g/l NaCl brine pH 4 solution with pure  $CO_2$  in a 1.2 Darcy glass bead pack at 40% ( $\diamond$ ) and 80%( $\square$ ) foam quality or a 30 Darcy sand pack at 80%(+) and 90% ( $\Delta$ ) foam quality at 120 °C (See reference 42). (B) Co-injecting 1% w/w  $C_{12-14}N(EO)_2$  in 22%TDS brine pH6 solution with  $CO_2$ ( $\diamond$ ), 0.2% w/w  $C_{12-14}N(EO)_2$   $CO_2$  solution with 22%TDS brine ( $\square$ ) or 1% w/w  $C_{12-14}N(EO)_2CH_3Cl$  22%TDS brine solution with  $CO_2$  ( $\Delta$ )at 120 °C, total superficial velocity 938 ft/day in 76 Darcy calcium carbonate packed bed with foam quality from 70% to 95%. (C) Co-injecting 1% w/w  $C_{12-14}N(EO)_2$  22%TDS brine pH 6 solution with  $CO_2$  at 24-120 °C, with a total superficial velocity 938 ft/day in 76 Darcy calcium carbonate pack.

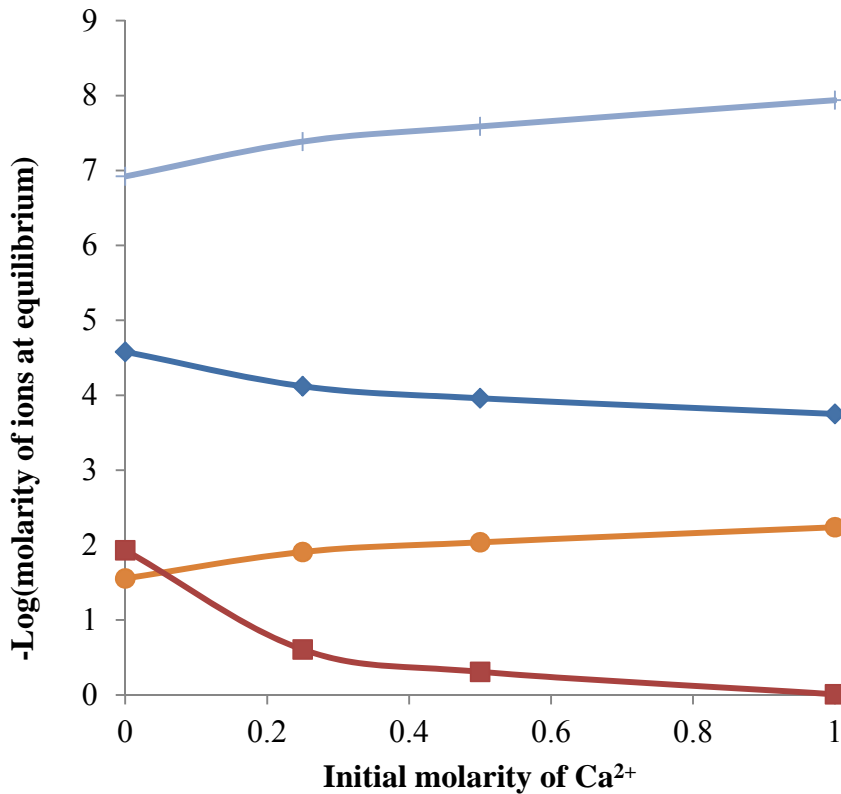


Figure 3.7: Effect of concentration of  $Ca^{2+}$  in injected brine on concentration of various species:  $CO_3^{2-}$ ( $\square$ ),  $H^+$ ( $\diamond$ ),  $HCO_3^-$ ( $\circ$ ) and  $Ca^{2+}$ ( $\square$ ) at equilibrium in the presence of excess calcium carbonate and  $CO_2$  at 120 °C and 3400 psia. The results are simulated using PHREEQC.

## **Chapter 4: CO<sub>2</sub>-in-Water Foam Stabilized with Cationic Ammonium Salt Surfactants at High Temperature**

The design of surfactants for stabilizing CO<sub>2</sub>-in-water (brine) foams at high temperature is challenging given the low density (solvent strength) of CO<sub>2</sub> and the interfacial and rheological properties of the thin lamellae films in the foam. Even though cationic surfactants may be expected to adsorb weakly on positively charged limestone in CO<sub>2</sub> enhanced oil recovery, they have received much less attention than anionic surfactants. Herein cationic alkyltrimethylammonium surfactants with an alkyl tail of average carbon number less than 15 were soluble in 22% total dissolved solids (TDS) brine up to 120 °C. The head group was properly balanced with a C<sub>12-14</sub> hydrocarbon tail for a sufficiently dense surfactant layer (area/ surfactant molecule of 154 Å<sup>2</sup>.) at the CO<sub>2</sub>-water interface to reduce the interfacial tension from ~40 mN/m to ~6 mN/m. For C<sub>12-14</sub>N(CH<sub>3</sub>)<sub>3</sub>Cl the solubility in brine and the surfactant adsorption were sufficient to stabilize CO<sub>2</sub>-in-water foam with an apparent viscosity of ~14 cP (~40 times higher than the value without added surfactant) at 120 °C in both a crushed calcium carbonate packed bed (76 Darcy) and a capillary tube downstream of the bed. The stability of the foam at high temperature may be attributed to the high surfactant solubility in brine and adsorption at the interface. In addition, the partition coefficient between oil and 22% TDS brine was below 0.15 at 24 and 90 °C. In CO<sub>2</sub> enhanced oil recovery, the low partition coefficient would be beneficial for low loss of the surfactant to the oil phase.

### **4.1 INTRODUCTION**

C/W macroemulsions (commonly referred to as foams) are of interest in various applications including chemical and pharmaceuticals processing, CO<sub>2</sub> EOR, and



hydraulic fracturing.<sup>5,8,18,76,77,85,114</sup> The dispersed CO<sub>2</sub> bubbles are stabilized through various mechanisms by the adsorption of surfactant molecules at the C-W interface to lower the interfacial tension. The solvation of the surfactant head groups produces a repulsive disjoining pressure between the two surfaces of the aqueous lamellae to resist the van der Waals attraction between the CO<sub>2</sub> bubbles.<sup>115</sup> The lowering of the interfacial tension and thus the capillary pressure between the dispersed CO<sub>2</sub> bubbles and the lamellae films slows down the draining and thinning of the lamellae.<sup>80</sup> Although these stability mechanisms have been studied for C/W foams, they are less well understood, given the complexity of solvation by supercritical CO<sub>2</sub> than in the case of more common gas-in-water foams.<sup>3,8,77</sup>

Despite numerous studies of C/W foams below ~ 60 °C, very few examples have examined high temperatures above 100 °C, due in part to limitations in surfactant solubility in the aqueous phase. Nonionic surfactants, for example alkyl EO/PO surfactants, are generally insoluble in aqueous media at temperatures above 100 °C, due to the relatively weak hydrogen-bonding between EO and surrounding water molecules.<sup>18,116</sup> Some anionic and cationic surfactants may be soluble given hydration of the charged head groups and the greater solvation of the tails, as the water becomes less structured.<sup>102,117</sup> For example, dodecyltrimethylammonium chloride (C<sub>12</sub>N(CH<sub>3</sub>)<sub>3</sub>Cl) is soluble in water at pH~7 up to ~200 °C<sup>118</sup>, In Chapter 3, a cationic tertiary amine surfactant bis(2-hydroxyethyl) cocoalkylamine (C<sub>12-14</sub>N(EO)<sub>2</sub>) in the protonated state up to pH 5.5 was reported soluble up to 120 °C even for a very high salinity of 22% TDS brine.<sup>40,86</sup> Basic surfactants, which are switchable between the cationic and nonionic states, are being exploited in a variety of surfactants and process concepts<sup>39,119</sup> including EOR at high temperature and pressure.<sup>40</sup>

The phase behavior and interfacial properties of a surfactant-CO<sub>2</sub>-water system is influenced by the interactions of surfactant head and tail with the fluid phases, as described by the HCB<sup>8,76,87-92</sup>

$$\frac{1}{HCB} = \frac{A_{TC} - A_{TT} - A_{CC}}{A_{HW} - A_{HH} - A_{WW}} \quad [4.1]$$

where  $A_{ij}$  is the interaction potential between CO<sub>2</sub> (C), the hydrocarbon tail (T), water (W) and the surfactant head group (H).<sup>85</sup> The HCB can be manipulated by varying surfactant structure, temperature, pressure, and salinity as depicted in Figure 4.1. When  $1/HCB < 1$ , the solvation of the surfactant head in water is stronger than that of the tail in CO<sub>2</sub>, which produces a low C-W partition coefficient and an interface curved around CO<sub>2</sub>, (C/W macroemulsion or foam).<sup>76,85,87</sup> When  $1/HCB > 1$ , the surfactant partitions more towards CO<sub>2</sub> than water and the interface curves about water to favor a W/C macroemulsion.<sup>88,90,91</sup> When  $HCB = 1$ , the surfactant exhibits an equal tendency for both phases and may form a C/W<sup>93,94</sup> or W/C<sup>29,57</sup> microemulsion. With an HCB a modest distance away from unity, the surfactants may adsorb to a sufficient degree at the C-W interface, reduce the interfacial tension, and stabilize a macroemulsion.<sup>80</sup> If the HCB is too close to 1, the macroemulsion may become unstable as it is easy to bend the interface and form a hole for coalescence of the dispersed droplets<sup>18</sup>. To date, the only study of interfacial tension (IFT) for a surfactant-CO<sub>2</sub>-water system at a temperature above 100 °C to our knowledge was with protonated C<sub>12-14</sub>N(EO)<sub>2</sub> as demonstrated in Chapter 3. However, for pH values above ~6, the surfactant is deprotonated and will precipitate in the aqueous phase. Thus, it would be of interest to find pH insensitive cationic surfactants that are soluble in brine at high temperature for studies of interfacial properties and the design of macroemulsions and foams.

Relative to ambient temperature, stabilization of the lamellae films in C/W foam at high temperatures above  $\sim 70$  °C is challenging for several reasons. First, the surfactant may become chemically unstable or it may precipitate in the aqueous phase.<sup>18</sup> Also, lamellae films drain more rapidly as the viscosity of the aqueous phase decreases as discussed in Chapter 3.<sup>45</sup> Furthermore, greater thermal fluctuations may produce holes in the lamellae films that lead to rupture and coalescence.<sup>44,96</sup>

Even at temperatures above 100 °C, anionic surfactants, such as sulfonates either alone or mixed with nonionic surfactants have been shown to stabilize foams.<sup>120,121</sup> However, anionic surfactants adsorb strongly on the surface of positively charged minerals, for example calcium carbonate in the presence of CO<sub>2</sub> and water at a pH below 6.<sup>38</sup> To attain low adsorption on calcium carbonate, Chen et al. used water-soluble cationic C<sub>12-14</sub>N(EO)<sub>2</sub> and to form C/W foam at 120 °C.<sup>40</sup> The positively charged surfactant head group is repelled by the cationic mineral surface,<sup>40</sup> However, the dissolution of the surfactant in water or brine required protonation by adding acids (for example, HCl or H<sub>2</sub>CO<sub>3</sub>). The surfactant was shown to stabilize C/W foams in porous media packed with glass beads or crushed calcium carbonate particles, and also in a capillary tube downstream of a foam generator. In the case of the crushed calcium carbonate packed bed, Ca<sup>2+</sup> and Mg<sup>2+</sup> were added to suppress dissolution of the basic calcium carbonate by the common ion effect to maintain a pH  $\sim 4$ . Here, the high degree of protonation resulted in strong foam formation at high temperature as explained in Chapter 3. To better understand the interfacial properties of these switchable surfactants in the protonated state, it would be instructive to study the equivalent permanent cationic quaternary ammonium surfactants. Furthermore, there is a need to discover additional classes of cationic surfactants that form C/W foams at high temperatures and salinities, particularly for EOR.

The objective of this study was to demonstrate cationic alkyltrimethylammonium salts are soluble in water and concentrated brine up to 120 °C, lower the interfacial tension, and consequently stabilize viscous C/W foams. The positively charged ammonium head group provides hydrophilicity over a broad range in pH, and may be expected to provide low adsorption on positively charged calcium carbonate surfaces in the presence of CO<sub>2</sub> at high pressure. For the chosen trimethylammonium head group, the highest carbon number in the surfactant tail is identified whereby the surfactant solubility is 1% w/w surfactant in 22% TDS brine up to 120 °C. This level of solubility is sufficient for studies of the IFT, critical micelle concentration (CMC), and surfactant adsorption at the C-W interface up to 120 °C. The results are compared with those for the switchable surfactant C<sub>12-14</sub>N(EO)<sub>2</sub> in the protonated state and found to be similar. The apparent viscosities of C/W foams are presented for a 76 Darcy crushed calcium carbonate packed bed and a downstream 762 μm inner diameter capillary tube. The apparent viscosities of the foams are characterized in terms of the alkyl tail length, temperature, foam quality (volumetric ratio of CO<sub>2</sub> in total injected fluid), and surfactant concentration. The apparent viscosity results are explained in terms of lamellae stabilization mechanisms and theories for bulk foam and foam in porous media<sup>42-46</sup>. The oil-water (O-W) partition coefficients of the surfactants are investigated in terms of alkyl tail length. The chemical stability of quaternary ammonium surfactants at high temperature is a concern, as they may undergo Hoffman elimination or nucleophilic substitution to form a tertiary amine. However, the surfactants may remain thermally stable at a temperature below 150 °C, based on tests for time periods up to 10 min.<sup>82,83,122</sup> From a practical point of view, alkyltrimethylammonium salts are of interest as foam stabilizers for hydraulic fracturing, as the process only takes several hours from fluid injection to gas production.

## **4.2 EXPERIMENTAL**

### **4.2.1 Materials**

Decyltrimethylammonium bromide ( $C_{10}N(CH_3)_3Br$ , 99%) was purchased from Acros. All other surfactants were gifts from Akzo Nobel and used without further purification (Table 4.1). The concentrations of surfactants reported in this study have been corrected for the surfactant purity (known at “activity”) of the stock solutions received from the manufacturer. Carbon dioxide (Metheson, Coleman grade, 99.99%) was used as received. Sodium chloride (NaCl, certified ACS, Fisher), calcium chloride dihydrate ( $CaCl_2 \cdot 2H_2O$ , 99+% Acros), and magnesium chloride hexahydrate ( $MgCl_2 \cdot 6H_2O$ , Fisher) were used as received. Model 22% TDS brine containing 182 g/L NaCl, 77 g/L  $CaCl_2 \cdot 2H_2O$ , 26 g/L  $MgCl_2 \cdot 6H_2O$  was used to prepare surfactant/brine solutions with surfactant concentration from 0.0001 to 1 % w/w ( $4 \times 10^{-6}$  to  $4 \times 10^{-2}$  M  $C_{12-14}N(CH_3)_3Cl$ ). Dodecane (Acros, 99%) was used without purification.

### **4.2.2 Surfactant aqueous solubility measurements**

Aqueous solubility measurements up to 120 °C were carried out with a sealed glass pipette method developed by Puerto et al.<sup>16,54</sup> following careful safety precautions. The sealed pipettes containing surfactant aqueous solution were placed inside a 10 mL test tube filled with the same oil as in a temperature controlled oil bath. The surfactant concentration was 1.0 % w/w. The uncertainty in the cloud point temperature was  $\pm 1$  °C.

### **4.2.3 Interfacial tension measurements at CO<sub>2</sub>-brine and air-brine interfaces**

The interfacial tension between CO<sub>2</sub> and surfactant brine solutions was determined from axisymmetric drop shape analysis of a captive bubble.<sup>56</sup> The detailed procedure was the same as in Chapter 3. Scheme and apparatus photos for interfacial

tension measurement at high pressures are shown in Figure C1. The standard deviation of the interfacial tension measurements was typically less than 4 % of the mean. Air-brine interfacial tension was determined using axisymmetric drop shape analysis of a pendant brine droplet containing a known concentration of surfactant using a procedure modified from a previous study.<sup>123</sup> The droplet was held for 2 minutes to equilibrate prior to recording droplet shape. The pendant drop was illuminated with a monochromatic light source and the digital images were recorded. The droplet shape profile was fitted according to the Young-Laplace equation with a software package (CAM200, KSV Ltd., Finland). The mean interfacial tension was taken of 10 measurements that were acquired 10 seconds apart, and the standard deviation of the measurements was typically less than 2 % of the mean.

The molar surface density of the surfactant monolayer was obtained from the Gibbs adsorption equation below the CMC:

$$\Gamma = -\frac{1}{RT} \left( \frac{\partial \gamma}{\partial \ln C_{surf}} \right)_{T,P} \quad [4.2]$$

where  $C_{surf}$  is the surfactant concentration. The slope was treated as a straight line given the challenges of high temperature measurements. The area occupied by a surfactant molecule in the monolayer is given by  $A_m = 1/(N_A \Gamma)$  where  $N_A$  is Avogadro's number. The efficiency of adsorption was defined as the negative logarithm of the concentration of surfactant in the bulk phase required to produce a 20 mN/m reduction in the interfacial tension:  $-\log C_{(-\Delta\gamma=20)} \equiv pC_{20}$ .<sup>60</sup>

#### 4.2.4 C/W foam formation and apparent viscosity measurements

The apparatus for measurement of the foam apparent viscosity up to 120 °C and 3400 psia is depicted in Figure 4.2. The experimental procedure for calculating the

apparent viscosity of C/W foam from the pressure drop, for both the porous media foam generator and a downstream capillary tube (762  $\mu\text{m}$  in inner diameter (ID), 195 cm in length) were the same as described in our previous publication.<sup>40</sup> In this work, the porous media was a crushed calcium carbonate packed bed (22.9 cm long, 0.62 cm inner diameter tube) with a permeability to water of 76 Darcy (calculated from Darcy's law for 1-D horizontal flow) and 38% porosity (2.6 mL pore volume) determined by the mass of loaded material. The crushed calcium carbonate (Franklin Industrial Minerals) was 420-840  $\mu\text{m}$  in diameter (20-40 mesh) and was washed with copious amounts of water and ethanol before use. The non-spherical calcium carbonate particles were held in place by two 100 mesh stainless steel wire screens.

#### **4.2.5 Partition coefficient of surfactant between 22% TDS brine and dodecane**

Equal volumes of 1 % w/w surfactant solution in the 22% TDS brine and dodecane were mixed by gentle hand-shaking. The mixtures were stored quiescent at 24 °C or at 90 °C for 48 h, and the partition coefficient of the surfactants between the brine and dodecane was investigated by measuring the surfactant concentration in a sample obtained from the aqueous phase. The concentration of surfactant in the aqueous phase was determined by Epton's method<sup>58</sup> of two-phase titration with methylene blue solution (0.03 g/L methylene blue, 50 g/L sodium sulfate ( $\text{Na}_2\text{SO}_4$ ), 10 mL/L sulfuric acid (98%)) as an indicator, and sodium dodecyl ether sulfate from Stepan (trade name: STEOL CS330, MW=422 g/mol) as titrant. Titrations were carried out to a colorless end point. All oil-water partitioning results contained an error below  $\pm 0.02$  in partition coefficients.

## **4.3 RESULTS AND DISCUSSION**

### **4.3.1 Solvation in water and brine**

All five alkyltrimethylammonium salt surfactants were examined at 1% w/w in water or 22% TDS brine (Table 4.2) and found to be soluble at up to 120 °C in water with no added salt. Both the solvation of surfactant ionic heads and hydrocarbon tails increased with an increase in temperature. For the surfactant ionic heads, the solubility depends on dissociation of the ammonium cations and bromide or chloride anions in water. This dissociation follows a Boltzmann distribution which is more favorable at a higher temperature.<sup>104</sup> For the hydrocarbon tail, the solvation increases as the water molecules at the surface of the hydrophobic tails become less structured at high temperature.<sup>102,117</sup> In 22% TDS brine, C<sub>10</sub>N(CH<sub>3</sub>)<sub>3</sub>Br, C<sub>12</sub>N(CH<sub>3</sub>)<sub>3</sub>Cl and C<sub>12-14</sub>N(CH<sub>3</sub>)<sub>3</sub>Cl were soluble up to 120 °C, while those with longer tails were insoluble. Here, the solubility of the surfactants decreased with the increase of tail length and salinity. The Gibbs free energy change for dissolving straight-chain aliphatic hydrocarbons becomes more unfavorable with an increase of carbon number because more water molecules are forced into contact with the chain.<sup>124</sup> As the salinity increases, the greater screening of the charge on the cationic head group, decreases the solvation by water and lowers the solubility.<sup>71</sup> The soluble alkyltrimethylammonium salt surfactants with less than 15 carbon atoms in the tail which were soluble up to 120 °C in concentrated brine will next be used for studies of interfacial properties and foams.

### **4.3.2 Interfacial properties at C-W and A-W interfaces**

#### **4.3.2.1 C-W IFT**

The IFT between CO<sub>2</sub> and 22% TDS brine measured in the presence of C<sub>12-14</sub>N(CH<sub>3</sub>)<sub>3</sub>Cl concentrations varied over four orders of magnitude at 3400 psia and 24-120



°C (Figure 4.3). Without surfactant, the IFT ranged from 33 to 44 mN/m at 2500-3900 psia and 25-125 °C.<sup>95</sup> Upon adding  $C_{12-14}N(CH_3)_3Cl$  at a concentration above the CMC, the IFT was reduced to 3.1-5.9 mN/m and increased with an increase of temperature at 3400 psia. The increase of IFT with temperature may be attributed to an increase in the HCB, as the surfactant moves from the interface towards water. Here, as the temperature increases at constant pressure, the cationic head group is better solvated in aqueous phase as explained above,<sup>104</sup> while the tail is less solvated by the less dense  $CO_2$ . Both factors drive  $C_{12-14}N(CH_3)_3Cl$  from the C-W interface towards water, resulting in an increase in the HCB and thus also in the C-W IFT as depicted in Figure 4.1. More importantly, the IFT still remains quite low at less than 6 mN/m at a surfactant concentrations above the CMC, even at 120 °C. This low IFT indicates significant solvation of the  $C_{12-14}$  tails by  $CO_2$  is still present despite the low  $CO_2$  density of only 0.48 g/mL. In addition, the C-W IFT results with  $C_{12-14}N(CH_3)_3Cl$  are very close to those (in the same brine) with a tertiary amine surfactant with the same tail,  $C_{12-14}N(EO)_2$  in the protonated state (Chapter 3). This similarity in IFTs may indicate similar HCBs and interactions of the surfactant heads and tails with the relevant phases. Apparently, the effect of three methyl groups in  $N^+(CH_3)_3$  was similar to that of two hydroxyethyl groups in  $NH^+(EO)_2$ . Relative to a  $CH_3$  group, the hydroxyethyl group has one more carbon adding hydrophobicity and a OH group giving hydrophilicity. The similar IFTs may suggest that the contribution from these two effects appeared to compensate each other.

The CMC of  $C_{12-14}N(CH_3)_3Cl$  increased by 6 times with an increase in temperature from 24 to 120 °C as listed in Table 4.3, which indicates the surfactant monomers were more favored than micelles. When temperature increases, the solvation of the cationic nitrogen head group and hydrocarbon tail group are increased in brine as explained previously, which disfavors micellization.<sup>108</sup> A similar increase of CMC with

an increase of temperature was also observed with  $C_{12-14}N(EO)_2$  under the same pressure and salinity.(Chapter 3)

#### ***4.3.2.2 Adsorption at the C-W interface and pC20***

The slope of the plot of the IFT versus the log of surfactant concentration was used to determine the adsorption of  $C_{12-14}N(CH_3)_3Cl$  as listed in Table 4.3. When temperature increased at constant pressure, the adsorption decreased from  $1.5 \times 10^{-6}$  mol/m<sup>2</sup> at 24 °C to  $1.1 \times 10^{-6}$  mol/m<sup>2</sup> at 120 °C. Here, the IFT in the absence of surfactant ( $\gamma_0$ ) increases<sup>95</sup> which provides a greater driving force for adsorption of surfactant at the C-W interface.<sup>33,110</sup> In contrast, the adsorption of  $C_{12-14}N(CH_3)_3Cl$  decreased with temperature likely due to the increase in HCB. This HCB increase is caused by the weaker tail solvation by the less dense CO<sub>2</sub> and stronger head solvation. Consequently, the adsorption of  $C_{12-14}N(CH_3)_3Cl$  decreased as the surfactant partitioned more from the interface to water. Finally, the increased thermal motion also leads to an increase of the area per surfactant molecule.<sup>60,125</sup> These factors also decreased the pC20 (negative logarithm of the concentration of surfactant in the bulk phase required to reduce IFT by 20 mM/m) modestly, as the surfactant was slightly less interfacially active.

At all tested temperatures, the adsorption of  $C_{12-14}N(CH_3)_3Cl$  at CO<sub>2</sub>-22% TDS brine interface was slightly higher than that of  $C_{12-14}N(EO)_2$ , giving a lower area per molecule. For example, at 120 °C, the area per molecule of  $C_{12-14}N(CH_3)_3Cl$  was 154 A<sup>2</sup> while that of  $C_{12-14}N(EO)_2$  was 207 A<sup>2</sup> (Chapter 3). The higher adsorption of  $C_{12-14}N(CH_3)_3Cl$  is consistent with the smaller surfactant head group.<sup>60</sup> In addition, at low or moderate temperatures, the adsorption of  $C_{12-14}N(CH_3)_3Cl$  (area per molecule of 111 A<sup>2</sup> at 24 °C) at the CO<sub>2</sub>-22% TDS brine interface was higher than that of several alkyl EO/PO nonionic surfactants (area per molecule of 200-300 A<sup>2</sup> ) at the C-W interface.<sup>36</sup>

Here, the concentrated ions in the 22% TDS brine screened the electrostatic repulsion between charged ammonium head which lowers the area per surfactant. Furthermore, similar to  $C_{12-14}N(EO)_2$ , the ammonium head group for  $C_{12-14}N(CH_3)_3Cl$  is much smaller than the head groups of previously studied nonionic alkyl EO/PO surfactants (for example, with 9 or more EO units<sup>36,57</sup>) and thus occupies a smaller area.

At 24 °C, similar to observations for  $C_{12-14}N(EO)_2$  in Chapter 3, the pC20 for  $C_{12-14}N(CH_3)_3Cl$  (6.1-6.5) for CO<sub>2</sub>-22% TDS brine system is higher than the value for the nonionic surfactant LA-EO<sub>12</sub>( $C_{12}(EO)_{12}$ ) (pC20~5) in the C-W system. The higher value of pC20 for the  $C_{12-14}N(CH_3)_3Cl$  may indicate a more balanced HCB compared with LA-EO<sub>12</sub>, since the relatively large EO number of 12 may be above the optimum. The high pC20 suggests that  $C_{12-14}N(CH_3)_3Cl$  has the potential to be effective for stabilizing C/W foams even at the high salinity.

#### ***4.3.2.3 Interfacial properties at A-W interface***

Interfacial tension measurements versus concentration of  $C_{12-14}N(CH_3)_3Cl$  surfactant at the air-22% TDS brine (Figure 4.4) and additional interfacial properties are listed in Table 4.3. At 24 °C, the adsorption of  $C_{12-14}N(CH_3)_3Cl$  at A-W interface ( $5.4 \times 10^{-6}$  mol/m<sup>2</sup>) was higher than that at the C-W interface ( $1.5 \times 10^{-6}$  mol/m<sup>2</sup>). This greater adsorption in the former may be explained by the greater driving force for adsorption given the higher  $\gamma_0$  at the air-22% TDS brine interface (~80 mN/m) relative to the CO<sub>2</sub>-22% TDS brine interface (~38 mN/m).<sup>110</sup>

At 24 °C, the CMC of  $C_{12-14}N(CH_3)_3Cl$  (0.13 mmol/L) in 22% TDS brine was lower than that of LA-EO<sub>12</sub> in water (~3 mmol/L).<sup>36</sup> In aqueous media, ionic surfactants usually have higher CMCs than nonionic surfactants containing equivalent hydrophobic groups given the greater head group solvation.<sup>108</sup> However, the presence of concentrated

electrolyte in 22% TDS brine will reduce the CMC of  $C_{12-14}N(CH_3)_3Cl$ , since the anions screen the electrostatic repulsion between the cationic head groups in the micellar surface (palisade region).<sup>108</sup>

The adsorption of  $C_{12-14}N(CH_3)_3Cl$  at the air-22% TDS brine interface, which corresponded to an area per molecule of  $31 \text{ \AA}^2$ , was higher than those of linear alkyl EO/PO nonionic surfactants (an area per molecule of  $40-100 \text{ \AA}^2$ ) at the A-W interface.<sup>36</sup> The high ionic strength in the aqueous phase screened the head repulsion during adsorption process. Also the head group for  $C_{12-14}N(CH_3)_3Cl$  is much smaller than the head groups of previously studied nonionic alkyl EO/PO surfactants and thus occupies a smaller area as discussed in the adsorption at C-W interface previously.

### **4.3.3 C/W foam formation and apparent viscosity**

#### ***4.3.3.1 Effect of tail length***

To generate C/W foam stabilized with alkyltrimethylammonium surfactants, 1% w/w surfactant in 22% TDS brine solutions were injected simultaneously with pure CO<sub>2</sub> into a 76 Darcy calcium carbonate packed bed at 120 °C, 3400 psia with total superficial velocity of 938 ft/day and 90% foam quality. As shown in Table 4.4, the apparent viscosity of the foam in the porous media decreased with a decrease of the alkyl tail length. With  $C_{12-14}N(CH_3)_3Cl$ , the highest apparent viscosity of 8.2 cP was observed, while no foam was formed with  $C_{10}N(CH_3)_3Br$ . With a longer alkyl tail, the efficiency of adsorption ( $pC_{20}$ ) at the interface increases due to the negative free energy of adsorbing a methylene group at the interface. Thus, surfactants with a longer alkyl tail would be more efficient in lowering the IFT and reducing capillary pressure to avoid bubble coalescence to enhance foam stability.<sup>60</sup> Further, longer surfactant tails may provide more resistance to hole formation as discussed below.

The coalescence of foam bubbles can occur through hole formation in the lamellae due to thermal fluctuations as depicted in Figure 4.1B. The surfactant tails from the two curved interfaces (hemispheres) are in close proximity to one another. Flocculation of the tails on the hemispheres, given weak solvation by CO<sub>2</sub>, may act to close and heal the hole and prevent coalescence.<sup>18</sup> With a longer alkyl tail, the stronger tail-tail interaction may enhance the healing process to give higher foam stability, and thus give higher apparent viscosity of the C/W foam in the porous media. However, when the length of tail is too long, the surfactant may aggregate too strongly or precipitate in the lamellae, which results destabilization of the foam.<sup>18</sup> Of the five alkyltrimethylammonium salt surfactants studied in this work, C<sub>16</sub>N(CH<sub>3</sub>)<sub>3</sub>Cl and C<sub>16-18</sub>N(CH<sub>3</sub>)<sub>3</sub>Cl were insoluble in 22% TDS brine and thus not suitable for stabilizing a C/W foam. C<sub>10</sub>N(CH<sub>3</sub>)<sub>3</sub>Br, C<sub>12</sub>N(CH<sub>3</sub>)<sub>3</sub>Cl did not stabilize viscous C/W foams at high temperature due their relatively short hydrocarbon tails. Therefore, the tail length for C<sub>12-14</sub>N(CH<sub>3</sub>)<sub>3</sub>Cl was optimal for forming a viscous foam.

#### ***4.3.3.2 Effect of temperature***

The effect of temperature on the apparent viscosity of C/W foam stabilized with 1% w/w C<sub>12-14</sub>N(CH<sub>3</sub>)<sub>3</sub>Cl in 22% TDS brine at the same conditions from 50 to 120 °C is shown in Figure 4.5. In the porous media, the apparent viscosity decreased from 15 cP at 50 °C to 8 cP at 120 °C. This decrease is due in part to a decrease in the viscosity of the aqueous (external) phase  $\mu_e$  when temperature increases (Equation A26).<sup>40</sup> As will now be explained below, high temperature also causes faster film drainage,<sup>18,45,46</sup> and more severe hole formation in the lamellae,<sup>44,96</sup> which reduce the lifetime of the lamellae. With a shorter lifetime, the number of lamellae in the porous media decreases and also does the apparent viscosity of the C/W foam.<sup>5,42</sup>

The difference in pressure between the film and plateau border,  $\Delta P_{film} = 2(P_c - \Pi_d)$  (where  $P_c = 2\gamma/R$  is capillary pressure of a bubble with a radius of R, and  $\Pi_d$  is disjoining pressure) creates a drainage velocity

$$V = -\frac{dh_f}{dt} = \frac{h_f^2}{3\mu_e R_f^2} \Delta P_{film} \quad [4.3]$$

where  $R_f$  and  $h_f$  are the radius and thickness for the thin film, respectively.<sup>46</sup> The reduction of  $\mu_e$  with an increase in temperature will lead to higher V indicating more rapid film drainage. Further, the increase in IFT shown in Figure 4.3 raises  $P_c$  and thus also  $\Delta P_{film}$  and V. In addition, more holes may appear due to greater thermal fluctuations.<sup>44,96</sup> If the hole radius is above a critical value, the hole will grow and lead rupture of the film and bubble coalescence. Here, as the aqueous lamellae become thinner, the reduction in work required to create a hole  $W_h \cong \frac{h_f^2 \gamma_h^2}{\gamma_p}$  (where  $W_h$  is the activation energy for hole formation,  $\gamma_p$  is the interfacial tension of the planar interface and  $\gamma_h$  is the interfacial tension of a curved border of the hole)<sup>44</sup> increases the probability of hole formation given by  $\exp(-W_h/kT)$ .<sup>44,96</sup> This probability is also increased by greater thermal energy fluctuations at higher temperature.<sup>44,96</sup> The formation of holes increases the rate of coalescence of the CO<sub>2</sub> bubbles. All of the above effects make the lamellae more unstable at higher temperature and thus induce coalescence of the flowing bubbles in the porous media.

In the capillary tube, the apparent foam viscosity also decreased with an increase of temperature from 50 to 120 °C. Here, the decrease of  $\mu_e$  directly contributes to the decrease of bulk foam apparent viscosity as shown in Equation 4.4 developed for concentrated O/W emulsions by Princen et al.<sup>126</sup>

$$\mu_{foam} = \frac{\tau_0}{\dot{\gamma}} + 32(\Phi_i - 0.73)\mu_e \left(\frac{\mu_e \dot{\gamma} R}{\gamma}\right)^{-1/2} \quad [4.4]$$

where  $\tau_0$  is the yield stress,  $\dot{\gamma}$  is the shear rate,  $\phi_i$  is internal phase volume fraction (referred to as the foam quality for a C/W system), R is radius of bubble, and  $\gamma$  is the interfacial tension. As described above for the foam in the porous media, high temperature also leads to faster film drainage,<sup>18,45</sup> and more severe hole formation in the lamellae.<sup>44,96</sup> All above effects make the lamellae more unstable at higher temperature and thus induce coalescence of the flowing bubbles in the capillary tube. The increase in bubble radius R and the decrease in  $\mu_e$  both contribute to lower  $\mu_{foam}$  as observed in Figure 4.5.

#### 4.3.3.3 Effect of foam quality

The effect of foam quality on apparent viscosity of C/W foams stabilized with 1% w/w C<sub>12-14</sub>N(CH<sub>3</sub>)<sub>3</sub>Cl in the 76 Darcy calcium carbonate packed bed and the downstream capillary tube is shown in Figure 4.6. All other parameters were held constant. As the quality increased above 50%, the apparent viscosity in the porous media increased gradually and reached a maximum at 95% with an apparent viscosity of ~14 cP (more than 40 times higher the value without any surfactant as depicted in Figure C2). At all qualities tested, the apparent viscosities were similar in the porous media and the downstream capillary tube. Above 95% foam quality, the pressure drop across the porous media became unstable and did not reach steady state. Also, as foam quality increased, the bulk foam occupied more area in the upper part of the high pressure view cell, for up to 95% foam quality (Figure 4.7). Moreover, significant coalescence was observed repeatedly at 98% foam quality; the nonuniform foam texture is shown in Figure 4.7.

In the porous media, at a low foam quality (e.g. 50%), aqueous films separate the CO<sub>2</sub> bubbles from (1) each other and (2) the wall of the channels in the porous media. As the foam quality increases, the increased gas fraction raises the number of bubbles (a

higher lamellae density)<sup>42</sup> and produces a thinner aqueous film between the bubbles and the wall.<sup>127</sup> Both factors result in an increase in flow resistance and thus the apparent viscosity.<sup>42,127</sup> Meanwhile as the foam quality increases, the water saturation in the porous media decreases and capillary pressure increases until reaching the limiting capillary pressure.<sup>43</sup> This limiting capillary pressure is set primarily by the disjoining pressure of the stabilizing surfactant.<sup>113,128</sup> Upon further increasing foam quality after reaching the limiting capillary pressure, the disjoining pressure does not resist the capillary pressure and the foam texture coarsens as the bubbles coalesce.<sup>43</sup> Additional discussion of limiting capillary pressure is given in Appendix A.

For the bulk foam, when the foam quality increased from 50% to 95%, the apparent viscosity in the capillary increased as expected from Equation 4.4 assuming all other parameters remained constant. Interestingly, the apparent viscosities of the foam were very similar in the porous media (where the foam generated) and the downstream capillary (where CO<sub>2</sub> bubbles flow as a bulk foam). We hypothesize that the similar viscosities were due to C<sub>12-14</sub>N(CH<sub>3</sub>)<sub>3</sub>Cl generating lamellae in the narrow channels in porous media (with ID close to diameter of CO<sub>2</sub> bubbles) and those lamellae remaining stable when the foam travelled into the capillary tube (with an ID much larger than CO<sub>2</sub> bubble sizes). Bubbles much smaller than the capillary tube have been observed by optical microscopy downstream of a porous media foam generator.<sup>18</sup>

From a practical point of view, viscous bulk foams could be utilized as hydraulic fracturing fluids, where the high apparent viscosity aids in transport of suspended proppant into fractures.<sup>129</sup> As hydraulic fracturing operations typically last only a few hours, long term chemical stability of the surfactant would not be required.



#### **4.3.3.4 Effect of surfactant concentration**

The effect of surfactant concentration on apparent viscosity of C/W foam is shown in Figure 4.8. When the surfactant concentration was  $\leq 0.1\%$  w/w in the brine, no foam formed. At surfactant concentration of 0.25 to 1% w/w, C/W foam with roughly constant apparent viscosity between 8-10 cP was stabilized in the porous foam generator and the downstream capillary tube. Note that the surfactant concentration of 0.25% w/w in the aqueous phase is more than 30 times higher than the CMC of the surfactant in CO<sub>2</sub>-22% TDS system as shown in Figure 4.3. Surfactant micelles trapped in lamellae act as reservoirs to provide surfactant to form new lamellae during the lamellae division when bubbles travel through porous media.<sup>5</sup> Similar critical surfactant concentrations in the plateau region for foam apparent viscosities were observed in core floods by others.<sup>130,131</sup>

#### **4.3.4 PARTITIONING OF SURFACTANTS BETWEEN BRINE AND DODECANE**

The partition coefficients of quaternary ammonium salts between 22% TDS brine solution and dodecane at 24 °C and 90 °C (1 atm) are presented in Table 4.5. All tested surfactants preferred the aqueous phase over the oil phase as indicated by the low partition coefficients below 0.3. The O/W partition coefficients of the surfactants decreased with an increase of temperature. For example, the partition coefficient of C<sub>12</sub>-<sub>14</sub>N(CH<sub>3</sub>)<sub>3</sub>Cl decreased from 0.14 at 24 °C to 0.06 at 90 °C. This decrease is due to improved solvation of both the surfactant cationic head<sup>104</sup> and hydrocarbon tail<sup>102</sup> in the aqueous brine phase with temperature as discussed above. Also, with an average number of carbon atoms in the alkyl tail less than 15, the partition coefficients were less than 0.1 at 90 °C, while for C<sub>16</sub>N(CH<sub>3</sub>)<sub>3</sub>Cl, the partition coefficient was higher at 0.27. The partition coefficients of quaternary ammonium salts increased with an increase of tail length due to a greater free energy penalty required to bring more water molecules in

contact with the more hydrophobic tails upon transfer of the surfactants from the oil phase to the aqueous phase.<sup>124</sup> In oil recovery applications, a low O/W partition coefficient would minimize loss of the surfactant to oil when the surfactant undergoes transport in reservoirs.

#### 4.4 CONCLUSIONS

Cationic alkyltrimethylammonium surfactants with an average carbon number less than 15 are sufficiently hydrophilic to enable solubility at 1% w/w in 22% TDS brine up to 120 °C. For  $C_{12-14}N(CH_3)_3Cl$ , the balance of the quaternary ammonium head with a  $C_{12-14}$  hydrocarbon tail led to a reduction in the IFT from ~40 mN/m to ~6 mN/m at 120 °C at a surfactant concentration above the CMC. The area/molecule of 154 Å<sup>2</sup> at 120 °C was smaller relative to that of a similar surfactant  $C_{12-14}N(EO)_2$ , with a larger head group as expected, despite similar IFT reductions.

$C_{12-14}N(CH_3)_3Cl$  stabilized C/W foams at 120 °C in the presence of 22% TDS brine, with a maximum apparent viscosity ~14 cP in both in a 76 Darcy crushed calcium carbonate packed bed and a downstream capillary tube at a quality of 95%. The presence of surfactant raised the apparent viscosity more than 40 times. The stability of the lamellae between CO<sub>2</sub> bubbles may be attributed to the high surfactant adsorption at the interface, and possibly strong tail-tail interaction for healing of holes that form in thin film lamellae, particularly with the  $C_{12-14}$  tail. For the surfactants with carbon numbers less than 15, the O-W partition coefficient was below 0.15 at both 24 and 90 °C which would favor minimal loss of the surfactants to oil during transport inside reservoirs. The viscous bulk foam is of interest for practical applications such as low

water hydraulic fracturing, where the process times of <1 day are amenable to the thermal stability of the surfactant.

Table 4.1: Composition and HLB of alkyltrimethylammonium surfactants

Sample	Composition	HLB*	Activity	Water	Impurities**
DTAB	Decyltrimethyl ammonium bromide (C <sub>10</sub> N(CH <sub>3</sub> ) <sub>3</sub> Br)	-	99%	-	-
Arquad 12- 37W	Dodecyltrimethyl ammonium chlorides (C <sub>12</sub> N(CH <sub>3</sub> ) <sub>3</sub> Cl)	23.3	35-39%	58- 63%	N,N-Dimethyl-1- dodecanamine hydrochloride, <1%; Lauryldimethylamine, <1%
Arquad C-33W	Cocoalkyltrimethyl ammonium chlorides (C <sub>12-14</sub> N(CH <sub>3</sub> ) <sub>3</sub> Cl)	22.9	32-35%	65- 67%	Cocoalkyldimethylamine, <2%
Arquad 16-29	Hexadecyltrimethyl ammonium chlorides (C <sub>16</sub> N(CH <sub>3</sub> ) <sub>3</sub> Cl)	21.2	29%	66- 71%	N, N-Dimethyl-1- hexadecanamine hydrochloride, <2%; N, N-Dimethyl-1- hexadecanamine, < 2%
Arquad T-27W	Tallowalkyltrimethyl ammonium chlorides (C <sub>16-18</sub> N(CH <sub>3</sub> ) <sub>3</sub> Cl)	20.8	27%	68- 73%	Dimethyltallowalkylamine hydrochloride, <2%; Dimethyltallowalkylamine, <2%

\* Davis scale, provided by manufacturer

\*\* From technical data provided by manufacturer

Table 4.2: Aqueous solubility of 1% w/w alkyltrimethylammonium surfactants from 25 to 120 °C in 22% total dissolved solids (see text for salt composition)

Surfactant	Solubility
C <sub>10</sub> N(CH <sub>3</sub> ) <sub>3</sub> Br	Soluble
C <sub>12</sub> N(CH <sub>3</sub> ) <sub>3</sub> Cl	Soluble
C <sub>12-14</sub> N(CH <sub>3</sub> ) <sub>3</sub> Cl	Soluble
C <sub>16</sub> N(CH <sub>3</sub> ) <sub>3</sub> Cl	Insoluble
C <sub>16-18</sub> N(CH <sub>3</sub> ) <sub>3</sub> Cl	Insoluble

Table 4.3: Properties of C<sub>12-14</sub>N(CH<sub>3</sub>)<sub>3</sub>Cl at the CO<sub>2</sub>-22% TDS brine and air-22% TDS brine interfaces

Interface	T (°C)	P (psia)	$\rho(\text{CO}_2)$ (g/mL)	CMC (% w/w)	CMC (mmol/L)	$\gamma_{\text{cmc}}$ (mN/m)	$\pi_{\text{cmc}}$ (mN/m)	$\Gamma_m * 10^6$ (mol/m <sup>2</sup> )	A <sub>m</sub> (Å <sup>2</sup> /molecule)	pC20
C-W	24	3400	0.94	0.0012	0.05	3.1	34-37	1.5	111	6.1-6.5
	90	3400	0.61	0.0035	0.15	4.7	-	1.2	139	
	120	3400	0.48	0.0071	0.30	5.9	34-38	1.1	154	
A-W	24	14.7	-	0.0031	0.13	31.7	50	5.4	31	4.7

Table 4.4: Apparent viscosities of CO<sub>2</sub>-in-brine foams with 1% w/w alkyl trimethyl ammonium salts in 22% TDS brine solution at 90% foam quality with total superficial velocity 938 ft/day in a 76 Darcy crushed calcium carbonate packed bed at 120 °C and 3400 psia

Surfactant	App. viscosity in porous media (cP)
C <sub>10</sub> N(CH <sub>3</sub> ) <sub>3</sub> Br	No foam
C <sub>12</sub> N(CH <sub>3</sub> ) <sub>3</sub> Cl	4.0
C <sub>12-14</sub> N(CH <sub>3</sub> ) <sub>3</sub> Cl	8.2

Table 4.5: Partition coefficient (weight fraction in oil/weight fraction in 22% TDS brine) of quaternary ammonium salts between aqueous solution and dodecane at 90 °C and 1 atm

Surfactant	24 °C	90 °C
C <sub>10</sub> N(CH <sub>3</sub> ) <sub>3</sub> Br	-	0.09
C <sub>12</sub> N(CH <sub>3</sub> ) <sub>3</sub> Cl	0.08	0.05
C <sub>12-14</sub> N(CH <sub>3</sub> ) <sub>3</sub> Cl	0.14	0.06
C <sub>16</sub> N(CH <sub>3</sub> ) <sub>3</sub> Cl	-	0.27

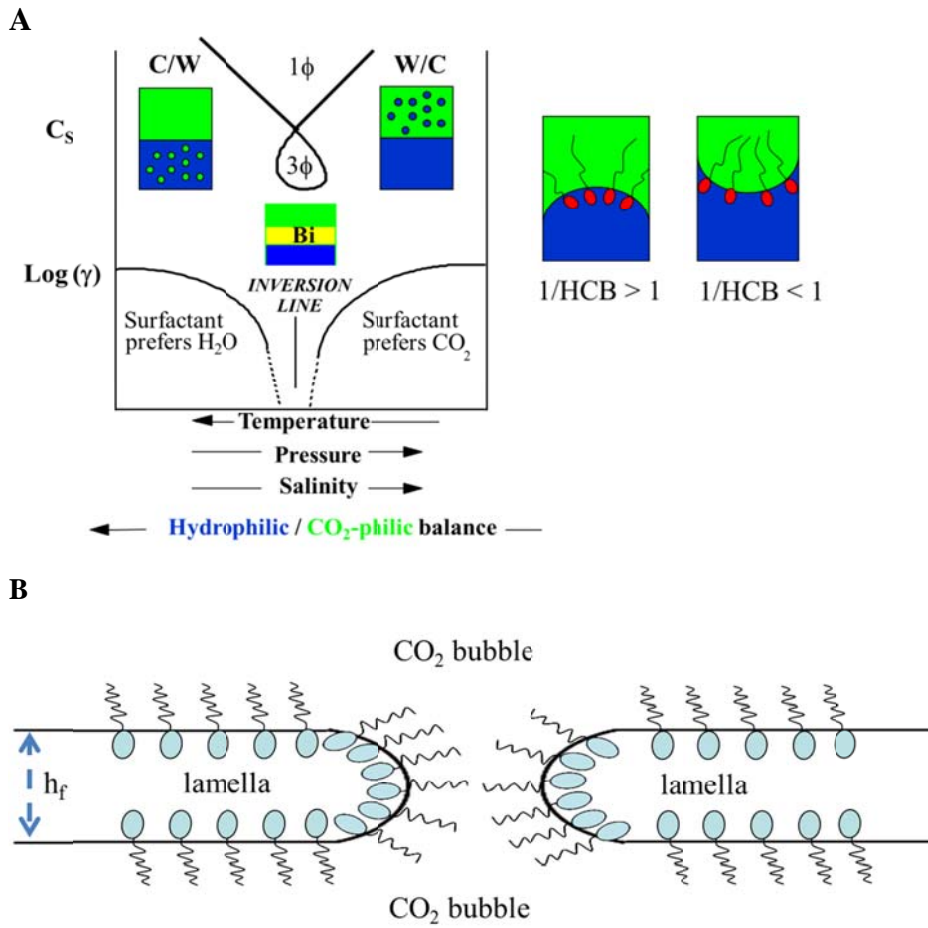


Figure 4.1: (A) Effect of formulation variables on the phase behavior and interfacial tension of CO<sub>2</sub>-water-ionic surfactant system; (B) Formation of a hole in a water lamella for a C/W foam

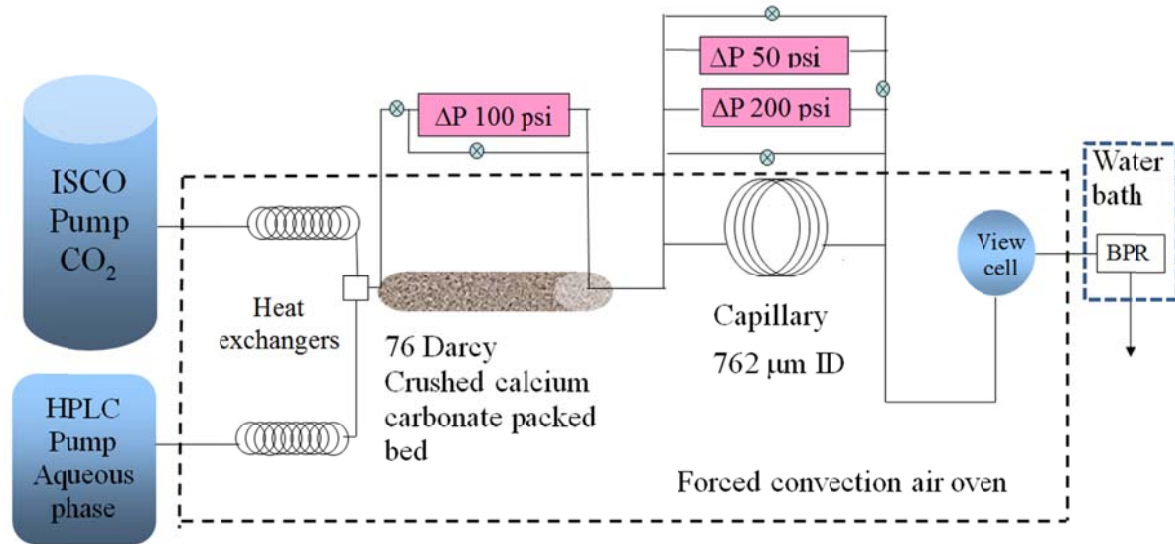


Figure 4.2: Apparatus for CO<sub>2</sub>-water foam viscosity measurements. BPR: back pressure regulator. The crushed calcium carbonate packed bed is used as the foam generator.



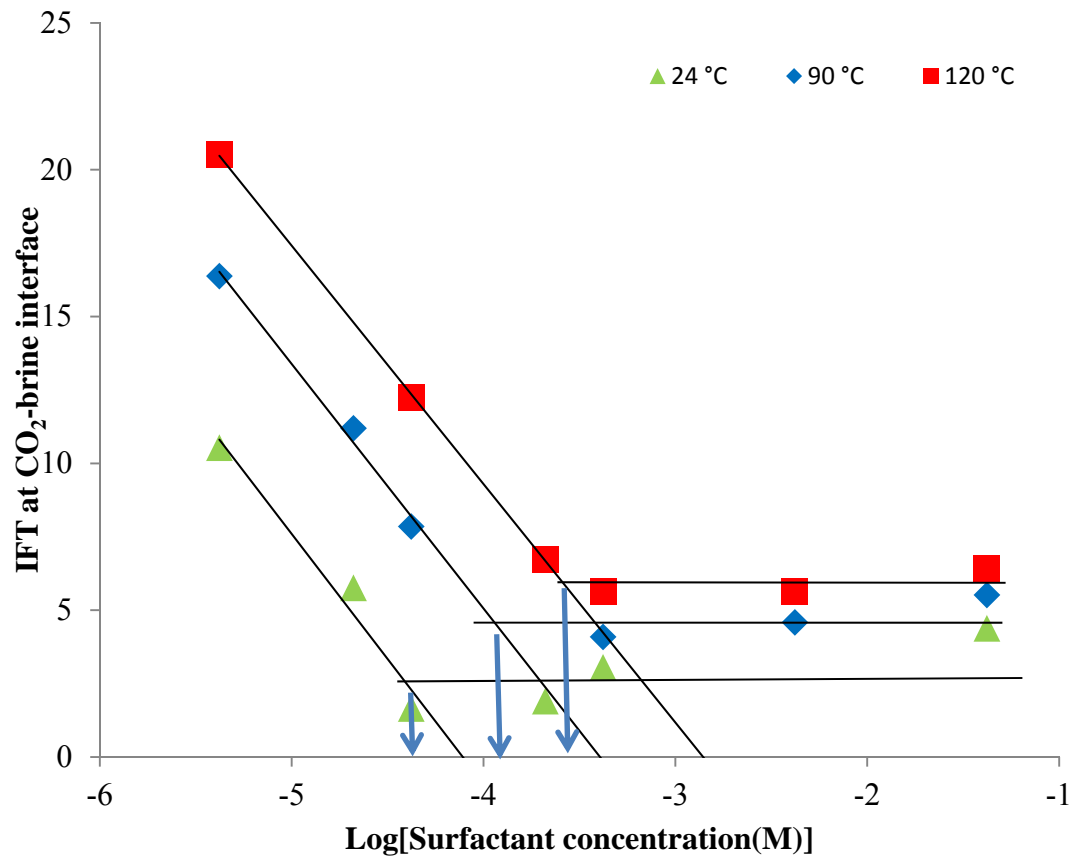


Figure 4.3: Interfacial tension (IFT) for  $C_{12-14}N(CH_3)_3Cl$  at the  $CO_2$ -22%TDS brine interface at 24, 90 and 120 °C. The arrows indicate the critical micelle concentrations.

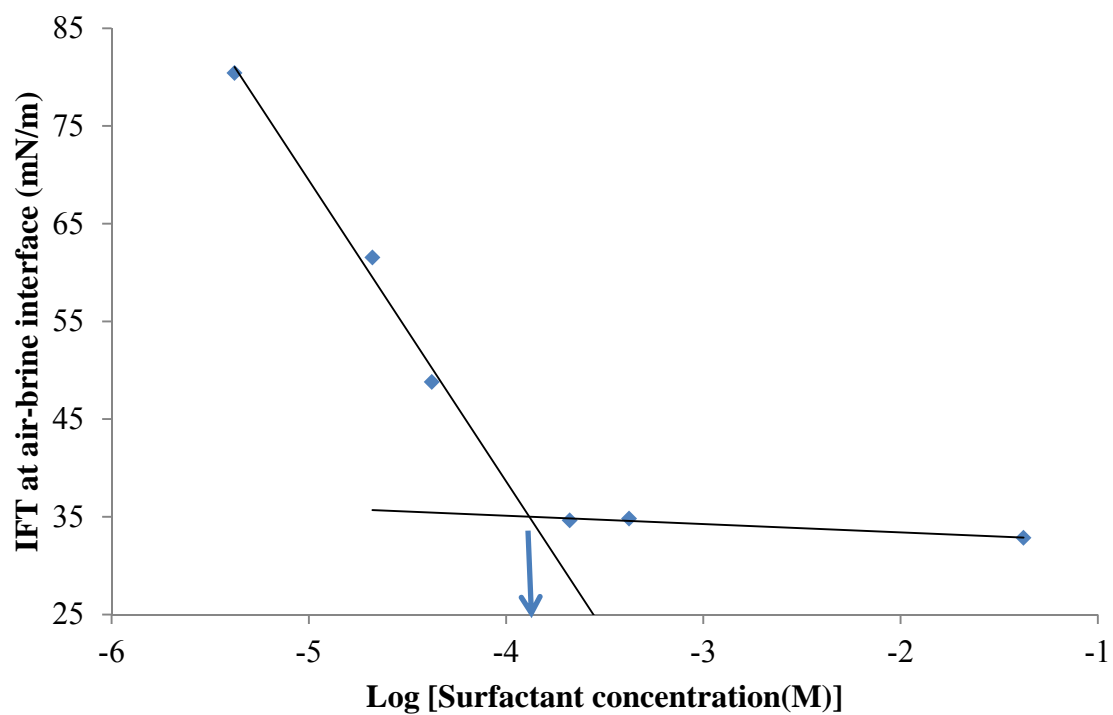


Figure 4.4: Surface tension for  $C_{12-14}N(CH_3)_3Cl$  at the air-22%TDS brine interface at 24 °C. The arrow indicates the critical micelle concentration

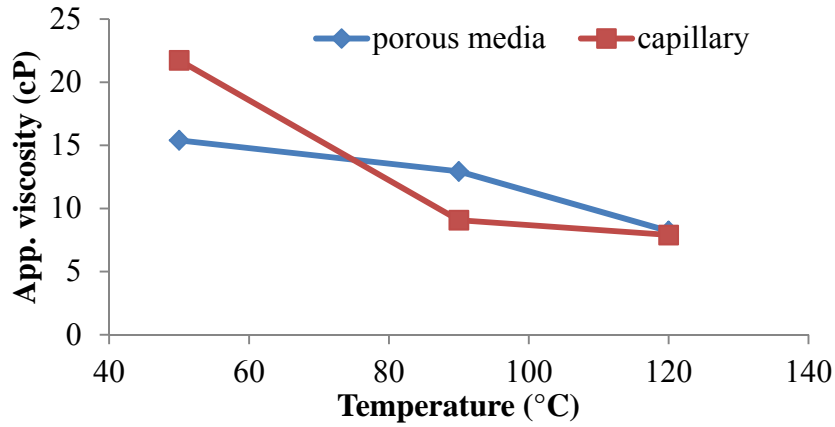


Figure 4.5: Effect of temperature on apparent viscosities of CO<sub>2</sub>-in-brine foams with 1% w/w C<sub>12-14</sub>N(CH<sub>3</sub>)<sub>3</sub>Cl in 22% TDS brine solution at total superficial velocity of 938 ft/day, 90% foam quality in a 76 Darcy calcium carbonate packed bed at 3400 psia

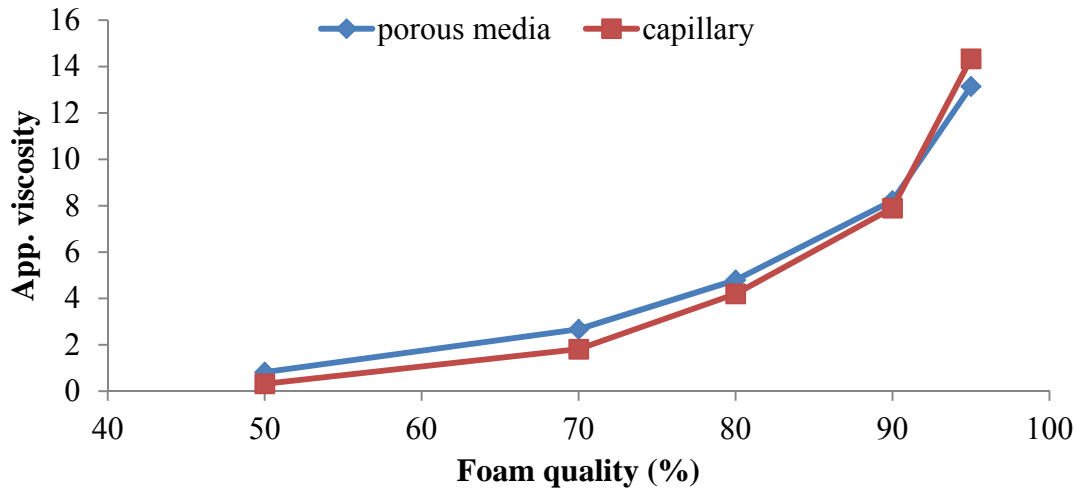


Figure 4.6: Effect of foam quality on apparent viscosities of CO<sub>2</sub>-in-brine foams stabilized with 1% w/w C<sub>12-14</sub>N(CH<sub>3</sub>)<sub>3</sub>Cl in 22% TDS brine solutions at total superficial velocity of 938 ft/day in a 76 Darcy calcium carbonate packed bed at 120 °C and 3400 psia

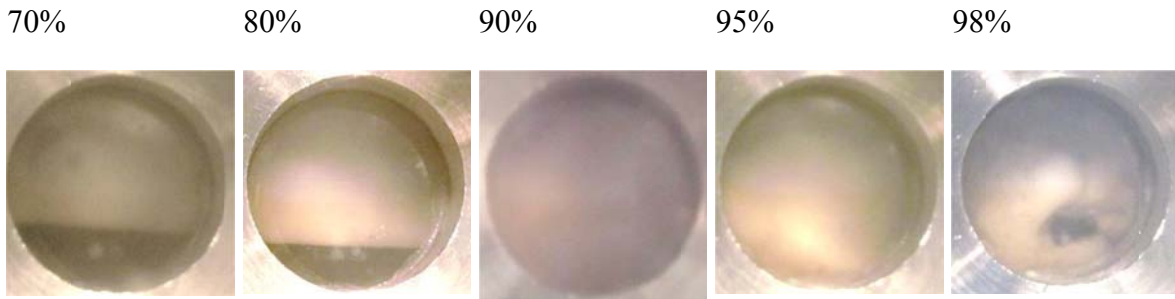


Figure 4.7: View cell photographs of CO<sub>2</sub>-in-brine foams stabilized with 1% w/w C<sub>12-14</sub>N(CH<sub>3</sub>)<sub>3</sub>Cl 22% TDS brine solutions at total superficial velocity 938 ft/day, 70-98% foam quality in 76 Darcy calcium carbonate packed bed, 120 °C and 3400 psia

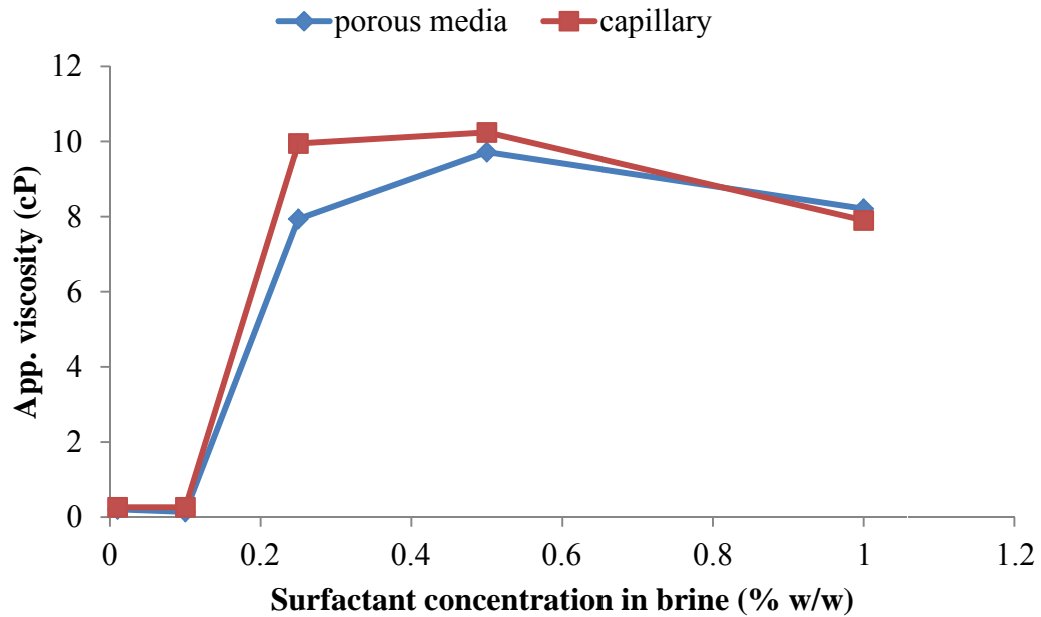


Figure 4.8: Effect of surfactant concentration in brine on apparent viscosities of CO<sub>2</sub>-in-brine foams stabilized with C<sub>12-14</sub>N(CH<sub>3</sub>)<sub>3</sub>Cl 22% TDS brine solutions at total superficial velocity 938 ft/day, 90% foam quality in a 76 Darcy calcium carbonate packed bed, 120 °C and 3400 psia

## **Chapter 5: CO<sub>2</sub>-in-Water Foam at Elevated Temperature and Salinity Stabilized with a Nonionic Surfactant with a High Degree of Ethoxylation**

The utilization of nonionic surfactants for stabilization of CO<sub>2</sub> foams has been limited by low aqueous solubilities at elevated temperatures and salinities. In this work, a nonionic surfactant C<sub>12-14</sub>(EO)<sub>22</sub> with a high degree of ethoxylation resulted in a high cloud point temperature of 83 °C even in 90 g/L NaCl brine. Despite the relatively high hydrophilic/CO<sub>2</sub>-philic balance (HCB), the surfactant adsorption at the C-W interface lowered the interfacial tension to ~7 mN/m at a CO<sub>2</sub> density of ~0.85 g/m, as determined with a captive bubble tensiometry. The adsorption was sufficient to stabilize a C/W foam with an apparent viscosity ~7 cP at 80 °C, essentially up to the cloud point temperature, in the presence of 90 g/L NaCl brine in a 30 Darcy sand pack. In a 1.2 Darcy glass bead pack, the apparent viscosity of the foam in the presence of 0.8% total dissolved solids (TDS) brine reached the highest viscosity of ~350 cP at 60% foam quality at a low superficial velocity of 6 ft/day. Shear-thinning behavior was observed in both the glass bead pack and the sand pack irrespective to the permeability difference. In addition, C<sub>12-14</sub>(EO)<sub>22</sub> stabilized C/W foam with an apparent viscosity of 80-100 cP in a 49 mD dolomite core formed through co-injection and a surfactant-alternating-gas process. The dodecane-0.8% TDS brine partition coefficient for C<sub>12-14</sub>(EO)<sub>22</sub> was below 0.1 at 40 °C and 1 atm. The formation of strong foam in the porous media and the low oil-brine partition coefficient indicates C<sub>12-14</sub>(EO)<sub>22</sub> has potential for CO<sub>2</sub> enhanced oil recovery (EOR).

## 5.1 INTRODUCTION

In CO<sub>2</sub> EOR, the sweep efficiency is limited by gravity override and viscous fingering resulting from the low density and viscosity of CO<sub>2</sub>.<sup>5</sup> In heterogeneous reservoirs, channeling through high permeability regions may leave low permeability oil-rich regions unswept.<sup>4,5</sup> By using a small amount of surfactant to form a CO<sub>2</sub>-in-water (C/W) foam (also called a concentrated macroemulsion), the mobility of CO<sub>2</sub> may be reduced up to thousands of times to stabilize the displacement front for improved sweep efficiency.<sup>4,5</sup> Also, some surfactants form “smart foams”<sup>10</sup> that are weak in oil-rich regions and strong in zones with lower oil amounts.<sup>3,132</sup> Thus, these foams may reduce CO<sub>2</sub> mobility selectively in regions where CO<sub>2</sub> would otherwise bypasses oil.

In a surfactant-CO<sub>2</sub>-water system, the surfactant partition coefficient between CO<sub>2</sub> and water phases may be characterized by the HCB.<sup>8,76,87-92</sup> To form a C/W macroemulsion, 1/HCB should be less than 1 so that the surfactant prefers the continuous aqueous phase and the interface is concave with respect to CO<sub>2</sub>, according to the Bancroft rule.<sup>76,85,87</sup> Furthermore, the HCB should not be too far away from unity (the balanced state) in order for the surfactant to reduce the interfacial tension (IFT) by > 10 mN/m as depicted in Figure 5.1. A decrease in the IFT reduces the energy penalty to generate new interfacial area, and thus aids foam generation. In porous media, a lower IFT also reduces the minimum pressure gradient required to mobilize lamellae for foam generation through mechanisms including snap-off and lamellae division.<sup>5,112,133,134</sup> It also decreases the capillary pressure between dispersed CO<sub>2</sub> bubbles and the aqueous lamellar films, which reduces the drainage and thinning of the films, and thus slows down film rupture and bubble coalescence.<sup>80</sup> If the HCB is too close to 1, however, the IFT can become low enough for forming a microemulsion.<sup>57,93,94</sup> Here, C/W macroemulsions tend to be

unstable as it is easy to bend the interface to generate holes in the lamellae which causes coalescence of foam bubbles.

Nonionic surfactants often exhibit low or moderate adsorption on various charged reservoir minerals such as sandstone and carbonate, whereas ionic surfactants tend to be less versatile.<sup>3,38</sup> For example, cationic surfactants adsorb strongly on negatively charged sandstone, while anionic surfactants adsorb strongly on carbonate formations which are positively charged in CO<sub>2</sub> EOR. Furthermore, nonionic surfactants also tend to adsorb at gas-water interfaces more strongly than ionic surfactants, given the lack of electrostatic repulsion between surfactant head groups.<sup>60</sup>

In addition, nonionic surfactants tend to be more soluble in CO<sub>2</sub> than charged surfactants given the weak intermolecular interactions especially with branched tails and/or small numbers of ethylene-oxide (EO) groups in the surfactant head.<sup>36,63</sup> The co-injection of surfactant-CO<sub>2</sub> solutions with an aqueous phase into porous media may produce C/W foams in both lab and field tests.<sup>49,135-138</sup> The injection of the surfactant in CO<sub>2</sub> may allow the surfactant to flow with the CO<sub>2</sub>-preferred flow path in a reservoir for foam formation. Also, by reducing the CO<sub>2</sub> mobility with viscous foam, CO<sub>2</sub> may be diverted into zones that had previously not seen CO<sub>2</sub> to raise the sweep efficiency as demonstrated in a field trial using a nonionic surfactant developed by Dow and the University of Texas at Austin.<sup>137</sup>

Despite the advantages of nonionic surfactants for foam formation, their solubilities may be limited at high temperature, particularly at high salinity. As temperature increases, hydrogen bonding between the nonionic EO head groups and water becomes weaker, and the surfactant phase separates at the cloud point temperature. The cloud point temperature of nonionic surfactants decreases with an increase in salinity as the ions weaken the hydrogen bonding between water and the EO groups.<sup>59,61,116,139</sup>



Additionally, upon approaching the cloud point temperature, the viscosity of foams stabilized with a nonionic surfactant typically decreases markedly.<sup>18</sup> At temperatures above the cloud point, foams do not tend to form.<sup>18</sup> So far, reports on foams generated in porous media with a nonionic surfactant are typically below 70 °C at salinities in the range of 0 to 5% TDS.<sup>3,18,135,138</sup> It remains uncertain to what degree the cloud points can be raised for nonionic surfactants at high salinity, and whether these surfactants will stabilize strong foams with high apparent viscosities at high temperatures and salinities.

The objective of this study was to identify a nonionic alkyl ethoxylate surfactant with a relatively high degree of ethoxylation ( $C_{12-14}(EO)_{22}$ ) and thus high cloud point temperature for stabilization of a viscous  $CO_2$  foam at temperatures up to 90°C and a salinity up to 30 g/L NaCl. To choose this surfactant, the cloud point and oil-water (O-W) partition coefficients of eight nonionic surfactants were studied as a function of surfactant structure and/or aqueous phase salinity. The C-W partition coefficients of the nonionic surfactants were investigated in terms of surfactant structure, temperature, and pressure to give insight on the curvature of the emulsion (C/W foam in this case) and ultimately, surfactant transport in the  $CO_2$  EOR process<sup>47-49</sup>. The effect of  $C_{12-14}(EO)_{22}$  on the C-W IFT was studied by over a wide range in temperature and pressure. The phase behavior and interfacial properties are explained in terms of the interaction of the surfactant head groups and tails with the relevant fluid phases. The high cloud point and substantial IFT reduction for  $C_{12-14}(EO)_{22}$  enabled the formation of viscous C/W foam in porous media. The effects of temperature, salinity, total superficial velocity, foam quality (volumetric ratio of  $CO_2$  in total injected fluid) and surfactant concentration on the apparent viscosity in a 30 Darcy sand pack or a 1.2 Darcy glass bead pack are presented and explained in terms of the phase behavior, interfacial properties and existing foam models..<sup>42,43</sup> Furthermore, shear-thinning C/W foams with an apparent viscosity over 200 cP were

observed at a low superficial velocity in a 1.2 Darcy glass bead pack. Finally, the surfactant is demonstrated to stabilize viscous C/W foam in a 49 mD dolomite core with both co-injection and surfactant-alternating-gas (SAG) processes indicating it is a potential candidate for future field tests.

## **5.2 EXPERIMENTAL**

### **5.2.1 Materials**

Surfactants were gifts from Huntsman, Shell, Stepan and Dow, and used without further purification (Table 5.1). Research-grade carbon dioxide was used as received. Sodium chloride (NaCl, certified ACS, Fisher), calcium chloride dehydrate ( $\text{CaCl}_2 \cdot 2\text{H}_2\text{O}$ , 99+% Acros), magnesium chloride hexahydrate ( $\text{MgCl}_2 \cdot 6\text{H}_2\text{O}$ , Fisher), and isopropanol (certified ACS plus, Fisher) were used as received. 30-120 g/L NaCl brine and 0.8% TDS brine (5.98 g/L NaCl, 1.18 g/L  $\text{CaCl}_2 \cdot 2\text{H}_2\text{O}$ , 2.03 g/L  $\text{MgCl}_2 \cdot 6\text{H}_2\text{O}$ ) were prepared with deionized (DI) water (Nanopure II, Barnstead, Dubuque, IA) to obtain surfactant/brine solutions with surfactant concentrations from 0.01 to 1 % w/w.

### **5.2.2 Cloud point temperature**

For all the samples in this work, the cloud point temperature of the aqueous surfactant solution at 1.0% w/w in water/brine was first measured in a synthetic oil bath equipped with a temperature controller (Julabo MP immersion circulator) heated from 24 °C to 90 °C.<sup>57</sup> The cloud point was observed visually when surfactant solutions turn from clear to cloudy. For some samples with a cloud point above 90 °C, a second technique with a sealed glass pipette method was used to as described in our previous

publication to withstand the elevated pressure.<sup>40</sup> Each test was repeated three times for giving an average cloud point temperature. The error was  $\pm 1$  °C.

### **5.2.3 CO<sub>2</sub>-brine partition coefficient determination**

To determine the equilibrium partition coefficient, equal masses (5 g for each) of CO<sub>2</sub> and 0.8% TDS brine plus 0.5 or 1 g surfactant, were loaded in the front part of a stirred variable volume view cell following our earlier procedure.<sup>40,57,86</sup> After equilibration for two hours, samples of the upper CO<sub>2</sub> phase were recovered via a 6-port valve (Valco Instrument Co., Inc.) and a 100  $\mu$ L stainless steel loop (Valco Instrument Co., Inc.). The first 100  $\mu$ L in the loop was discarded and a composite sample was obtained by discharging five loads of the loop (500  $\mu$ L in total) into a vial with 3 mL DI water. The loop was flushed with a total of 2 ml of DI water followed with 10 mL of air (1 atm) to recover all of the surfactant and water. The sampling procedure was repeated twice to collect two separate samples. The surfactant concentrations of the collected sample solutions were determined with a pendant-drop surface tension measurement as reported previously<sup>57</sup> (The curve of surface tension versus surfactant concentration of C<sub>12-14</sub>(EO)<sub>22</sub> in 0.8% TDS brine is shown as an example of a calibration curve in Figure D1). The average surfactant concentrations were used to calculate the CO<sub>2</sub>-brine partition coefficients.

### **5.2.4 Interfacial tension measurement between CO<sub>2</sub> and aqueous surfactant solutions**

The interfacial tension between CO<sub>2</sub> and aqueous surfactant solution was determined from axisymmetric drop shape analysis of a captive bubble,<sup>56</sup> as described in detail previously.<sup>40,57,86</sup>

### 5.2.5 Foam formation and apparent viscosity in sand/glass bead packs

The apparatus for measurement of the foam viscosity in sand/glass bead packs up to 100 °C and 2551 psia is depicted in Figure 5.2. The experimental procedure for calculating the apparent viscosity of C/W foam from the pressure drop, for both the porous media foam generator and downstream capillary tube were the same as described in our previous publication<sup>40</sup>. In this work, the first porous media was a sand pack (14.7 cm long, 0.76 cm inner diameter (ID) tube) with a water permeability of 30 Darcy (calculated from Darcy's law for 1-D horizontal flow) and 32% porosity (2.1 mL pore volume) determined from the mass of loaded material. The non-spherical sand was 420-840  $\mu\text{m}$  in diameter (20-40 mesh). It was washed with copious amounts of water and ethanol. The sand was held in place by a 100 mesh wire screen at each end of the pack. The second porous media was a 1.2 Darcy (determined by the same method described above) glass bead pack (a 20.9 cm long, 1.73 cm inner diameter tube holding pre-washed 30-50  $\mu\text{m}$  in diameter spherical particles from Polysciences, Inc.). The glass beads were held in place by two cylindrical stainless steel screen holders (1.5 cm long, 1.70 cm outer diameter, 0.42 ID), each of which held a 100 mesh and 500 mesh wire screens in series to give an effective pack length of 17.9 cm. A Buna N O-ring (McMaster-Carr, Dash number 014) sealed each screen holder against the inner wall of the pressure vessel. (Photos for the screen holder is shown in Figure D2.) The porosity of the glass bead pack was 36%, and the pore volume is 15.2 mL. The stainless steel capillary tube for measuring bulk foam viscosity had a 762  $\mu\text{m}$  ID was 1.95 m in length. In addition to the three original differential pressure transducers in the setup from our previous work<sup>40</sup>; one additional transducer (Validyne, model DP22) with a 1000 psi diaphragm was inserted. Also, a Swagelok 177-R3A-K1-D spring (1500-2250 psia) or a 177-R3A-K1-E spring (2250-3000 psia) was used to maintain the system pressure in a heated (75 °C,

with a water bath) back pressure regulator (BPR) (Swagelok model SS-4R3A adjustable relief valve) at the end of the apparatus.

### **5.2.6 Core flood**

The schematic of the core flooding apparatus is shown in Figure 5.3. High pressure CO<sub>2</sub> and surfactant solution were injected by ISCO dual-pump system (E260, from Teledyne ISCO Inc.) and HPLC pump (Lab Alliance Series III), respectively. A Silurian dolomite core (3.81 cm in diameter, 7.59 cm in length) was vacuumed to approximately 0 pisa, and then saturated with water to obtain the pore volume (15.5 mL) and porosity (17.9%). The permeability was measured with the same method in the literature<sup>40</sup>, and was equal to 49 mD. The system pressure at the outlet of the core and pressure drop across the core was measured by two pressure transducers (Validyne, model DP 303) with ranges of 5000 psi and 500 psi respectively. The surfactant water solution and CO<sub>2</sub> were either co-injected at 80% foam quality or alternately with a repeated pattern of 0.1 PV surfactant solution/0.4 PV CO<sub>2</sub> both at a total superficial velocity of 4 ft/day, 25 °C and 3400 psia. The pressure drop across the core was recorded, and foam apparent viscosity was calculated through the same method reported previously based on Darcy's law.<sup>40</sup> The effluent out of the core flew into a two-stage relief valves (RV) (Swagelok, SS-4R3A-KZ). The upstream RV (with a 177-R3A-K1-F spring, 3000-4000 psia) was set at 3400 psia as the system pressure, while the downstream one (with a 177-R3A-K1-C spring, 750-1500 psia) was set at 1200 psia. Water is injected through the RVs to keep them open for reducing fluctuation in back pressure. Heating tapes (BriskHeat, HSTAT051006) were used to maintain the BPR system at 82 °C. After each test, the core was depressurized to atmosphere pressure and flushed by water to restore

the original permeability before the next experiment. Core flood experiments were conducted by Dr. Leyu Cui at Rice University.

### **5.2.7 Oil-brine partition coefficient determination**

The partition coefficient of a surfactant between 0.8% TDS brine and dodecane was determined at 40 °C and 1 atm. 3.5 mL of dodecane was added to an equal volume of 1 % w/w surfactant solutions in 0.8% TDS brine. The mixtures were equilibrated in an oven at 40 °C for 48 h. The partition coefficient of surfactant between the brine and dodecane was investigated by measuring the surfactant concentration in a sample obtained from the aqueous phase with a pendant-drop surface tension measurement procedure reported previously<sup>57</sup>.

## **5.3 RESULTS AND DISCUSSION**

### **5.3.1 Cloud point temperature**

An aqueous micellar surfactant solution separates into a surfactant rich and a surfactant poor phase as the temperature is raised to the cloud point.<sup>139</sup> The phase separation results from dehydration of the surfactant head group, which weakens electrostatic repulsion between micelles relative to van der Waals attraction.<sup>139</sup> For EO head groups, the dehydration at high temperatures is due to the loss of the hydrogen bonding between water and the ether oxygen atoms.<sup>98</sup>

Table 5.2 shows the effect of surfactant structure and salinity on the cloud point of a series of nonionic surfactants at different salinities. Increasing the EO number or decreasing the carbon tail length caused an increase in the cloud point in agreement with well-established trends.<sup>59,140</sup> For example, at 90 g/L NaCl, increasing the number of EO

groups from 9 to 22 with a C<sub>12-15</sub> tail raised the cloud point from 58 °C to 83 °C. Here, the larger number of EO groups adds hydrophilicity, given the hydrogen bonding with water.<sup>139</sup> For C<sub>9-11</sub>(EO)<sub>8</sub> versus C<sub>12-15</sub>(EO)<sub>9</sub> in DI water, decreasing the tail length raised the cloud point by 9 °C. For longer alkyl tails, the added hydrophobicity increases micelle aggregation number and micellar size which enhances van der Waals attractions and consequently lowers the cloud point.<sup>141</sup> The effect of addition of NaCl for all tested surfactants was similar whereby added salt weakened the head group hydration and depressed the cloud point, so called “salting out”.<sup>32</sup> The reduction in hydration is attributed to the water structure making nature of Na<sup>+</sup> which decreases the number of water molecules available for hydrogen bonding with the EO head.<sup>59,142</sup> Among all tested surfactants, C<sub>12-14</sub>(EO)<sub>22</sub> showed the highest salt tolerance with a cloud point of 76 °C at a salinity of 120 g/L NaCl. Notice the addition of propylene-oxide (PO) units as a linker between the hydrocarbon tail and the EO head causes a decrease in the cloud point.<sup>143</sup> Perez et al gave two reasons for this behavior: first, an increase in the lipophilicity of the surfactant and secondly, the dehydration of the PO groups as temperature increases.<sup>143</sup>

### 5.3.2 CO<sub>2</sub>-brine partition coefficient

The CO<sub>2</sub>-brine partition coefficients of three nonionic surfactants with very similar hydrocarbon tails (C<sub>12-14</sub>(EO)<sub>22</sub>, C<sub>12-15</sub>(EO)<sub>12</sub> and C<sub>12-15</sub>(EO)<sub>9</sub>) between CO<sub>2</sub> and 0.8% TDS brine solution at 24 and 40 °C, 1700 psia are presented in Table 5.3. In each case, the partition coefficient decreased (higher HCB) with an increase of EO number as the increase in hydrogen bonding drove the surfactants towards the aqueous phase. Also, the partition coefficient decreased when temperature increased at a constant pressure. Here, the decrease in density and thus solvent strength of CO<sub>2</sub> lowered tail solvation. Moreover, the increase in temperature also weakened the hydrogen bonding of

the head groups.. In total, reduction of tail solvation in the CO<sub>2</sub> phase was greater than the weakening of the head group hydration since the HCB increased.

In addition, the partition coefficients of both C<sub>12-14</sub>(EO)<sub>22</sub> (0.020) and C<sub>12-15</sub>(EO)<sub>9</sub> (0.226) between CO<sub>2</sub> and the low salinity 0.8% TDS brine were much lower than that of 2-ethxylhexyl-(PO)<sub>5</sub>(EO)<sub>8</sub> (~3) at 24 °C, 2000 psia (CO<sub>2</sub> density ~0.87) as reported previously<sup>57</sup>. Here, the higher partition coefficient for 2-ethxylhexyl-(PO)<sub>5</sub>(EO)<sub>8</sub> at the same temperature and similar CO<sub>2</sub> density may be attributed to the lower degree of ethoxylation,<sup>144</sup> the more CO<sub>2</sub>-philic tail due to branching<sup>36</sup> and the additional CO<sub>2</sub>-philic PO groups.<sup>144</sup>

### 5.3.3 Interfacial tension at CO<sub>2</sub>-brine interface

The IFT between CO<sub>2</sub> and 0.8% TDS brine in the presence of 1% w/w C<sub>12-14</sub>(EO)<sub>22</sub> in the aqueous phase as a function of CO<sub>2</sub> pressure (density) at 24-60 °C is presented in Table 5.4. At 24 °C, the IFT decreased from 8.2 mN/m at 940 psia to 7.3 mN/m at 1700 psia. Also, at a constant pressure of 1700 psia, the IFT increased with temperature from 7.3 mN/m at 24 °C to 9.3 mN/m at 60 °C. The decrease in IFT with an increase of pressure may be explained by: 1) the decrease of the IFT for the CO<sub>2</sub>-aqueous binary system without surfactant ( $\gamma_0$ ).<sup>57,95</sup> and 2) an increase in CO<sub>2</sub> density, whereby the tail solvation increases and the HCB decreases towards a more balanced state that is, the surfactant migrates from the aqueous phase to the interface (Figure 5.1). When temperature increases at a constant pressure,  $\gamma_0$  increases for a CO<sub>2</sub>-aqueous binary system without a surfactant.<sup>57,95</sup> Furthermore, the increase of temperature at a constant pressure leads to a decrease of head solvation in aqueous phase ( HCB decreases) and a decrease in tail solvation in CO<sub>2</sub> as the density decreases (HCB increases). The combination of all of these changes leads to an increase in  $\gamma$ .



### **5.3.4 Foam formation and apparent viscosity in sand/glass bead pack**

#### ***5.3.4.1 Effect of temperature and salinity on apparent viscosity at high superficial velocity***

The apparent viscosity of C/W foams stabilized with 1% w/w C<sub>12-14</sub>(EO)<sub>22</sub> brine solution in a 30 Darcy sand pack at 90% foam quality, total superficial velocity 622 ft/day and constant CO<sub>2</sub> density of 0.413 g/mL is shown in Table 5.5. The condition of constant CO<sub>2</sub> density was chosen to maintain relatively constant tail solvation in CO<sub>2</sub>. In the presence of 90 g/L NaCl, stable C/W foams (apparent viscosity > 7 cP) were formed at temperatures up to 80 °C. At 30 g/L NaCl, C/W foams were stable to an even higher temperature of 90 °C. At lower temperatures (for example, 60 °C or below) at a constant pressure of 1700 psia, the apparent viscosity of the foam was insensitive to salinity as shown in Figure 5.4. For example, at 60 °C the apparent viscosities were 9.6 at 0.8% TDS and 11.6 at 90 g/L NaCl. In addition, the apparent viscosity decreased when temperature was increased. For example, at 90 g/L NaCl and 1700 psia, it decreased from 23 cP at 25 °C to 12 cP at 60 °C, as also demonstrated in Figure 5.4.

The surfactant C<sub>12-14</sub>(EO)<sub>22</sub> stabilized a C/W foam in the porous media at 80 °C at a high salinity brine of 90 g/L NaCl. To our knowledge, it is very unusual to form C/W foam in porous media with a nonionic surfactant at such high salinity and temperature.<sup>3,18</sup> For nonionic surfactants, the viscosity of foams typically decreases significantly upon approaching the cloud point.<sup>18</sup> For C<sub>12-14</sub>(EO)<sub>22</sub> the high cloud point of 83 °C in 90 g/L NaCl (Table 5.2) ensured that the surfactant remained well solvated in the aqueous thin film lamellae to stabilize the foam despite the harsh temperature and salinity conditions. However, at 90 °C, the foam was not formed as the temperature exceeded the cloud point. Here the precipitation of a surfactant rich phase destabilizes the aqueous lamellae.<sup>145</sup> At

a lower salinity of 30 g/L NaCl, as the cloud point increased to 111 °C (Table 5.2), foam was formed at an even higher temperature of 90 °C.

At a constant salinity and pressure, the decrease of apparent viscosity of the C/W foams in the porous media with temperature will now be partially explained in terms of the reduction of the viscosity of the aqueous phase viscosity,  $\mu_e$ . This behavior may be described with a model for foam flow in porous media developed by Hirasaki and Lawson with smooth capillaries.<sup>42</sup> Here, the foam flows as bubbles through a bundle of interconnected parallel capillaries with diameters smaller than the gas bubble diameter. The apparent viscosity of foam in this capillary model is the sum of three terms on the right side of Equation 5.1 in sequence: (1) resistance from slugs of liquid between bubbles, (2) the resistance to deformation of the interface of a bubble passing through the capillary, and (3) the surface tension gradient that results when surface active materials is swept from the front of a bubble and accumulates at the back edge

$$\begin{aligned} \frac{\mu_{foam}}{\mu_e} = & L_s n_L + 0.85 \frac{(n_L R_c)}{(r_c/R_c)} \left( \frac{3\mu_e U}{\gamma} \right)^{-\frac{1}{3}} [(r_c/R_c)^2 + 1] \\ & + (n_L R_c) \left( \frac{3\mu_e U}{\gamma} \right)^{-\frac{1}{3}} \sqrt{N_s} \frac{(1 - e^{-N_L})}{(1 + e^{-N_L})} \end{aligned} \quad [5.1]$$

where  $L_s$  is length of liquid slugs,  $n_L$  is lamellae density (the number of equivalent lamellae per unit length),  $r_c$  is radius of curvature of gas-liquid interface,  $R_c$  is capillary radius,  $U$  is velocity of bubble, and  $N_s$  is a dimensionless number for interfacial tension gradient effect, and  $N_L$  is a dimensionless bubble length. A decrease in the viscosity of the aqueous phase viscosity,  $\mu_e$  with an increase in temperature will produce an increase in  $\mu_{foam}/\mu_e$  with a weak exponent of -1/3 in the second two terms, but overall an decrease in  $\mu_{foam}$ .

Furthermore, a higher temperature will now be shown to lead to a higher film drainage velocity<sup>18,45</sup>, and a greater degree of hole formation and thus rupture of thin film lamellae<sup>44,96</sup>. Both the faster drainage and greater hole formation cause a shorter lifetime for the lamellae, resulting in a decrease in lamellae density and thus a decrease in the apparent viscosity of the foams in the porous media.<sup>5,42</sup> The pressure difference in the lamellae between the plateau border and the thin film,  $\Delta P_{film} = 2(P_c - \Pi_d)$ <sup>46</sup> (where  $P_c = 2\gamma/R$  is capillary pressure at the plateau border of a curvature radius of R, and  $\Pi_d$  is disjoining pressure) gives a drainage velocity

$$V = -\frac{dh_f}{dt} = \frac{h_f^2}{3\mu_e R_f^2} \Delta P_{film} \quad [5.2]$$

where  $R_f$  and  $h_f$  are the radius and thickness for the thin film.<sup>98</sup> As  $\mu_e$  decreases when temperature increases,  $V$  increases as shown in Equation 5.2. Further, more rapid formation of holes may occur in the thin film lamellae from greater thermal fluctuations at a higher temperature.<sup>44,96</sup> When the radius of the hole is higher than a critical value, it causes rupture of the lamellae. As the films become thinner, the work for creating a hole  $W_h \cong \frac{h_f^2 \gamma_h^2}{\gamma_p}$  (where  $W_h$  is the activation energy for hole formation,  $\gamma_p$  and  $\gamma_h$  are the interfacial tensions at the planar interface and a curved border of the hole) decreases.<sup>44</sup> This change increases the probability of hole formation,  $\exp(-W_h/kT)$ <sup>44,96</sup> resulting in faster coalescence of the dispersed phase bubbles. The faster drainage, and greater hole formation and coalescence reduce the number of lamellae and lower the apparent viscosity of the foam.

At temperatures well below the cloud point at constant pressure, the apparent viscosity was affected only slightly by salinity over a wide range (0.8% TDS to 90 g/L NaCl). This result is desirable for industrial application in CO<sub>2</sub> EOR, as the surfactant may be injected in an aqueous media at a different salinity than that inside reservoir. In

this case, the surfactant may be able to produce foam and reduce CO<sub>2</sub> mobility throughout the reservoir even with salinity variation based on the injected fluid.

#### ***5.3.4.2 Minimum pressure gradient for foam generation***

Figure 5.5 shows the effect of total superficial velocity on the pressure gradient in the 30 Darcy sand pack upon simultaneous injection of 1% w/w C<sub>12-14</sub>(EO)<sub>22</sub> 0.8% TDS brine solution and CO<sub>2</sub> at 90% foam quality, 40 °C, and 1700 psia. When the total superficial velocity was below ~80 ft/day, the pressure gradient across the sand pack was low (<1 psi/ft) and foam was not formed. As the velocity was increased to 83 ft/day, an abrupt increase in the pressure gradient was observed at ~ 0.56 psi/ft, indicating an generation of stronger foam.<sup>133</sup> This value of 0.56 psi/ft is the minimum pressure gradient (MPG) for foam generation<sup>133</sup>, which is consistent with an earlier study<sup>112</sup> as discussed in Appendix A. Above this pressure gradient, lamellae were mobilized to allow foam generation through mechanisms including lamellae division and repeated snap-off.<sup>5,134</sup> Foam generation at a low pressure gradient (~1 psi/ft) is important for EOR when the injection rate is low.<sup>133</sup> It may be aided further in reservoir rock due to heterogeneity, which promotes lamella generation through snap-off because of local fluctuations in capillary pressure as permeability changes.<sup>146</sup>

#### ***5.3.4.3 Effect of total superficial velocity and shear thinning on apparent viscosity***

In Figure 5.6, the results are combined for both 30 Darcy sand pack and 1.2 Darcy glass bead pack to illustrate the effect of shear thinning on the apparent viscosity. For the 30 Darcy sand pack at a relative low velocity (<80 ft/day), the pressure gradient is low as shown in Figure 5.5 giving an apparent viscosity below 2 cP. As shown in Figure 5.6, the apparent viscosity increased to a maximum of ~16 cP at ~160 ft/day as the increase in superficial velocity produces a pressure gradient that exceeds the minimum

pressure gradient for foam generation. As the density of lamellae increases, a strong foam forms in the porous media with an apparent viscosity an order of magnitude higher than at the lowest superficial velocity as depicted in Figure 5.6. At higher superficial velocities, the apparent viscosity decreased to  $\sim 10$  cP at  $\sim 600$  ft/day indicating shear-thinning behavior.

The effect of total superficial velocity on apparent viscosity of C/W foam stabilized with 1% w/w  $C_{12-14}(EO)_{22}$  or  $C_{12-15}(EO)_9$  0.8% TD brine solution in a 1.2 Darcy glass bead pack at 80% foam quality, at the same temperature is shown in Figure 5.6. The apparent viscosities of the two surfactants with similar  $C_{12-14}$  and  $C_{12-15}$  alkyl tails but different EO chain lengths were very similar over the range of the total superficial velocity tested. At a low total superficial velocity between 6-10 ft/day, both surfactants stabilized C/W foams with high apparent viscosity of 210 to 220 cP. When the velocity further increased to  $\sim 200$  ft/day, the foam viscosity decreased by about one order of magnitude, which also indicates a shear thinning behavior in the 1.2 Darcy glass bead pack as well.. For industrial application in  $CO_2$  EOR, a shear-thinning foam is beneficial for low apparent viscosity in the near well-bore area for high injectivity and yet a higher viscosity for low gas mobility and oil displacement in the areas that are far away from the injection well at a much lower flow velocity.

For both of the porous media in Figure 5.6, the shear-thinning behavior for foam flow in the porous media may be explained from the model developed by Hirasaki and Lawson<sup>42</sup> with smooth capillaries as shown in Equation 5.1. When a single bubble moves inside one single capillary tube, the thickness of a thin liquid film between the bubble and the wall of the capillary increases when gas phase velocity increases given greater bubble deformation. This increase in thickness changes the curvature of the bubble and also increases the pressure drop across the bubble.<sup>127</sup> The pressure drop across the bubble

becomes proportional to the 2/3 power of the gas phase velocity<sup>127</sup>, and thus, the apparent viscosity decreases as the -1/3 power of the gas phase velocity (as shown by the second term on the right side of Equation 5.1)<sup>42</sup>. Moreover, as the bubbles flow in the capillary, surfactant is dragged to the rear side of the bubbles, generating interfacial tension gradients disfavoring flow of the bubble, due to the Gibbs-Marangoni effect. Here, the contribution from the interfacial tension gradient on apparent viscosity is also proportional to the -1/3 power of gas phase velocity (as shown by the third term on the right side of Equation 5.1)<sup>42</sup>. Thus both the second and third terms in Equation 5.1 describe the shear thinning of the foam in porous media as seen in Figure 5.6. .

#### ***5.3.4.4 Effect of surfactant concentration on apparent viscosity***

The effect of surfactant concentration on apparent viscosity of C/W foam stabilized C12-14(EO)22 0.8% TDS brine solution in the 1.2 Darcy glass bead pack is shown in Figure 5.7. When the surfactant concentration was <0.1% w/w in the brine, no foam was formed. Above 0.1% w/w surfactant, apparent viscosity increased abruptly reaching a roughly constant value of ~200 cP at 0.5% w/w surfactant., This threshold surfactant concentration of 0.5% w/w in the aqueous phase is usually many times higher than the CMC of the surfactant.<sup>147</sup> Surfactant micelles present in lamellae act as reservoirs to provide surfactant to form new lamellae during the lamellae division.<sup>5,80</sup> . With further increasing surfactant concentration up to 1% w/w, the large number of micelles did not appear to contribute to the apparent viscosity. Similar critical surfactant concentrations and plateaus in foam viscosities were observed in core floods by others.<sup>130,131</sup>

#### ***5.3.4.5 Effect of foam quality on apparent viscosity***

The effect of foam quality on the apparent viscosity of C/W foams stabilized with 1% or 0.1% w/w C12-14(EO)22 0.8% TDS brine solution in the 30 Darcy sand pack at a total superficial velocity of 156 ft/day, at 40 oC and 1700 psia is shown in Figure 5.8. At a surfactant concentration of 1% w/w, as the foam quality increased from 35%, the apparent viscosity first increased and reached a maximum of 16 cP at 90% foam quality. With a further increase foam quality from 90% to 95%, the apparent viscosity declined dramatically and no foam was formed at 95% as indicated by the low apparent viscosity of 0.3 cP. When the surfactant concentration in the brine was only 0.1% w/w, a similar trend was observed. However, at this lower surfactant concentration, a plateau value in the apparent viscosity of ~6 cP was observed at 64-80% foam quality in contrast with a sharp peak at 90% foam quality in the case of 1% w/w surfactant. Below 64% or above 80%, the apparent viscosity was below 3.5 cP. Figure 5.9 shows the effect of foam quality on the apparent viscosity of C/W foams stabilized with 1% w/w C12-14(EO)22 0.8% TDS brine in the 1.2 Darcy glass bead pack at total superficial velocity 6 ft/day. As was also seen in Figure 5.7, the apparent viscosity went through a maximum, but with a much larger value reaching 348 cP given the small amount of shear thinning at the low superficial velocity.

In porous media, aqueous films separate the CO<sub>2</sub> bubbles from each other, and from the wall of the inner channels of the porous media. As the foam quality increases from a low value (for example below 40%), the bubble population and number of lamellae increases since bubble size can be assumed to be a constant.<sup>67,134</sup> The higher lamellae density<sup>42</sup> and also the thinner aqueous films between the bubbles and the channel wall increase the flow resistance and thus the apparent viscosity.<sup>42, 127</sup> At the same time as the foam quality increases for mineral surfaces wet by water, the water

saturation in the porous media decreases and capillary pressure increases until a “limiting capillary pressure” is reached in the porous media<sup>43</sup>. Upon increasing foam quality beyond the limiting capillary pressure, the surfactant provides insufficient disjoining pressure against the capillary pressure.<sup>113,128</sup> , . Here the lamellae rupture and the coarser foam texture (i.e. lower lamellae density) leads to a reduction of the apparent viscosity as shown at 90-95% foam quality at the surfactant concentration of 1% w/w in the brine, Figure 5.8.<sup>43</sup> Further discussion of limiting capillary pressure is given in Appendix A. As shown in Figure 5.8, the higher surfactant concentration stabilized lamellae at a higher quality, indicating a higher limiting capillary pressure. Other researchers, for example, Lee and Heller, also found that a higher surfactant concentration resulted in greater mobility control using CO<sub>2</sub> foam.<sup>131</sup> This finding in C/W foam is also consistent with the results of Alvarez et al<sup>68</sup> on the relationship between the surfactant concentration and the foam quality.

In addition to the behavior in the 30 Darcy sand pack, the effect of foam quality on the apparent viscosity of the foams stabilized with 1% w/w C<sub>12-14</sub>(EO)<sub>22</sub> 0.8% TDS brine solution in a capillary (ID: 762 μm) downstream of the porous media was also investigated as shown in Figure D3. The apparent viscosity in the capillary was very close to that in the 30 Darcy sand pack, which was observed similarly in our previous foam study with ethoxylated amine surfactants<sup>40</sup>.

In the 1.2 Darcy glass bead pack at a low total superficial velocity of 6 ft/day, the highest viscosity (~350 cP) was achieved at a foam quality of 60% lower than the value of 90% in the 30 Darcy sand pack at 156 ft/day. This shift of the foam quality at the viscosity maximum has been explained by the higher capillary resistance in a lower permeability system.<sup>67,68</sup> For the foam in the capillary.in the downstream of the 1.2



Darcy glass bead pack, the apparent viscosity in the capillary was much lower than the value in the porous media (Figure D4).

### 5.3.5 Apparent viscosity of C/W foam in core floods

C/W foams stabilized with  $C_{12-14}(EO)_{22}$  were investigated in core floods through co-injection and SAG process at total superficial velocity 4 ft/day, 25 °C, 3400 psia. The apparent viscosity history for co-injection of 1% w/w  $C_{12-14}(EO)_{22}$  water solution or DI water and  $CO_2$  in a 49 mDarcy dolomite core at 80% foam quality is shown in Figure 5.10. In the presence of  $C_{12-14}(EO)_{22}$ , the apparent viscosity increased gradually and reached ~60 cP at 2 PV. With further injection, the apparent viscosity remained at a plateau value indicating steady state. In the absence of the surfactant, the apparent viscosity was below 3 cP. In addition, the apparent viscosity history for SAG process of injecting 1% w/w  $C_{12-14}(EO)_{22}$  water solution or DI water and  $CO_2$  in the 49 mDarcy dolomite core at, 80% foam quality (0.1 PV aqueous solution /0.4 PV  $CO_2$ ) is shown in Figure 5.11. The apparent viscosity in the SAG process also generally increased with an increase of the number of injected PVs. The highest apparent viscosity of ~100 cP was reached at ~2.5 PV at the end of a  $CO_2$  injection cycle as shown in Figure 5.11. Without the surfactant, similar as the co-injection process, the apparent viscosity was low (<5 cP) in the porous media.

For both injection strategies, apparent viscosity in the porous media was ~30 times higher in the presence of 1% w/w the surfactant in the aqueous phase than the cases without any surfactant. This demonstrates that  $C_{12-14}(EO)_{22}$  is a good agent for stabilizing viscous C/W foams in a core (49 mD) at a low velocity close to the conditions away from the injection well in reservoirs for gas mobility control. For the SAG process, the capillary pressure increases during  $CO_2$  injection and decreases in aqueous injection

in each injection cycle. The fluctuation in the capillary pressure is beneficial for foam generation through snap-off mechanism.<sup>5,146</sup> Also, lamellae form through leave-behind during the injection of CO<sub>2</sub> in the SAG process.<sup>5</sup> The above two effects may explain the higher apparent viscosity in the SAG process than in the co-injection process.

### **5.3.6 Partition coefficient between dodecane and 0.8%TDS brine**

Table 5.6 shows the dodecane/brine partition coefficient of several nonionic surfactants between dodecane and 0.8% TDS brine at 40 °C below the cloud point temperature for all surfactants. The partition coefficient was found to decrease with an increase in EO number or a decrease in hydrocarbon tail length as expected. For example, with the same C<sub>12-14</sub> tail, as the number of EO groups increased from 12 to 22, the partition coefficient decreased from 0.43 to 0.09. These trends are consistent with previous data reported and can be attributed to the enhanced hydrogen bonding between the head groups and the water molecules.<sup>98,148,149</sup> Furthermore, increasing the hydrophobic tail length requires an unfavorable free energy for solubilizing the methyl group in water resulting in an increase in the surfactant partitioning to oil.<sup>124</sup> As a result of these factors, the partition coefficient was lowest for C<sub>12-14</sub>(EO)<sub>22</sub>. This low value is important to produce low losses of surfactant to residual oil in CO<sub>2</sub> EOR<sup>52</sup>.

## **5.4 CONCLUSIONS**

The high EO number for C<sub>12-14</sub>(EO)<sub>22</sub> provided a high cloud point of 83 °C even in 90 g/L NaCl brine) and enabled formation of C/W foams up to 80 °C. The high EO number resulted in a low oil/brine partition coefficient, which is beneficial for lowering loss of surfactant to oil in the reservoir. The strong hydration of the head group and relatively weak solvation of the alkyl tail in CO<sub>2</sub>, resulted in a low C-W partition coefficient and thus a C/W curvature consistent with the Bancroft rule. The C-W

partition coefficient decreased with CO<sub>2</sub> density and thus tail solvation, or an increase in the number of EO groups. Despite the low C-W partition coefficient at a CO<sub>2</sub> density of ~0.85 g/mL, there was still sufficient affinity for C<sub>12-14</sub>(EO)<sub>22</sub> to the C-W interface to lower the IFT to ~7 mN/m.

The favorable HCB and interfacial properties led to stable C/W foam with an apparent viscosity of ~11 cP at 60 °C in a high permeability (30 darcy) sand pack in the presence of 90 g/L NaCl brine. At lower velocities, the apparent viscosity increased abruptly above the minimum pressure gradient required to overcome capillary forces and mobilize the lamellae, and then decreased at high superficial velocities due to shear thinning. In a lower permeability (1.2 darcy) glass bead pack, the maximum viscosity reached ~350 cP at a low superficial velocity of 6 ft/day at 60% foam quality. Shear-thinning behavior was observed in both the glass bead pack and the sand pack, as described in Hirasaki and Lawson's model for smooth capillaries.<sup>42</sup> This shear-thinning behavior in porous media may be beneficial for field applications, where a low viscosity foam is desired near the well-bore for high injectivity and a more viscous foam is desired away from the well-bore for mobility control. In addition, C<sub>12-14</sub>(EO)<sub>22</sub> stabilized C/W foam with an apparent viscosity of 80-100 cP in a 49 mD dolomite core with both co-injection and a SAG process.

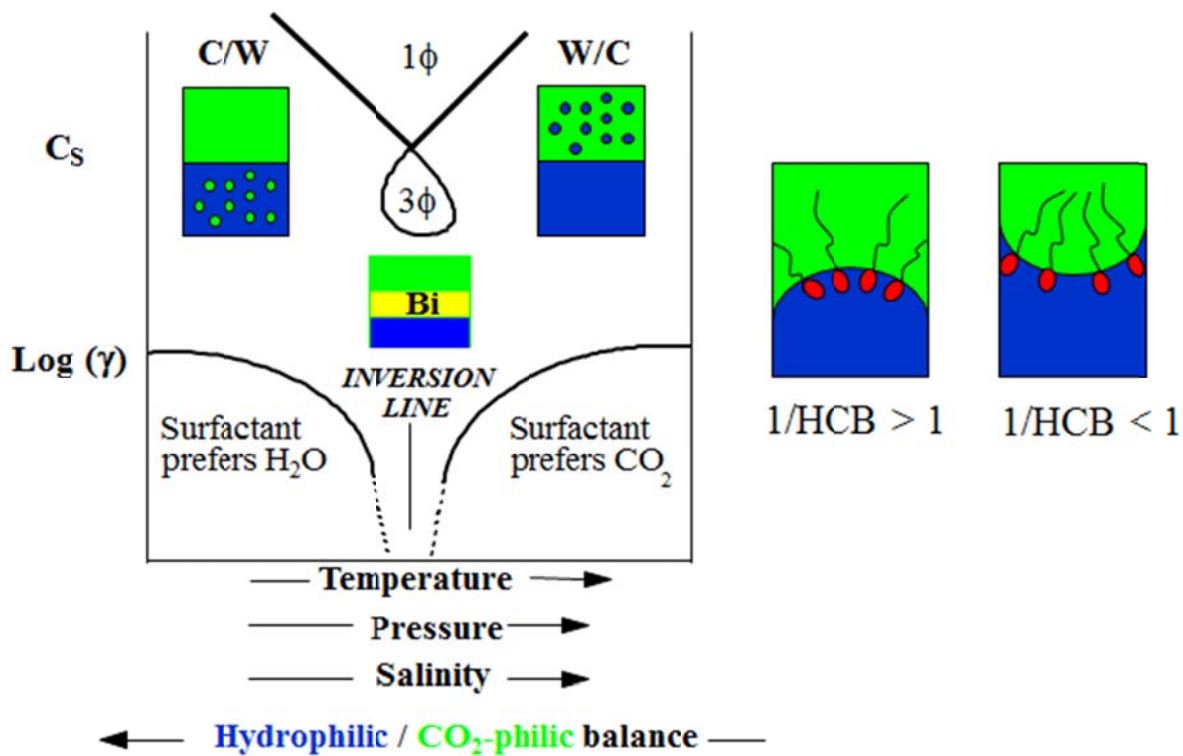


Figure 5.1: Effect of formulation variables on the phase behavior and interfacial tension of CO<sub>2</sub>-water-nonionic surfactant system

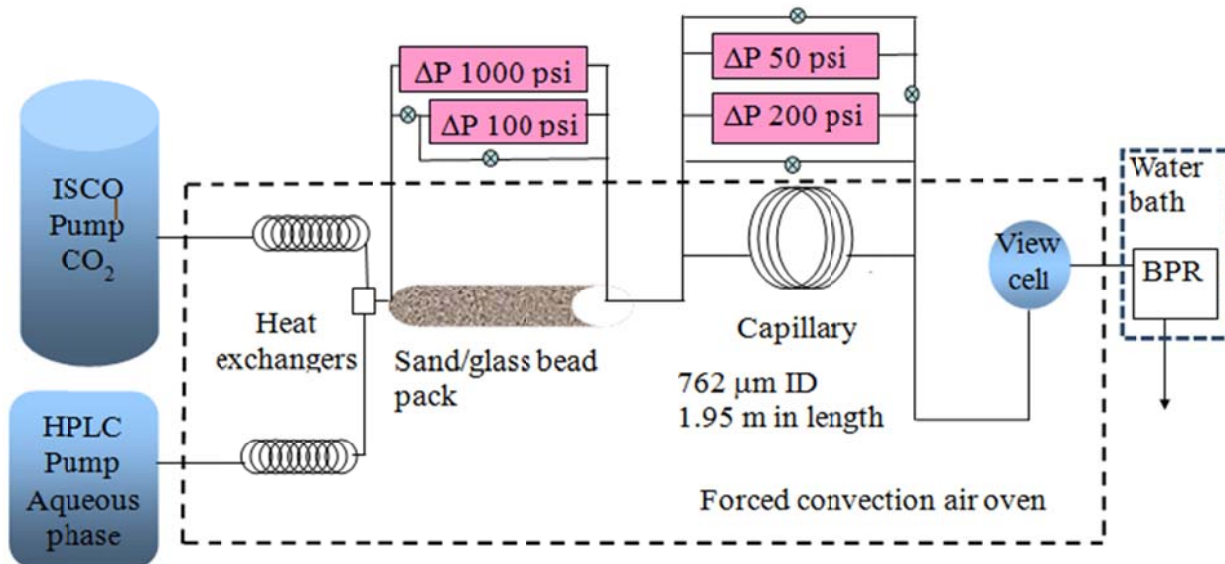


Figure 5.2: Schematic of equipment used for CO<sub>2</sub>-water foam viscosity measurements. BPR: back pressure regulator.

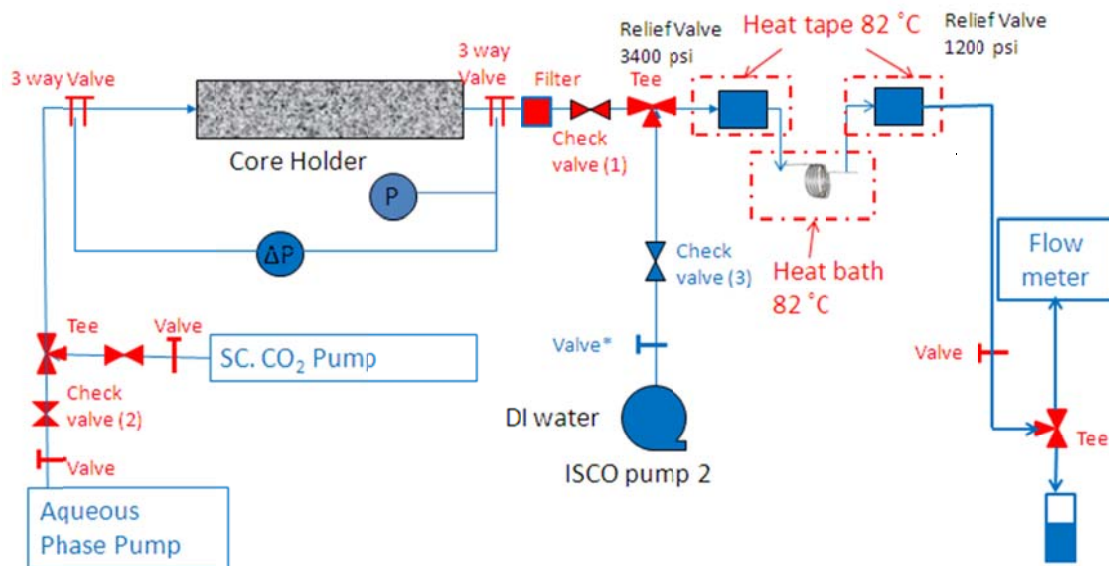


Figure 5.3: C/W foam core flood apparatus

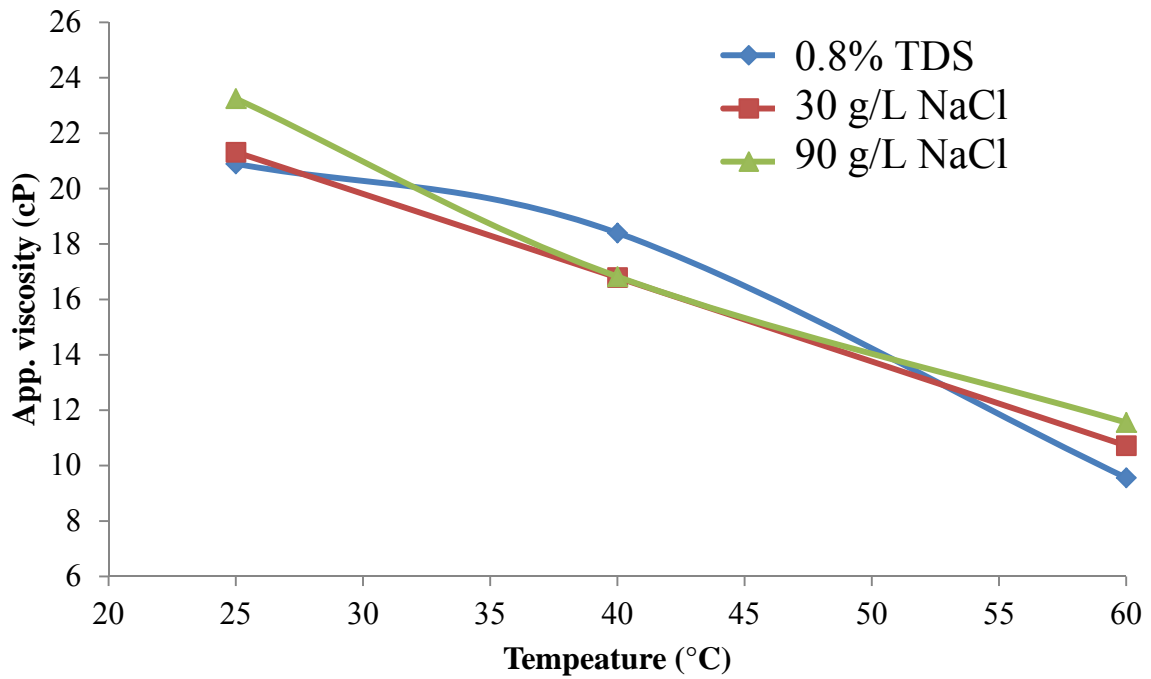


Figure 5.4: Temperature and salinity effects on the apparent viscosity of C/W foams stabilized with 1% w/w  $C_{12-14}(EO)_{22}$  brine solution in a 30 Darcy sand pack at 25-60 °C, in the presence of 0.8% TDS brine, 30 g/L NaCl brine or 90 g/L NaCl brine at 90% foam quality, total superficial velocity 622 ft/day and 1700 psia

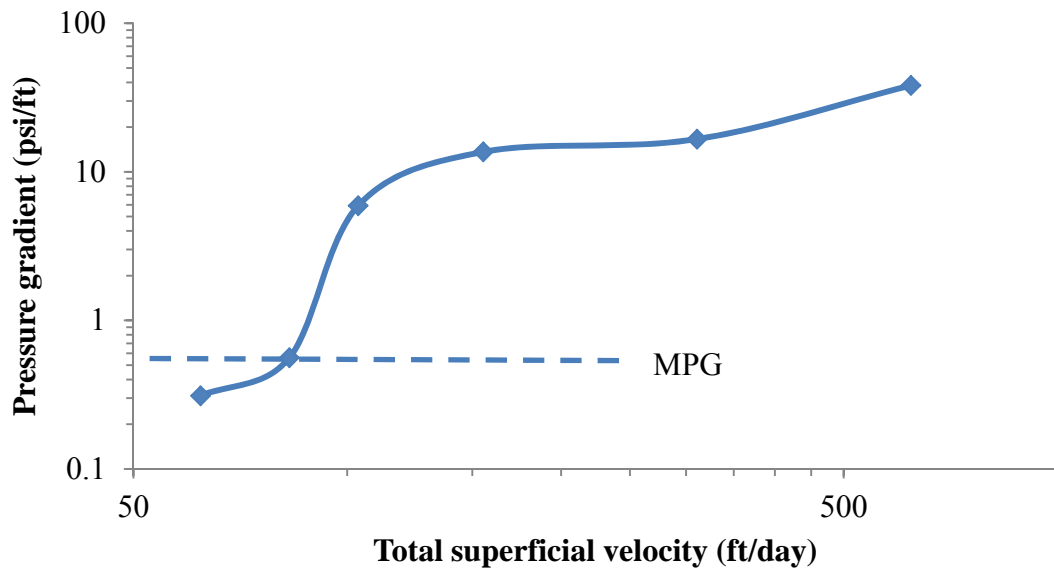


Figure 5.5: Effect of total superficial velocity on the pressure gradient in a 30 Darcy sand pack for co-injection of 1% w/w  $C_{12-14}(EO)_{22}$  0.8% TDS brine with  $CO_2$  at 90% foam quality, 40 °C and 1700 psia. The minimum pressure gradient (MPG) for foam generation is marked with a dash line.

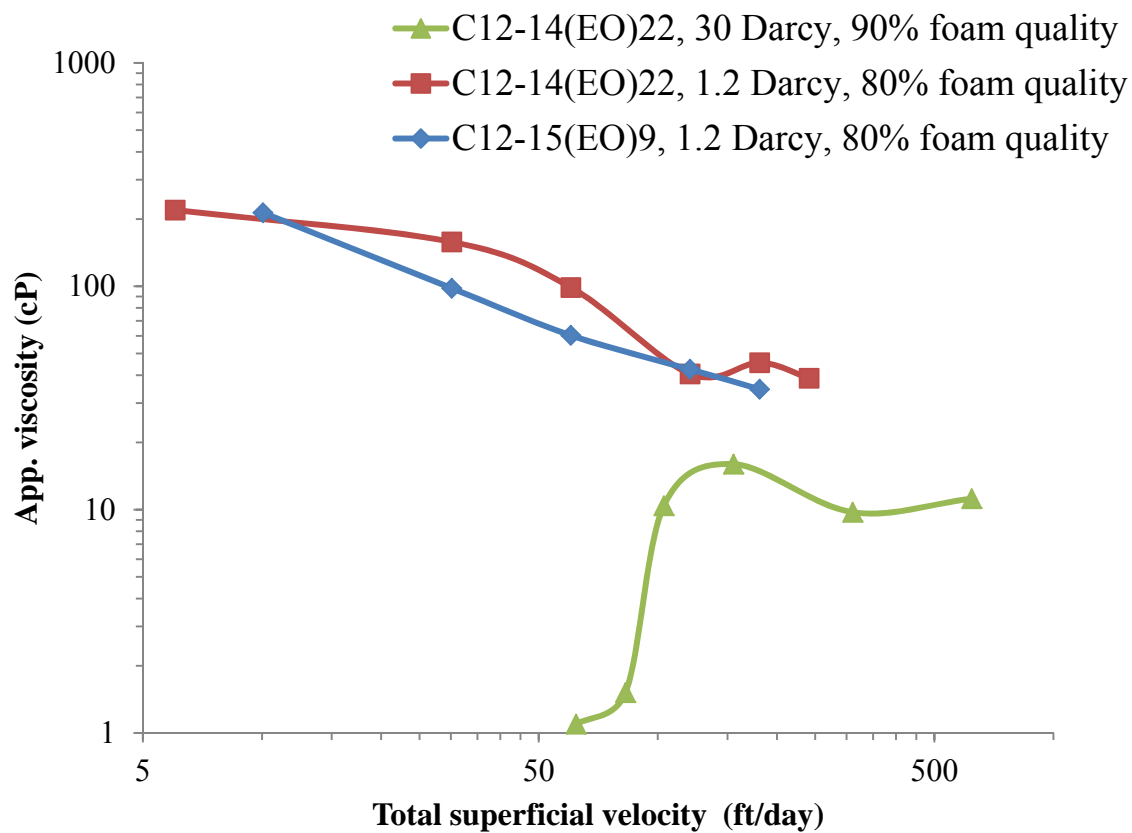


Figure 5.6: Effect of total superficial velocity on apparent viscosity of C/W foams stabilized with 1% w/w C<sub>12-14</sub>(EO)<sub>22</sub> or C<sub>12-15</sub>(EO)<sub>9</sub> 0.8% TDS brine solution in 30 Darcy sand pack or 1.2 Darcy glass bead pack at 40 °C, and 1700 psia



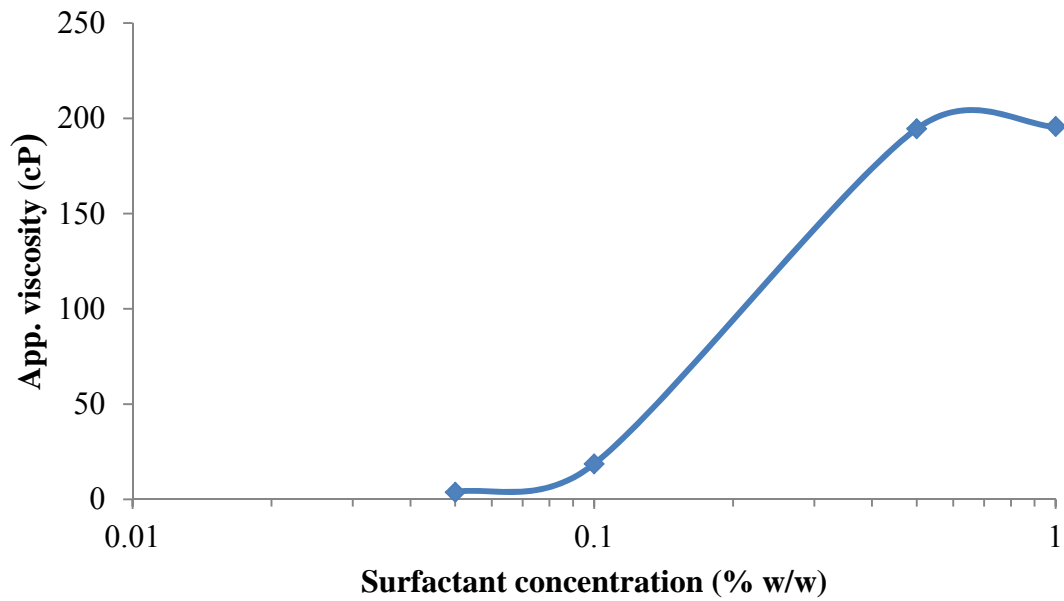


Figure 5.7: Effect of  $C_{12-14}(EO)_{22}$  concentration in brine on foam apparent viscosity in 1.2 Darcy glass bead pack at superficial velocity 10 ft/day, foam quality 60%, 40 °C, 1700 psia with 0.8% TDS brine

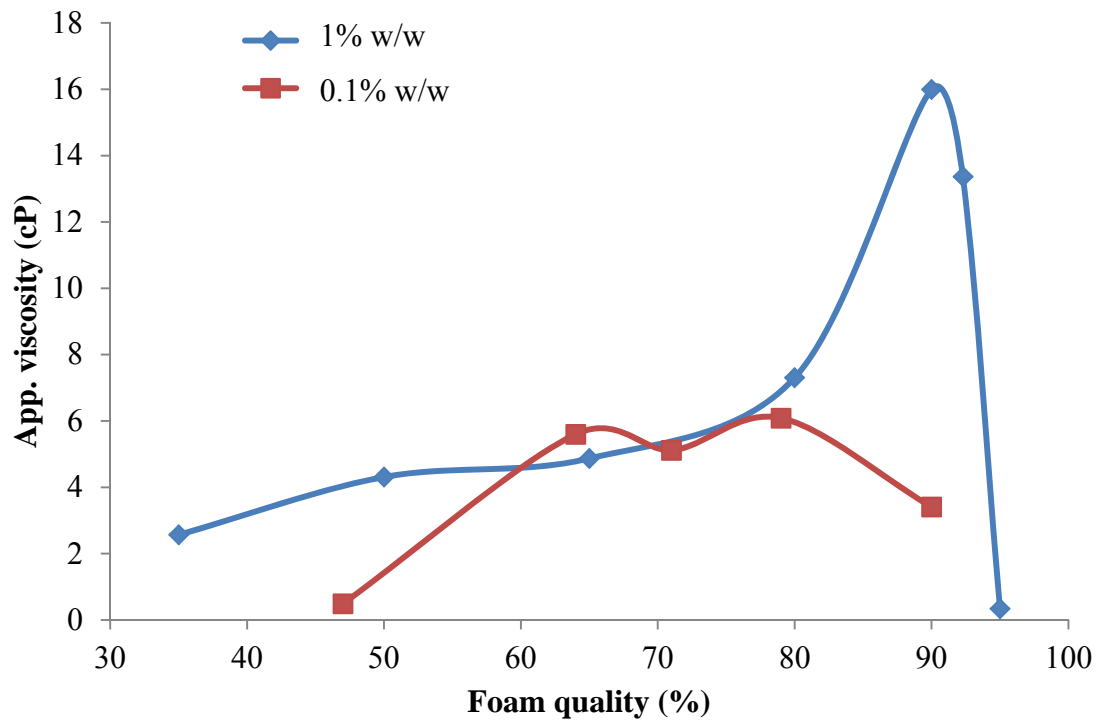


Figure 5.8: Effect of foam quality on the apparent viscosity of C/W foams stabilized with 1% and 0.1% w/w  $C_{12-14}(EO)_{22}$  0.8% TDS brine solution in 30 Darcy sand pack at total superficial velocity of 156 ft/day, 40 °C, and 1700 psia in a 30 Darcy sand pack

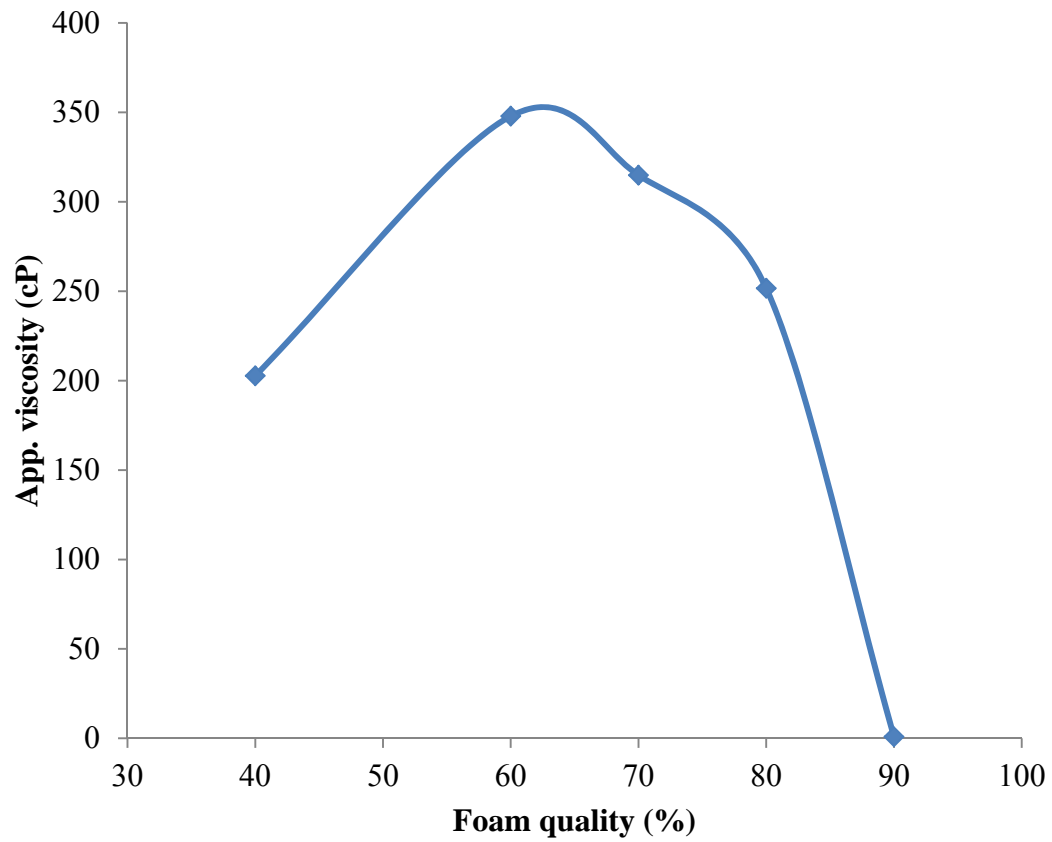


Figure 5.9: Effect of foam quality on apparent viscosity of C/W foam stabilized with 1% w/w  $C_{12-14}(EO)_{22}$  0.8% TDS brine solution, 40 °C, and 1700 psia in a 1.2 Darcy bead pack at total superficial velocity 6 ft/day

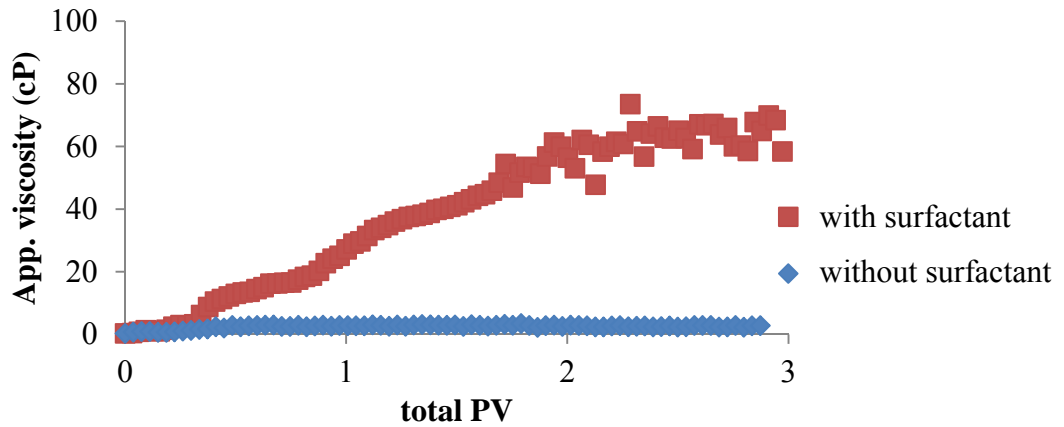


Figure 5.10: The apparent viscosity history for co-injection of 1% w/w  $C_{12-14}(EO)_{22}$  water solution or DI water and  $CO_2$  in a 49 mDarcy dolomite core at total superficial velocity 4 ft/day, 80% foam quality, 25 °C and 3400 psia

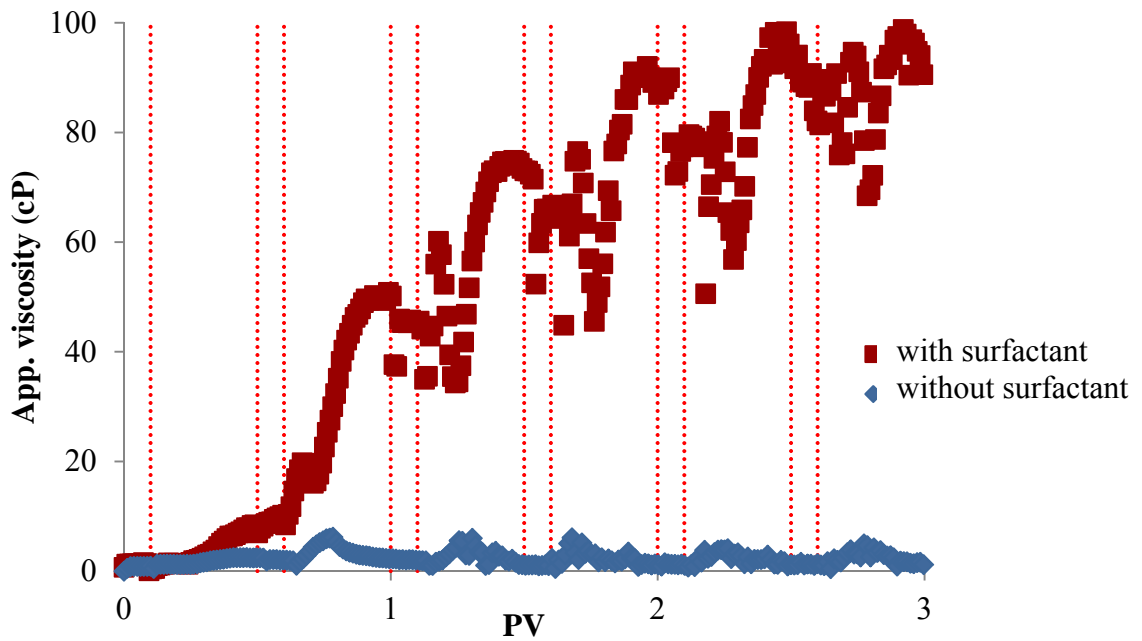


Figure 5.11: The apparent viscosity history for SAG process of injecting 1% w/w  $C_{12-14}(EO)_{22}$  water solution or DI water and  $CO_2$  in a 49 mDarcy dolomite core at total superficial velocity 4 ft/day, with an injection pattern of 0.1 PV aqueous solution /0.4 PV  $CO_2$ , 25 °C and 3400 psia

Table 5.1: Structures of surfactants

Surfactant name	Structure	HLB	Supplier
2EH-PO5-EO8	2-ethxylhexyl-(PO) <sub>5</sub> (EO) <sub>8</sub>	13.2	Dow
2EH-PO5-EO15	2-ethxylhexyl-(PO) <sub>5</sub> (EO) <sub>15</sub>	15.6	Dow
2EH-EO11.8	2-ethxylhexyl-(EO) <sub>11.8</sub>	16.2	Dow
Bio-soft N91-8	C <sub>9-11</sub> (EO) <sub>8</sub>	13.9	Stepan
Surfonic L24-12	C <sub>12-14</sub> (EO) <sub>12</sub>	14.4	Huntsman
Surfonic L24-22	C <sub>12-14</sub> (EO) <sub>22</sub>	16.6	Huntsman
Neodol N25-9	C <sub>12-15</sub> (EO) <sub>9</sub>	13.2	Shell
Neodol N25-12	C <sub>12-15</sub> (EO) <sub>12</sub>	14.4	Shell

Table 5.2: Effect of salinity on cloud points of nonionic surfactants

Surfactant	HLB	Salinity					
		0	0.8% TDS	30 g/L NaCl	90 g/L NaCl	100 g/L NaCl	120 g/L NaCl
2-ethylhexyl-(PO) <sub>5</sub> (EO) <sub>8</sub>	13.2	54 °C*					
2-ethylhexyl-(PO) <sub>5</sub> (EO) <sub>15</sub>	15.6	95 °C			65 °C		
2-ethylhexyl-(EO) <sub>12</sub>	16.2	>80 °C*					
C <sub>9-11</sub> (EO) <sub>8</sub>	13.9	81 °C					
C <sub>12-14</sub> (EO) <sub>12</sub>	14.4					68 °C	
C <sub>12-14</sub> (EO) <sub>22</sub>	16.6	>120 °C	>120 °C	111 °C	83 °C		76 °C
C <sub>12-15</sub> (EO) <sub>9</sub>	13.2	72 °C		63 °C	58 °C		45 °C
C <sub>12-15</sub> (EO) <sub>12</sub>	14.4			89 °C	75 °C		67 °C

\* published<sup>18</sup>

Table 5.3: Partition coefficients of C<sub>12-14</sub>(EO)<sub>22</sub>, C<sub>12-15</sub>(EO)<sub>12</sub> and C<sub>12-15</sub>(EO)<sub>9</sub> between CO<sub>2</sub> and 0.8% TDS brine at 1700 psia, 24 and 40 °C

Surfactant	Temperature (°C)	CO <sub>2</sub> density (g/mL)	CO <sub>2</sub> -brine partition coefficient
			(% w/w in CO <sub>2</sub> /% w/w in brine)
C <sub>12-14</sub> (EO) <sub>22</sub>	24	0.849	0.020
	40	0.709	<0.006
C <sub>12-15</sub> (EO) <sub>12</sub>	40	0.709	0.035
C <sub>12-15</sub> (EO) <sub>9</sub>	24	0.849	0.226
	40	0.709	0.077

Table 5.4: Interfacial tension between CO<sub>2</sub> and 1 % w/w C<sub>12-14</sub>(EO)<sub>22</sub> 0.8% TDS brine at 24-60 °C, 940 or 1700 psia

Temperature (°C)	Pressure (psia)	CO <sub>2</sub> density (g/mL)	IFT (mN/m)
24	940	0.736	8.2
	1700	0.849	7.3
40	1700	0.709	8.5
50	940	0.152	15.2
60	1700	0.413	9.3

Table 5.5: Apparent viscosity of C/W foams stabilized with 1% w/w C<sub>12-14</sub>(EO)<sub>22</sub> brine solution in a 30 Darcy sand pack at 90% foam quality, total superficial velocity 622 ft/day at a CO<sub>2</sub> density of 0.413 g/mL. (Temperature and pressure was adjusted to give the constant CO<sub>2</sub> density)

Salinity	Temperature (°C)	Pressure (Psia)	Apparent viscosity (cP)
0.8% TDS	60	1700	9.6
30 g/L NaCl	60	1700	10.7
	90	2341	6.1
	100	2551	0.4 (no foam)
90 g/L NaCl	60	1700	11.6
	80	2128	7.3
	90	2341	0.5 (no foam)

Table 5.6: Partition coefficients of nonionic surfactants between dodecane and 0.8% TDS brine at 40 °C, 1 atm.

Surfactant	HLB	Oil-brine partitioning coefficients
2-ethxylhexyl-(PO) <sub>5</sub> (EO) <sub>8</sub>	13.2	2.10
2-ethxylhexyl-(PO) <sub>5</sub> (EO) <sub>15</sub>	15.6	0.70
2-ethxylhexyl-(EO) <sub>11.8</sub>	16.2	0.43
C <sub>9-11</sub> (EO) <sub>8</sub>	13.9	2.22
C <sub>12-14</sub> (EO) <sub>12</sub>	14.4	0.43
C <sub>12-14</sub> (EO) <sub>22</sub>	16.6	0.09
C <sub>12-15</sub> (EO) <sub>9</sub>	13.2	0.72
C <sub>12-15</sub> (EO) <sub>12</sub>	14.4	0.62



## **Chapter 6: Conclusions and Recommendations**

### **6.1 CONCLUSIONS**

By utilizing high HCB surfactants, high temperature CO<sub>2</sub>-in-water foams were stabilized. This was accomplished with three classes of surfactants: switchable nonionic-to-cationic ethoxylated amine surfactant, cationic alkyltrimethylammonium surfactant and nonionic alkyl ethoxylate surfactant with a high degree of ethoxylation. By designing surfactants with high HCB, the solubility in high salinity brines was maintained at high temperature. The high aqueous solubility enabled phase behavior and interfacial tension studies for a surfactant-CO<sub>2</sub>-water system at high temperatures and salinities that had not been studied previously. In addition, the strong solvation in brine and affinity for CO<sub>2</sub> provided an appropriate HCB for significant adsorption of the surfactant at the C-W interface and reduction of the IFT. Furthermore, viscous C/W foams were stabilized with these surfactants at a wide range of temperatures, foam qualities and total superficial velocities and explained in terms of destabilization mechanisms such as film drainage and thermally activated hole formation, and theories for foam generation and viscosity in porous media.

### **6.2 RECOMMENDATIONS**

To demonstrate the foaming capability of a surfactant for foam mobility control at reservoir condition, it is necessary to understand the influence of oil on the foam generation and propagation process, as oil may destabilize C/W foam through multiple mechanisms such as bridging of foam film by oil droplet and pinch-off<sup>52</sup>. For a high temperature, high salinity system, oil-foam interaction in porous media has not been

studied and can be interesting and useful information on evaluating surfactant candidates for further field trials.

In Chapter 5, the apparent viscosity of foam in a 30 Darcy sand pack was found close to that of the bulk foam in a downstream capillary, when CO<sub>2</sub> and surfactant solution were injected simultaneously into the porous media at a high total superficial velocity of ~600 ft/day. However, when CO<sub>2</sub> and surfactant solution were injected into a 1.2 Darcy glass bead pack at a low total superficial velocity of ~10 ft/day, apparent viscosity up to ~350 cP was achieved in the glass bead pack, but less than 5 cP achieved in the downstream capillary. It is still not clear why lamellae survived in the earlier case, but were unstable in the latter one. This destabilization may result from the smaller size of bubbles generated from the lower permeability porous media, which produces a higher capillary pressure for faster lamellar film drainage and a shorter lifetime for the lamellae. When foam travels from a low permeability region to a much higher permeability region, understanding the stability of lamellae in this process can be very useful for surfactant selection for foam mobility control in fractured reservoir condition. Microscopic observation on bubble sizes at the outlet of the foam generator may be useful for understanding this process.

## Appendix A

Theories and equations for bulk foam and foam in porous media related in this work are summarized as below.

### A.1 THEORY OF BULK FOAM FORMATION, APPARENT VISCOSITY, AND STABILITY

For CO<sub>2</sub> in water foams given that the viscosity for the external or continuous phase  $\mu_e$  (water) is higher than that of the internal or dispersed phase  $\mu_i$  (CO<sub>2</sub>), the application of shear deforms the CO<sub>2</sub> into elongated cylinders which can break up into small droplets (or bubbles). The bubbles form when the ratio of the shear stress ( $\mu_e \dot{\gamma}$ ) to the interfacial stress ( $\gamma/R_0$ ), reaches a critical value (always >1), defined by the capillary number,

$$C_a = \frac{\mu_e \dot{\gamma} R_0}{\gamma} \quad [A1]$$

where  $\dot{\gamma}$  is the shear rate,  $\gamma$  is the interfacial tension, and  $R_0$  is the droplet radius before the shear force is applied as illustrated in Figure A1.<sup>150</sup>

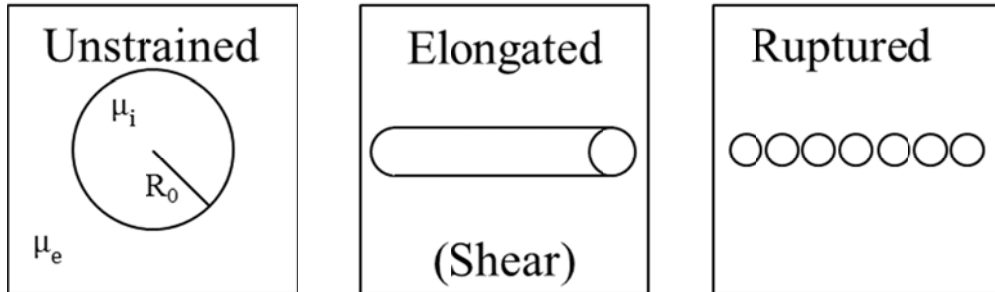


Figure A1: Schematic of an “isolated” droplet deforming in an external phase composed of either a concentrated surfactant solution or a concentrated emulsion

As the internal phase fraction  $\phi_i$  (referred to as the foam quality for C/W foam) increases, lamellae become thinner and bubbles become polyhedral. As depicted in Figure A2 for a two-dimensional array of droplets with a high  $\phi_i$ , as shear is applied

emulsion droplets are distorted from the original hexagonal shape until they are transformed into parallelograms with a higher total film area. The parallelograms are unstable and revert back to a hexagonal configuration, where the droplets in one layer are shifted with respect to the adjacent layers. The energy requirement for this translation is described by the yield stress  $\tau_0$  in Equation 2.<sup>150</sup> The viscosity of a bulk foam or concentrated emulsion was given by Princen et al.<sup>126</sup> as

$$\mu_{foam} = \frac{\tau_0}{\dot{\gamma}} + 32(\phi_i - 0.73)\mu_e \left(\frac{\mu_e \dot{\gamma} R}{\gamma}\right)^{-1/2} \quad [A2]$$

where R is the radius of a spherical droplet, Equation A2<sup>151</sup> indicates that the viscosity of a bulk foam decreases with an increase in the shear rate (shear thinning behavior).

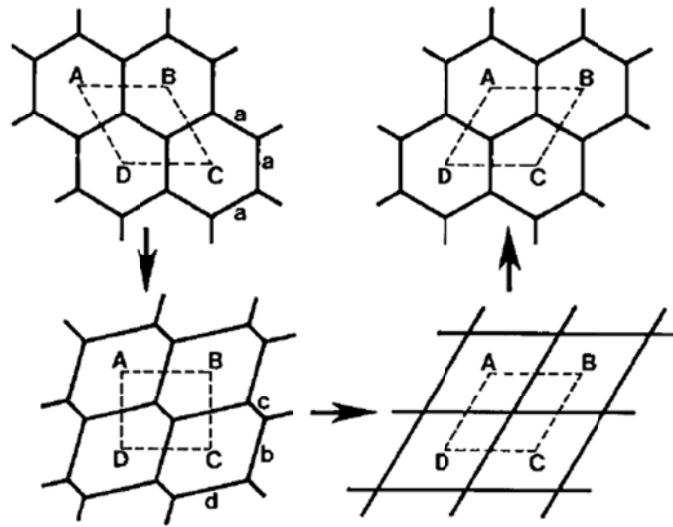


Figure A2: Scheme of emulsion droplets are distorted and shifted as shear is applied

Stabilization of bulk foams is vitally important for the maintenance of high viscosities, as bubble size (R) increases as bubbles coalesce. Bulk foams can be destabilized by many mechanisms, including drainage of the lamellae film between the dispersed droplets.<sup>18,45,46</sup> Drainage is driven by the difference in pressure between the thin film section of the lamellae film and plateau border,  $\Delta P_{film} = 2(P_c - \Pi_d)$  (where  $P_c$  is

capillary pressure, and  $\Pi_d$  is disjoining pressure). The drainage velocity, described by Reynolds for approaching flat plates, is given as

$$V = -\frac{dh_f}{dt} = \frac{h_f^2}{3\mu_e R_f^2} \Delta P_{film} \quad [A3]$$

where  $R_f$  and  $h_f$  are the radius and thickness for the thin film, respectively.<sup>18,45,46</sup> Once the lamellae are thinned to a critical level, coalescence of foam bubbles can occur by the formation of a thermally-activated hole in the lamellae film.<sup>18,44,96</sup> The probability of hole formation is  $\exp(-W_h/kT)$ <sup>44,96</sup>, where the activation energy is

$$W_h \cong \frac{h_f^2 \gamma_h^2}{\gamma_p} \quad [A4]$$

where  $\gamma_p$  is the interfacial tension of the planar interface and  $\gamma_h$  is the interfacial tension of a curved border of the hole.<sup>44</sup>

In addition, bulk foam destabilization also occurs via Ostwald ripening due to gas diffusion from small bubbles at high capillary pressure to larger bubbles at lower pressure.<sup>152</sup> Due to the lack of data on bubble size distribution, this effect is not discussed in this work. The effect of Ostwald ripening on stability of bulk C/W foam in capillary tube can be found in a previous paper from our group based on the microscopic observation of bubble size verse time.<sup>18</sup>

## A.2 FOAM IN POROUS MEDIA

### A.2.1 Single-phase fluid flow in porous media

Foam flow in a horizontal porous media (sand/bead pack or core) is usually simplified as one dimensional (1-D) single-phase flow and described by Darcy's law<sup>153</sup>

$$q = -\frac{kA}{\mu} \frac{dP}{dx} \quad [A5]$$

where  $q$  is flow rate,  $k$  is permeability,  $A$  is cross-sectional area,  $\mu$  is viscosity, and  $dP/dx$  is pressure gradient. Integration of Equation A5, followed by substitution of porous medium length  $L$  for distance  $x_0$  to  $x_1$  along porous media gives

$$q = \frac{kA \Delta P}{\mu L} \quad [A6]$$

where  $\Delta P$  is pressure drop across the porous medium. Equation A7 can be used to experimentally determine  $k$  of a porous medium of known  $A$  and  $L$ , by passing a fluid with known  $\mu$  through the porous media at a known  $q$ . In the present work, all permeabilities were determined using water at a known  $T$  using the equation

$$k = \frac{q\mu L}{A\Delta P} \quad [A7]$$

After the permeability of the porous media to water was determined with Equation A7, the apparent viscosity,  $\mu_{app}$  of a fluid or fluid mixture (treating the mixture as 1 phase) can be determined by rearranging Equation A7.

$$\mu_{app} = \frac{kA\Delta P}{qL} \quad [A8]$$

Note that *apparent* viscosity is used to describe foam because the foam is treated as “one phase”. Foam apparent viscosities were calculated using Equation A8, treating the foam as one phase. Equation A7 can be reformulated in terms of mobility  $\lambda$ <sup>4,5,153</sup>

$$\lambda = \frac{k}{\mu} = \frac{qL}{\Delta P A} \quad [A9]$$

Comparison of two fluids, a low viscosity fluid 1 and high viscosity fluid 2, with constant  $q$ ,  $A$ , and  $L$  can be accomplished by calculation of mobility reduction factor (MRF), which may be expressed in terms of  $\Delta P$  or  $\mu_{app}$  using Equations 8 and 9

$$MRF = \frac{\lambda_2}{\lambda_1} = \frac{\Delta P_1}{\Delta P_2} = \frac{\mu_{app,1}}{\mu_{app,2}} \quad [A10]$$

When the porous medium is a bead pack composed of uniform spheres, the empirical Carmen-Kozeny equation can be used to predict the permeability<sup>153</sup>

$$k_{beadpack} = \frac{1}{72t} \frac{\phi^3 D_p^3}{(1-\phi)^2} \quad [A11]$$

where  $\phi$  is porosity,  $t$  is tortuosity and  $D_p$  is particle diameter. The equivalent shear rate in a bead pack is calculated with the following equation<sup>153</sup>

$$\dot{\gamma}_{eq} = \frac{4q}{A\sqrt{8k\phi}} \quad [A12]$$

Pore throat sizes can be estimated from geometric arguments<sup>141</sup>, where for cubic packing of spheres

$$D_{throat,cubic} = D_p (\sqrt{2} - 1) \approx \frac{D_p}{2.41} \quad [A13]$$

and for hexagonal packing of spheres

$$D_{throat,hexagonal} \approx \frac{D_p}{6.46} \quad [A14]$$

### A.2.2 Foam generation

Generation of a foam in porous media encompasses two steps: lamella generation and lamella mobilization. Creation and mobilization of the lamellae were not visually observable in our metal apparatus, but the processes by which they occurred are described in this section.

### A.2.2.1 Lamellae creation

Lamellae creation is the first step in foam generation. There are four ways to create lamellae in porous media: snap-off, leave-behind, lamella division, and gas evolution within liquid (gas is generated by a surfactant solution within a porous medium chemically or physically). The first three lamellae creation mechanisms will be explained below. It is important to note that for bulk foam, viscous forces (shear flow) disrupt large bubbles to create smaller bubbles (and more lamellae) as explained above. However, for foam in porous media lamellae are created by snap-off, leave-behind and lamellar division, which are influence by capillary forces.

#### Snap-off

In porous media, the capillary pressure<sup>153</sup> (Equation A15) in the neck is higher than in less curved regions. Assuming gas phase pressure is equal everywhere, then the liquid pressure in the neck is lower than the rest of the capillary. Driven by the pressure difference, liquid flows in the constriction and accumulates in a collar. As the collar swells and bridges the throat, a new lamella is created. as shown in Figure A3.<sup>5,146</sup>

$$P_c = P_{nonwetting} - P_{wetting} = \frac{2\gamma\cos\theta}{R} \quad [A15]$$

where, R is the radius of pore and  $\theta$  is contact angle.



Figure A3: Scheme of liquid accumulating in a pore throat



For pore throats with a circular cross-section, there is capillary entry pressure of the throat,  $P_c^e$ , which is the capillary pressure above which gas would displace liquid filling the same throat,<sup>5</sup>.

$$P_c^e = \frac{2\gamma}{R_t} \quad [A16]$$

where  $R_t$  is the radius of the pore throat. Then, snap-off requires that capillary pressure in the throat then falls to a lower value (Equation A17) to let snap-off occurs.

$$P_c^{sn} = P_c^e / 2 \quad [A17]$$

Here, the ratio of  $P_c^{sn}/P_c^e$  depends on pore geometry and the wettability of the solid surface.<sup>146</sup> A scheme for snap-off process is shown in Figure A4<sup>154</sup>.

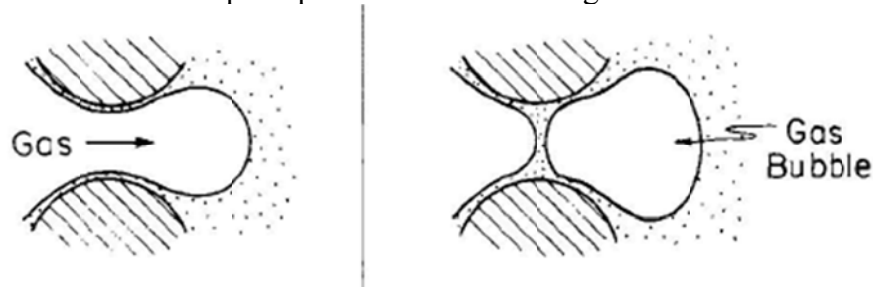


Figure A4: Scheme of snap-off in a pore throat

### Leave-behind

When gas enters a porous medium saturated with surfactant aqueous solution, lamellae can be created by “leave-behind.” Leave-behind (Figure A5<sup>154</sup>) creates a lamella in the throat at adjacency between pore bodies when they are invaded by gas from different paths. Note that only during drainage (decreasing water saturation) can lamellae be created through leave-behind, which makes foam generation easier than in steady flow processes (i.e. where water saturation remains constant)<sup>5</sup>

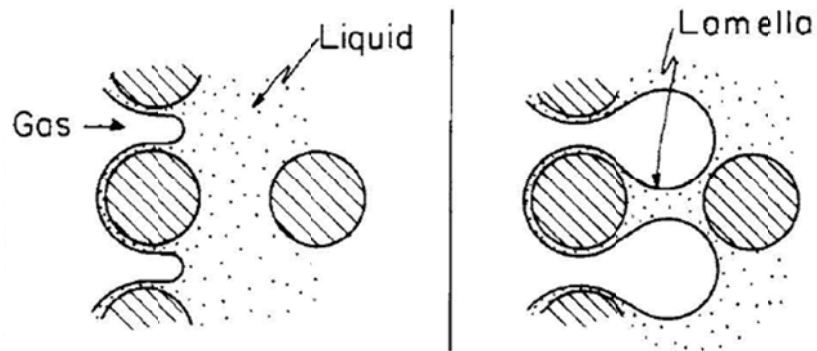


Figure A5: Scheme of leave-behind a pore throat

### Lamellae division

As a lamella enters a pore body with several pore throats, the lamella stretches across the pore body and either (1) breaks or (2) deposits a new lamella in each unblocked pore throat (Figure A6<sup>154</sup>). This process can create large numbers of lamellae when they survive being stretched through pore bodies.<sup>5</sup>

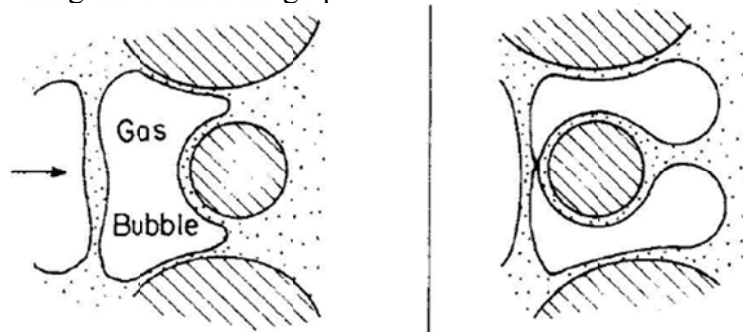


Figure A6: Scheme of lamellae division a pore throat

### A.2.2.2 Lamellae mobilization

After lamellae are created by one or more processes described above, the they must be mobilized for foam generation to occur in porous media.<sup>5</sup> For lamellae mobilization, a minimum pressure gradient (MPG) across the porous media is required.

The pressure gradient must be large enough to produce a sufficient pressure difference across lamellae trapped in the pore throats to exceed the "yield" pressure to mobilize the lamellae.<sup>112,133</sup> For each lamella, this yield pressure is the minimum pressure drop across it (Equation A18) required to displace it from the pore throat as a function of the interfacial tension between the liquid and gas, the geometry of the pore throat, and the capillary pressure<sup>155</sup>:

$$\Delta p^{max} = \frac{4\gamma}{\bar{r}_{min}} \quad [A18]$$

where  $\Delta p^{max}$  is the maximum pressure drop across the lamella as it is displaced from the pore throat, that is, the minimum pressure drop required to displace it completely.  $\gamma$  is the interfacial tension and  $\bar{r}_{min}$  is the minimum value of  $\bar{r} \equiv 2/(1/r_1 + 1/r_2)$  during the displacement, with  $r_1$  and  $r_2$  are the principal radii of curvature of the lamella. If the radius of the pore throat<sup>156</sup> (Equation A19) is substituted for  $\bar{r}_{min}$  in Equation A18, the yield pressure for a lamella  $\Delta P_{y1}$  is obtained by Equation A20<sup>112,155</sup>:

$$R_t = \sqrt{\frac{50k}{3\phi}} \quad [A19]$$

$$\Delta P_{y1} = \frac{\gamma}{\sqrt{k/\phi}} \quad [A20]$$

where  $k$  is permeability and  $\phi$  is porosity. For a series of lamellae over system length  $L$ , the yield pressure drop  $\Delta P_y$  is:

$$\Delta P_y = n\Delta P_{y1} = n\left(\frac{\gamma}{\sqrt{k/\phi}}\right) \quad [A21]$$

where  $n$  is the number of lamellae over system length. For foam generation by injecting aqueous and CO<sub>2</sub> phase simultaneously (as typically done in this dissertation), there is a uniform pressure gradient,  $\nabla p_y$ :

$$\nabla p_y = \Delta P_y / L = (n/L) \Delta P_{y1} \quad [A22]$$

Where  $(n/L)$  is the lamellae density (number of lamellae per unit length). In the case of a geometrically similar porous media where the lamellae density is similar

$$(n/L) \propto 1 / \sqrt{k/\phi} \quad [A23]$$

Therefore,

$$\nabla p_y \propto \gamma \phi / k \quad [A24]$$

For foam generation by co-injection of CO<sub>2</sub> and surfactant solution, Tanzil *et al.*<sup>112</sup> defined a normalized pressure gradient,  $N_{\nabla p}$  by:

$$N_{\nabla p} \equiv \frac{\nabla p}{\gamma \phi / k} \quad [A25]$$

### A.3 SMOOTH CAPILLARIES MODEL AND SHEAR THINNING IN POROUS MEDIA

Hirasaki and Lawson developed a model for predicting foam flow behavior in a natural porous medium. In this model, foam flow in porous media is described as flow of bubbles through a bundle of parallel capillaries with inner diameters smaller than the diameter of the bubbles. The apparent viscosity of foam in this capillary model is the sum of three contributions as listed in Equation A26: (1) slugs of liquid between bubbles, (2) the resistance to deformation of the interface of a bubble passing through a capillary, and (3) the surface tension gradient that results when surface active materials is swept from the front of a bubble and accumulates at the back of it.

$$\begin{aligned} \frac{\mu_{foam}}{\mu_e} = & L_s n_L + 0.85 \frac{(n_L R_c)}{(r_c/R_c)} \left( \frac{3\mu_e U}{\gamma} \right)^{-\frac{1}{3}} [(r_c/R_c)^2 + 1] \\ & + (n_L R_c) \left( \frac{3\mu_e U}{\gamma} \right)^{-\frac{1}{3}} \sqrt{N_s} \frac{(1 - e^{-N_L})}{(1 + e^{-N_L})} \end{aligned} \quad [A26]$$

Where  $L_s$  is the length of liquid slugs,  $n_L$  is lamellae density,  $r_c$  is the radius of curvature of gas-liquid interface,  $R_c$  is the capillary radius,  $U$  is the velocity of bubbles,  $N_s$  is a dimensionless number for interfacial tension gradient effect, and  $N_L$  is a dimensionless bubble length.<sup>42</sup>

As a bubble moves inside a single capillary, the thickness of a thin liquid film between the bubble and the capillary wall increases with an increase of velocity, which results in the change of bubble curvatures and the pressure drop across the bubble.<sup>127</sup> This pressure drop is proportional to the 2/3 power of the gas velocity<sup>127</sup>, which gives a viscosity contribution proportional to the -1/3 power of the velocity (as demonstrated in the second term on the right side of Equation A26)<sup>42</sup> and thus a shear-thinning effect. In addition, as the bubbles flow in the capillary tube, surfactant gets dragged to the rear side of the bubbles, resulting interfacial tension gradient disfavoring moving of the bubbles due to Gibbs-Marangoni effect. The contribution on foam viscosity from interfacial tension gradient is also proportional to the -1/3 power of gas phase velocity (the third term on the right side of Equation A26) and thus a shear-thinning effect. Therefore, the foam in the porous media is shear-thinning.

#### **A.4 LIMITING CAPILLARY PRESSURE AND DISJOINING PRESSURE**

In water-wet porous media, water forms a meniscus that spans the pair of grains in contact with water as shown in Figure A7. When an aqueous phase and  $\text{CO}_2$  are injected simultaneously into pores initially occupied with water, the water saturation

decreases such that the meniscus moves closer towards the contact point. This change results in a smaller radius of curvature at the interface as shown in Figure A7. As the radius of curvature decreases, the capillary pressure increases until it reaches a “limiting capillary pressure”<sup>43</sup> above which the capillary pressure exceeds disjoining pressure (Figure A8).<sup>113,128</sup> Here, lamellae become unstable and several lamellae rupture simultaneously to produce a foam with a coarser texture. The increase of the average bubble size causes a decrease in the capillary pressure.<sup>43</sup> Thus, as the coarser foam is displaced, the capillary pressure increases again which leads to further bubble coalescence. This repeated coalescence and displacement of the coarse-textured foam keeps the average capillary pressure near the limiting capillary pressure.<sup>43</sup>

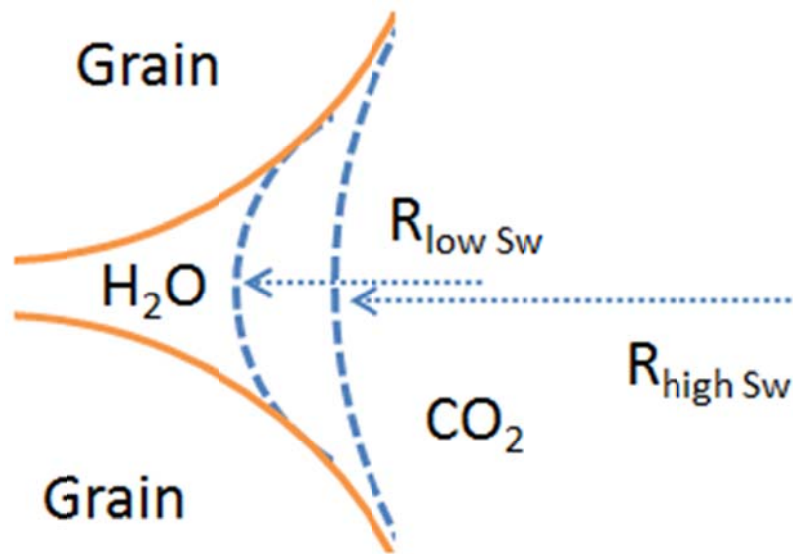


Figure A7: Effect of water saturation on the curvature of CO<sub>2</sub>-water interface in water-wet porous media:  $R_{low Sw}$  and  $R_{high Sw}$  are the radii of the curvatures at relative low and high water saturation

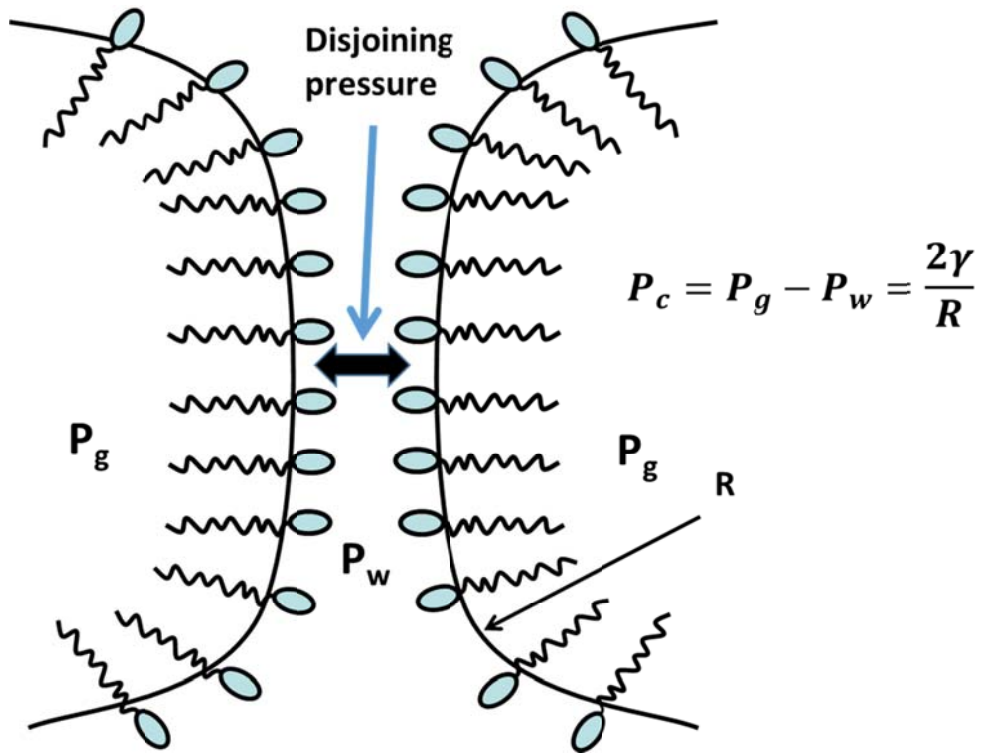


Figure A8: Stability of lamellae: disjoining pressure versus capillary pressure

## Appendix B

### B.1 POTENTIOMETRIC TITRATION FOR DETERMINATION OF THE DEGREE OF PROTONATION

$C_{12-14}N(EO)_2$  (1% w/w) water/brine mixtures (about 50 mL in total) were titrated with 400 or 800 mM HCl brine solutions at 24 or 90 °C, 1 atm. The ionic strength of the titrant was kept constant by using HCl at the same ionic strength. The titration was carried in a 250 mL three-neck flask merged in an oil bath heated with Corning PC-420D stirring hot plate with a temperature controller. To minimize loss of water, a refluxing condenser was used. The amount of titrant and pH was recorded.

The overall degree of protonation was measured by titration of the amine with 400 or 800 mM HCl titrant along with the charge balance<sup>157</sup> for electrical neutrality (assuming ideal solution behavior) according to

$$\theta = \frac{C_a \times V_{titrant} + (C_{OH^-} - C_{H^+}) \times V_{titrand}}{C_{total} \times V_{titrand_0}} \quad [B1]$$

where  $\theta$  is the overall fraction of protonated amine,  $C_a$  is the concentration of HCl and  $C_{H^+}$  and  $C_{OH^-}$  are the concentration of free  $H^+$  and  $OH^-$  determined from the pH of the solution.  $C_{total}$  is the total concentration of the unprotonated amine before adding HCl, which was 1% w/w (40 mM).  $V_{titrand_0}$  is the volume of the amine solution before adding HCl, whereas  $V_{titrand}$  is the total volume of titrand at any stage of titration.

During titration process, the  $C_{12-14}N(EO)_2$  water/brine mixture was always cloudy initially as the solubility of the unprotonated amine is limited. Upon adding HCl,  $C_{12-14}N(EO)_2$  was protonated and the mixture turned clear. The phase boundaries where the pH of the cloudy mixture turned clear are shown in red circles. We note that it was not feasible to titrate from low to high pH as the base would precipitate the  $Ca^{2+}$  in the brine solution.



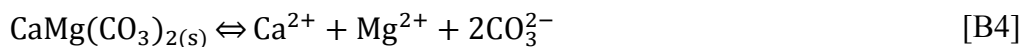
## B.2 APPARATUS FOR APPARENT VISCOSITY MEASUREMENT

In addition to the three original differential pressure transducers in the setup from our previous work,<sup>40</sup> one additional transducer (Validyne, model DP22) with a 1000 psi diaphragm was inserted to measure even high pressure drops. Also, instead of using one BPR as in our previous study,<sup>40</sup> two BPRs (Swagelok model SS-4R3A adjustable relief valve, heated to over 75 °C with water bath) were connected in series for controlling system pressure (reported by the pressure at the upstream BPR) to prevent CO<sub>2</sub> liquid formation. A Swagelok 177-R3A-K1-F spring (3000-4000 psia) was used in the upstream one, and a 177-R3A-K1-D spring (1500-2250 psia) was used in the other. In some experiments, pH of effluent from the downstream BPR was measured by the same pH meter used in potentiometric titration.

## B.3 PHREEQC SIMULATION (CONTINUED)

PHREEQC stands for “PH(pH), RE(redox), EQ (equilibrium), C (program written in C)”; it is a public-domain program developed by Parkhurst et al.<sup>156</sup> PHREEQC is used to determine thermodynamic equilibrium of geochemical reactions with a comprehensive database, along with phase equilibria of CO<sub>2</sub> between the gas and liquid phases. In the presence of salt, PHREEQC utilizes the modified Debye Hückel expressions to account for non-ideality of ions in aqueous solution. In this study, the relevant chemical equilibria reactions are given below.<sup>41,156</sup>

Solid phase dissolution:



Reaction equilibria in aqueous phase:

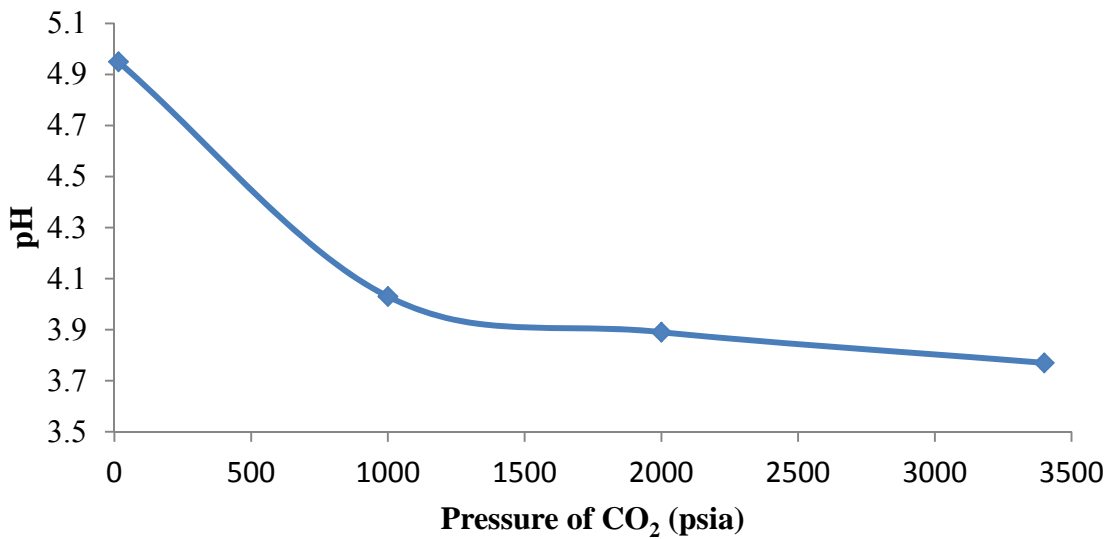
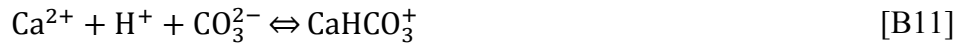


Figure B1: Effect of CO<sub>2</sub> pressure on simulated pH of effluent at 120 °C in the presence of 22% TDS brine and excess calcium carbonate

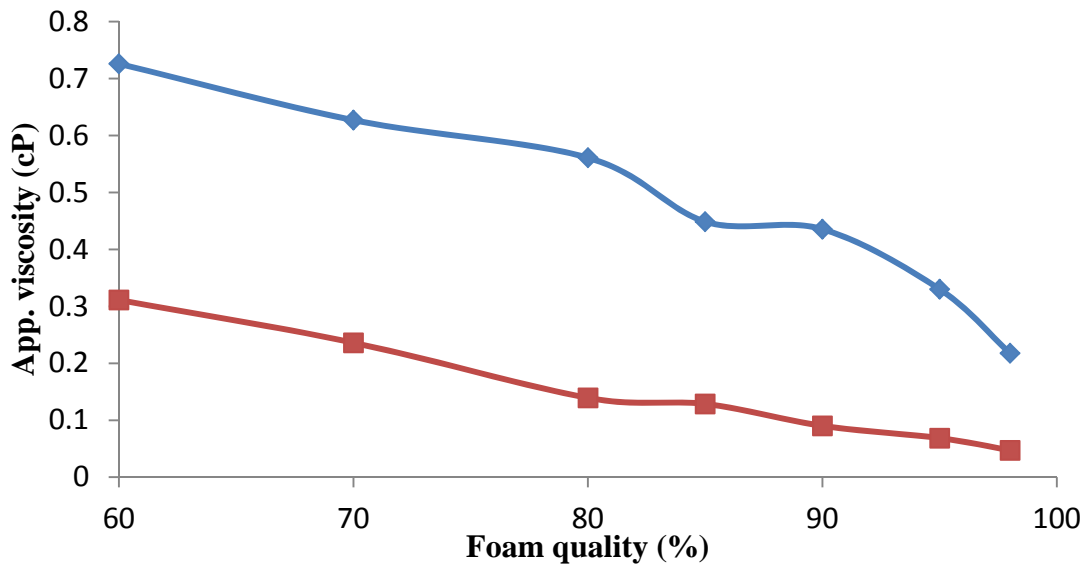


Figure B2: Effect of foam quality on apparent viscosity of CO<sub>2</sub>/brine mixture without surfactant in a 76 Darcy crushed calcium carbonate packed bed (◇) and a downstream capillary tube (660 μm ID) (□) at total superficial velocity 938 ft/day in the calcium carbonate packed bed, 120 °C and 3400 psia

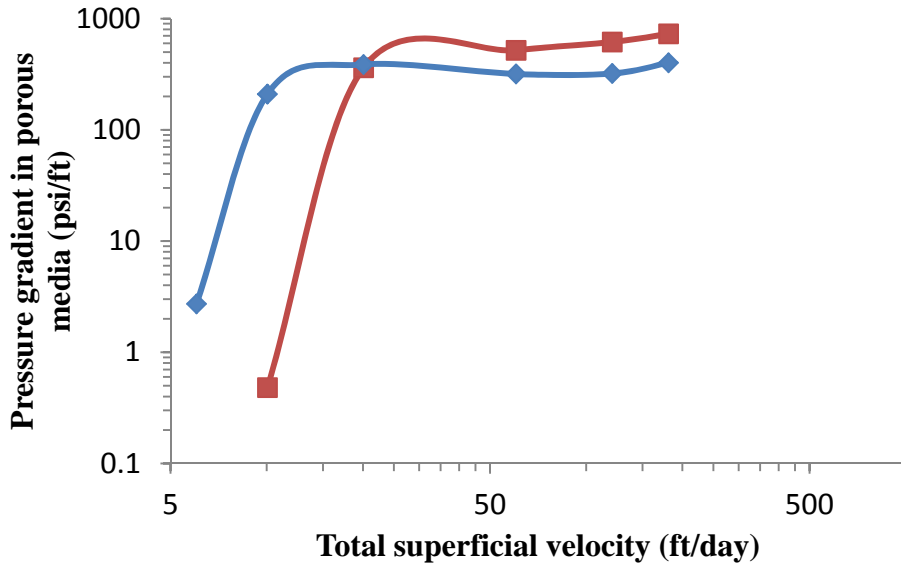


Figure B3: Effect of total superficial velocity on the pressure gradient in 1.2 Darcy glass bead pack by injecting 1% w/w  $C_{12-14}N(EO)_2$  182 g/L NaCl brine pH 4 (adjusted by HCl initially) solution with  $CO_2$  at 40% (◇) or 80% (□) foam quality at 120 °C and 3400 psia.

#### B.4 MINIMUM PRESSURE GRADIENT FOR FOAM GENERATION

From the MPG at 40% Foam quality (2.7 psi/ft as shown in Figure B3), For co-injection process of 1% w/w  $C_{12-14}N(EO)_2$  182 g/L NaCl brine pH 4 (adjusted by HCl initially) solution and  $CO_2$  into a 1.2 Darcy glass bead pack, the normalized pressure gradient  $N_{vp}$  (Equation A25) was determined to be  $4.4 \times 10^{-5}$ , assuming a  $\gamma$  between this surfactant brine solution and  $CO_2$  equal to 5.1 mN/m, the value measured above between  $CO_2$  and 22% TDS brine in Figure 3.4. The  $N_{vp}$  from our data was on the same order as the value of  $N_{vp}=2.6 \times 10^{-4}$  calculated from Gauglitz et al.'s data<sup>112,133</sup> at low temperature, perhaps suggesting similar foam generation mechanisms.

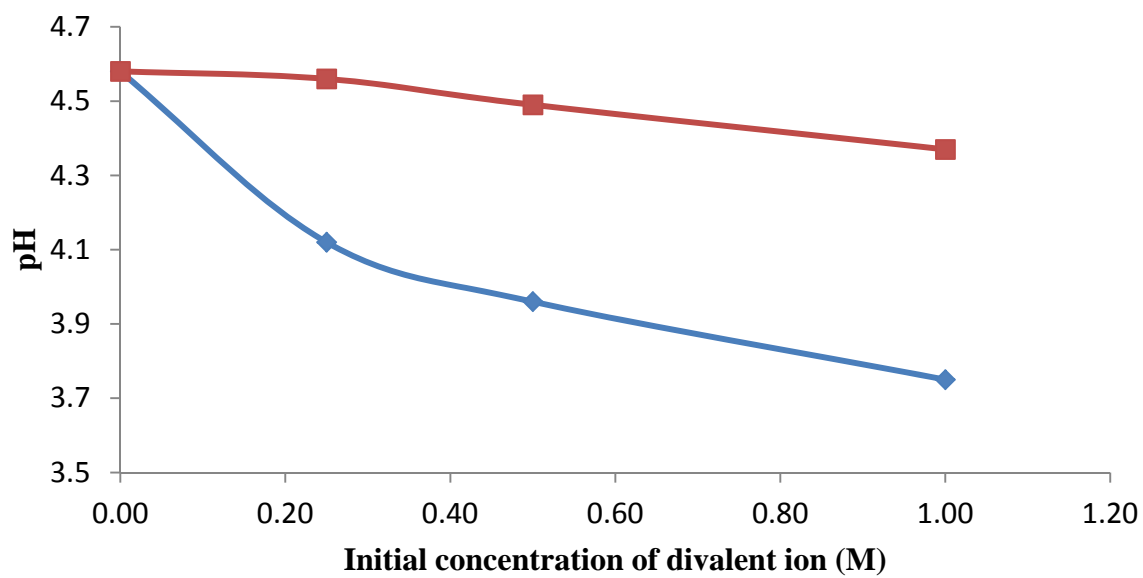


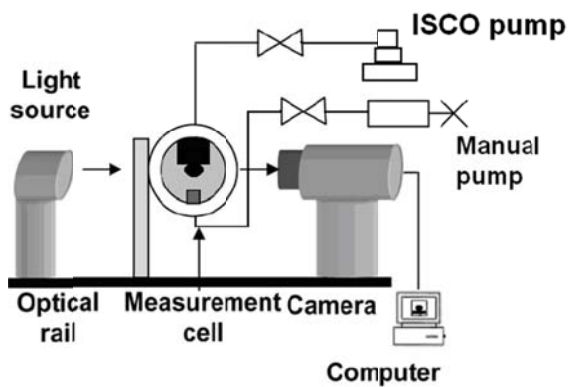
Figure B4: Effect of initial concentration of Ca<sup>2+</sup> (◇) or Mg<sup>2+</sup> (□) on simulated pH at equilibrium at 120 °C, 3400 psia in the presence of excess calcium carbonate and CO<sub>2</sub>

Table B1: Apparent viscosity of C/W foam stabilized with 1% w/w C<sub>12-14</sub>N(EO)<sub>2</sub> 22%TDS brine or 182 g/L NaCl brine solution (pH of aqueous phase was adjusted to 6 by HCl initially.) at 120 °C, 3400 psia, total superficial velocity 938 ft/day in a 76 Darcy calcium carbonate packed bed with foam quality from 70% to 95%

Salinity	Foam quality (%)	Foam viscosity (cP) in calcium carbonate packed bed	Foam viscosity (cP) in capillary	Effluent pH (~30 °C)
22% TDS	70	4.6	2.4	4.8
	80	7.3	4.9	-
	85	9.2	4.9	4.5
	90	14.5	5.7	-
	92	11.9	1.6	5.2
	95	No foam	No foam	4.5
182 g/L NaCl	90	7.9	3.8	5.7

## Appendix C

A



B

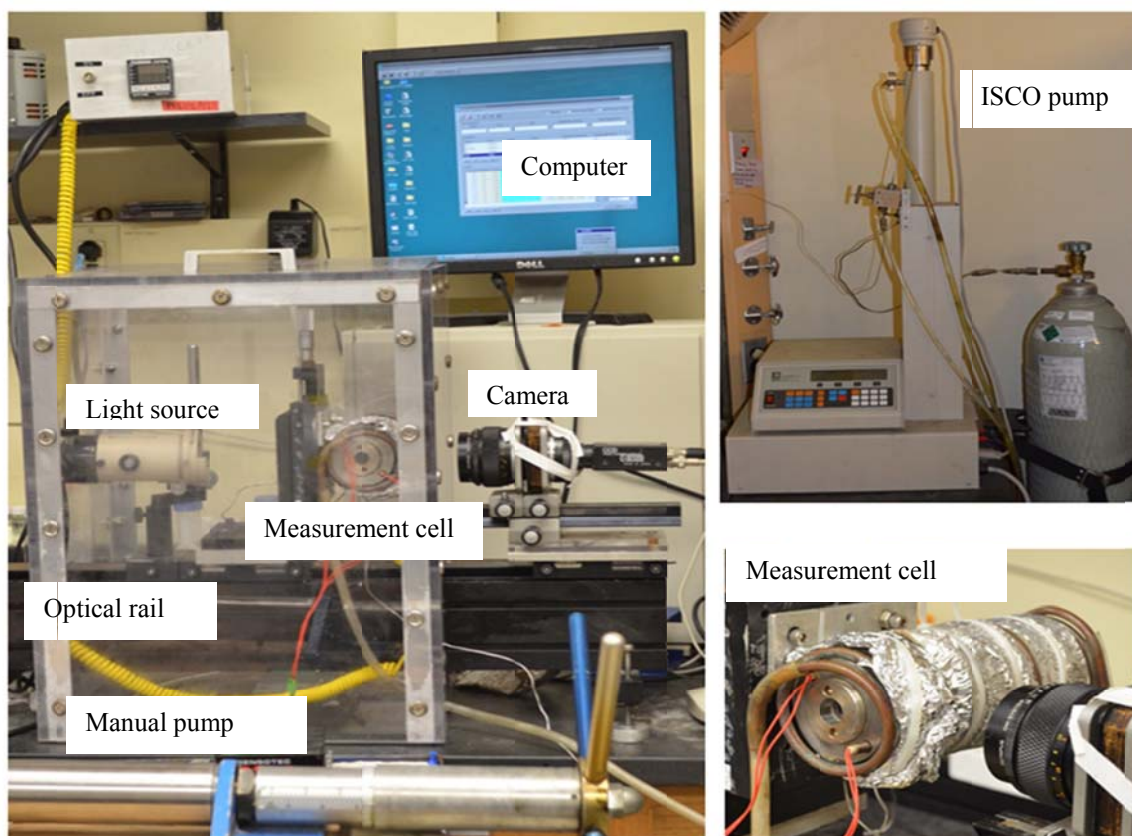


Figure C1: Scheme (A) and apparatus photos (B) for IFT measurement at high pressures

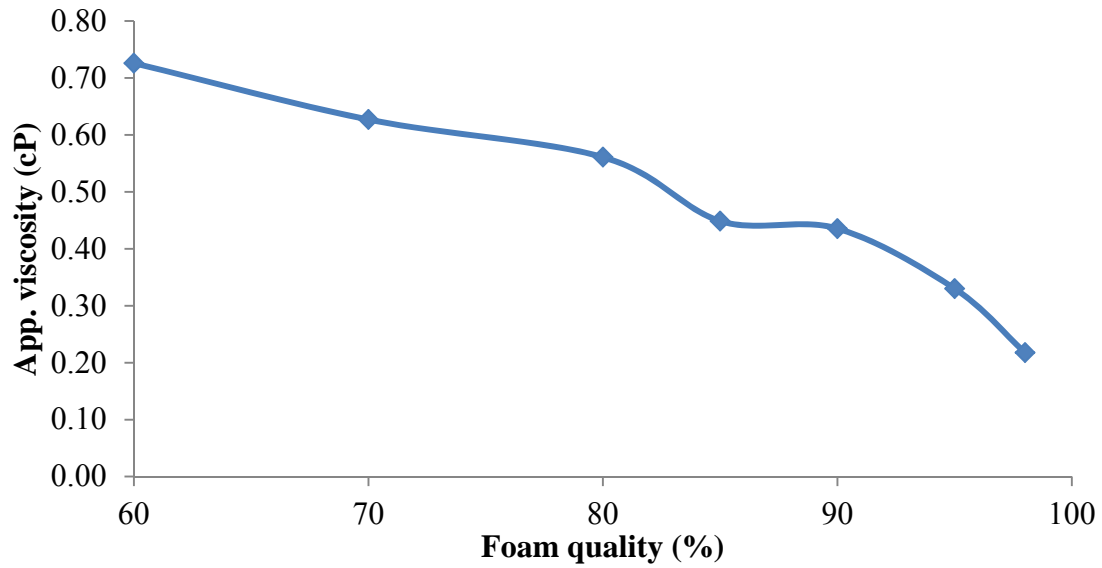


Figure C2: Effect of foam quality on apparent viscosity of CO<sub>2</sub>-brine mixture without surfactant in a 76 Darcy crushed calcium carbonate packed bed at total superficial velocity 938 ft/day, 120 °C and 3400 psia



## Appendix D

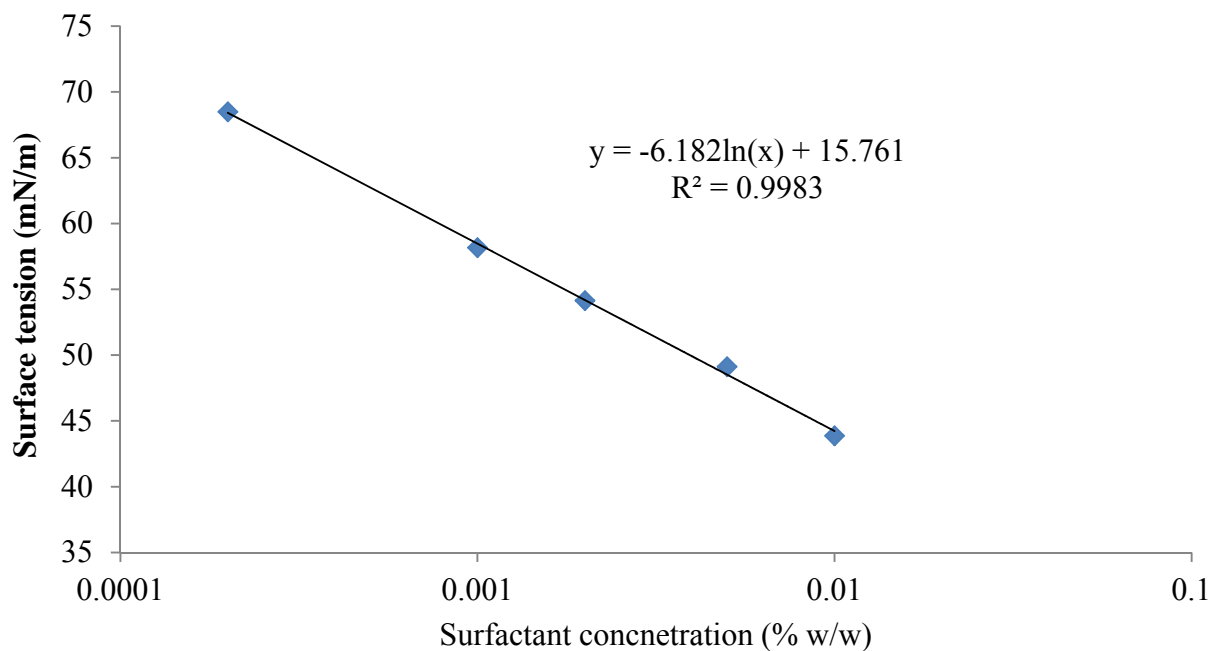


Figure D1: Effect of surfactant concentration on the surface tension for  $C_{12-14}(EO)_{22}$  at the air-0.8 TDS brine interface at 24 °C and 1 atm (an example of a calibration curve used for measuring surfactant concentration in a sample for  $CO_2$ -brine or oil-brine partition coefficient determination)

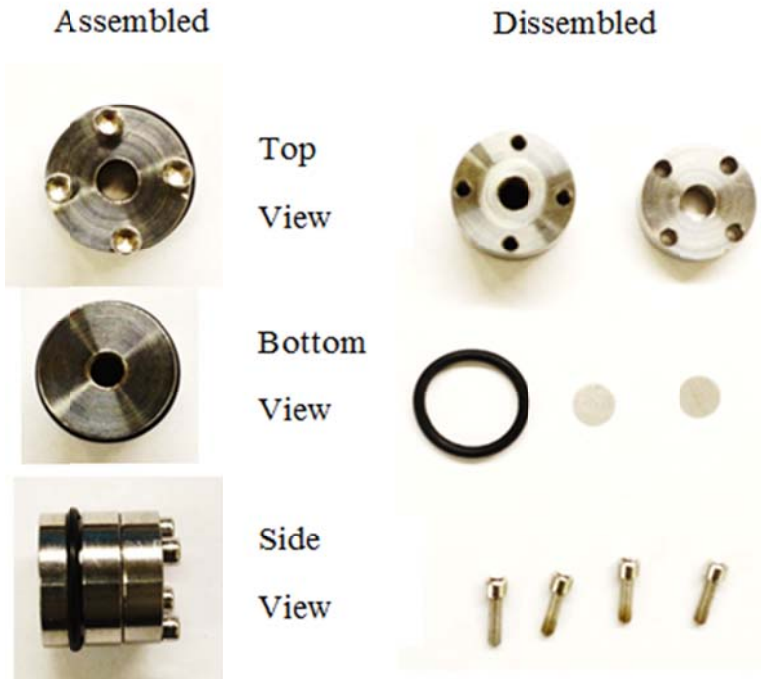


Figure D2: Photos for screen holder used in 1.2 Darcy glass bead pack

### Minimum pressure gradient for foam generation

From the MPG in the 30 Darcy sand pack (0.56 psi/ft as shown in **Figure 5.5**), *normalized pressure gradient*,  $N_{\nabla p}$  was determined *from Equation A25* to be  $1.4 \times 10^{-4}$ , based on a  $\gamma$  equal to 8.5 mN/m (**Table 5.4**). The  $N_{\nabla p}$  from our data was on the same order as the value of  $N_{\nabla p}=2.6 \times 10^{-4}$  calculated from Gauglitz et al.'s data<sup>112,133</sup> for simultaneous injection, possibly suggesting similar foam generation mechanisms.

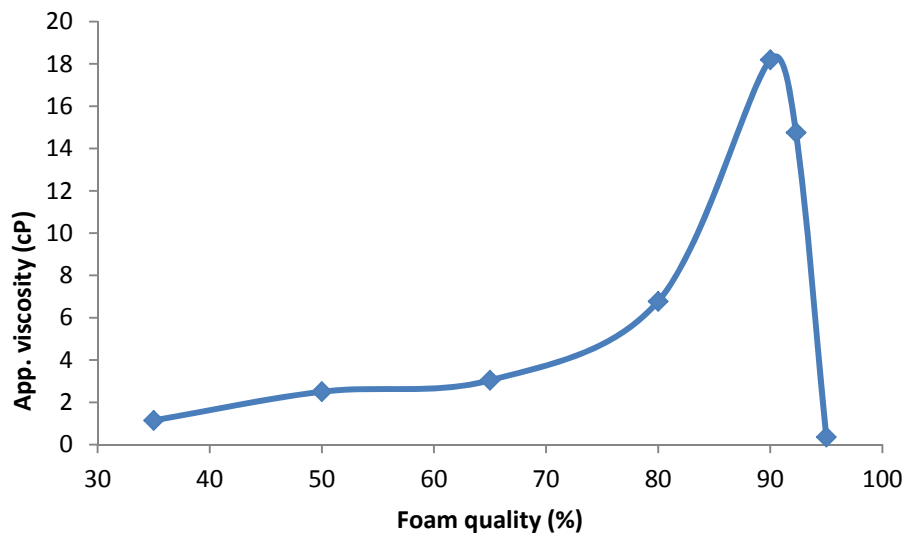


Figure D3: Effect of foam quality on apparent viscosity of C/W foams stabilized with 1% w/w  $C_{12-14}(EO)_{22}$  0.8% TDS brine solution at 15500 ft/day, 40 °C and 1700 psia in a capillary at the downstream of a 30 Darcy sand pack (total superficial velocity 156 ft/day in the porous media)

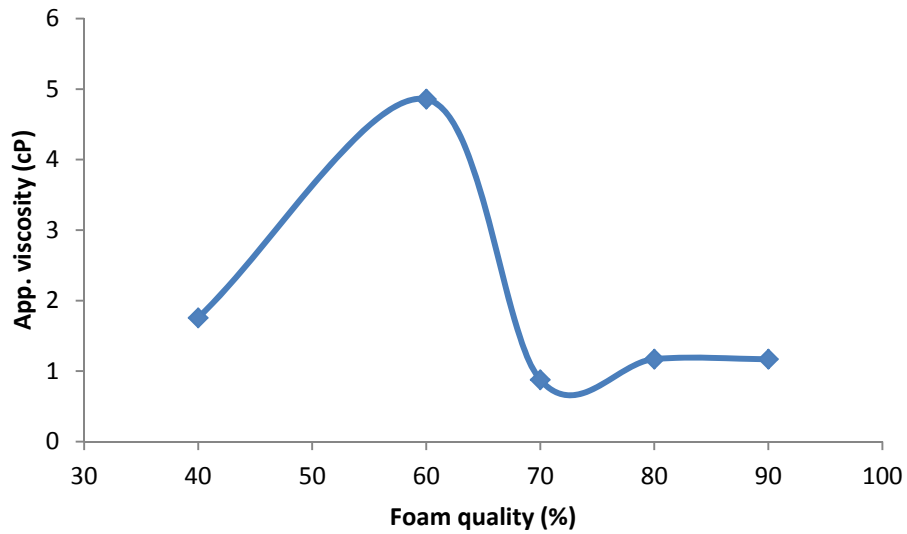


Figure D4: Effect of foam quality on apparent viscosity of C/W foams stabilized with 1% w/w  $C_{12-14}(EO)_{22}$  0.8% TDS brine solution at 3100 ft/day, 40 °C and 1700 psia in a capillary at the downstream of a 1.2 Darcy bead pack (total superficial velocity 6 ft/day in the porous media)

## Bibliography

- (1) Stevens, S.; Kuns kraa, V.; O'Donnell, J. *Enhanced oil recovery scoping study*; EPRI: Palo Alto, CA, 1999.
- (2) Gozalpour, F.; Ren, S. R.; Tohidi, B. *Oil & gas science and technology* **2005**, *60*, 537.
- (3) Enick, R.; Olsen, D. *Mobility and Conformance Control for Carbon Dioxide Enhanced Oil Recovery (CO<sub>2</sub>-EOR) via Thickeners, Foams and Gels- A Detailed Literature Review of 40 Years of Research*, 2011.
- (4) Heller, J. P. *Foams: Fundamentals and Applications in the Petroleum Industry* **1994**, 242(*Foams: Fundamentals and Applications in the Petroleum Industry*), 201.
- (5) Rossen, W. R. In *Foams: Theory, Measurements, and Applications*; Prudhomme, R. K., Khan, S. A., Eds.; Marcel Dekker: New York, 1996.
- (6) Zhu, T.; Ogbe, D. O.; Khataniar, S. *Industrial & Engineering Chemistry Research* **2004**, *43*, 4413.
- (7) Rossen, W. R. *Theory, Measurements, and Applications*; Marcel Dekker: New York, 1996.
- (8) Johnston, K. P.; Da Rocha, S. R. P. *J. Supercritical Fluids* **2009**, *47*, 523.
- (9) Eckert, C. A.; Knutson, B. L.; Debenedetti, P. G. *Nature* **1996**, *383*, 313.
- (10) Tsau, J.; Yaghoobi, H.; Grigg, R. B. In *SPE/DOE Improved Oil Recovery Symposium* Tulsa, Oklahoma, USA, 1998, p 247.
- (11) Renkema, W. J.; Rossen, W. R. In *SPE Annual Technical Conference and Exhibition* Anaheim, California, USA, 2007, p 1.
- (12) Lee, H. O.; Heller, J. P.; Hoefler, A. M. W. *SPE Reservoir Engineering* **1991**, 421.
- (13) Holm, L. W.; Josendal, V. A. *Journal of Petroleum Technology* **1974**, *26*, 1427.
- (14) Stalkup, F. I. *Journal of Petroleum Technology* **1978**, *30*, 1102.
- (15) Puerto, M.; Hirasaki, G. J.; Miller, C. A.; Barnes, J. R. *SPE Journal* **2012**, *17*, 11.
- (16) Barnes, J. R.; Smit, J. P.; Smit, J. R.; Shpakoff, P. G.; Raney, K. H.; Puerto, M. C. In *the SPE/DOE Improved Oil Recovery Symposium* Tulsa, Oklahoma, USA., 2008, p 1.

- (17) Algharaib, M. In *the SPE Middle East Oil & Gas Show and Conference* Kingdom of Bahrain, 2009.
- (18) Adkins, S. S.; Chen, X.; Chan, I.; Torino, E.; Nguyen, Q. P.; Sanders, A. W.; Johnston, K. P. *Langmuir* **2010**, *26*, 5335.
- (19) Levitt, D. B.; Jackson, A. C.; Heinson, C.; Britton, L. N.; Malik, T.; Dwarakanath, V.; Pope, G. A. *SPE Reservoir Evaluation & Engineering* **2009**, *12*, 243.
- (20) Adams, W. T.; Schievelbein, V. H. *SPE Reservoir Engineering* **1987**, *2*, 619.
- (21) Liu, S.; Zhang, D. L.; Yan, W.; Puerto, M.; Hirasaki, G. J.; Miller, C. A. *SPE Journal* **2008**, *13*, 5.
- (22) Hirasaki, G. J.; Miller, C. A.; Puerto, M. *SPE Journal* **2011**, *16*, 889.
- (23) Holland, P. M.; Rubingh, D. N. In *Cationic Surfactants: Physical Chemistry*; Rubingh, D. N., Holland, P. M., Eds.; Marcel Dekker, Inc.: New York, USA, 1990, p 141.
- (24) Lee, C. T., Jr.; Psathas, P. A.; Ziegler, K. J.; Johnston, K. P.; Dai, H. J.; Cochran, H. D.; Melnichenko, Y. B.; Wignall, G. D. *Journal of Physical Chemistry B* **2000**, *104*, 11094.
- (25) Smith, P. G.; Dhanuka, V. V.; Hwang, H. S.; Lim, K. T.; Johnston, K. P. *Ind. Eng. Chem. Res.* **2007**, *46*, 2473.
- (26) McLendon, W. J.; Koronaios, P.; McNulty, S.; Enick, R. M.; Biesmans, G.; Miller, A.; Salazar, L.; Soong, Y.; Romanov, V.; Crandall, D. In *The Eighteenth SPE Improved Oil Recovery Symposium* Tulsa, Oklahoma, USA, 2012.
- (27) Gupta, R. B.; Shim, J. *Solubility in Supercritical Carbon Dioxide*; CRC Press: Boca Raton, Florida, USA, 2007.
- (28) Wolthers, M.; Charlet, L.; Van Cappellen, P. *American Journal of Science* **2008**, *308*, 905.
- (29) McFann, G. J., Univ. Texas, 1993.
- (30) Kuhlman, M. I. *Journal of Petroleum Technology* **1990**, *42*, 902.
- (31) McFann, G. J.; Johnston, K. P. *Langmuir* **1993**, *9*, 2942.
- (32) Harrison, K. L.; Da Rocha, S. R. P.; Yates, M. Z.; Johnston, K. P.; Canelas, D.; DeSimone, J. M. *Langmuir* **1998**, *14*, 6855.
- (33) da Rocha, S. R. P.; Johnston, K. P. *Langmuir* **2000**, *16*, 3690.
- (34) da Rocha, S. R. P.; Johnston, K. P.; Rossky, P. J. *Journal of Physical Chemistry B* **2002**, *106*, 13250.

- (35) Harrison, K. L.; Johnston, K. P.; Sanchez, I. C. *Langmuir* **1996**, *12*, 2637.
- (36) Adkins, S. S.; Chen, X.; Sanders, A.; Nguyen, Q. P.; Johnston, K. P. *Journal of Colloid and Interface Science* **2010**, *346*, 455.
- (37) Holmes, J. D.; Ziegler, K. J.; Audriani, M.; Lee, C. T.; Bhargava, P. A.; Steytler, D. C.; Johnston, K. P. *J. Phys. Chem B* **1999**, *103*, 5703.
- (38) Tabatabal, A.; Gonzalez, M. V.; Harwell, J. H.; Scamehorn, J. F. *SPE Reservoir Engineering* **1993**, *8*, 117.
- (39) Liu, Y.; Jessop, P. G.; Cunningham, M.; Eckert, C. A.; Liotta, C. L. *Science* **2006**, *313*, 958.
- (40) Chen, Y.; Elhag, A. S.; Poon, B. M.; Cui, L.; Ma, K.; Liao, S. Y.; Reddy, P. P.; Worthen, A. J.; Hirasaki, G. J.; Nguyen, Q. P.; Biswal, S. L.; Johnston, K. P. *SPE Journal* **2014**, *19*, 249.
- (41) Zou, B.; McCool, C. S.; Green, D. W.; Willhite, G. P. *SPE Reservoir Evaluation & Engineering* **2000**, *3*, 209.
- (42) Hirasaki, G. J.; Lawson, J. B. *Society of Petroleum Engineers Journal* **1985**, 176.
- (43) Khatib, Z. I.; Hirasaki, G. J.; Falls, A. H. *SPE Reservoir Engineering* **1988**, *3*, 919.
- (44) Babak, V. G.; Stebe, M.-J. *Journal of Dispersion Science and Technology* **2002**, *23*, 1.
- (45) Langevin, D. *Advances in Colloid and Interface Science* **2000**, *88*, 209.
- (46) Ivanov, I. B.; Kralchevsky, P. A. *Colloids and Surfaces A: Physicochemical and Engineering Aspects* **1997**, *128*, 155.
- (47) Ma, K.; Lopez-Salinas, J. L.; Puerto, M. C.; Miller, C. A.; Biswal, S. L.; Hirasaki, G. J. *Energy & Fuels* **2013**, *27*, 2363.
- (48) Ren, G.; Zhang, H.; Nguyen, Q. P. In *the SPE Enhanced Oil Recovery Conference* Kuala Lumpur, Malaysia, 2011, p 1.
- (49) Ren, G.; W., S. A.; Nguyen, Q. P. *The Journal of Supercritical Fluids* **2014**, *91*, 77.
- (50) Enick, R. M.; Olsen, D. K. *Mobility and conformance control for carbon dioxide enhanced oil recovery (CO<sub>2</sub>-EOR) via thickeners, foams, and gels- a detailed literature review of 40 years of research*, 2012.
- (51) Borchardt, J. K.; Bright, D. B.; Dickson, M. K.; Wellington, S. L. In *The 60th Annual Technical Conference and Exhibition of the society of Petroleum Engineers* Las Vegas, Nevada, USA, 1985.

- (52) Farajzadeh, R.; Andrianov, A.; Krastev, R.; Hirasaki, G. J.; Rossen, W. R. *Advances in Colloid and Interface Science* **2012**, 183-184, 1.
- (53) Reck, R. A. In *Cationic Surfactant Organic Chemistry*; Richmond, J. M., Ed.; Marcel Dekker, Inc.: New York, 1990, p 163.
- (54) Puerto, M.; Hirasaki, G. J.; Miller, C. A. In *2010 SPE improved oil recovery symposium* Tulsa, Oklahoma, USA, 2010.
- (55) Lemert, R. M.; Fuller, R. A.; Johnston, K. P. *J. Phys. Chem.* **1990**, 94, 6021.
- (56) Prokop, R. M.; Jyoti, A.; Eslamian, M.; Garg, A.; Mihaila, M.; del Rio, O. I.; Susnar, S. S.; Policova, Z.; Neumann, A. W. *Colloids and Surfaces, A: Physicochemical and Engineering Aspects* **1998**, 131, 231.
- (57) Chen, X.; Adkins, S. S.; Nguyen, Q. P.; Sanders, A. W.; Johnston, K. P. *J. of Supercritical Fluids* **2010**, 55, 712.
- (58) Epton, S. R. *Nature* **1947**, 160, 795.
- (59) Li, J.; Bai, D.; Chen, B. *Colloids and Surfaces A: Physicochemical and Engineering Aspects* **2009**, 346, 237.
- (60) Rosen, M. J. In *Surfactants and Interfacial Phenomena*; 3rd Edition ed.; Rosen, M. J., Ed.; John Wiley & Sons, Inc.: New York, 2004, p 34.
- (61) Hulbers, P. D. T.; Shah, D. O.; Katritzky, A. R. *Journal of Colloid and Interface Science* **1997**, 198, 132.
- (62) Florin, E.; Kjellander, R.; Eriksson, J. C. *Journal of the Chemical Society, Faraday Transactions 1: Physical Chemistry in Condensed Phases* **1984**, 80, 2889.
- (63) O'Neill, M. L.; Cao, Q.; Fang, M.; Johnston, K. P.; Wilkinson, S. P.; Smith, C. D.; Kerschner, J. L.; Jureller, S. H. *Ind. Eng. Chem. Res.* **1998**, 37, 3067.
- (64) Chalbaud, C.; Robin, M.; Lombard, J. M.; Bertin, H.; Egermann, P. *Oil & Gas Science and Technology* **2010**, 65, 541.
- (65) Szulczewski, M. L.; Cueto-Felgueroso, L.; Juanes, R. *Energy Procedia* **2009**, 3421.
- (66) Richmond, J. M. *Cationic surfactants* New York, 1990; Vol. 34.
- (67) Rossen, W. R.; Wang, U. *SPE Journal* **1999**, 4, 92.
- (68) Alvarez, J. M.; Rivas, H. J.; Rossen, W. R. *SPE Journal* **2001**, 6, 325.
- (69) Friedmann, F.; Jensen, J. A. In *SPE California Regional Meeting*; Society of Petroleum Engineers, Inc.: Oakland, CA, 1986.



- (70) Falls, A. H.; Musters, J. J.; Ratulowski, J. *SPE Reservoir Engineering* **1989**, 155.
- (71) Kahlweit, M. *J. Phys. Chem.* **1995**, *99*, 1281.
- (72) Salager, J. L. In *Emulsions and Emulsion Stability*; Sjöblom, J., Ed.; CRC Press: 2006, p 185.
- (73) Kosmulski, M. *Chemical properties of material surfaces*; Marcel Dekker: New York, 2001.
- (74) Qun, X.; Vasudevan, T. V.; Somasundaran, P. *Journal of Colloid and Interface Science* **1991**, *142*, 528.
- (75) Siracusa, P. A.; Somasundaran, P. *Journal of Colloid and Interface Science* **1986**, *114*, 184.
- (76) Dhanuka, V. V.; Dickson, J. L.; Ryoo, W.; Johnston, K. P. *Journal of Colloid and Interface Science* **2006**, *298*, 406.
- (77) Eastoe, J.; Gold, S.; Steytler, D. C. *Langmuir* **2006**, *22*, 9832.
- (78) Johnston, K. P.; Harrison, K. L.; Clarke, M. J.; Howdle, S. M.; Heitz, M. P.; Bright, F. V.; Carlier, C.; Randolph, T. W. *Science* **1996**, *271*, 624.
- (79) Worthen, A. J.; Bagaria, H. G.; Chen, Y.; Bryant, S. L.; Huh, C.; Johnston, K. P. *Journal of Colloid and Interface Science* **2013**, *391*, 142.
- (80) Schramm, L. L.; Wassmuth, F. In *Foams: Fundamentals and Applications in the Petroleum Industry*; Schramm, L. L., Ed.; American Chemical Society: Washington, DC, 1994, p 1.
- (81) Rosen, M. J. In *Surfactants and Interfacial Phenomena*; 3rd Edition ed.; Rosen, M. J., Ed.; John Wiley & Sons, Inc.: New York, 2004, p 178.
- (82) Xie, W.; Gao, Z.; Pan, W.; Hunter, D.; Singh, A.; Vaia, R. *Chem. Mater.* **2001**, *13*, 2979.
- (83) Cui, L.; Khramov, D. M.; Bielawski, C. W.; Hunter, D. L.; Yoon, P. J.; Paul, D. R. *Polymer* **2008**, *49*, 3751.
- (84) Consani, K. A.; Smith, R. D. *Journal of Supercritical Fluids* **1990**, *3*, 51.
- (85) da Rocha, S. R. P.; Psathas, P. A.; Klein, E.; Johnston, K. P. *J. Colloid Interface Sci.* **2001**, *239*, 241.
- (86) Chen, Y.; Elhag, A. S.; Poon, B. M.; Cui, L.; Ma, K.; Liao, S. Y.; Omar, A.; Worthen, A. J.; Hirasaki, G. J.; Nguyen, Q. P.; Johnston, K. P. In *SPE Improved Oil Recovery Symposium* Tulsa, Oklahoma, USA, 2012.
- (87) Lee, C. T., Jr.; Psathas, P. A.; Johnston, K. P.; DeGrazia, J.; Randolph, T. W. *Langmuir* **1999**, *15*, 6781.

- (88) Aveyard, R.; Binks, B. P.; Clark, S.; Fletcher, P. D. I. *Journal of the Chemical Society, Faraday Transactions* **1990**, *86*, 3111.
- (89) Salager, J. L.; Quintero, L. R., Ennodio; Anderez, Jose M. *J. Colloid Interface Sci.* **1980**, *77*, 288.
- (90) Johnston, K. P.; Cho, D.; da Rocha, S. R. P.; Psathas, P. A.; Ryoo, W.; Webber, S. E.; Eastoe, J.; Dupont, A.; Steytler, D. C. *Langmuir* **2001**, *17*, 7191.
- (91) Eastoe, J.; Chatfield, S.; Heenan, R. *Langmuir* **1994**, *10*, 1650.
- (92) Psathas, P. A.; Janowiak, M.; Garcia-Rubio, L. H.; Johnston, K. P. *Langmuir* **2002**, *18*, 3039.
- (93) Ryoo, W.; Webber, S. E.; Johnston, K. P. *Industrial & Engineering Chemistry Research* **2003**, *42*, 6348.
- (94) da Rocha, S. R. P.; Dickson, J. L.; Cho, D.; Rossky, P. J.; Johnston, K. P. *Langmuir* **2003**, *19*, 3114.
- (95) Bachu, S.; Bennion, D. B. *J. Chem. Eng. Data* **2009**, *54*, 765.
- (96) Kabalnov, A.; Wennerstrom, H. *Langmuir* **1996**, *12*, 276.
- (97) Cui, L.; Hirasaki, G. J.; Chen, Y.; Elhag, A. S.; Abdala, A. A.; Lu, L. J.; Pueto, M.; Ma, K.; Tanakov, I.; Pudasaini, R.; Johnston, K. P.; Biswal, S. L. In *Abu Dhabi International Petroleum Exhibition and Conference Abu Dhabi, UAE*, 2014.
- (98) Bergeron, V.; Radke, C. J. *Langmuir* **1992**, *8*, 3020.
- (99) Matulis, D.; Bloomfield, V. A. *Biophysical Chemistry* **2001**, *93*, 37.
- (100) Golec, K.; Hill, E. C.; Kazemi, P.; Skold, R. O. *Tribology International* **1989**, *22*, 375.
- (101) Bergstrom, S.; Olofsson, G. *Journal of Solution Chemistry* **1975**, *4*, 535.
- (102) Tanford, C. In *Hydrophobic Effect*; Tanford, C., Ed.; John Wiley & Sons, Inc.: USA, 1980, p 21.
- (103) Hirasaki, G. J.; Lawson, J. B. *SPE Reservoir Engineering* **1986**, *1*, 119.
- (104) Israelachvili, J. N. In *Intermolecular and Surface Forces*; 3rd ed.; Israelachvili, J. N., Ed.; Elsevier Inc.: USA, 2011, p 1.
- (105) Consani, K. A.; Smith, R. D. *Journal of Supercritical Fluids* **1990**, *3*, 51.
- (106) Holmes, J. D.; Ziegler, K. J.; Audriani, M.; Lee Jr., C. T.; Bhargava, P. A.; Steytler, D. C.; Johnston, K. P. *J. Phys. Chem. B* **1999**, *103*, 5703.
- (107) Bourrel, M.; Schechter, R. S. *Microemulsions and Related Systems: Formation, Solvency, and Physical Properties*; Marcel Dekker: New York, 1988; Vol. 30.

- (108) Rosen, M. J. In *Surfactants and Interfacial Phenomena*; 3rd Edition ed.; Rosen, M. J., Ed.; John Wiley & Sons, Inc.: New York, 2004, p 105.
- (109) Flockhart, B. D. *Journal of Colloid Science* **1961**, *16*, 484.
- (110) van Voorst Vader, F. *Trans. Faraday. Soc.* **1960**, *56*, 1067.
- (111) Narsimhan, G.; Ruckenstein, E. In *Foams: Theory, Measurements and Applications*; Prud'homme, R. K., Khan, S. A., Eds.; Marcel Dekker, Inc.: New York, 1995, p 99.
- (112) Tanzil, D.; Hirasaki, G. J.; Miller, C. A. In *the SPE/DOE Improved Oil Recovery Symposium* Tulsa, Oklahoma, USA, 2002.
- (113) Kovscek, A. R.; Radke, C. J. In *Foams: Fundamentals and Application in the Petroleum Industry*; Schramm, L. L., Ed.; ACS Washington DC, 1994.
- (114) Chambers, D. J. In *Foams: Fundamentals and Applications in the Petroleum Industry*; Schramm, L. L., Ed.; American Chemical Society: Washington, DC, 1994, p 355.
- (115) Kralchevsky, P. A.; Danov, K. D.; Ivanov, I. B. In *Foams: Theory, Measurements and Applications*; Prud'homme, R. K., Khan, S. A., Eds.; Marcel Dekker, Inc.: New York, 1995, p 1.
- (116) Aveyard, R.; Binks, B. P.; Clark, S.; Fletcher, P. D. I. *Journal of Chemical Technology and Biotechnology* **1990**, *48*, 161.
- (117) Frank, H. S.; Evans, M. W. *J. Chem. Phys.* **1945**, *13*, 507.
- (118) Laughlin, R. G. In *Cationic Surfactants: Physical Chemistry*; N., R. D., Holland, P. M., Eds.; Marcel Dekker, INC.: New York, 1990, p 1.
- (119) Scott, L. M.; Robert, T.; Harjani, J. R.; Jessop, P. G. *RSC Advances* **2012**, *2*, 4925.
- (120) Friedmann, F.; Chen, W. H.; Gauglitz, P. A. *SPE Reservoir Engineering* **1991**, *6*, 37.
- (121) Muijs, H. M.; Keijzer, P. P. M.; Wiersma, R. J. In *SPE Enhanced Oil Recovery Symposium* Tulsa, 1988.
- (122) Galimberti, M.; Martino, M.; Guenzi, M.; Leonardi, G.; Citerio, A. *e-Polymers* **2009**, *9*, 686.
- (123) Yoon, K. Y.; Li, Z.; Neilson, B. M.; Lee, W.; Huh, C.; Bryant, S. L.; Bielawski, C. W.; Johnston, K. P. *Macromolecules* **2012**, *45*, 5157.
- (124) Tanford, C. In *Hydrophobic Effect*; Tanford, C., Ed.; John Wiley & Sons, Inc.: USA, 1980, p 5.

- (125) Hiemenz, P. C.; Rajagopalan, R. In *Principles of Colloid and Surface Chemistry*; Hiemenz, P. C., Rajagopalan, R., Eds.; Marcel Dekker, Inc.: New York, 1997, p 297.
- (126) Princen, H. M.; Kiss, A. D. *Journal of Colloid and Interface Science* **1989**, *128*, 176.
- (127) Bretherton, F. P. *Journal of Fluid Mechanics* **1961**, *10*, 166.
- (128) Aronson, A. S.; Bergeron, V.; Fagan, M. E.; Radke, C. J. *Colloids and Surface A: Physicochem. Eng. Aspects* **1994**, *83*, 109.
- (129) Chambers, D. J. In *Advances in Chemistry Series*; Schramm, L. L., Ed.; American Chemical Society: Washington, DC, 1994; Vol. 242 (Foams: Fundamentals and Applications in the Petroleum Industry), p 335.
- (130) Tsau, J.-S.; Heller, J. P. In *Permian Basin Oil and Gas Recovery Conference*; Society of Petroleum Engineers, Inc.: Midland, TX, 1992.
- (131) Lee, H. O.; Heller, J. P. *SPE Reservoir Engineering* **1990**, *5*, 193.
- (132) Yaghoobi, H.; Heller, J. P. In *the 1996 Permian Basin Oil and Gas Recovery Conference* Midland, U. S. A., 1996.
- (133) Gauglitz, P. A.; Friedmann, F.; Kam, S. I.; Rossen, W. R. *Chemical Engineering Science* **2002**, *57*, 4037.
- (134) Falls, A. H.; Hirasaki, G. J.; Patzek, T. W.; Gauglitz, D. A.; Miller, D. D.; Ratulowski, T. *SPE Reservoir Engineering* **1988**, *3*, 884.
- (135) Xing, D.; Wei, B.; McLendon, W.; Enick, R.; McNulty, S.; Trickett, K.; Mohamed, A.; Cummings, S.; Eastoe, J.; Rogers, S.; Crandall, D.; Tennant, B.; McLendon, T.; Romanov, V.; Soong, Y. *SPE Journal* **2012**, *17*, 1172.
- (136) Le, V. Q.; Nguyen, Q. P.; Sanders, A. W. In *SPE/DOE Improved Oil Recovery Symposium* Tulsa, Oklahoma, USA, 2008, p 1.
- (137) Sanders, A. W.; Jones, R. M.; Linroth, M.; Nguyen, Q. P. In *SPE Annual Technical Conference and Exhibition* San Antonio, Texas, USA, 2012.
- (138) McLendon, W. J.; Koronaios, P.; Enick, R. M.; Biesmans, G.; Salazar, L.; Miller, A.; Soong, Y.; McLendon, T.; Romanov, V.; Crandall, D. *Journal of Petroleum Science and Engineering* **2014**, *Accepted*.
- (139) Mukherjee, P.; Padhan, S. K.; Dash, S.; Patel, S.; Mishra, B. K. *Advances in Colloid and Interface Science* **2011**, *162*, 50.
- (140) Huibers, P. D.; Shah, D. O.; Katritzky, A. R. *Journal of colloid and interface science* **1997**, *193*, 132.
- (141) Adkins, S. S., The University of Texas at Austin, 2009.

- (142) Rosen, M. J. In *Surfactants and Interfacial Phenomena*; 3rd ed.; Rosen, M. J., Ed.; John Wiley & Sons, Inc.: New York, 2004, p 1.
- (143) Miñana-Perez, M.; Graciaa, A.; Lachaise, J.; Salager, J.-L. *Colloids and Surfaces A: Physicochemical and Engineering Aspects* **1995**, *100*, 217.
- (144) da Rocha, S. R. P.; Harrison, K. L.; Johnston, K. P. *Langmuir* **1999**, *15*, 419.
- (145) Bonfillon-Colin, A.; Langevin, D. *Langmuir* **1997**, *13*, 599.
- (146) Rossen, W. R. *Colloids and Surface A: Physicochem. Eng. Aspects* **2003**, *225*, 1.
- (147) Liu, Y.; Grigg, R. B.; Bai, B. In *SPE International Symposium on Oilfield Chemistry* Woodland, Texas, 2005.
- (148) Marquez, N.; Anton, R.; Graciaa, A.; Lachaise, J.; Salager, J.-L. *Colloids and Surfaces A: Physicochemical and Engineering Aspects* **1995**, *100*, 225.
- (149) Salager, J.-L.; Marquez, N.; Graciaa, A.; Lachaise, J. *Langmuir* **2000**, *16*, 5534.
- (150) Welch, C. F.; Rose, G. D.; Malotky, D.; Echersley, S. T. *Langmuir* **2006**, *22*, 1544.
- (151) Princen, H. M. *Journal of Colloid and Interface Science* **1983**, *91*, 160.
- (152) Wagner, C. Z. *Elektrochem* **1961**, *65*, 581.
- (153) Lake, L. *Enhanced Oil Recovery*; Prentice Hall: Englewood Cliffs, NJ, 1989.
- (154) Ransohoff, T. C.; Radke, C. J. *SPE Reservoir Engineering* **1988**, *3*, 573.
- (155) Rossen, W. R.; Gauglitz, P. A. *AIChE Journal* **1990**, *36*, 1176.
- (156) Parkhurst, D. L.; Appelo, C. **1999**.
- (157) Wang, W.; Lu, W.; Jiang, L. *J. Phys. Chem. B* **2008**, *112*, 1409.